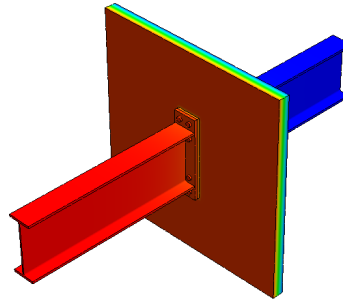
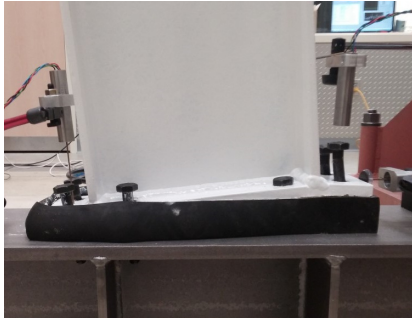


# **THERMO-MECHANICAL MODELING AND TESTING OF THERMAL BREAKS IN STRUCTURAL STEEL JOINT TRANSMITTANCES**

## **FINAL PROJECT REPORT**



by

Scott Hamel, P.E., Ph.D.  
Sava White, M.S.  
University of Alaska Anchorage

for

American Institute of Steel Construction  
130 East Randolph Street Suite 2000  
Chicago, IL 60601-6219



August 29, 2016

THIS PAGE INTENTIONALLY LEFT BLANK

## **Abstract**

Thermal bridging through structural steel members in building envelopes poses issues with heat loss and condensation in cold regions. Structural steel thermal breaks serve to reduce heat flow through the steel element and have seen extensive use in the construction industry. These breaks generally take the form of high-strength and stiffness materials with low-thermal conductivity placed between the faying surfaces of a steel connection. Current steel construction code provisions in the US, however, prohibit the use of compressible materials in a steel connection. While the practical benefits of thermal breaks in structural steel beams and columns have been well demonstrated, there is no accepted guidance on the structural design of these thermal breaks, nor is there information on the thermal efficacy of thermal break design parameters.

The objective of this project was to determine the thermal and mechanical behavior of structural steel beam thermally broken connections, and their corresponding continuous beam thermal bridges. Heat flow through a thermally broken steel end-plate connection was determined experimentally using a calibrated hot box. Results were used to validate a finite element heat transfer model, which was then used to perform a parametric analysis on the thermal break configuration using different break and bolt materials. From the analyses, it was determined that heat flow reduction and condensation potential are highly dependent on the thickness of the break material. In addition, the use of stainless steel or fiber-reinforced bolts provides a significant reduction in heat flow and condensation potential. The mechanical behavior of a thermally-broken connection with an elastomeric pad as the break material was evaluated using cantilever bending tests and shear tests. The mechanical and thermal tests were conducted on an identical set of connections with three different thicknesses of neoprene pad. Results showed that the rotational stiffness of the connection was reduced approximately linearly with increasing neoprene pad thickness. Shear stiffness was reduced exponentially with increased pad thickness. Structural experimental results were validated against a finite element model which was used to investigate stresses in the end-plate and the bolt. Bolt rupture was found to occur at a reduced applied bolt bending moment due to the increased rotation of the end-plate.

THIS PAGE INTENTIONALLY LEFT BLANK



## Table of Contents

|   |           |
|---|-----------|
| Abstract.....   | iii       |
| List of Figures.....  | vii       |
| List of Tables .....  | ix        |
| Acknowledgments.....  | x         |
| <b>Chapter 1: Introduction .....</b>  | <b>13</b> |
| 1.1 Background.....   | 13        |
| 1.2 Objectives .....  | 14        |
| 1.3 Methodology .....   | 15        |
| <b>Chapter 2: Literature Review .....</b>                                   | <b>17</b> |
| 2.1 Calibrated Hot-Box .....  | 17        |
| 2.2 Thermal Performance.....  | 21        |
| 2.2.1 Thermal bridging in structural steel frames .....                     | 23        |
| 2.2.2 Calculating thermal bridging transmittances .....                     | 26        |
| 2.2.3 Structural steel thermal break strategies for point penetrations..... | 27        |
| 2.2.4 Condensation considerations .....                                     | 28        |
| 2.3 Mechanical Performance .....  | 29        |
| 2.3.1 Thermal bridging and breaks in point penetrations .....               | 29        |
| 2.3.2 Structural considerations.....  | 30        |
| <b>Chapter 3: Method .....</b>  | <b>35</b> |
| 3.1 Industry Survey of Thermal Break Practices .....                        | 35        |
| 3.2 Calibrated Hot-Box Testing.....   | 36        |
| 3.2.1 Description of Calibrated Hot Box .....                               | 36        |
| 3.2.2 Calibration of Hot Box.....   | 41        |
| 3.2.3 Uncertainty analysis.....   | 46        |
| 3.2.4 Thermal Transmittance Measurement .....                               | 48        |
| 3.3 Structural Testing.....   | 53        |
| 3.3.1 Bending Tests.....  | 54        |
| 3.3.2 Shear Tests .....   | 58        |
| 3.4 Finite-element Modeling.....  | 61        |

|  |     |
|--|-----|
| 3.4.1 Model Information .....                              | 61  |
| 3.4.2 Material Properties .....                            | 62  |
| 3.4.3 Boundary Conditions .....                            | 65  |
| 3.4.4 Mesh Parameters .....                                | 65  |
| 3.4.5 Steps and Solution.....                              | 66  |
| Chapter 4: Results and Discussion.....                     | 67  |
| 4.1 Industry Survey .....                                  | 67  |
| 4.2 Calibrated Hot-Box Testing.....                        | 68  |
| 4.3 Structural Testing.....                                | 69  |
| 4.3.1 Bending Tests.....                                   | 69  |
| 4.3.2 Shear Tests .....                                    | 74  |
| 4.4 Finite-element Modeling.....                           | 76  |
| 4.4.1 Thermal Modeling .....                               | 76  |
| 4.4.2 Mechanical Behavior .....                            | 95  |
| 4.5 Limitations .....                                      | 102 |
| Chapter 5: Conclusions and Recommendations .....           | 105 |
| 5.1 Hot-Box.....   | 105 |
| 5.2 Structural Testing.....                                | 105 |
| 5.3 Finite-element Modeling.....                           | 107 |
| 5.4 Recommendations.....                                   | 109 |
| 5.5 Future Research .....                                  | 110 |
| References .....   | 111 |
| Appendices .....   | 113 |
| Appendix A Industry Survey of Thermal Break Practices..... | 115 |
| Appendix B Experimental Test Drawings.....                 | 125 |
| Appendix C End-plate Design.....                           | 151 |
| Appendix D Neoprene Material Model .....                   | 159 |
| Appendix E Material Reports.....                           | 163 |
| Appendix F Drawings and Photos of Calibrated Hot Box.....  | 170 |

## List of Figures

|  |    |
|--|----|
| Figure 2-1: Example of a structural steel (a) thermal bridge and (b) thermal break .....           | 18 |
| Figure 2-2: Schematic of a calibrated hot box .....  | 21 |
| Figure 2-3: Thermal bridging in a stud wall .....  | 22 |
| Figure 2-4: Structural steel shelf angle supporting facade elements .....                          | 24 |
| Figure 2-5: Example of a structural steel beam thermal bridge.....                                 | 24 |
| Figure 2-6: Example of a rooftop penetration thermal bridge .....                                  | 25 |
| Figure 3-1: Schematic cross section of the constructed hot box.....                                | 37 |
| Figure 3-2: Constructed calibrated hot box .....   | 37 |
| Figure 3-3: Example air temperatures for an entire run period (24-hr) .....                        | 39 |
| Figure 3-4: Air temperature in the metering chamber at steady-state (18:00-24:00). ....            | 40 |
| Figure 3-5: Heat flow balance in the metering chamber.....   | 41 |
| Figure 3-6: Flanking loss for the calibrated hot box.....  | 43 |
| Figure 3-7: Surround panel temperature characterization sensor locations.....                      | 45 |
| Figure 3-8: Schematic of thermal bridge configuration.....   | 49 |
| Figure 3-9: Sensor arrangement for the continuous beam thermal bridge.....                         | 50 |
| Figure 3-10: End plate connection geometry.....  | 51 |
| Figure 3-11: Temperature sensor arrangement for the beam-to-beam thermal break connection          | 52 |
| Figure 3-12: An idealized neoprene thermal break end-plate connection .....                        | 53 |
| Figure 3-13: End plate connection geometry.....  | 55 |
| Figure 3-14: Bending test configuration .....  | 56 |
| Figure 3-15: Constructed bending test assembly .....   | 57 |
| Figure 3-16: Bolt tightening sequence .....  | 58 |
| Figure 3-17: Shear test configuration .....  | 59 |
| Figure 3-18: Constructed shear test setup .....  | 60 |
| Figure 3-19: Assembled and meshed model (1.5-in. neoprene) .....                                   | 62 |
| Figure 3-20: Material definition for (a) bolts and nuts and (b) beam and end-plate .....           | 63 |
| Figure 4-1: Dot density map of survey respondents .....  | 67 |
| Figure 4-2: Heat flow results from calibrated hot box testing.....                                 | 68 |
| Figure 4-3: Shear deflection of the end-plate. Measured at edge of tension side of end plate. .... | 70 |
| Figure 4-4: Moment-rotation curves .....   | 71 |
| Figure 4-5: Deformation of the neoprene under ultimate moment .....                                | 73 |
| Figure 4-6: Measured deflection of the compression flange for each bending test .....              | 74 |
| Figure 4-7: Comparison of deflection and load for all shear tests .....                            | 75 |
| Figure 4-8: Bending in a bolt under shear load with a soft neoprene layer .....                    | 76 |
| Figure 4-9: Idealized continuous beam thermal bridge model .....                                   | 77 |
| Figure 4-10: Effective versus nominal R-value for a structural steel thermal bridge.....           | 78 |

|  |     |
|--|-----|
| Figure 4-11: Temperature variation along a long W-section of uniform cross-sectional area .....                  | 80  |
| Figure 4-12: Total heat flow versus length of beam extending from insulation face .....                          | 81  |
| Figure 4-13: Temperature distribution along the surface of the beam flange.....                                  | 82  |
| Figure 4-14: Relationship of heat flow rate to perimeter and area for all W-shapes.....                          | 83  |
| Figure 4-15: Comparison of heat flow rate and the area moment of inertia.....                                    | 84  |
| Figure 4-16: Covering insulation applied to an extended steel beam .....   | 85  |
| Figure 4-17: Temperature and heat flux for a continuous and covered beam thermal bridge.....                     | 86  |
| Figure 4-18: Optimum insulation covering. $TI = 0.91$ . Heat flow = $0.927 \text{ Btu/hr } ^\circ\text{F}$ ..... | 87  |
| Figure 4-19: Beam-to-beam end-plate connection .....   | 88  |
| Figure 4-20: Finite element model of the thermal break connection.....   | 89  |
| Figure 4-21: Comparison of heat flow rate and thermal break pad thickness .....                                  | 90  |
| Figure 4-22: Comparison of heat flow against neoprene pad thickness for different bolt types ..                  | 91  |
| Figure 4-23: Comparison of heat flow through the pad material and steel bolts.....                               | 92  |
| Figure 4-24: Comparison of surface temperatures along the beam for continuous beam test.....                     | 95  |
| Figure 4-25: Deformed isometric view of each connection.....   | 96  |
| Figure 4-26: Experimental and FEA moment-rotation curves for steel connection.....                               | 97  |
| Figure 4-27: Experimental and FEA moment-rotation curves all bending tests .....                                 | 98  |
| Figure 4-28: Deformation of connection for each thickness of neoprene. ....                                      | 100 |
| Figure 4-29: von Mises stress distribution in bolt 8 at 200 kip-in applied moment. ....                          | 101 |
| Figure 4-30: 1.5-in. neoprene pad for (a) experimental bending and (b) FEA stresses.....                         | 101 |

## **List of Tables**

|  |    |
|--|----|
| Table 3-1: Comparison of thermal conductivity values obtained for the characterization panel . | 44 |
| Table 3-2: Surface heat transfer coefficient values for surround panel .....                   | 45 |
| Table 3-3: Calibrated Hot-Box Thermal-Break Testing Parameters .....                           | 51 |
| Table 3-4: Cantilever bending test matrix .....  | 56 |
| Table 3-5: Shear test matrix .....   | 60 |
| Table 3-6: Ogden coefficients used for neoprene material model .....                           | 64 |
| Table 4-1: Heat flow measurement results .....   | 69 |
| Table 4-4: Bending test summary .....  | 69 |
| Table 4-5: Comparison between experimental and finite-element analysis results.....            | 93 |

THIS PAGE INTENTIONALLY LEFT BLANK

### **Acknowledgments**

I would like to recognize and thank Sava White, whose tireless work on this project made it possible. I would also like to acknowledge significant contributions from Nathaniel Cox. I would also like to thank AISC, the UAA College of Engineering, and the Structural Engineers Association of Alaska (SEAAK) for funding that made the project possible.

THIS PAGE INTENTIONALLY LEFT BLANK



# Chapter 1: Introduction

## 1.1 Background

A building's thermal envelope should ideally encompass entirely the conditioned space of the structure. However, there are common construction situations where a structural element must pass between the interior conditioned space and the exterior environment creating a thermal bridge. Thermal bridging in buildings occurs when a highly conductive building element crosses between the interior conditioned space and the exterior creating a localized region of excessive heat flow. Thermal bridging is present in a variety of conditions including wall studs, balcony supports, façade supports, rooftop penetrations, etc. Thermal bridges in cold regions pose a significant issue with heat flow and condensation due to the greater temperature difference between the interior and exterior environments.

Thermal bridging has been addressed by building energy code requirements, which often require a layer of continuous insulation to be applied to the exterior face of the building, atop the stud wall cavity insulation [1]. Best practices suggest minimizing or eliminating thermal bridging. A common solution to thermal bridging is to replace the highly conductive material with a material that has a lesser conductivity such as wood, vinyl, or fiberglass. This is done easily with façade features, but in cases where the thermal bridge consists of a load-bearing structural element, reducing or eliminating the thermal bridge creates additional engineering considerations.

Commonly, structural elements that protrude through the building envelope create a load path from exterior elements to interior structural supports. Structural steel has a thermal conductivity that is several orders of magnitude higher than that of the building envelope insulation. Hence, structural steel elements protruding through the building envelope result in acute and consequential thermal bridging.

A common solution has been to use a gasket material such as wood or fiberglass to split the structural element in the plane of the thermal envelope [2]. This method has been applied by both the structural engineering community and the building envelope industry to develop thermally-broken structural steel connections. These connections often take the form of a low-conductivity,

but high-strength and stiffness, material placed in a steel connection located inside the layer of the building insulation. These type of connections are becoming increasingly common. One the most popular thermal break connection types consists of a steel end-plate connection that is bolted through a low-conductivity gasket, such as neoprene or fiberglass, to the structural element on the outside of the structure [3].

Design and installation of thermal breaks in structural applications is currently not addressed by any structural engineering governing organization, but nonetheless, structural engineers specify thermal break strategies in their designs. This situation has prompted manufacturers of thermal breaks to develop and market thermally insulating structural materials and products that have properties and a mechanical behavior guaranteed by the manufacturer, which alleviating the design burden on the structural engineer. However, the American Institute of Steel Construction (AISC) and the Research Council on Steel Connections (RCSC) prohibits the placement of non-steel materials in the grip of a bolted connection [4], hereby restricting the use of structural steel thermal breaks of the aforementioned type.

Research is necessary to quantify and characterize the thermal and mechanical behavior of structural steel point thermal break connections. Determining effective ways of reducing thermal bridging in structural steel elements can increase the energy efficiency of buildings and reduce the negative effects of thermal bridges, such as condensation and cold spots.

## **1.2 Objectives**

The main goal of this project was to experimentally and numerically evaluate the thermal and mechanical characteristics of a set of common structural steel thermal break details. The specific objectives of the research were to:

- Determine what details are currently available, identify where they have been used successfully, and determine which thermal break strategies are most common.
- Use finite element methods to:
  - evaluate the thermal effectiveness of a set of common thermal break details
  - characterize the structural performance of the break details

- Perform experimental measurement of a thermal break details to evaluate the validity of the finite element analysis models.

### **1.3 Methodology**

To meet the project's objectives, this work was divided into several phases. The following tasks were performed:

- A survey of literature and structural engineering industry survey on structural steel thermal bridging and thermal break practices.
- Experimental calibrated hot box testing on thermal bridge and thermal break specimens.
- Experimental testing of a thermally-broken end-plate moment connection under cantilever bending and shear.
- A parametric sensitivity analysis on thermal break and thermal bridge details for heat flow and condensation potential using a finite element heat transfer model.
- Development and calibration of a finite-element model to predict the behavior of the experimentally-tested end-plate connection.

THIS PAGE INTENTIONALLY LEFT BLANK

## Chapter 2: Literature Review

This section will review literature on previous and related research on thermal-breaks and thermal bridging, and associated experimental standards.

### 2.1 Calibrated Hot-Box

Thermal bridges are a type of building envelope thermal anomaly caused by heat conduction and produce localized excessive heat flow [2]. A variety of common building assembly features lead to thermal bridging (e.g. wall studs, canopies, balconies, and rooftop penetrations). Thermal bridging results in an unanticipated and localized increase in heat flow, and without proper detailing, can result in condensation on elements inside or outside of the structure, potentially leading to building degradation.

There are two general categories of thermal bridging; linear and point. A linear thermal bridge is one that can be characterized per unit length, such as a wall stud, roof rafter, or steel shelf angle, while a point thermal bridge is generally a single penetration through the building envelope, such as a beam penetrating through a wall, or a post penetrating through an insulated roof.

Thermal transmittance (U-value) is the rate of heat transfer through an area of the building under a certain temperature difference. A building envelope area not affected by a thermal bridge is referred to as the clear field. Thermal bridging and related building thermal anomalies are accounted for by comparing the heat flow through an area with a thermal bridge, to the same area without the thermal bridge. The difference in magnitude of heat flow is attributed to the effect the thermal anomaly has on the clear field assembly, a value conventionally represented by  $\Psi$  for linear thermal transmittances (Btu/hr·°F·ft) and  $\chi$  for point thermal transmittances (Btu/hr·°F).

Figure 2-1 shows an example of a typical structural steel thermal bridge (a) and a structural steel thermal break (b).

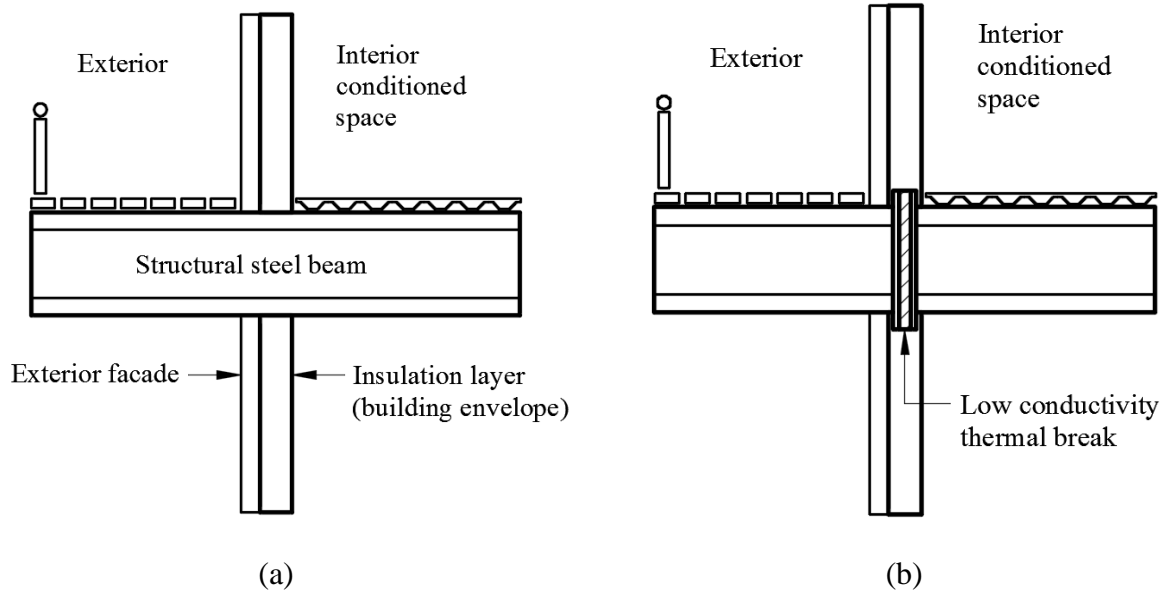


Figure 2-1: Example of a structural steel (a) thermal bridge and (b) thermal break

Linear thermal bridges have been studied extensively using experimental and numerical methods, and recent emphasis on sustainable buildings has once again prompted increased attention on thermal bridging. Oak Ridge National Laboratories has previously performed numerous measurements and simulations of various wall configurations [5]. More recently, Morrison Hershfield, as part of an extensive research project for ASHRAE into thermal bridging, used three-dimensional finite element software to provide thermal performance data of a number of common building envelope details for mid- and high-rise construction [6]. Oak Ridge and Morrison Hershfield, along with other researchers[7]–[10], have largely concentrated their efforts on studying linear thermal bridges (e.g. wall studs, floor slabs, shelf angles) as opposed to point transmittances (e.g. a steel beam penetrating the building envelope normal to the plane of the envelope).

In cases where the thermal bridge consists of a load-bearing structural steel element, reducing or eliminating the thermal bridge requires additional non-traditional structural engineering methods, and requires prudent engineering judgement with an awareness of the thermal envelope. The relatively high thermal conductivity of structural steel linear and point thermal bridges exacerbates the issues caused by thermal bridges. A common solution has been to use a relatively high-strength pad material, such as rubber or fiberglass, to cut the structural steel element in the

plane of the thermal envelope, as shown in Figure 2-1(b). This, however, requires special attention as the pad material must be designed and engineered to resist the applied forces present in the otherwise un-broken structural element.

A number of manufacturers have developed and are marketing thermal break materials engineered to be placed in between the faying surfaces of structural steel connections. Fabreeka [11], Armadillo [12], Schock [13], Farrat [14], and Insula [15] are a few among several that market thermal break products (Fabreeka-TIM, Armatherm FRR, Isokorb, Farrat TBK/TBL, and ThermConX, respectively) that are specifically designed to be used in structural steel applications.

Thermal bridges that consist of structural steel beam or column penetrations are made complicated by air leakage and condensation issues. Many complex thermal bridging problems can be addressed using commercially-available software for modeling and simulating steady-state and transient heat flow in two and three dimensions. While this software can be utilized to determine the total heat flow for a specific idealized configuration of thermal bridging, finite element software, in its current state, cannot predict air leakage or condensation effects. Experimental testing is required to simulate and quantify these effects in order to fully assess the impact of thermal bridging on thermal performance.

There exist several methods for experimentally determining the thermal transmittance of building elements. A calibrated or a guarded hot-box apparatus is used to determine heat transfer and thermal properties of building elements of different materials and configurations. Typical uses for a calibrated or guarded hot box include measuring the R-value of insulating materials and wall configurations of varying geometries and complexities as well as fenestration systems such as windows and curtain walls. The hot box method has also been used to determine heat flow generated by thermal bridges [5], [10], [16], [17]. The American Society of Testing and Materials (ASTM) has two active standards that deal with the hot box measurement method. ASTM C1199 - Standard Test Method for Measuring the Steady-State Thermal Transmittance of Fenestration Systems Using Hot Box Methods [18] is used for the measurement of fenestration systems, while ASTM C1363 - Standard Test Method for Thermal Performance of Building

Materials and Envelope Assemblies by Means of a Hot Box Apparatus [19] is more suited for the measurement of various building element assemblies. There are also several ISO standards that describe a similar hot box apparatus (e.g., ISO 12567, ISO 8990). The Russian standard GOST 26602.1 [20] is regarded as a higher precision method with respect to the ASTM and ISO standards [21], but is more applicable to fenestration systems rather than thermal bridging elements.

While there have been a number of hot box experiments performed on thermal bridges, all of them have investigated heat flow in enclosed linear thermal bridges within a wall or roof system, such as cold-formed steel stud wall assemblies. Finite element models have been calibrated to agree with experimental results in those scenarios [5], [10], [22]. However, experimental studies performed on extended point transmittances of structural steel thermal bridges or breaks using the hot box method have not been found.

There are two basic configurations for a hot box. The first is the guarded hot box, which has a smaller metering chamber located inside a guard chamber. The second configuration is the calibrated hot box, which is similar to the guarded hot box with the exception of the guard chamber. A cross-sectional schematic of a typical calibrated hot box is shown in Figure 2-2.

The calibrated hot box is better suited to larger and non-homogenous test specimens, because it lacks the requirement for a secondary guard chamber, which can be cost and space prohibitive. In general, a calibrated hot box must be operated in a conditioned laboratory space, as well as be highly insulated to reduce heat flow through the metering chamber walls.

The calibrated hot box method is designed and operated to maintain a constant temperature difference across the test specimen for a period of time required for heat flow to come to a constant rate (i.e., steady-state). The temperature difference between the metering chamber and the climatic chamber drives a heat flow across the test specimen. By measuring the total energy entering the metering chamber, and accounting for the measured extraneous heat flows from the metering chamber, the heat flow across the test specimen is determined.



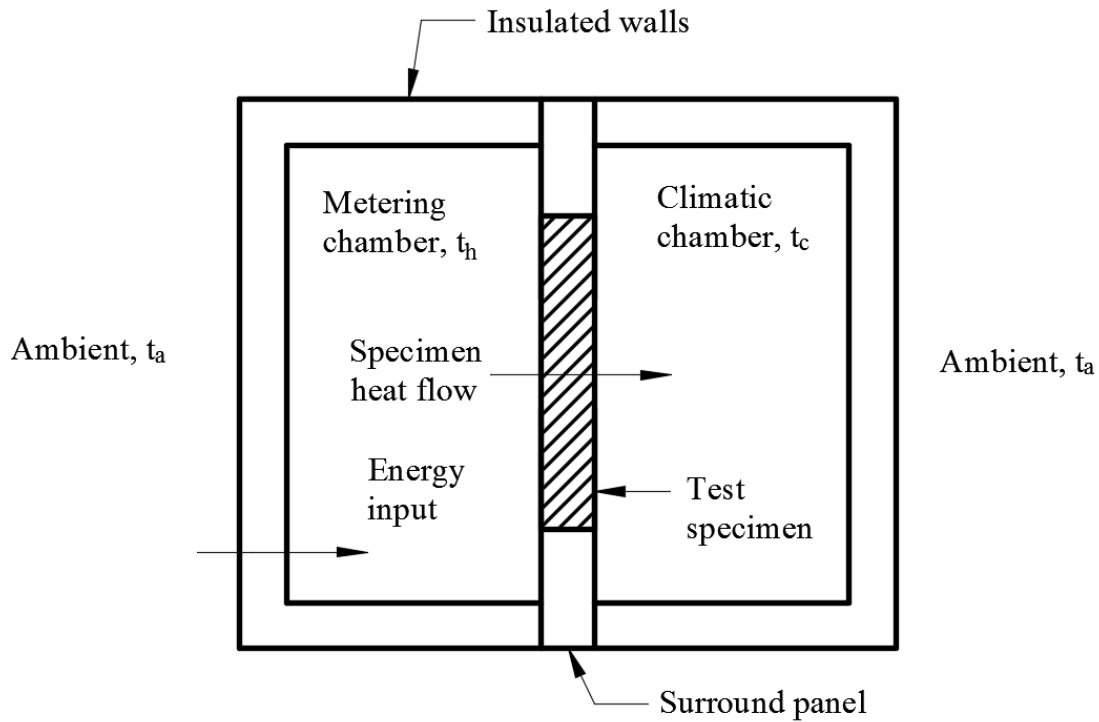


Figure 2-2: Schematic of a calibrated hot box

## 2.2 Thermal Performance

Thermal bridges are characterized as thermal anomalies in a building envelope. Simply, a thermal bridge occurs when a building element of higher thermal conductivity than the surrounding insulation layer ‘bridges’ between the outside space and the conditioned inside space. A thermal bridge can exist even if the element does not cross entirely from one space to the other, such as a wall stud encased between the exterior sheathing and the interior wall coverings, as shown in Figure 2-3. In this case, a region of high heat flow, relative to the surrounding envelope, exists in the thermal bridge due to the higher thermal conductivity of the bridging element.

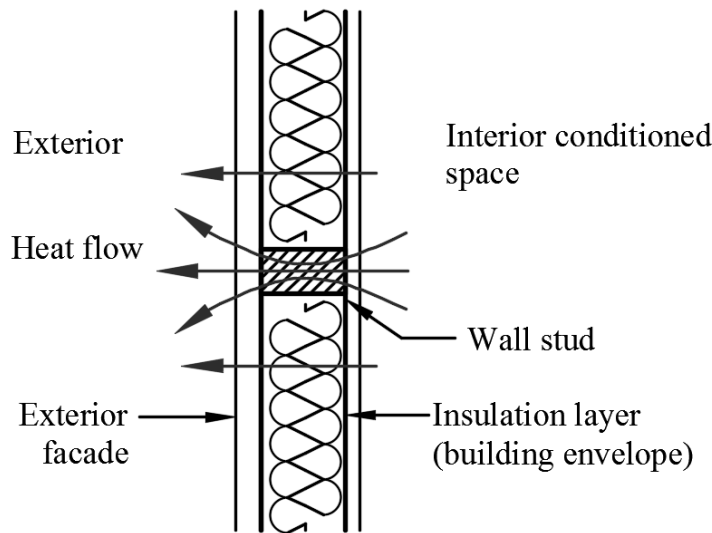


Figure 2-3: Thermal bridging in a stud wall

Excessive heat flow is not the only consequence of a thermal bridge through a building envelope. In cold weather, the high heat flow in the area of a thermal bridge can produce a localized region of low temperature on the inside surface of the building envelope [7]. This low-temperature area can result in condensation of moisture from the interior air, which, in turn, can lead to mold growth, staining, and possible deterioration of the building envelope. Conversely, the temperature on the exterior surface is raised to an extent where it melts snow and ice on the exterior surface of the building envelope, which then freezes back to ice when the water travels past the location of the thermal bridge forming a mass of continually expanding ice. In addition to posing the danger of falling ice, this can cause corrosion as well as structural loading issues due to pooling of water or other unanticipated loadings.

In most cases, the effects of thermal bridging have not been catastrophically detrimental to a building's health, nor its occupants. But, as the industry tends towards more sustainable buildings, typical insulation thickness is increasing, which could lead to more significant negative effects caused by thermal bridges. The diminishing return of reduced heat flow by increasing the thickness of the building envelope insulation is well known. However, as the insulation capacity of the building envelope is increased, the heat flow through the thermal bridge remains constant. Therefore, the practice of increasing the thickness of the building

envelope in an attempt to reduce the overall heat flow through the envelope area becomes even less important without first acknowledging the contributing effects of thermal bridging.

Thermal bridging has been studied extensively in the past few decades, but recent emphasis on sustainable buildings has again prompted increased attention on thermal bridges [23]–[25]. Oak Ridge National Laboratories in particular has performed numerous measurements and simulations of various wall configurations [22], [26]. As part of an ASHRAE research project into thermal bridging, Morrison Hershfield performed an in-depth analysis of a variety of thermal bridging configurations for typical commercial construction details. They, along with a number of other researchers [8], [27], however, have largely concentrated their efforts on studying linear thermal bridges such as wall studs and floor slabs.

### 2.2.1 Thermal bridging in structural steel frames

The presence of steel elements in thermal bridges amplifies their detrimental effects due to the relatively high thermal conductivity of steel. The thermal conductivity of steel is roughly 1,500 times the thermal conductivity of typical insulations used in a building envelope. Most thermal bridges in structural steel frames take the form of either linear or point penetrations through the building envelope. Linear thermal bridges are those that can be expressed per a unit length, such as shelf angles shown in Figure 2-4.

Point transmittances are single penetrations through the building envelope than can be repeating or non-repeating, such as the single beam penetration shown in Figure 2-5.

Two of the most common structural steel point transmittances take the form of either cantilever beams crossing through the wall, such those shown in Figure 2-5, and rooftop columns penetrating horizontal plane of a roof surface such as the one shown in Figure 2-6. In each case, the size and shape of the steel beam can vary, as well as the thickness, insulation, and layering of the clear wall or roof.

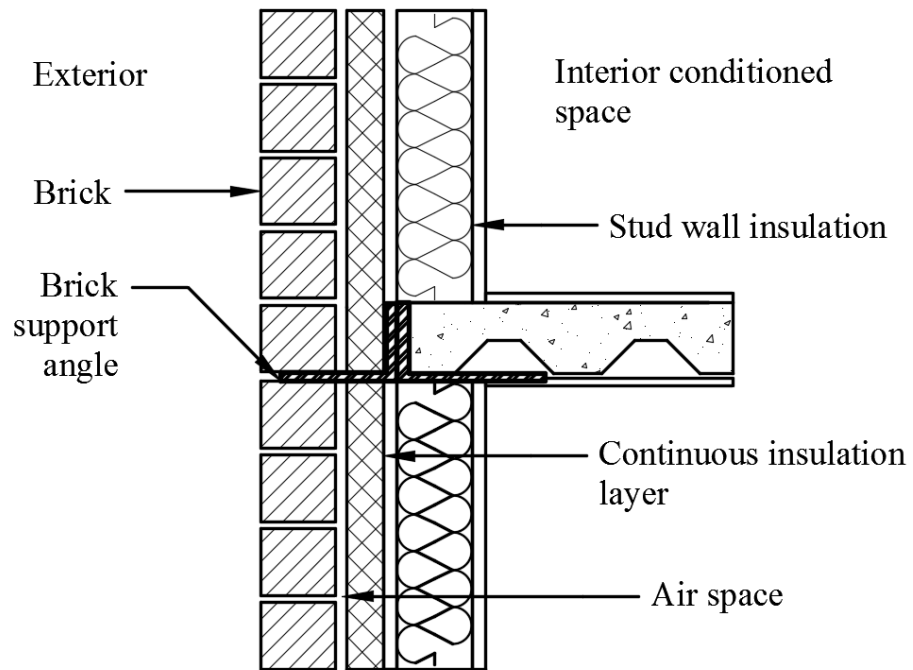


Figure 2-4: Structural steel shelf angle supporting facade elements

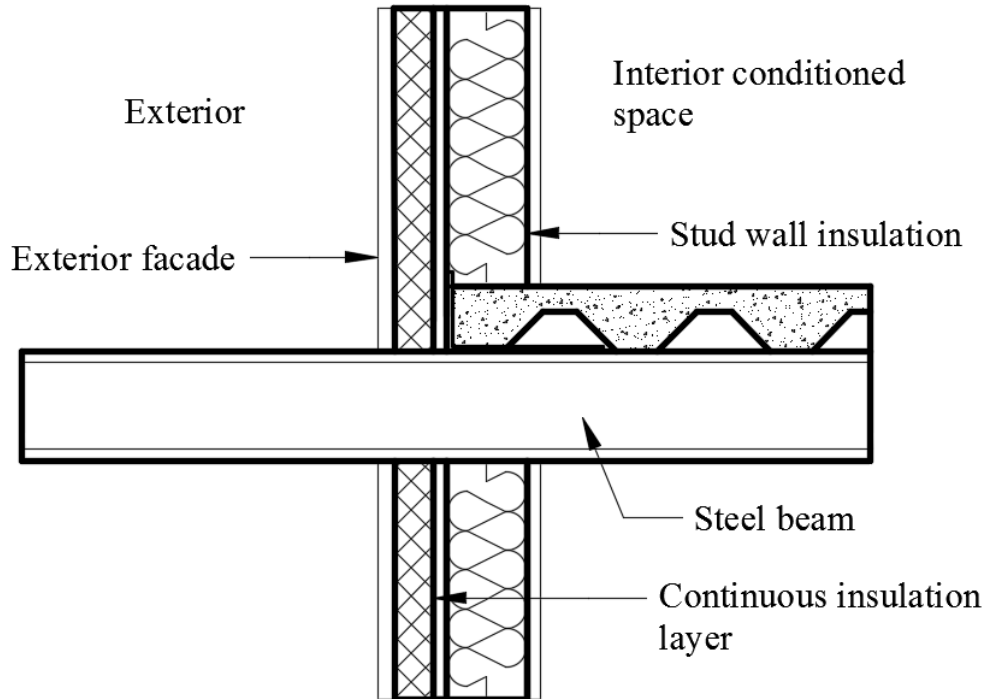


Figure 2-5: Example of a structural steel beam thermal bridge

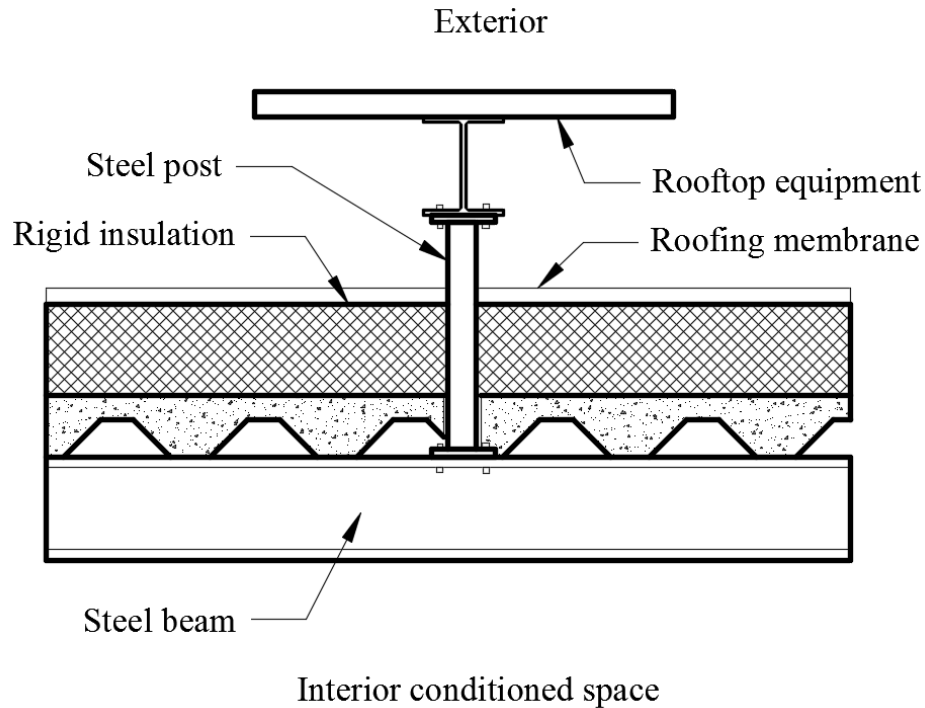


Figure 2-6: Example of a rooftop penetration thermal bridge

Structural steel members that penetrate the building envelope normal to the plane of the insulation, and protrude into the outside air act as cooling fins. This increases the rate of heat transfer to the environment by increasing convection. The geometry of the steel shape can affect the resulting rate of heat transfer due to an increase or decrease in the surface area exposed to the outside air with a corresponding change in convective heat transfer.

Building envelopes that subscribe to the code requirements of ASHRAE 90.1-2004 and later [1] are comprised of two serial layers of insulation. These consist of the cavity, or stud wall, insulation and a continuous insulation layer which is defined in ASHRAE 90.1 as “insulation that is continuous across all structural members without thermal bridges other than fasteners and service openings. It is installed on the interior, exterior, or is integral to any opaque surface of the building envelope”. Typically, for commercial structures, this is an insulation layer of 1 to 4in. thick, depending on the climate zone, rigid insulation applied to the exterior of the wall studs. Thus, a continuous thermal bridging structural member passing through both planes of insulation, does not meet the insulation requirements of ASHRAE 90.1.

A study by Morrison Hershfield [25] identified that point transmittances due to steel beams penetrating the thermal envelope can have a significant impact on the thermal resistance of a wall. Simulations revealed that that one beam penetration (HSS 3x3x1/8) on a wall 10 ft. tall and 10 ft. wide causes a 9 % increase in overall thermal transmittance, 17 % for two beams placed horizontally, 25 % for three and so on. This study included a variety of other linear detailing scenarios and provided thermal transmittance values for each. A subsequent investigation by Morrison Hershfield in 2014 [27] expanded on the already extensive catalogue of common construction details adding a number of structural beam point transmittance details. The simulated construction details included a structural beam penetrating a clear wall, and several thermally-broken structural steel beam connections.

### 2.2.2 Calculating thermal bridging transmittances

Current North American practices use the area-weighted approach to calculate U-values or effective R-values of wall assemblies and construction details. While this method is simple and effective when dealing with plane wall areas, it becomes burdensome to apply effective areas to complex three-dimensional thermal bridges. A more appropriate method, the method of utilizing linear and point transmittances, is becoming the recognized method for quantifying all thermal anomalies [28]. The concept of linear and point transmittances is based on European literature and standards [29], and has only recently gained attention in North American energy codes.

The method of utilizing linear and point transmittances is relatively straightforward. The heat flow through an area of the building envelope with a thermal bridge is compared to the same area without the thermal anomaly, the clear wall. The difference in the magnitude in heat flow is the heat flow that can be attributed to the effect that the thermal bridge has on the clear wall [28]. The sum of the heat flow added due to the thermal bridges is added to the clear wall U-value to determine the overall thermal transmittance of the building. Linear ( $\Psi$ ) and point ( $\chi$ ) transmittance values are determined using the following equations:

$$\psi = \frac{Q - Q_0}{L} = (U - U_0) \cdot \frac{A_{total}}{L} \quad (\text{Eq. 2-1})$$

$$\chi = Q - Q_0 = (U - U_0) \cdot A_{total} \quad (\text{Eq. 2-2})$$

where  $Q$  is the heat flow through the area of the clear wall with the thermal bridge,  $Q_0$  is the heat flow through the area of the clear wall without the thermal bridge,  $U$  is the respective U-value for the area  $A_{total}$ , and  $U_0$  is the respective U-value for the representative area.

The total heat loss in a building is the sum of the heat loss due to the clear field and the heat loss due to the anomalies, as follows:

$$\frac{Q}{\Delta T} = \frac{U_0}{A_{total}} + \sum (\Psi \cdot L) + \sum (\chi \cdot n) \quad (\text{Eq. 2-3})$$

where  $\Delta T$  is the temperature difference across the clear wall,  $L$  is the length of the linear thermal bridge for the respective  $\Psi$ -value, and  $n$  is the number of point transmittances for the respective  $\chi$ -value. In this study, the results for  $\chi$ -value value are presented and used interchangeably with the term heat flow rate.

### 2.2.3 Structural steel thermal break strategies for point penetrations

A thermal break is a construction material or engineering method applied to a building detail in order to reduce or eliminate a thermal bridge. A common solution to thermal bridging is to replace the highly conductive steel element with a material that has a lesser conductivity such as wood, vinyl, or fiberglass. This method is common with façade features, such as insulation panel supports, door and window frames, and utility connections, but in cases where the thermal bridge consists of a load-bearing structural element, reducing or eliminating the thermal bridge requires additional engineering consideration. As noted, a common solution has been to use a low-conductivity pad material such as wood or fiberglass to split the structural element in the plane of the thermal envelope [2].

In a survey of structural engineering practices regarding thermal bridges (see Appendix A) in 2014, respondents indicated that most thermal bridging detailing situations involving steel are cantilever beams and floors, façade elements, and roof penetrations. The most common thermal break strategy for structural steel thermal bridges employed by structural engineers surveyed is to surround the protruding steel member with insulation, followed by using a pad

material placed between two steel bearing plates and bolted together. Of the most common materials placed as a break in a steel connection, neoprene stands out, followed by wood and high-density polyethylene.

Manufactured structural thermal break assemblies (MSTBAs) have been used for a number of years, but have relatively recently gained popularity in the United States with the introduction of new guidance on thermal bridging in ASHRAE 90.1 [1] and a forward push by industry to confront the negative effects of thermal bridging. A typical MSTBA configuration consists of a low-conductivity material placed between the faying surfaces of an end-plate moment-resisting beam-to-beam or beam-to-column connection. In general, MSTBAs are made from fiber-reinforced polymer (FRP) or other thermoset-based composites.

#### 2.2.4 Condensation considerations

Condensation of water vapor from the indoor air will occur on a surface that is below the dew point temperature. To evaluate the potential for condensation on interior surfaces of thermal bridging details across the thermal envelope, a temperature index is determined for each model using the following equation as defined by EN ISO 10211:

$$TI = \frac{T_s - T_o}{T_i - T_o} \quad (\text{Eq. 2-4})$$

Where  $TI$  is the temperature index, or factor as its sometimes referred to,  $T_s$  is the coldest indoor surface temperature,  $T_i$  is the inside air temperature, and  $T_o$  is the outside air temperature.

The coldest indoor surface temperature is determined from the results of a numerical analysis. There are limitations, however, to the use of the temperature index. The temperature factors determined in this study are due to average steady-state conductive heat flow. The actual surface temperatures are affected by several factors (localized geometry conditions, air transport, moisture variations, etc.) which directly influence the resulting temperature factor. Temperature factors provided by this project are used only to illustrate the variation in the temperature factor depending on the condition of the thermal break.



The temperature index is a dimensionless ratio that remains stable regardless of the temperature difference between the outside and inside air [30]. Some European countries have codified lower limits on the temperature index to ensure that condensation is avoided [32]. Although ASHRAE has not yet codified limits to the temperature factor, it has been suggested that 0.7 is an appropriate lower limit based on an interior temperature of 68°F and a relative humidity of 50 % [30], [33]. The lower limit that will actually cause condensation, however, is a function of the dew point temperature, which is controlled by both the temperature and relative humidity of the air space.

## **2.3 Mechanical Performance**

### **2.3.1 Thermal bridging and breaks in point penetrations**

Thermally broken steel connections, low-conductivity material placed as an intermediate layer between connecting steel surfaces, with relatively thick bearing pads have been shown to be effective [27]. However, thin pads have been proven to be ineffective, and may worsen the total heat flow compared to a continuous beam [3], [27]. Additionally, steel bolts in the connection used to clamp the end-plates together act as a thermal bridge, effectively reducing the benefit of the thermal break connection for thin pads. The increased demand for high-performance green buildings and tighter building envelopes has prodded the emergence of proprietary thermal break materials and assemblies. Manufactured structural thermal break assemblies (MSTBA) are proprietary products that are similar in nature to a thermal break pad, but feature high-strength connecting elements and have the capacity to transfer axial, shear, and bending stresses [3]. Similar to a thermal break pad, MSTBAs feature a low thermal conductivity and are designed to be installed in the splice of a structural steel beam or column located in the plane of the building envelope. MSTBAs are an attractive option to structural engineers, since the structural design, testing, and research is performed by the manufacturer with the designer only having to specify the applied load, and the manufacturer's engineer specifies and provides the appropriate sized thermal break.

### 2.3.2 Structural considerations

As noted, there is currently no North American structural engineering governance or recommendations to the use of intermediate elastomeric bearing pads in structural steel connections. In fact, quite the opposite is true, the inclusion of non-steel elements between the faying surfaces of steel connections is prohibited. This prohibition can be found in the Research Council on Structural Connection (RCSC) Specification for Structural Joints Using High-Strength Bolts [4] (Section 3.1, p. 16.2-17). It has been suggested that this prohibition stems from the Kemper Arena collapse in 1979 in Kansas City, Missouri where a 1/4-in. thick Micarta plate was used in a critical joint as an insulator to prevent condensation. However, the RCSC prohibition on non-steel materials in steel connections pre-dates the design and construction of the arena. The report on the collapse identified the cause as the failure of two high-strength bolts due to fatigue and repeated loading [34]. It was suggested that the Micarta plate could have been a contributor to the bolt failure, but no further research or investigations were conducted to explore that possibility.

Despite the RCSC specification, one of the most popular thermal break strategies is to place a low-conductivity bearing pad in an end-plate moment connection. End-plate moment connections have become the most widely used moment connection in the construction of metal building and steel portal frame due to ease of fabrication and erection [35]. Bolted end-plates have been studied extensively, with design guidance proffered for many common types of end-plate configurations. Of note, AISC Design Guide 16 [35] and AISC Design Guide 4 [36] combined the research efforts of Murray [37], Sumner [38], Borgsmiller [39], among many others, to develop cumulative design guidance on flush and extended end-plate moment connection of various configurations. Although simple in construction and assembly, the mechanical behavior of bolted end-plates is influenced by many parameters, such as bolt positions, spacing, end-plate and column dimensions, pretension in the bolts, and properties of the steel. An understanding of the behavior of these connections has been developed using experimental tests, finite-element simulations, and analytical approaches [35], [40], [41]. Since the behavior of end-plate connections has been extensively researched and is relatively well understood, the next logical step is to experimentally and analytically develop knowledge on these connections with the inclusion of a non-steel intermediate bearing pad.

In a practical sense, a rigid moment connection with an intermediate bearing pad is similar to a semi-rigid moment connection, due to the relatively low stiffness of the pad which provides additional rotation under compression loads. In conventional steel frame analysis, steel connections are idealized as either rigid or pinned, whereas the actual behavior lies between the two extremities, deemed semi-rigid. In analysis and design of steel frames, moment connections are generally divided into two categories; fully-restrained and partially-restrained. Fully restrained connections assume that the connections are rigid and the original angle between connecting members remains unchanged under load. Partially-restrained, or semi-rigid, connections are classified as connections that don't meet the criteria of a rigid nor a pinned joint. AISC groups these connections into Type 1, Type 2, and Type 3 as fully-restrained, simple shear, and partially-restrained, respectively. Some research has been performed in the field of semi-rigid end-plate connections and there exists a broad field of knowledge related to analyzing their behavior using experimental, analytical, and numerical methods [42]–[44].

The analysis of the behavior of semi-rigid connections has historically been an exclusively academic pursuit, as the majority of constructed connections are prescriptively designed according to common practices and design guide procedures. However, the expansion of seismic code requirements and broad availability of software programs capable of analyzing complex connection behaviors has spurred the efforts of researchers to refine the understanding of the behavior of semi-rigid connections so as to utilize their high ductility in seismic-resisting steel frame analyses. A review on semi-rigid joint behavior in steel frames was performed by Daz et. al. [45] in 2011. This review presented a comprehensive and detailed accounting of nearly 180 publications on the experimental, analytical, and numerical research methods and results of semi-rigid joint behavior. A brief review of research efforts and results that co-align with this study are presented here.

Although prohibited by AISC, elastomeric bearing pads, such as neoprene or FRP, in structural steel connections are commonly used. Reasons for which include thermal breaks, seismic isolators, and vibration dampeners. Rubber and neoprene elastomeric bearing pads are often used as bridge bearing pads to accommodate changes in length of the bridge deck without transmitting excessive lateral forces to the bridge supports [46]. The majority of research into elastomeric pads has been performed by bridge engineering groups seeking to determine the

compression, shear, and long-term mechanical properties of reinforced neoprene and rubber bearing pads [47]–[51]. Plain pads, steel-reinforced, and cotton duck elastomeric bearing pads are the most commonly used bearing pad types. Glass fiber reinforced polymer (FRP) bearing pads are similar to reinforced bearings, but due to the sudden failure characteristics of the fiberglass, the compressive stresses are limited, and are not very popular in bridge bearing pad design [52]. Plain elastomeric bearing pads rely upon friction at the contact surfaces to resist bulging. Local slip resulting from friction loss leads to increased strain, thus limiting the load carrying capacity of the bearing. The allowable stress is a function of the shape factor so plain pads must be relatively thin to carry the maximum compressive load, and therefore can accommodate only small horizontal translations and rotations [52].

Although a significant amount of research has been performed on the behavior of elastomeric bearing pads for use in bridge bearing applications, very little research or guidance has been put forth to determine and quantify the behavior of structural steel frame connections with elastomeric pads. Common practices suggest that typical uses for elastomeric bearing pads in buildings are not for structurally critical connection, but rather low-load applications, such as support members for rooftop mechanical equipment and façade support elements. The main advantage of an elastomeric pad is its relatively high load-bearing capacity and resistance to compressive stresses. The high strength, stiffness, and durability of elastomeric bearing pads allows their use in a variety of loading conditions such as bridge-bearings, base isolations, and expansion joints. The use of elastomeric pads in structural applications such as beam-to-column joints and end-plate connections is very attractive for the aforementioned reasons, including thermal breaks.

Application of elastomeric bearing pads as seismic dampeners has been investigated by a few researchers, notably Lee et. al. who investigated the use of hyperelastic high dampening materials in reinforced concrete frame buildings [53]. A significant amount of research has also been performed towards the goal of defining a hyperelastic elastomeric material model for use in numerical modeling [54], [55]. However, the complexity of the material and variety of elastomeric formulations makes it difficult to develop design guidance that can be applied to all elastomeric bearing pad and end-plate configurations. To that effect, there have been a few

attempts at investigating the behavior of such connections, and to develop a few basic design rules using guidance from elastomeric bridge bearings literature.

Milani and Milani [56] experimental and numerically investigated the behavior of elastomeric seismic isolators undergoing large deformations. Using test data on several different rubber and neoprene compounds, they applied the Mooney-Rivlin and exponential hyperelastic models to fit the data. Applying the hyperelastic model to a finite element material definition, they investigated the global behavior of a seismic steel-reinforced isolator under compression and shear loads. It was concluded that neoprene had sufficient stiffness and was well suited for use as an elastomeric bearing.

Cleary and Riddell [57] carried out moment-rotation tests of the Armatherm thermal barrier plates under monotonic loading. The Armatherm thermal barrier is a proprietary fiber-reinforced resin material. They concluded that under loading conditions that reached the elastic limit of the beam under bending, the connection with the thermal barrier and without the thermal barrier exhibited comparable stiffness. At further stress levels, the thermal barrier exhibited non-linear behavior that resulted in permanent plastic deformation. Shear [58] and compression [59] tests were also performed on the connection. Results of the shear tests showed that the slope of the shear-displacement curve is reduced, as well as the friction coefficient compared to a connection with no thermal break. Time-dependent compression tests showed clamping loss in the bolts.

Nasdala et. al. [60] developed an analytical design concept for an end-plate connection with a proprietary elastomeric bearing pad and validated their design equations using finite element analysis. They determined that the most significant stresses in the pad material under load is between the bolts due to the bulging of the material out from the sides. They found that friction conditions between the elastomer and the steel have a large influence on the load bearing capacity of the connection. Creep processes were also explored and it was determined that the rotational stiffness of the connection is decreased if creep deflection is considered. This study only investigated and formulated an analytical model for flush end-plate connection, and they suggested the use of extended end-plates to increase the load-bearing capacity.

Šulcová et. al. [61] performed compression and bending tests on the plastic material Erthacetal H. The influence of different thicknesses of the plastic and the steel end-plate was

explored. Empirical equations relating the width of the compression area to an effective width were developed. It was found that creep and temperature had a significant influence on the resulting rotation of the joint. This study, however, lacked any realizations to the behavior of end-plate connections with elastomeric bearing pads nor presented any results to the mentioned full-scale end-plate connection test.

The results reviewed indicate that the complexity of the end-plate behavior coupled with the complexity of the pad material behavior provides a significant challenge for researchers. Due to the complexity of the material behavior, variety of materials, and lack of design rules, there exists a need to further research into structural steel moment connection that include non-steel materials.

## **Chapter 3: Method**

The methodology of this study was to survey the structural engineering industry on structural steel thermal bridging and thermal break practices, experimentally test thermal bridge and thermal break specimens using a calibrated hot box, experimentally test thermally-broken end-plate moment connection under cantilever bending and shear, and utilize the experimental data to calibrate and analyze the thermal and mechanical performance of thermal-break details using finite-element models.

### **3.1 Industry Survey of Thermal Break Practices**

In 2014, the authors initiated a survey of structural engineering practices regarding thermal breaks and thermal bridges in structural steel construction. This survey collected information via an online survey and in-person interviews of structural engineering and architecture firms in the Anchorage, Alaska area. The online survey was distributed to members of the AISC mailing list via email on May 14, 2014.

The body of the email was written as follows:

“Engineers and Architects:

Thermal efficiency and performance are important aspects to the design of steel buildings, particularly as we strive to design more sustainable structures. Steel members that penetrate the building envelope act as thermal bridges, channeling heat into or out of the building, and it can be a significant problem to the building’s thermal performance. Dr. Scott Hamel of University Alaska at Anchorage is currently conducting a research investigation sponsored by AISC on steel connection details that provide adequate thermal breaks in the building envelope. We would like your help in completing a short survey to gather information on how engineers and architects currently address the thermal bridging issue when it is encountered in practice. The results of the survey will be consolidated into a report and made publicly available. The short survey can be completed at the following link:”

The structural engineering and architecture firms that were interviewed in the Anchorage, Alaska area were Kumin Associates Inc (A), Livingston Slone Inc (A), PND Engineers Inc (E), PDC Engineers Inc (E), R&M Engineering (E), Reid Middleton (E), URS Corporation (AE), and USKH Inc (AE), (A = Architecture, E = Engineering, AE = Architecture and Engineering). The objective of the surveys and interviews was to determine the current methods that structural engineers in the U.S. use to deal with thermal bridges in structural steel frames and how they apply thermal breaks into their designs. The authors also sought to qualitatively determine how common thermal breaks were used in structural steel construction and what materials are used.

The survey questions and detailed responses can be found in Appendix A.

### **3.2 Calibrated Hot-Box Testing**

The calibrated hot box method is designed to maintain a constant temperature difference across the test specimen long enough to allow the heat flow to reach steady-state. The temperature difference between the metering chamber and the climatic chamber drives a heat flow across the test specimen. By measuring the total energy entering the metering chamber, and accounting for the measured extraneous heat flows out of the metering chamber, the heat flow across the test specimen can be determined.

#### **3.2.1 Description of Calibrated Hot Box**

Figure 3-1 shows the cross-sectional schematic of the hot box system. The system consists of four main components: metering chamber, surround panel, test specimen, and climate chamber. Figure 3-2 shows an image of the constructed hot box.

##### ***3.2.1.1 Metering chamber***

The metering chamber has inside dimensions of 40 in. (height) x 40 in. (width) x 31 in. (depth). The walls are 6 in. thick extruded polystyrene (XPS) board (FOAMULAR 250, Owens Corning) with a 7/16 in. oriented strand board (OSB) exterior skin. No paints or coatings were applied to the exterior or interior of the metering chamber. Adjoining walls were sealed together using adhesive (PL300 Foamboard Adhesive, Loctite) and the inside corners were sealed with a ½in bead of insulating spray foam (Great Stuff Pro – Gaps & Cracks, DOW Chemical Company).



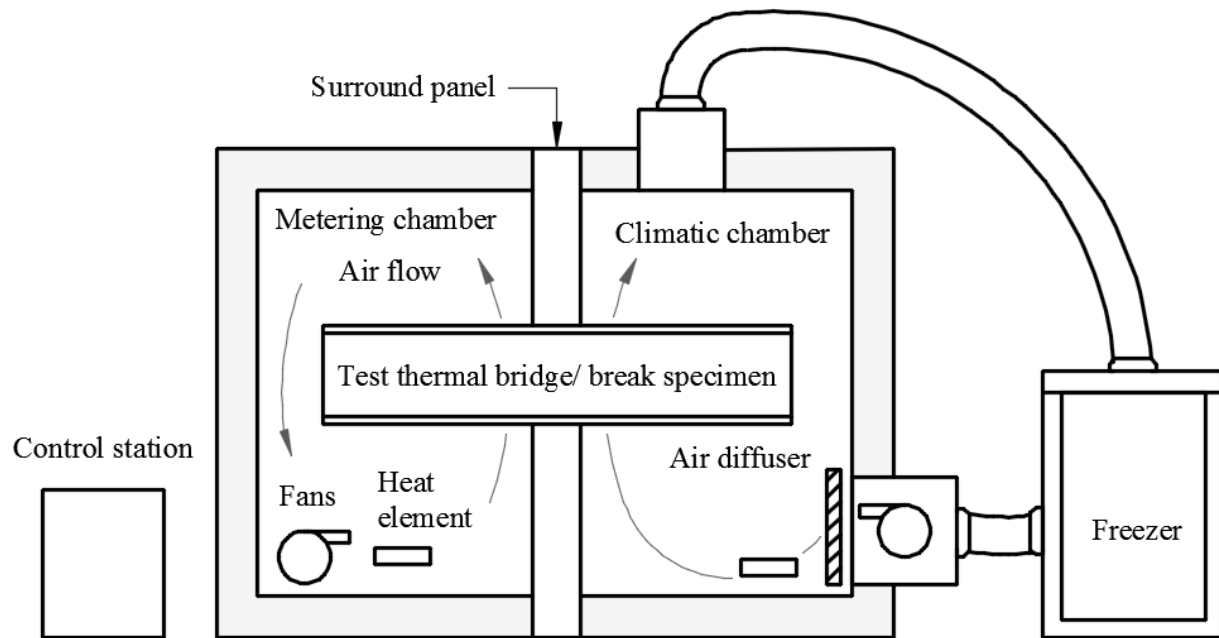


Figure 3-1: Schematic cross section of the constructed hot box



Figure 3-2: Constructed calibrated hot box

Temperature sensors were attached to the five interior faces of the chamber to monitor the interior surface temperatures of the walls. A sixth temperature sensor was hung 12 in. below the ceiling of the metering chamber to monitor and control the metering chamber air temperature. An additional 6 temperature sensors with extended leads were placed inside the metering chamber for the purpose of attaching to the specimen. The temperature sensors were LM34 Precision Fahrenheit Temperature Sensors (LM34CAZ, Texas Instruments) with a typical accuracy of  $\pm 0.5$  °F and self-heating of less than 0.2 °F in still air. The temperature sensors were powered by 5.0 V and used approximately 90 $\mu$ A each. The LM34 outputs a linearized voltage of 10.0 mV/°F. Each sensor's output was verified using a multi-point calibration in a stirred oil bath at the expected operating temperature range using a known and calibrated thermometer (Fluke 54 II B Digital Thermometer, Fluke).

The analog temperature readings were collected using a Labjack T7, a multifunction data-acquisition device (Labjack T7, Labjack Corporation) through a single multiplexer (Labjack MUX80, Labjack Corporation). The Labjack's T7s 22-bit effective resolution analog to digital converter (ADC) was utilized to acquire all analog readings.

Two DC-powered fans were placed at the bottom of the metering chamber against the rear wall in order to prevent thermal stratification. The voltage and current powering the fans was measured using their DC power supply (Agilent 3616A, HP Agilent) and maintained at a constant level for all test and calibration runs.

Energy input to the metering chamber was achieved using a DC-powered 4in wide by 24in long carbon fiber heating fabric spanning the width of the chamber. The heater was powered by a linear DC power supply (Agilent 6010A, HP Agilent). The voltage output was fine-tuned by a software proportional-integral-differential (PID) controller. Programming of the data collection and heater output was achieved using LabVIEW (NI LabVIEW, National Instruments). Power input to the metering chamber was measured by means of a scaled analog voltage output of the voltage and current from the dedicated DC power supply. The scaled product of the output voltage and output current resulted in apparent resolution steps, the error of which is calculated in Section 3.2.2 .

The design air temperature in the metering chamber was between 65 °F and 80 °F. The design air temperature in the climatic chamber was between 20 °F and the metering chamber

temperature. Since no active cooling was constructed for the metering chamber, heat loss from the metering chamber is only possible through the surround panel and/ or specimen and the metering chamber walls. As such, a greater time was required for the metering chamber to return to the set temperature. Figure 3-3 shows an example of a test run for set temperatures of 80 °F and 30 °F, metering chamber and climate chamber, respectively. It can be seen that temperature stability is reached within nine hours. Temperature and power data is collected for the entire 24-hour period. Excellent temperature stability of less than  $\pm 0.025$  °F was achieved in both the metering chamber and the climatic chamber, as shown in Figure 3-4.

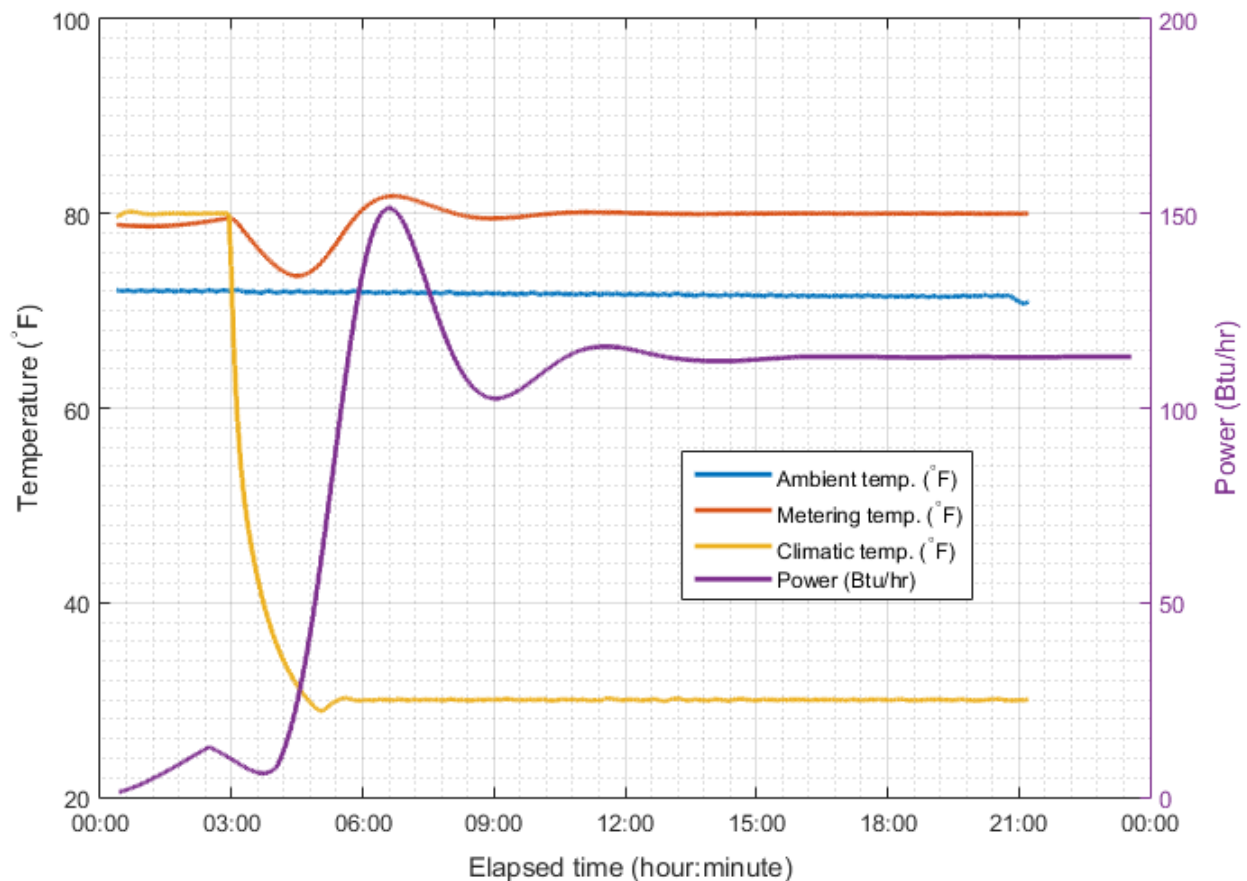


Figure 3-3: Example air temperatures for an entire run period (24-hr)

### 3.2.1.2 Climate chamber

The climate chamber was identical to the metering chamber in its construction and temperature sensor arrangement. A single in-line duct fan with an air diffuser was placed at the bottom rear of the climatic chamber and attached to an insulated duct from the 5 cubic foot exterior freezers. Temperature stability in the climatic chamber was achieved using a heating element placed directly in front of the air diffuser. The heating element was powered by three DC power supplies operated in series in order to produce the necessary current output (200V/17A Agilent 3616A, HP Agilent). The heater output was fined-tuned by a software PID controller in the same manner as the PID control for the metering chamber.

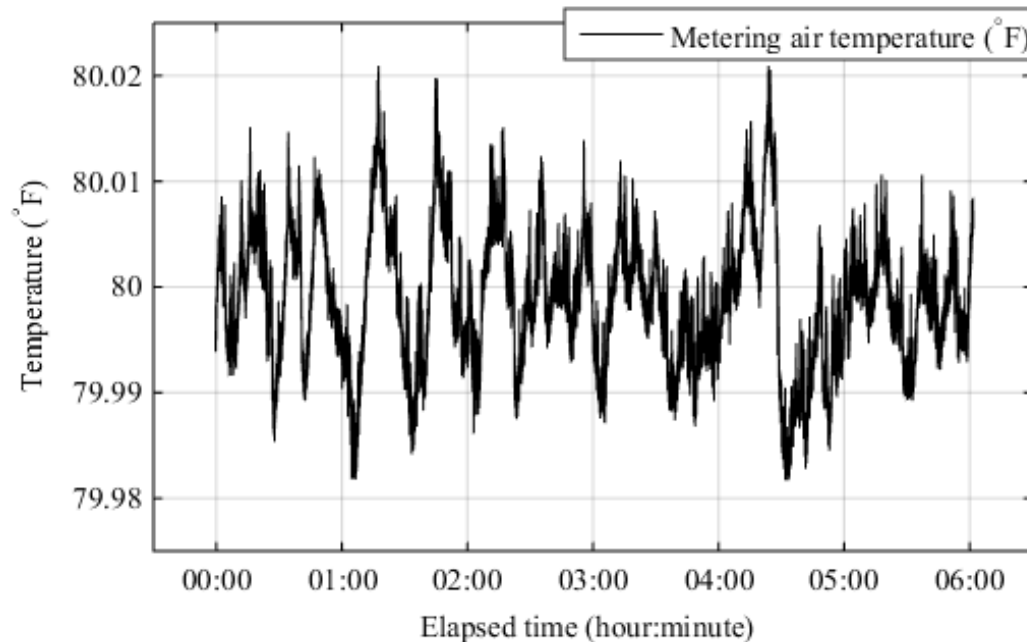


Figure 3-4: Air temperature in the metering chamber at steady-state (18:00-24:00).

### 3.2.1.3 Surround panel

The surround panel was a 2 in. thick XPS rigid insulation panel (FOAMULAR 250, Owens Corning). The perimeter joints between the surround panel and the metering chamber and climatic chamber were sealed using 0.25 in. thick compressible foam (Foam Seal-R, Owens Corning). The surround panel was clamped between the metering chamber and climate chamber

using bar clamps ensuring an airtight seal. Additionally, at the initiation of each test run, the joint perimeter was sealed by tape to ensure air-tightness.

### 3.2.2 Calibration of Hot Box

Calibration of a hot box is necessary to accurately obtain the net heat transfer through the test specimen. At steady state, the time rate of heat flow through the specimen,  $Q_s$ , is determined from the heat balance:

$$Q_s = Q_h + Q_f - Q_{mw} - Q_{fl} \quad (\text{Eq. 3-1})$$

where  $Q_h$  is the heat added by the heater,  $Q_f$  is the heat added due to the fans,  $Q_{mw}$  is heat flow of the metering chamber to ambient air, and  $Q_{fl}$  is the flanking heat loss. Figure 3-5 shows the heat flow balance in the metering chamber.

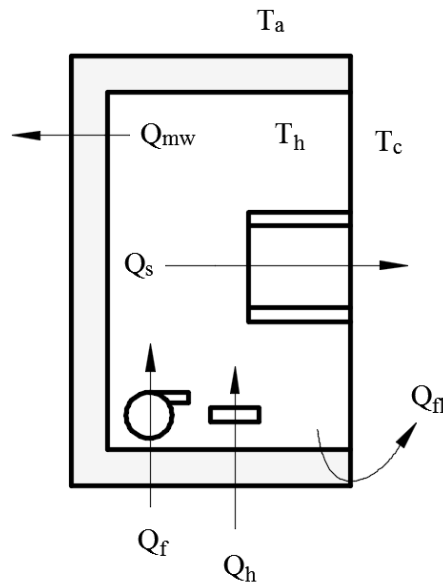


Figure 3-5: Heat flow balance in the metering chamber

#### *3.2.2.1 Metering Chamber Wall Loss*

In order to determine the metering chamber wall loss,  $Q_{mw}$ , a characterization panel (2 in. thick FOAMULAR 250 XPS rigid insulation), identical to the surround panel used in all test

runs, but without a penetration hole, was placed between the metering chamber and the climate chamber. The air temperature was maintained equal in the metering chamber and the climate chamber, so that the heat flow through the characterization panel was negligible, and flanking loss could be ignored; since at equal temperature negligible heat flow exists between the two chambers. At steady-state the heat flow through the metering chamber becomes:

$$Q_{mw} = Q_h + Q_f \quad (\text{Eq. 3-2})$$

For a calibrated hot chamber, standardized metering wall loss calibration procedures recommend three calibration tests, with the metering chamber air temperature higher than, equal to, and lower than the ambient air temperature. Since the metering chamber does not have the capability to perform cooling, three tests were performed with the metering chamber temperature at 5 °F, 10 °F, and 15 °F above the ambient temperature. A linear relation was fit to the data to obtain:

$$Q_{mw} = 1.58(T_h - T_a) [\pm 0.05] \frac{\text{Btu}}{\text{hr} \cdot ^\circ\text{F}} - 0.1 [\pm 0.5] \frac{\text{Btu}}{\text{hr}} \quad (\text{Eq. 3-3})$$

ASTM C1363 recommends that the metering chamber wall loss be kept under 10% of the net heat flow through the specimen in order to reduce its contributing uncertainty. Under the greatest temperature difference between ambient temperature and metering box temperature, metering chamber wall losses for the constructed hot box were below 15% of the total heat flow through the specimen.

### 3.2.2.2 Flanking Loss

Due to the nature of the determination of point transmittance values, the flanking losses can be neglected using this hot box method for the purposes of testing thermal breaks/ bridges to determine the  $\chi$ -value, provided that the surround panel configuration remains the same. The point transmittance value,  $\chi$ , is determined using the difference between heat flow in the clear wall assembly and the clear wall assembly with the inclusion of the thermal bridge. The manner in which a thermal break/ bridge is tested using this hot box precludes the necessity for determining the flanking loss, since the surround panel is identical to the characterization panel and the test specimen flanking loss is considered to be a part of the point transmittance value.

However, it is necessary for the thermal break/ bridge to maintain a certain separation distance from the area of the greatest heat flow and the edges of the metering chamber in order to prevent heat flow interaction between different mechanisms, that is, to minimize boundary condition effects. The flanking loss interface and interaction for the hot box and test arrangement described herein is shown in Figure 3-6.

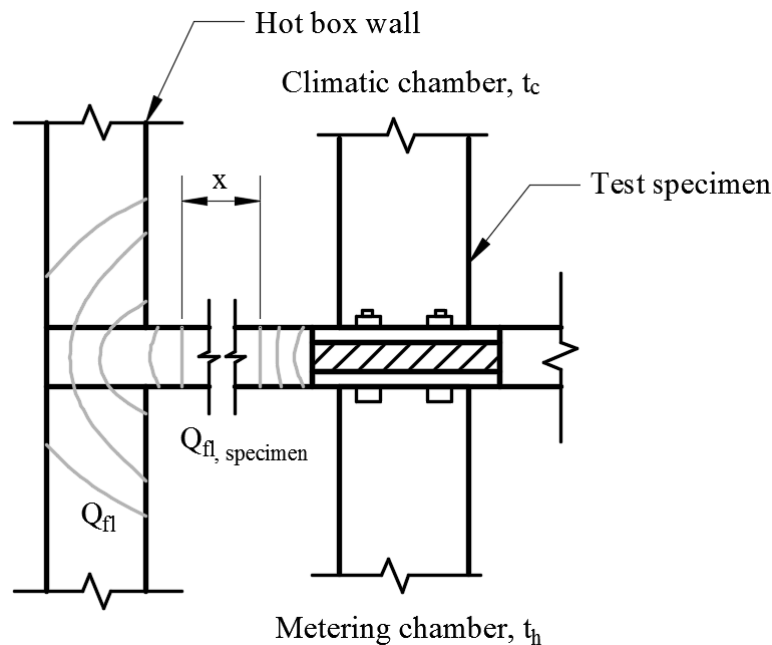


Figure 3-6: Flanking loss for the calibrated hot box

The determination of the surround panel flanking loss is necessary when the clear wall field assembly heat flow is also desired, or when testing specimens with different hot boxes, because of the uncertainties inherent between testing institutions [21]. The flanking loss for the specific surround panel (2in thick XPS rigid insulation) used for all test and calibration runs was determined using finite element analysis and compared to the value determined experimentally during the metering chamber wall loss calibration. It was determined that because the ambient lab temperature and the temperature difference across the test specimen were held constant and identical for all calibration and test runs, the flanking loss can be considered a constant. Though the flanking losses were found to be a small percentage of the total heat flow (between 2.2% to 3.5% depending on the test conditions), neglecting their contribution would result in large

percent error when comparing the test specimen heat flow results between different surround panel configurations.

### 3.2.2.3 Surround Panel

The surround panel is used in this calibrated hot box to represent the insulated layer of the building envelope in a thermal bridging/ break configuration (i.e., the clear field). It is necessary to determine the heat flow through the surround panel in order to apply the acquired value to the equation for determining the chi value of the thermal bridge and/ or thermal break. The surround panel's heat flow was measured and compared against the value specified by the manufacturer's product data sheet. The results are reported in Table 3-1.

Table 3-1: Comparison of thermal conductivity values obtained for the characterization panel

| Sample               | Hot box<br>Btu·in/(hr·ft <sup>2</sup> ·°F) | Literature Btu·in/(hr·ft <sup>2</sup> ·°F) |
|----------------------|--|--|
| XPS rigid insulation | 0.197 ± 0.011                              | 0.20                                       |

It is important to maintain relatively fixed temperature and airflow conditions for all calibrations and test runs. Most of the parameters, with the exception of the ambient laboratory temperature, were maintained with no measurable variation between calibrations and test runs.

### 3.2.2.4 Surface Film Coefficients

The determination of surface film coefficient values on the metering and climatic side was loosely based on the procedure described in ASTM C1199 [18]. The surface film coefficient is calculated as the heat flow through a specimen divided by the difference in the surface and air temperature for each side, per unit area. The test configuration used to determine the thermal transmittance of the surround panel was also used for this test. Temperature sensors were affixed to both faces of the surround panel at points shown in Figure 3-7.

The metering chamber and climatic chamber heat transfer coefficients are calculated as follows:

$$h_h = \frac{Q_s}{A_s(t_h - t_{h,s})} \quad (\text{Eq. 3-4})$$



where  $h_h$  is the surface film coefficient,  $Q_s$  is the heat flow through the specimen,  $A_s$  is the total heat flow surface area, and  $t_h$  and  $t_{h,s}$  are the air temperature and the area averaged surface temperatures, respectively. ASHRAE provides values for typical ranges for the combined exterior and interior surface film coefficients and resistances [62], which are also specified by ASTM C1199 [18]. The resulting surface film coefficient values are specified in Table 3-2 along with ASHRAE typical values.

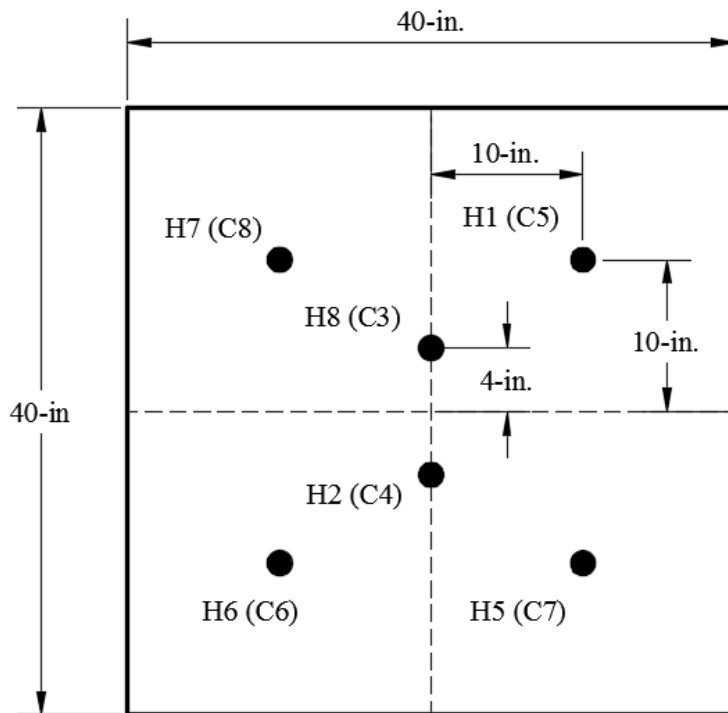


Figure 3-7: Surround panel temperature characterization sensor locations

Table 3-2: Surface heat transfer coefficient values for surround panel

|  | <b>Heat transfer<br/>coefficient<br/>Btu/hr·ft<sup>2</sup>·°F</b> | <b>ASHRAE values<br/>(Ch. 26, Table 10)<br/>Btu/hr·ft<sup>2</sup>·°F</b> |
|--|---|--|
| <b>Metering chamber side, <math>h_h</math></b> | 2.53  | 1.29 to 1.41   |
| <b>Climatic chamber side, <math>h_c</math></b> | 3.40  | 5.12 to 5.64   |

No attempt was made to straighten airflow and control across the specimen, since the protrusion of the beam would interfere with any attempt to provide a uniform omnidirectional airflow. As such, the air velocity was adjusted to provide a relatively reasonable (in terms of building envelope conditions and temperatures) value for the overall surface film coefficient. However, in situations where a large percentage of the overall thermal resistance is the surface film coefficient, as is the case in a thermal bridge/ break where the steel beam acts as a large heat sink/source, it can be especially challenging to determine an overall surface film coefficient. The difficulty lies in measuring the airflow on every surface of the thermal bridging specimen. Because the design heat transfer coefficient is coupled with the convective and radiative heat transfer coefficient, the temperature along the specimen can affect the resulting heat transfer coefficient. As such, determination of an accurate heat transfer coefficient comes with a significant experimental resource cost.

### 3.2.3 Uncertainty analysis

It is impractical to estimate the uncertainty of a measurement using this hot box by means of statistical sampling. Therefore, the uncertainty of experimental measurement using this hot box was estimated by the law of propagation of errors based on the root-sum square formula and the methods outlined by Yuan et. al. [63], [64]. The measured value of thermal transmittance of a test specimen using this hot box, and its uncertainty, must be combined with the overall uncertainty of the elements associated with the hot box itself. The net heat transfer through a test specimen is:

$$Q_s = Q_h + Q_f - Q_{mw} - Q_{fl} \quad (\text{Eq. 3-5})$$

The individual uncertainty for each term in the equation must be estimated, resulting in the following equation for the absolute uncertainty for the net heat transfer through the specimen:

$$\Delta Q_s = \sqrt{(\Delta Q_h)^2 + (\Delta Q_f)^2 + (\Delta Q_{mw})^2 + (\Delta Q_{fl})^2} \quad (\text{Eq. 3-6})$$

The uncertainty of the  $Q_h$ , the power input, is obtained from the steady-state voltage and amperage readings, which depend on the accuracy of the power supply and the accuracy of the analog readings. The uncertainty for  $Q_h$  varies with each test, depending on the length of the test

and the temperature difference between the metering chamber and the ambient laboratory temperature. The uncertainty in  $Q_f$  is obtained using the same manner.

The uncertainty for  $Q_{mw}$  requires a few additional steps, since the value for  $Q_{mw}$  is the product of the slope and intercept from the metering chamber wall loss calibration. Therefore, the error in  $Q_h$  and  $Q_f$  must be propagated into the error for  $Q_{mw}$ . The value of  $Q_{mw}$  for each test is calculated using:

$$Q_{mw} = \frac{dQ}{dT}(t_h - t_a) + Q_0 \quad (\text{Eq. 3-7})$$

Where  $dQ/dT$  and  $Q_0$  is the slope and intercept determined by a linear regression of total power input divided by the difference in the metering chamber temperature and ambient laboratory temperature. Both the dependent and independent variable ( $Q_h$  and  $\Delta t_{(h-a)}$ , respectively) in the linear regression have a particular uncertainty. Maximum and minimum slopes were determined using the calculated uncertainties of the first and last calibration values. The uncertainty in the intercept was determined from the resulting slope and the maximum and minimum values. All test and calibration runs were performed with  $(t_h - t_a)$  within the limits of the maximum and minimum values used to determine the gradient uncertainty. Taking into account the uncertainties of each term on the right hand side of Eq. 2-7, the equation for the resulting absolute uncertainty for  $Q_{mw}$  is:

$$\Delta Q_{mw} = \sqrt{\left( (t_h - t_a) \cdot \Delta \frac{dQ}{dT} \right)^2 + \left( \frac{dQ}{dT} \cdot \Delta t_h \right)^2 + \left( \frac{dQ}{dT} \cdot \Delta t_a \right)^2 + (\Delta b)^2} \quad (\text{Eq. 3-8})$$

The overall heat transfer coefficient is typically reported as a per temperature-degree difference per unit area:

$$U = \frac{Q_s}{A_s \cdot (t_h - t_c)} \quad (\text{Eq. 3-9})$$

Therefore, the parameter of dimension and temperature is propagated into the global equation resulting in the following equation for the uncertainty of the overall heat transfer coefficient:

$$\Delta U = \sqrt{\left(\frac{1}{A_s \cdot dt_{(h-c)}} \Delta Q_s\right)^2 + \left(\frac{Q_s}{A_s^2 \cdot dt_{(h-c)}} \Delta A_s\right)^2 + \left(\frac{Q_s}{A_s \cdot dt_{(h-c)}^2} \Delta dt_{(h-c)}\right)^2} \quad (\text{Eq. 3-10})$$

To determine the  $\chi$ -value of the resulting thermal bridge/ break, the difference between the heat flow through the surround panel with no thermal bridge/ break and the heat flow through the surround panel with the thermal bridge/ break:

$$\chi = \frac{Q_{cf} - Q_b}{dt_{(h-c)}} \quad (\text{Eq. 3-11})$$

and the uncertainty is calculated:

$$\Delta \chi = \sqrt{\left(\frac{1}{dt_{(h-c)}} \Delta Q_b\right)^2 + \left(\frac{1}{dt_{(h-c)}} \Delta Q_{cf}\right)^2 + \left(\frac{Q_{cf} - Q_b}{dt_{(h-c)}^2} \Delta dt_{(h-c)}\right)^2} \quad (\text{Eq. 3-12})$$

where  $Q_{cf}$  is the heat flow through the un-broken surround panel, and  $Q_b$  is the heat flow through the surround panel with the inclusion of a thermal break/ bridge. All calculated uncertainty values presented herein are normalized to the 95 % confidence level.

### 3.2.4 Thermal Transmittance Measurement

The purpose of this calibrated hot box was to determine the point transmittance values of structural steel thermal bridge and thermal break configurations. A thermal bridge and a thermal break were tested using the hot box described herein.

#### *3.2.4.1 Continuous Beam*

The thermal bridge consisted of a steel beam passing through an insulated panel. The schematic of the thermal bridge configuration is shown in Figure 3-8. A W10x19 steel beam with a cross sectional area of 5.62 in<sup>2</sup> was tested. The steel beam was received from the steel fabrication shop unpainted and cut to a length of 61in. The surround panel was a 2in thick sheet

of XPS insulation (FOAMULAR 250, Owens Corning) measuring 56in by 56in, identical to the surround panel used in the calibration. The shape of the W10x19 beam was traced in the center of the panel and cut out. The gap between the steel beam and the rigid insulation (approximately 1/8in) was filled with insulating spray foam (Great Stuff Pro – Gaps & Cracks, DOW Chemical Company).

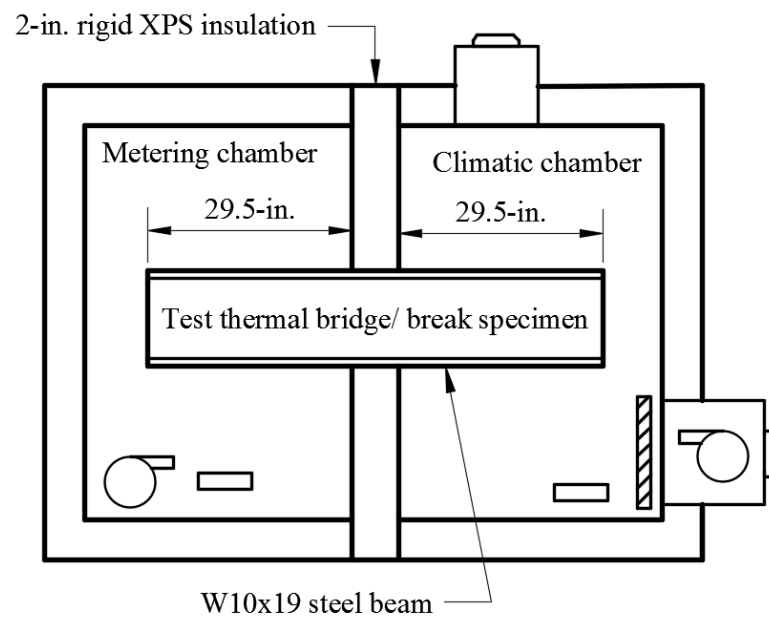


Figure 3-8: Schematic of thermal bridge configuration

Temperature sensors were attached to the beam along the center of the web and the flange in the arrangement shown in Figure 3-9. The temperature sensors were placed flat against the unpainted steel face and fixed fast using masking tape. The beam was supported in the center by the insulated panel and at the ends on 2in by 4in a height measured to position the beam in the center of the box.

The temperature of the metering chamber was held at 80 °F, and the climatic side was brought to 30 °F.

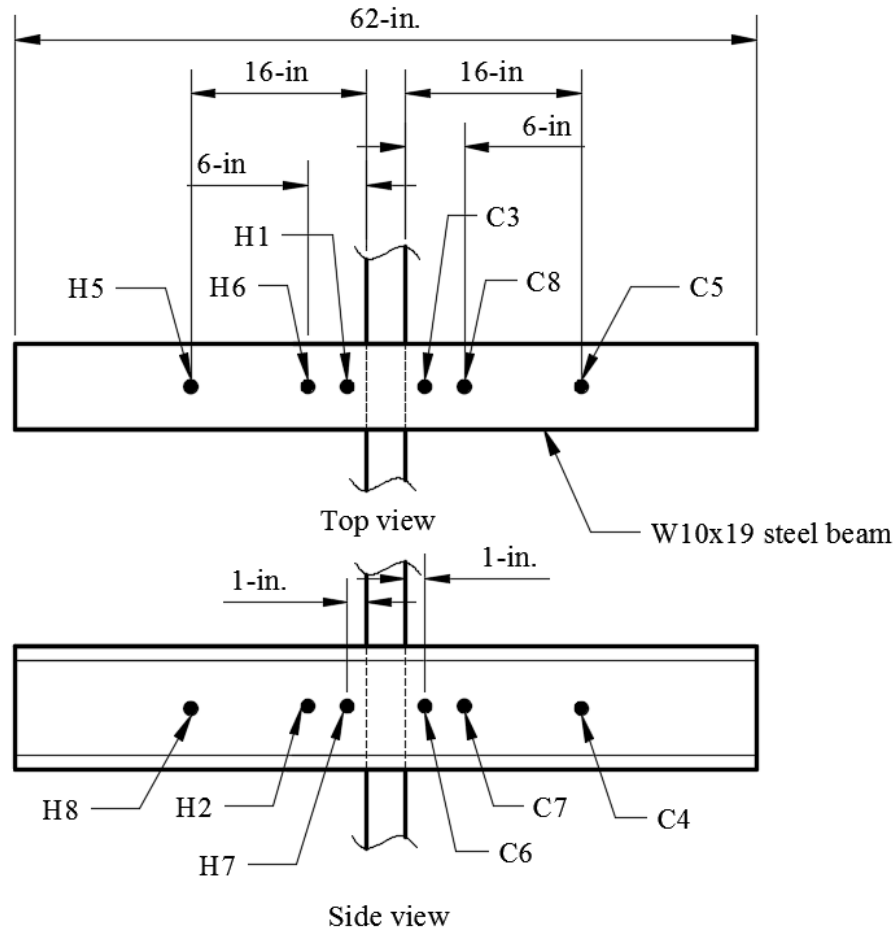


Figure 3-9: Sensor arrangement for the continuous beam thermal bridge

#### 3.2.4.2 Beam-to-Beam Thermal Break Connection

The thermal break connection consisted of various pad materials placed between the faying surfaces of a steel beam-to-beam end-plate connection. The end-plate connection was a doubly-symmetric unstiffened 4-bolt end-plate moment connection that attached to 29.5in long W10x19 steel beams (A992 steel) with 1/2in thick steel end-plates (A572 Gr. 50 steel). The bolt holes were 9/16in diameter and the dimensions of the end-plate measure 4.25in by 14.75in. The end-plate was welded to the beam with a 5/16in nominal weld size all around using an E70XX filler metal. The end plate connection geometry is shown in Figure 3-10.

A variety of different pad materials, thicknesses, and bolt material combinations were tested, as shown in Table 3-3.

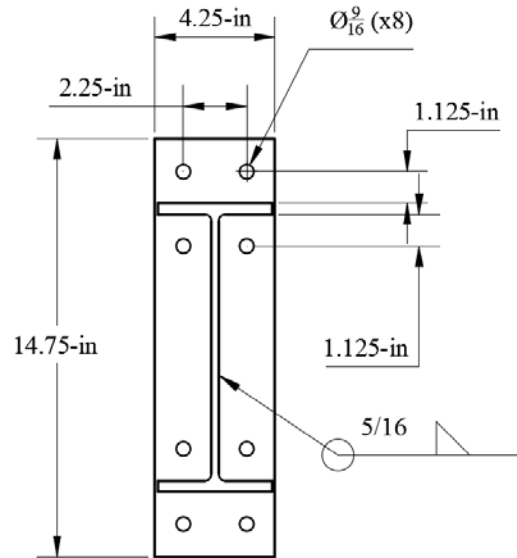


Figure 3-10: End plate connection geometry

Table 3-3: Calibrated Hot-Box Thermal-Break Testing Parameters

| Test #          | Break material | Break thickness (in.) | Bolt material | Description                        |
|-----------------|----------------|-----------------------|---------------|------------------------------------|
| TT-CP           | n/a            | 0                     | n/a           | 2in. XPS rigid insulation          |
| TT-CS           | n/a            | 0                     | n/a           | Continuous beam (W10x19)           |
| TT-00           | None           | 0                     | Steel         | Connection w/ no break             |
| TT-NP-05-ST     | Neoprene       | 0.5                   | Steel         | 0.5in. neoprene break, steel bolts |
| TT-NP-10-ST     | Neoprene       | 1                     | Steel         | 1.0in. neoprene break, steel bolts |
| TT-NP-15-ST     | Neoprene       | 1.5                   | Steel         | 1.5in. neoprene break, steel bolts |
| TT-NP-05-SS     | Neoprene       | 0.5                   | Stainless     | 1.5in. neoprene break, steel bolts |
| TT-NP-10-SS     | Neoprene       | 1                     | Stainless     | 1.5in. neoprene break, steel bolts |
| TT-FR-05-ST     | FRP            | 0.5                   | Steel         | 1.5in. neoprene break, steel bolts |
| TT-FR-10-ST     | FRP            | 1                     | Steel         | 1.5in. neoprene break, steel bolts |
| TT-FR-05-SS     | FRP            | 0.5                   | Stainless     | 1.5in. neoprene break, steel bolts |
| TT-FR-10-SS     | FRP            | 1                     | Stainless     | 1.5in. neoprene break, steel bolts |
| TT-FP-10-SS-INS | FRP            | 1                     | Stainless     | 1.5in. neoprene break, steel bolts |

A shop coating was applied to all exposed surfaces of the beams and end-plates (2-mil Inhibitive Shopcoat Primer 100R7713 Red, Sumter Coatings). Figure 3-11 shows a cross-sectional schematic of the test configuration and the temperature sensor arrangement. Temperature sensors were attached to the steel in the same manner as that of the continuous beam test.

The assembled end-plate connection used eight ½ inch diameter, 2-¾ inch long A325, Type 1 steel bolts with 1/2in diameter A563 Grade C steel nuts. Other thermal break tests used identically-sized stainless-steel bolts and nuts.

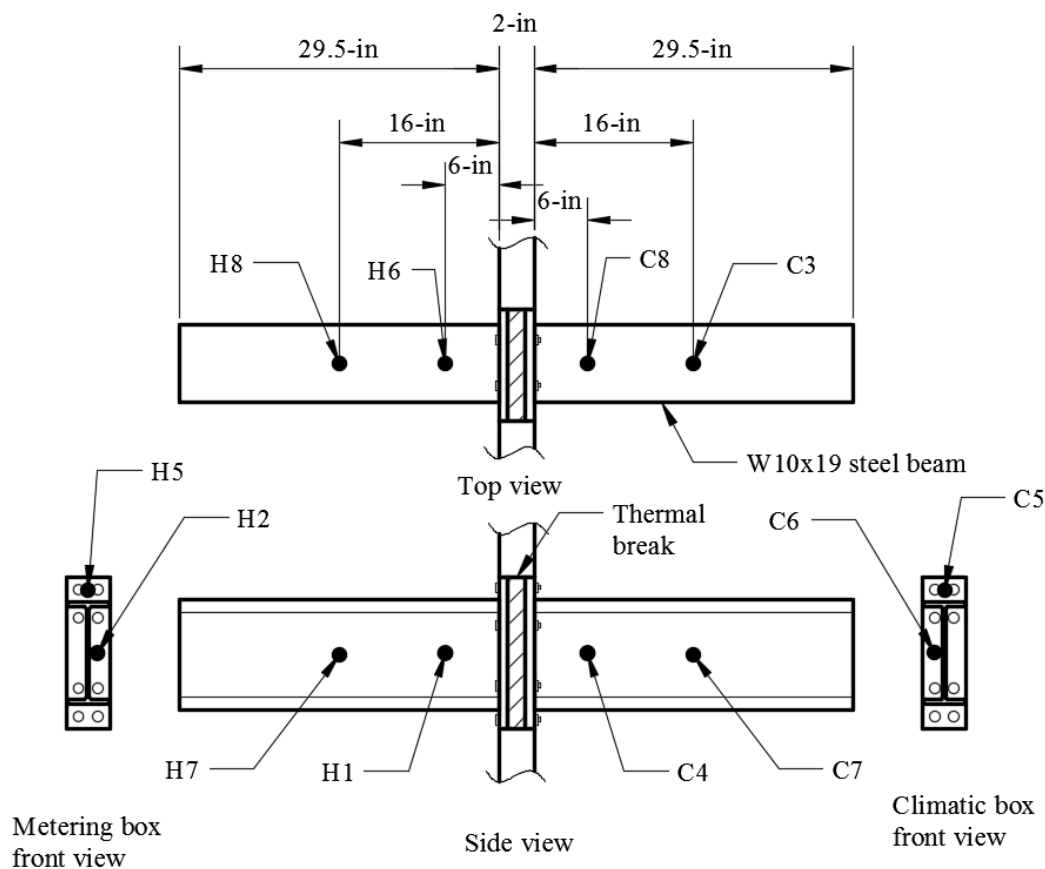


Figure 3-11: Temperature sensor arrangement for the beam-to-beam thermal break connection

The surround panel was a 2in thick sheet of XPS insulation (FOAMULAR 250, Owens Corning) measuring 56in by 56in, identical to the one used for the continuous beam thermal bridge. A rectangular hole in the center of the surround panel was cut to fit the end-plate and



thermal break. The thermal break was arranged so that it remained fixed in the center of the surround panel (length-, depth-, and width-wise). The end-plate connection was bolted through the thermal break to the opposite end-plate connection. The gap between the steel end-plates and the rigid insulation (approximately 1/8in) was filled with insulating spray foam (Great Stuff Pro – Gaps & Cracks, DOW Chemical Company), allowed to dry and harden, and sealed over with tape. The temperature of the metering chamber was held at 80.0 °F, and the climatic side was brought to 30.0 °F.

### 3.3 Structural Testing

A representative thermally-broken connection was formulated for investigation in this study. The idealized representative connection consists of an end-plate connection bolted through a neoprene pad to a column, as shown in Figure 3-12.

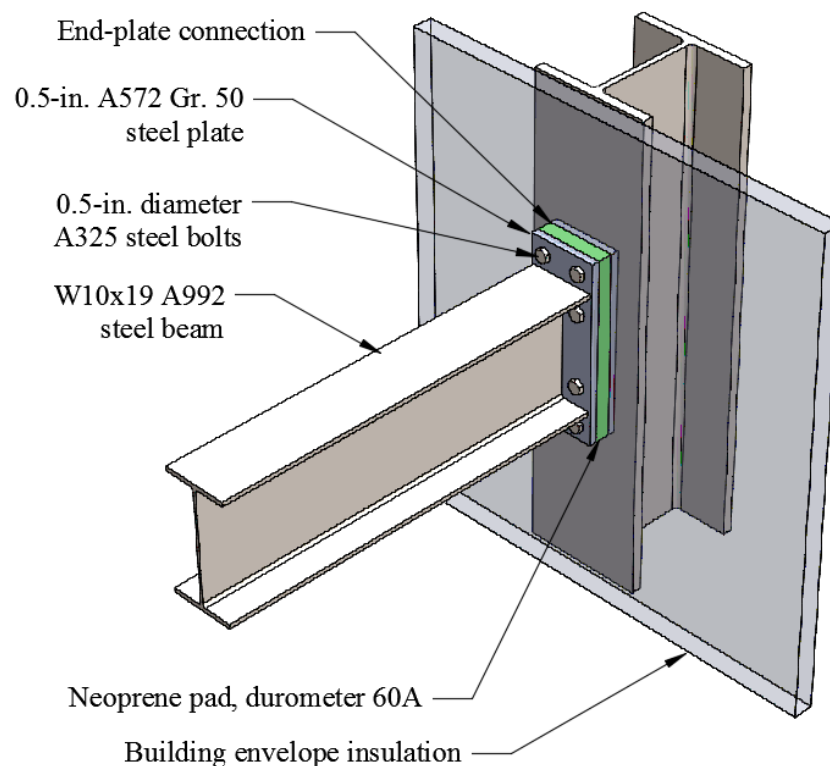


Figure 3-12: An idealized neoprene thermal break end-plate connection

Neoprene was selected as the thermal break material based on heat flow results from Finite-element studies showing that it exhibits nearly identical heat resistance properties as more rigid FRP materials. Neoprene is commonly used for structural engineering bearing applications, notably seismic isolators and bridge bearing pads [52]. For these reasons, neoprene is a suitable candidate for use as a bearing pad material in a thermally-broken end-plate connection.

Finite-element studies also identified that both stainless-steel and FRP bolts provided a significant reduction in heat flow compared to steel fasteners. However, due to lack of extensive literature available regarding stainless-steel and FRP bolts in combination with end-plate connection design, steel bolts were chosen for use in the experimentally tested thermal break connection.

To experimentally determine the response of the steel end-plate connection with the inclusion of a non-steel material in the faying surface of the connection, two experimental test procedures were conducted, bending tests and shear tests, which were performed on a representative steel connection using neoprene pads.

### 3.3.1 Bending Tests

The tested end-plate connection was designed using AISC Steel Design Guide 16 [35] using the thick end-plate, smaller diameter bolts procedure. This procedure produces an end-plate connection that uses a thicker end-plate and smaller diameter bolts, which presumes that bolt rupture will occur prior to plate yield with no contribution due to prying forces. This design was selected as it represents a relatively typical end-plate moment connection, and choice of the small-bolt option was justified by finite-element studies that show thinner bolts will reduce heat flow. The tested connection is a doubly-symmetric unstiffened 4-bolt end-plate moment connection that uses a W10x19 A992 steel beam with a 1/2" thick A572 Gr. 50 end-plate and 1/2-in. diameter A325 Type 1 structural steel bolts. The end-plate was welded to the beam with 5/16-in. fillet E70XX welds. A diagram of the connection geometry is shown in Figure 3-13.

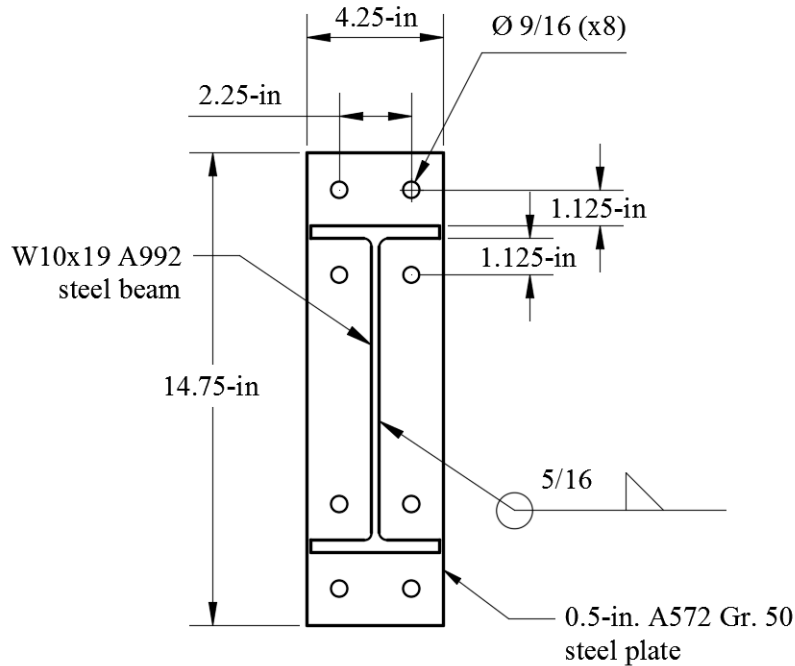


Figure 3-13: End plate connection geometry

An identical end plate was attached to both ends of a 60-in. beam. Two such beam specimens were fabricated, for a total of four identical end-plate connections (see Appendix B). The specimens were fabricated by STEELFAB in Anchorage, Alaska in accordance with AISC and American Welding Society (AWS) specifications. In order to reduce experimental variability in material strengths, specimen components were cut from the same length of beam and steel plate.

The neoprene material was specified as durometer 60A cut from sheet stock and sourced locally (Anchorage, Alaska). It was cut to measure the end-plate dimensions and the bolt holes were machined to 0.5-in diameter.

Four bending tests were conducted, three using different thicknesses of neoprene and an additional control test to serve as a baseline for a connection without the neoprene pad. The test matrix is shown in Table 3-4.

The connection was tested by applying both a moment and shear force. A W10x45 stiffened beam was used as the rigid support, hereafter referred to as the column. 1/2-in. continuity plates were welded to the column at the centerline of the tension and compression

flanges of the beam. The column was bolted to a strong floor using 1-1/2 in. diameter ACME threaded rod. A schematic of the test configuration is shown in Figure 3-14.

Table 3-4: Cantilever bending test matrix

| Test            | Test ID  | Neoprene pad thickness (in.) | Bolt type | Bolt diameter (in.) | Bolt length (in.) |
|-----------------|----------|------------------------------|-----------|---------------------|-------------------|
| No neoprene     | TB-NP-00 | None                         | A325      | 0.5                 | 2.0               |
| 0.5in. neoprene | TB-NP-05 | 0.50                         | A325      | 0.5                 | 2.5               |
| 1.0in. neoprene | TB-NP-10 | 1.0                          | A325      | 0.5                 | 3.0               |
| 1.5in. neoprene | TB-NP-15 | 1.5                          | A325      | 0.5                 | 3.5               |

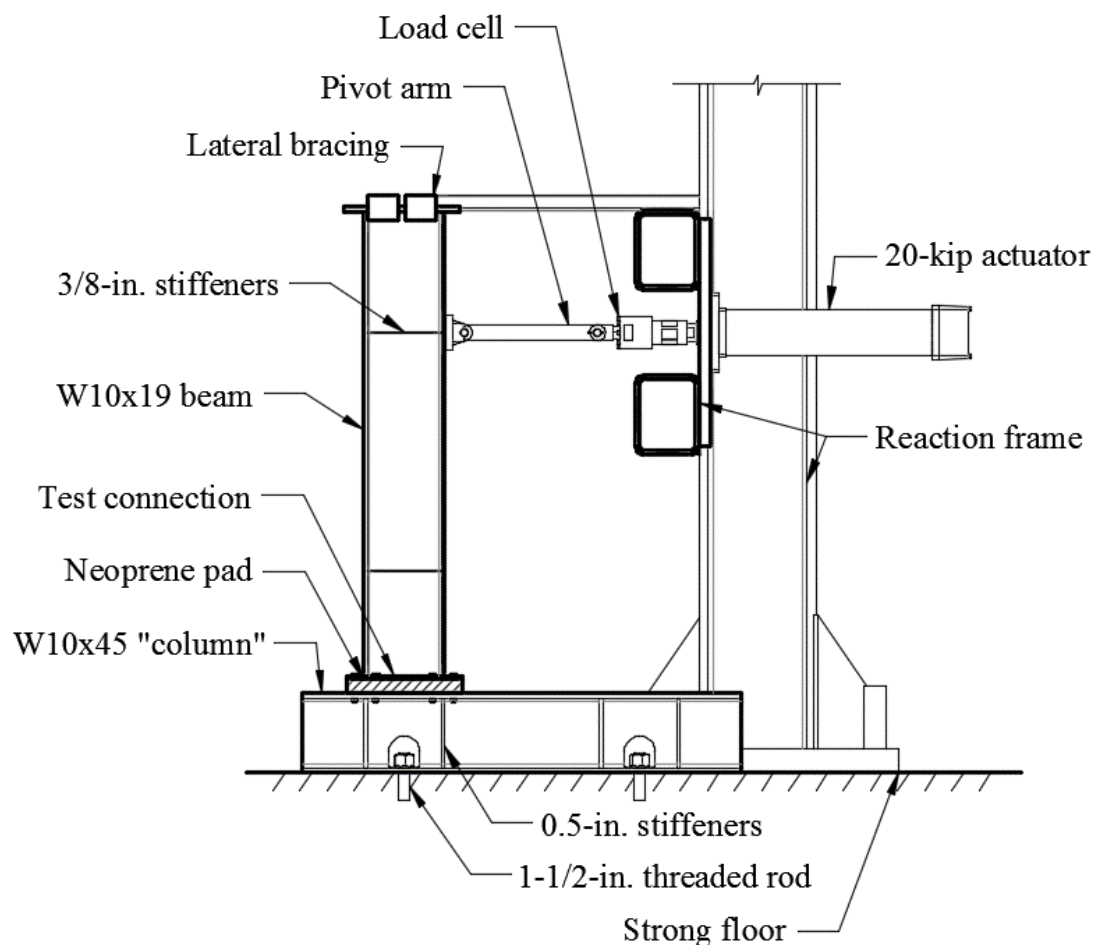


Figure 3-14: Bending test configuration

The test was configured for load to be applied horizontally at a distance of 45.9-in. from the face of the column flange with the column anchored rigidly to the floor. Lateral displacement of the beam was prevented by roller wheels placed on each side of the free end of the beam. A picture of the constructed and instrumented bending test setup is shown in Figure 3-15.



Figure 3-15: Constructed bending test assembly

The beam specimen was bolted to the W10x45 column using eight 1/2in. diameter A325 Type 1 (black) bolts with A563 bearing-face nuts. Washers were omitted from the connection. AISC Design Guide 16 [35] recommends that all bolts be tightened to 75% of the minimum pretension force defined in Table J3.1 of the AISC Specification for Structural Steel Buildings [65]. It was determined experimentally that tightening the bolts to the recommended force (9kip for 0.5in diameter bolts) resulted in excessive squeezing of the neoprene material. Therefore, bolts were tightened to 2 kips of axial force using a calibrated torque wrench. The torque

required was determined to be 200in-lbs by using a calibrated torque wrench and a compression load cell washers. The bolts were tightened sequentially following the pattern shown in Figure 3-16.

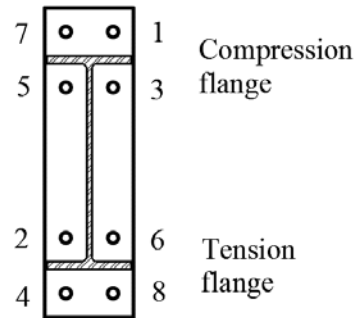


Figure 3-16: Bolt tightening sequence

All the bolts were snug-tightened by hand, and the pattern was repeated until all bolts achieved the required torque of 200-in-lbs. For the 0.5-in. thick neoprene, three complete patterns were required for all bolts to reach their required torque. For the thickest neoprene, 1.5-in., five complete patterns were required. Bolt numbers hereafter refer to the numbering shown in Figure 3-16.

Bending tests were carried out under monotonic displacement control with a constant speed of 0.14-in/min up to bolt rupture. The measured parameters were load, displacement at the location of the load, displacement 12-in. above the column face on the beam, displacement at the outer row of bolts (both compression and tension), and shear displacement of the end-plate. The displacements were measured at a collection period of 100 Hz using linear variable displacement transducers (LVDTs). Load was measured using a 25-kip pancake-style load cell. Instrumentation data was collected using a National Instruments data acquisition system.

### 3.3.2 Shear Tests

The purpose of the shear tests was to determine the shear deformation of a bolted bearing pad connection, and how the interaction of bolt shear stiffness and neoprene shear stiffness affects the shear stiffness of the assembled connection. Bearing pads in compression are often un-bonded to the support concrete or steel, relying solely on friction to transfer shear forces. In

an end-plate connection with a neoprene pad, however, bolts passing through the pad and clamping the connection together provide a portion of the shear resistance through the connection. There is a need to determine whether the shear stiffness of the neoprene has any contribution, and if so, to what extent.

Shear tests were carried out using a 110-kip capacity hydraulic test machine. This test consisted of clamping the neoprene specimen between two 0.5-in. A572 Gr. 50 steel plates and applying load to the end of the plates, in a manner shown schematically in Figure 3-17 and pictured in Figure 3-18.

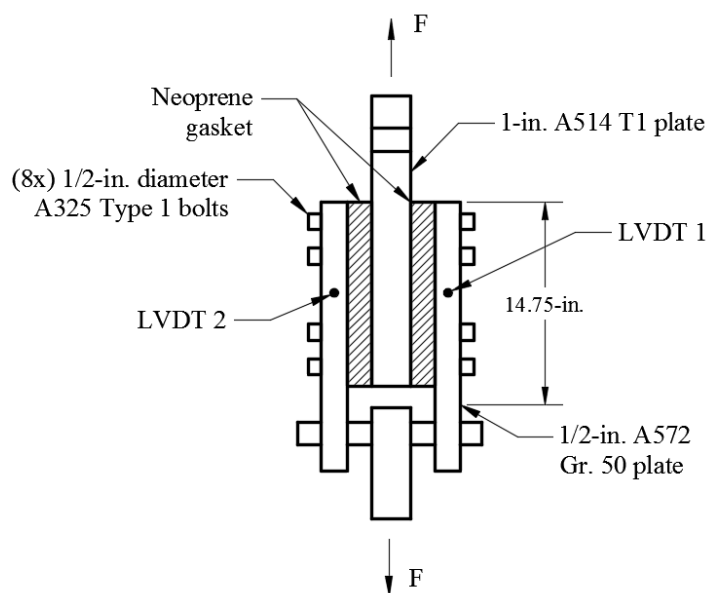


Figure 3-17: Shear test configuration

The 1/2-in. plates on either side of the assembly and the bolt hole pattern matched the end-plate dimensions of the bending tests, shown in Figure 3-13, albeit without the W10x19 and connecting welds. The neoprene specimens were identical in geometry to those used in the bending test, though the shear tests required two neoprene specimens for each test. The plates used for the shear test were cut from the same sheet stock as those used for the bending tests. The mating surfaces between the neoprene and steel were given no special preparations apart from being cleaned of oil and dirt and dried before being bolted together. The shear test matrix is shown in Table 3-5.

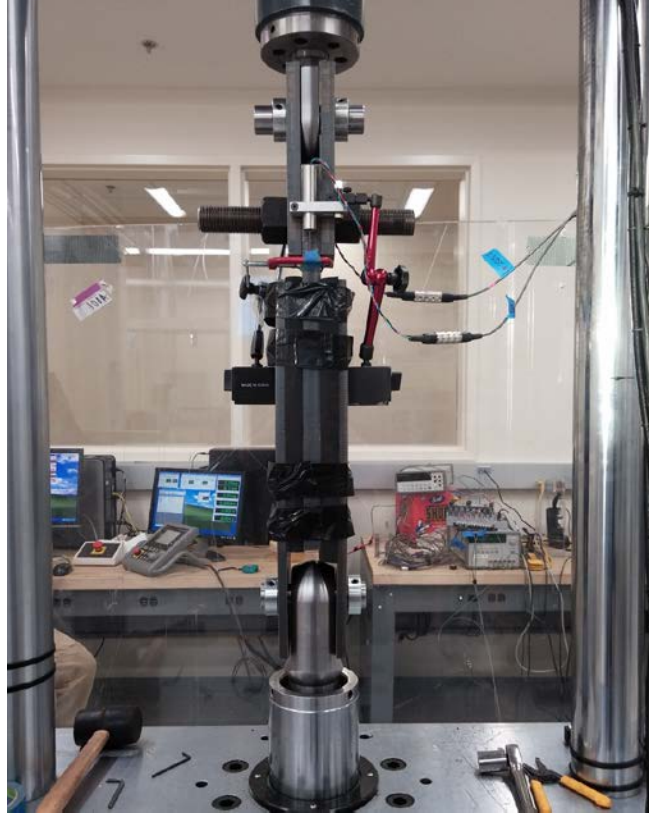


Figure 3-18: Constructed shear test setup

Table 3-5: Shear test matrix

| Test     | Neoprene pad thickness (in.) | Bolt type | Bolt diameter (in.) | Bolt length (in.) |
|----------|------------------------------|-----------|---------------------|-------------------|
| TS-NP-00 | None                         | A325      | 0.5                 | 2.5               |
| TS-NP-05 | 0.50                         | A325      | 0.5                 | 3.5               |
| TS-NP-10 | 1.0                          | A325      | 0.5                 | 4.5               |
| TS-NP-15 | 1.5                          | A325      | 0.5                 | 5.5               |

Prior to testing, the center pull-plate was fixed to the upper cross-beam with the center of the plate co-aligned to the center of the applied load. The neoprene pad and plates were applied to each side of the center plate, and bolted through the entire assembly. The bolts were then tightened in an identical manner as the bending test. However, because the test assembly



consisted of two neoprene specimens instead of one, approximately twice as many tightening patterns were required to achieve the desired torque of 200-in·lbs.

Shear tests were carried out under displacement control with a constant speed of 0.072-in/min up to 90-kips total load. Load was measured using a 120-kip cylinder-style load cell. Displacement was measured at the center of each plate with reference to the edge of the pull-plate. In this manner, the additional displacements due to dishing of the clevis pin on the pull-holes were excluded from displacement data. The displacements were measured using  $\pm 0.25$ in. LVDTs. Instrumentation data was collected using a National Instruments data acquisition system.

### **3.4 Finite-element Modeling**

The objective of the finite-element modeling was to calibrate a non-linear finite element model to predict the behavior of the end-plate connection under the influence of a relatively soft bearing pad. Experimental testing of steel end-plate connections has been compared to numerical simulation results and has produced excellent agreement for moment-rotation curves of various configurations [66]–[68]. An extensive literature review on the application of the finite element method to end-plate connections is given in [45] and [69]. These recent studies using contemporary finite element programs have concluded that end-plate behavior can be accurately analyzed using finite element modeling. However, the lack of sufficient information on the effect of elastomeric pads in moment end-plate connections exposes the need to further investigate the behavior of such connections.

#### **3.4.1 Model Information**

Abaqus was employed as the finite element analysis simulation program for this study. To verify and validate the FEA model, it was determined that the experimental bending test presented in Section 3.3.1 was to be modeled and analyzed. In order to model the experimental setup, the geometry of all the parts was created with their respective dimensions. Several simplifications were made from true conditions in order to enable convergence and ease-of-use. Bolts were modeled as two simple cylindrical volumes, and nuts were modeled as one cylindrical volume. The outside diameter of the modeled nut and bolt head measured the inside hex dimension. The stiffeners on the W10x19 beam were omitted from the model to reduce element

quantity. A complete model that included the W10x45 column and W10x19 beam and end-plate was modeled and compared against the results of a model that substituted the W10x45 column with a rigid plate. It was determined from this preliminary analysis that the W10x45 column acts as a rigid element, providing negligible contribution to the rotation of the connection, and could therefore be represented by a rigid plate. The assembled model is shown in Figure 3-19.

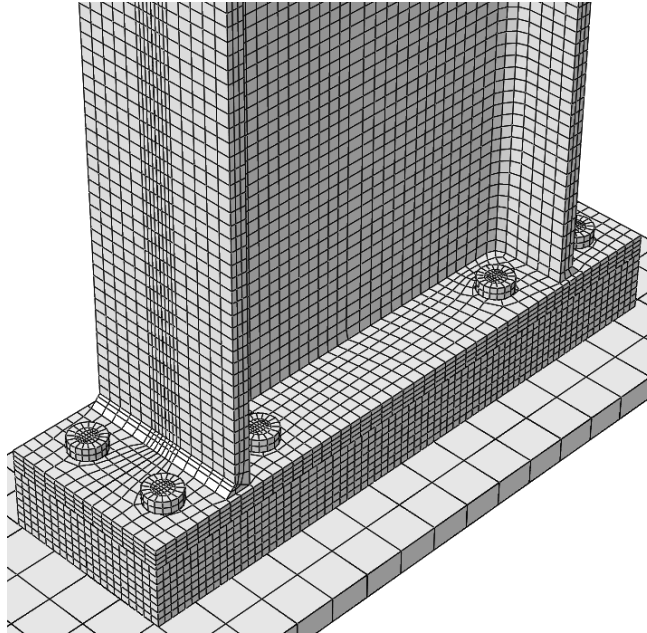


Figure 3-19: Assembled and meshed model (1.5-in. neoprene)

#### 3.4.2 Material Properties

There have been several stress-strain relationships proposed in literature that account for plasticity and strain hardening in high-strength bolts for finite element modeling purposes. Abel [70], as part of thesis research into extended unstiffened end-plate connections in 1993, proposed a bilinear model relating bolt stress and bolt strain and applied it to finite-element analyses and experimental data. More recently, faster processors enabled Sherbourne and Baharri [40] to develop an idealized trilinear curve which they used to parametrically evaluate a number of end-plate configurations. The most popular bolt material model used to model end-plate connection behavior in use today was developed by Mays [71] and uses a slightly modified trilinear model. This material model was used successfully in a number of finite element analyses to predict the experimental behavior of bolted end-plate connections [67], [72], [73]. Stress-strain curves used in this study utilize the material models proposed by Mays and are shown in Figure 3-20.

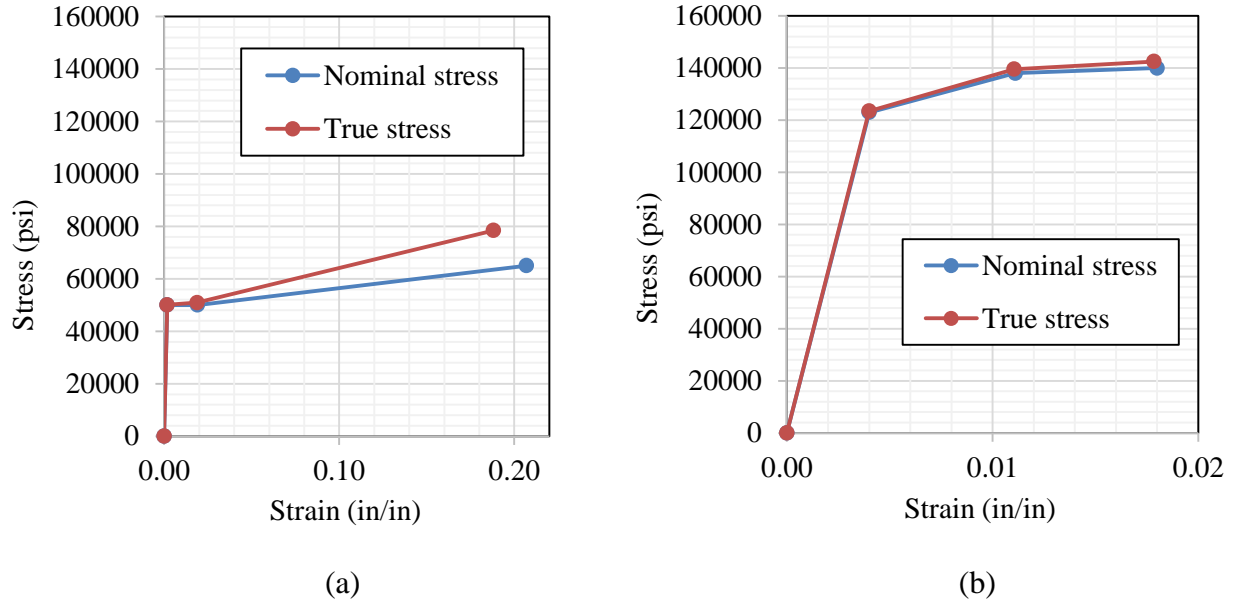


Figure 3-20: Material definition for (a) bolts and nuts and (b) beam and end-plate

In the absence of material test data, minimum yield and minimum tensile strengths were used with the Mays model to construct the stress-strain curves shown in Figure 3-20. A factor of 1.1 was applied to the yield and ultimate stress values in order to compensate for the difference between true strength and specified minimum strength. All steel components were modeled as isotropic elasto-plastic material in both compression and tension. A Poisson's ratio of 0.3 and an elastic modulus of 29,000-ksi was assumed. Abaqus requires input of true-stress and true-strain values, which were determined from nominal stress and nominal strain values using the following relationships between nominal (engineering) stress and strain, and true stress and strain:

$$\sigma_{true} = \sigma_{engr}(1 + \varepsilon_{engr}) \quad (\text{Eq. 3-13})$$

$$\varepsilon_{true} = \ln(1 + \varepsilon_{engr}) \quad (\text{Eq. 3-14})$$

The extensive amount of numerical work that has been performed on hyperelastic materials for a variety of industrial applications makes it difficult to select an appropriate

material model to approximate the behavior of a specific formulation of neoprene. However, there exist several examples in literature that have used hyperelastic material definitions to model and simulate elastomeric bearing pads in combination with steel plates [55], [74], [75]. Nearly incompressible hyperelastic materials, such as rubber and neoprene, are treated in continuum mechanics using the principles of stretch and strain energy potential to determine their constitutive relationship. The strain energy potential defines the energy stored in the material per unit of reference volume as a function of the strain at that point in the material [76].

While there exist a number of models that have been developed to describe the behavior of hyper-elastic materials, the Ogden model was selected based on work by Kim et. al. [77] who made a comparison between the Neo-Hookean, Mooney-Rivlin, and Ogden models for use as a finite element material model for neoprene. The strain-energy density function for the Ogden model [78] is:

$$W = \sum_{i=1} \frac{\mu_i}{\alpha_i} (\lambda_1^{\alpha_i} + \lambda_2^{\alpha_i} + \lambda_3^{\alpha_i} - 3) \quad (\text{Eq. 3-15})$$

where  $\alpha_i$  and  $\mu_i$  are constants, and  $\lambda_1, \lambda_2$ , and  $\lambda_3$ , are the three principal stretch ratios, or stretch invariants, since they are independent from the used coordinate system. The material constants are generally derived from experimental material test data fitted to the Ogden model, or another strain energy potential model. The neoprene material used in this study was defined as a coefficient based Ogden model with a second-order strain energy potential. The coefficients used to define the neoprene were derived from the work by Xiao et. al. [79] and are shown in Table 3-6.

Table 3-6: Ogden coefficients used for neoprene material model

|            | 1        | 2       |
|------------|----------|---------|
| $\mu_i$    | 0.104347 | 158.099 |
| $\alpha_i$ | 7.78077  | 2.24987 |
| D          | 0        | 0       |

The term,  $D$ , is related to the initial bulk modulus,  $K_0$ , by the expression,  $K_0 = 2/D$ , which is a function of the materials Poisson's ratio and initial shear modulus.

### 3.4.3 Boundary Conditions

A fixed boundary condition (no rotations, no displacements) was applied to the rigid plate. Bolts were pre-loaded using the applied force method. A force of 2000-lbs was applied to the center of each bolt. At the start of the subsequent step, bolt deformation was fixed at its current stretch. The load was applied as a pressure to a 4-in by 4-in. region on the beam at 45.9-in. from the column face.

Contact definitions between parts is one of the most critical processes in defining an accurate finite element model. For contact between the end-plate, neoprene, and column, tangential and normal interaction properties were defined using finite-sliding and surface-to-surface contact. It is recognized that the friction coefficient between the steel and neoprene can have a large effect on the compressive response of the nearly incompressible neoprene material. A value of 0.4 was chosen for the tangential interaction between neoprene and steel, and 0.3 for steel-to-steel interaction. Normal behavior between contacting parts was defined using hard contact with the penalty method and a stiffness scale factor of 1.0. Nuts were bonded to the bolts using a tie constraint, which allows no relative displacement between contacting surfaces. A tie constraint was applied to connect the beam end to the end-plate to simulate the welds.

### 3.4.4 Mesh Parameters

A study by Augusto et. al. [80] performed a mesh sensitivity analysis using a contemporary version of Abaqus on three different solid elements. Each element formulation produced relatively similar results. However, comparison with experimental test results on an end-plate connection identified the C3D8RH solid element (an 8-node linear brick element with reduced integration, hourglass control, and hybrid formulation) as the best choice based on the criteria of efficiency and accuracy. Therefore, the beam, column, end-plates, bolts, and nuts were modeled using the three-dimensional eight node solid element with reduced integration element and hybrid formulation (C3D8RH). The neoprene material was also modeled using a C3D8RH solid element formulation. A solid brick element lacks any rotational degrees of freedom, so the number of elements through the thickness of any geometry must be carefully selected in order to

yield accurate results. Bursi and Jaspart [81] recommended that a minimum of 3 elements through any geometry should be used for any bending-dominated regions using the aforementioned continuum element formulations. However, at least five elements through the thickness were used in regions of expected bending to negate any inaccuracies due to insufficient element layering.

#### 3.4.5 Steps and Solution

The analysis was performed using two consecutive steps, each with a different solution target. The first step was to tighten all the bolts to the specified force for each bolt. The second step applied the load to the cantilever beam. Both steps were defined to use automatic increment controls, as well as consider second-order effects which accounts for large displacements. The Abaqus/Standard solver, which iteratively solves a system of equilibrium equations implicitly for each step increment [76], was used for all simulations.

## Chapter 4: Results and Discussion

This chapter contains the results of all phases of the study including the industry survey, calibrated hot box testing, structural testing, and finite-element simulations.

### 4.1 Industry Survey

The interviews with local firms in Anchorage, Alaska proved fruitful in assessing the perspectives of a selection of engineers in sub-arctic regions where there are a much higher number of heating degree days than in the contiguous US. Several engineers expressed more concern for the issue of condensation than heat loss. When heat loss and heat flow was discussed, it was in reference to structures built on permafrost. In several instances it was stated that steel construction was avoided because of concerns about potential thermal bridging. Thermal bridging through foundation elements is a critical issue in the arctic as it can thaw permafrost or melt the active layer, imposing large up-lift forces on the structure. As such, a common practice is to use wood or neoprene as a thermal break between the foundation and the superstructure.

In the nationwide survey to AISC members a total of 269 responses were started with 140 completed, resulting in a 52% completion rate. Figure 4-1 shows a map of survey respondents in the U.S.

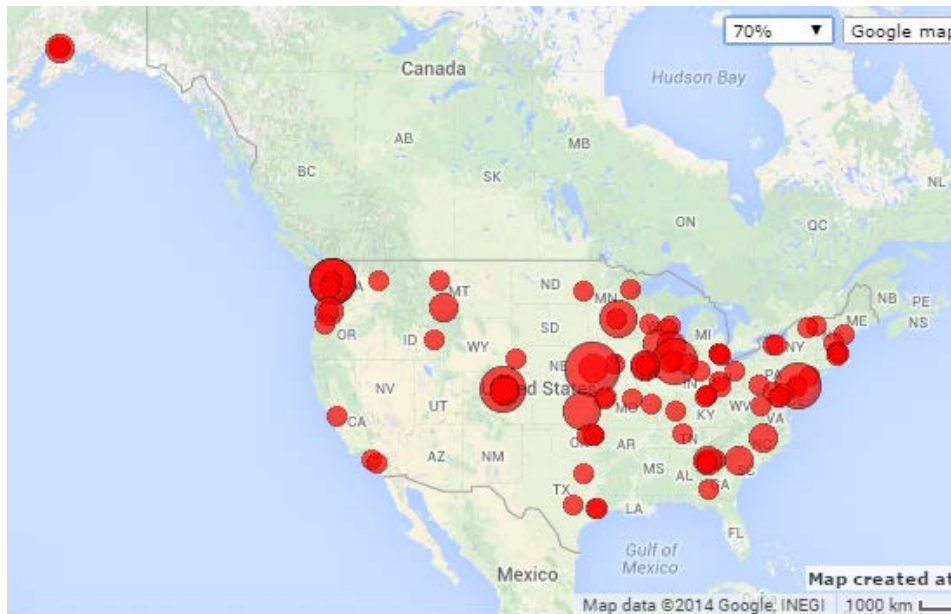


Figure 4-1: Dot density map of survey respondents

The full results of the survey can be found in Appendix A. In general, it was found that the majority of engineers attempt to avoid thermal-bridging. If avoidance is not possible, the most popular strategy was to surround the bridging element with insulation, followed by inserting an insulating pad. “Do nothing” was also a popular answer. The most popular pad materials were neoprene and wood, and the most common situations where thermal bridging is encountered were cantilever beams, façade element, and rooftop supports.

## 4.2 Calibrated Hot-Box Testing

Heat flow results for the surround panel, continuous beam, and beam-to-beam end-plate connection are shown in Figure 4-2. The 2in XPS insulated panel (control) had a specimen heat flow in Btu/(hr·°F) of  $1.02 \pm 0.03$ . Selected  $\chi$  values can be seen in Table 4-1

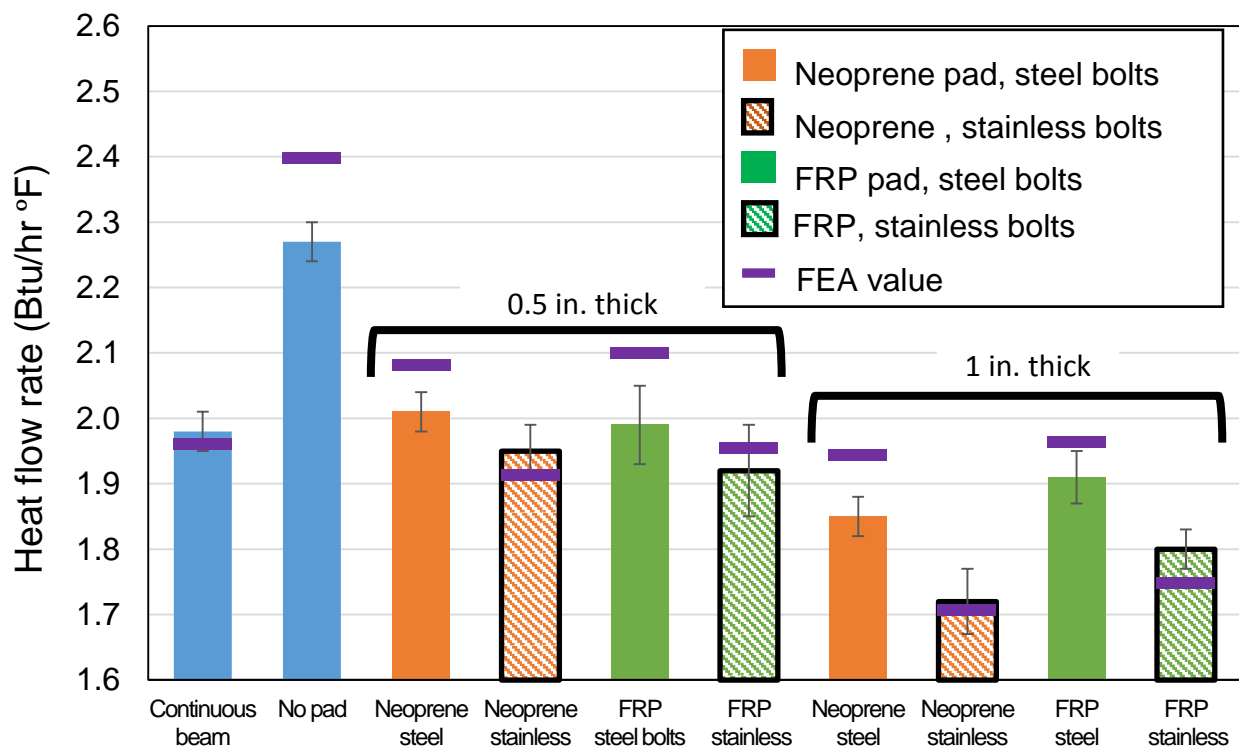


Figure 4-2: Heat flow results from calibrated hot box testing



It is evident that a thermal bridge caused by a continuous beam penetrating an insulated layer causes a severe increase in heat flow (81 % increase). The results from the thermal break tests indicate a slight decrease in heat flow compared to the continuous beam, but have overlapping uncertainties at their extreme ends.

Table 4-1: Heat flow measurement results

| <b>Test</b>   | <b><math>\chi</math><br/>Btu/(hr·°F)</b> |
|---|--|
| 2in XPS insulated panel                               | 0  |
| Continuous beam                                       | $0.96 \pm 0.04$                          |
| Thermal break (1in thick GRFP, steel bolts)           | $0.89 \pm 0.04$                          |
| Thermal break (1in thick GRFP, stainless-steel bolts) | $0.78 \pm 0.04$                          |

## 4.3 Structural Testing

### 4.3.1 Bending Tests

The observed failure mode in all tests was bolt rupture at the tension group of bolts. Tests were stopped after rupture of the first bolt. A summary of the results is presented in Table 4-2.

Table 4-2: Bending test summary

| <b>Test</b>     | <b>Test ID</b> | <b>Observed failure mode</b> | <b>Bolt number</b> | <b>Applied displacement at load (in.)</b> | <b>Applied load at rupture (kip)</b> |
|-----------------|----------------|------------------------------|--------------------|---|--------------------------------------|
| No neoprene     | TB-NP-00       | Bolt rupture                 | 2 & 6              | 0.936                                     | 17.80                                |
| 0.5in. neoprene | TB-NP-05       | Bolt rupture                 | 6                  | 2.00                                      | 15.54                                |
| 1.0in. neoprene | TB-NP-10       | Bolt rupture                 | 2 & 6              | 3.31                                      | 14.97                                |
| 1.5in. neoprene | TB-NP-15       | Bolt rupture                 | 4 & 8              | 5.00                                      | 12.00                                |

Beam-to-column connection behavior can be represented by the moment-rotation curve ( $M-\theta$ ). This curve represents the relationship between the bending moment applied to a joint and the resulting rotation between the connection members. The bending moment acting on the connection corresponds to the applied load multiplied by the distance between the location of the

load and the face of the end-plate,  $L$ . The rotation of the connection is then the sum of the shear deformation of the column web panel zone and the connection rotational deformation [82]. Connection rotation is then defined as the change in angle between the beam and column axes,  $\theta_b$  and  $\theta_c$ , respectively. In these tests, the column deformation in bending and panel zone shear is considered negligible, and that it behaves as a rigid element. However, shear deflection of the connection due to shear force is not negligible for tests with a neoprene pad. This topic is discussed in greater detail in the next section. Shear deflection was also measured in the bending tests, and is presented in Figure 4-3.

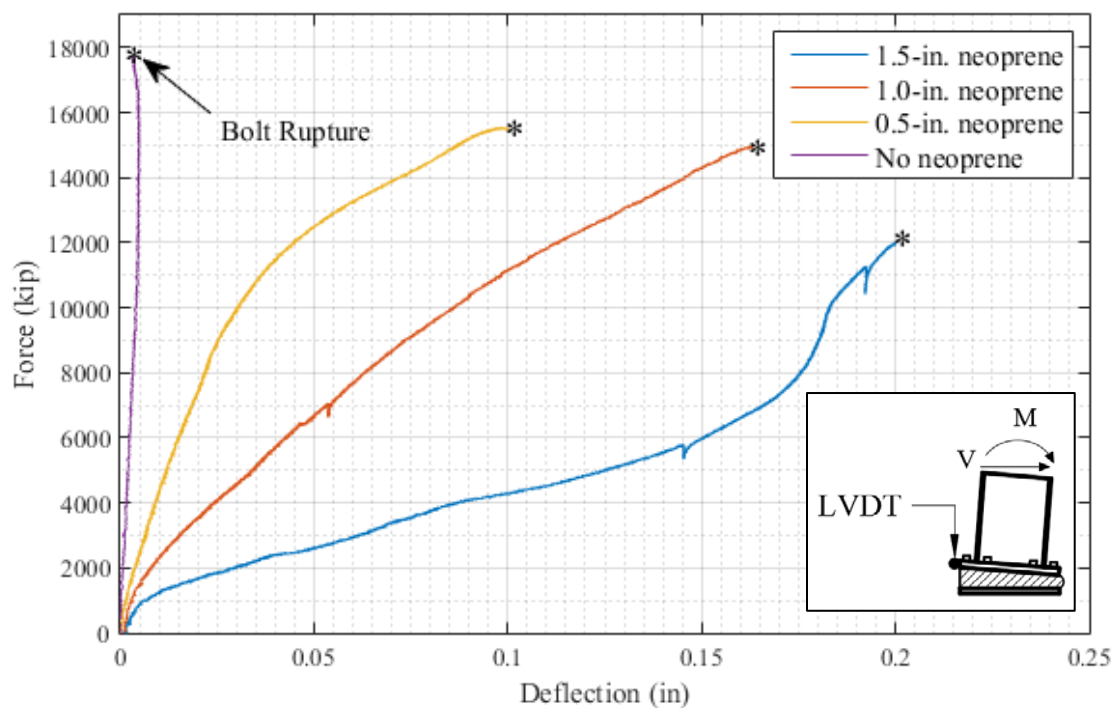


Figure 4-3: Shear deflection of the end-plate. Measured at edge of tension side of end plate.

It can be seen in Figure 4-3 that for the unaltered connection, the shear deflection could be considered negligible, but for the connections with a neoprene pad, this no longer holds true. Therefore, shear deflection was subtracted from the total deflection used to calculate rotation. Downward spikes in the 1.5-in. neoprene and 1.0-in. neoprene tests indicate when the test was paused briefly to adjust the range of the compression flange LVDT.

The experimental values of the rotation were obtained using the displacement at the load, 45.9-in from the column face, and displacement at 12-in. from the column face. With the

assumption that the column behaves as a rigid element, the rotation using displacement data at 12-in. and 45.9-in. from the column face is approximately given by:

$$\theta = \tan^{-1}\left(\frac{d_1}{12 \text{ in.}}\right) - \theta_{b,\text{elastic}} - \theta_{\text{shear}} = \tan^{-1}\left(\frac{d_2}{45.9 \text{ in.}}\right) - \theta_{b,\text{elastic}} - \theta_{\text{shear}} \quad (\text{Eq. 4-1})$$

where  $\theta_{b,\text{elastic}}$  is the additional rotation due to the elastic deflection of the beam,  $\theta_{\text{shear}}$  is the deformation due to shear displacement of the connection, and  $d_1$  and  $d_2$  are the displacements at 12-in. and 45.9-in from the column face, respectively. The resulting moment-rotation curves for all four tests are shown in Figure 4-4.

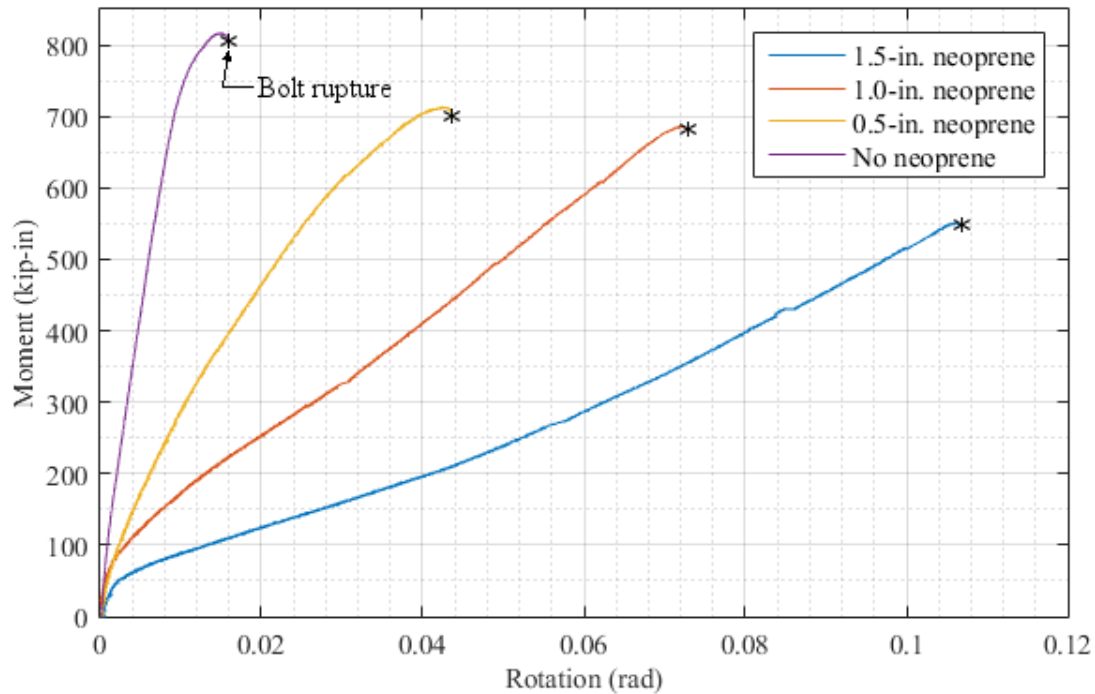


Figure 4-4: Moment-rotation curves

These curves show that the behavior of the end-plate with no neoprene exhibits a much higher stiffness and higher ultimate load than the same connection with a neoprene pad. The connection with no neoprene behaves in the expected manner for a fully-restrained moment connection, with a moment equal to 96-% of the fixed end moment for the loading, greater than the traditionally established limit of  $0.9 \cdot M_F$  [35].

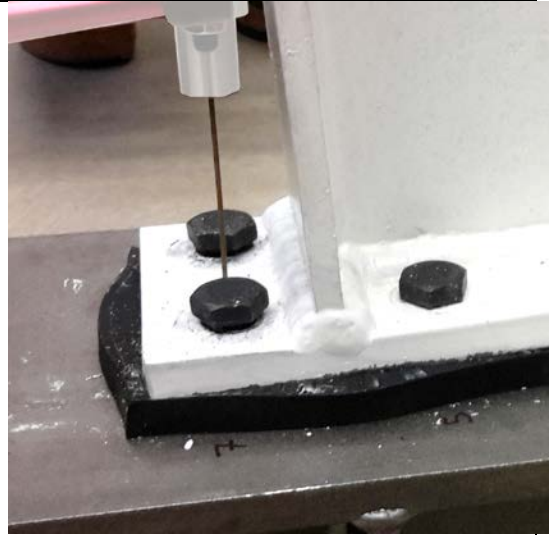
The difference in stiffness between tests is nearly linear. Although, for the thicker neoprene, 1.0-in. and 1.5-in., an inflection between the initial stiffness and apparent resulting stiffness is evident at a small moment, approximately 70-kip·in. and 50-kip·in, respectively. This phenomenon, however, is not apparent for the connection with no neoprene and the 0.5-in. neoprene connection.

Bolt rupture in tests with a neoprene pad occurred at less than the expected load for a connection without a pad. This indicates that there is a contribution to the bolt load from sources other than direct tension. Significant deformation of the neoprene in the compression flange region of the beam indicates that prying forces contribute to stresses in the tension bolts. As the thickness of the neoprene increases, it can be seen that the contribution of prying forces to bolt failure is significant, because bolt rupture occurs prematurely. However, prying forces cannot be determined as the sole cause of premature bolt failure based on these experimental tests. For the thicker neoprene tests, bolts in the compression region of the connection almost immediately lose all pre-load with the application of a moment load (curve-over region shown in Figure 4-4 where initial stiffness changes to resulting apparent stiffness), due to the low stiffness of the neoprene, and are left to rotate freely in place for the duration of the test with no contribution to the resistance of the connection. Thus, the applied shear force is transferred to the tension bolts resulting in combined bending and tension stresses on the bolts.

Significant deformation and damage was evidenced in the neoprene pad in the region of the compression flange, as shown in Figure 4-5. Figure 4-5(a) also shows the non-contributing nature of the compression group of bolts to the shear resistance of the connection, which are only kept in place by the neoprene pad. The deflection of the end-plate at the compression was measured in each bending test, and the results are shown in Figure 4-6.



(a) 1.5in neoprene



(b) 0.5in neoprene



(c) 1.5in neoprene



(d) 0.5in neoprene

Figure 4-5: Deformation of the neoprene under ultimate moment

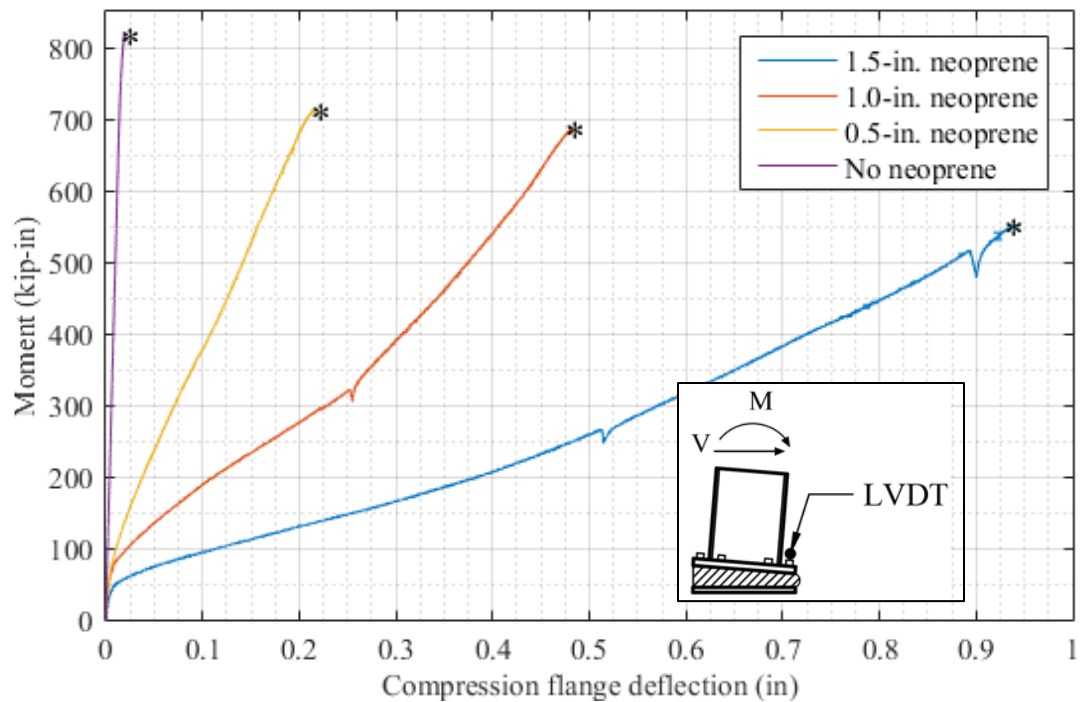


Figure 4-6: Measured deflection of the compression flange for each bending test

It can be seen from Figure 4-6 that the deflection of the compression flange is relatively linear up to bolt rupture.

#### 4.3.2 Shear Tests

Shear deflection is characterized in Figure 4-7 as the load applied in shear to the end plate and compared against the deflection parallel to the load. Deflections from both LVDTs was evaluated, and it was found that the deflections of each plate on were identical to within a 5-% difference at the greatest discrepancy value. Deflection shown in Figure 4-7 is from LVDT 1, which is on the plate with bolt heads.

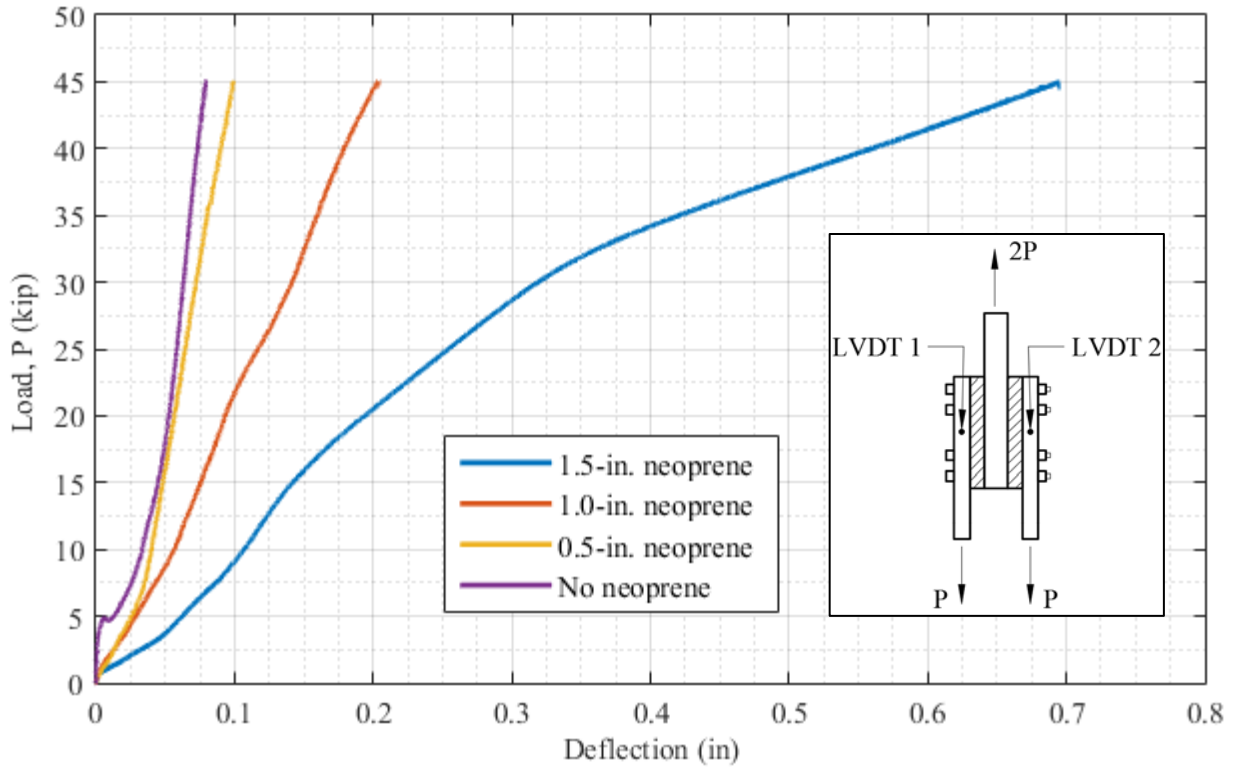


Figure 4-7: Comparison of deflection and load for all shear tests

It is evident that an increased thickness of neoprene leads to a seemingly exponential decrease in shear stiffness. The relative difference in maximum deflection between each test is approximately 0.025in, 0.1in, and 0.5in. From Figure 4-7, it can be seen that the test without a neoprene pad experiences a slip condition at approximately 5 kips where the load resistance changes from frictional resistance to bolt bearing. The test with the ½ in. neoprene showed no clear transition between frictional bearing and bolt bearing, because the presence of the neoprene precludes any frictional resistance between faying surfaces. The shear stiffness between the connection with no neoprene and ½ in. thick neoprene, however, is similar. This indicates that the contribution of bending forces to the total shear deflection for the ½ in. thick neoprene is minimal, as it closely resembles the shear stiffness of the connection with no neoprene pad. Although the tests were not continued until bolt rupture, bending forces in the bolts are significant, and the bending curvature of the bolts approximates the fixed-end moment condition of fixed-fixed with applied end displacement. Bending of the bolts due to an applied shear force at the plate diminishes with reduced pad thickness to the limit of pure shear deformation in the

bolts, shown in Figure 4-7 as the curve with no neoprene. Due to the low shear resistance of the neoprene pad, the bolts in the connection undergo double-curvature bending in a manner shown in Figure 4-8.

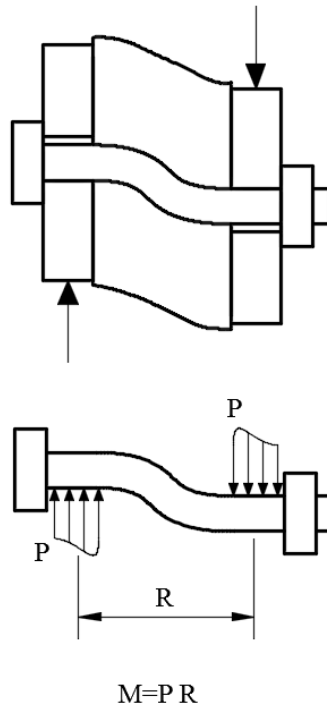


Figure 4-8: Bending in a bolt under shear load with a soft neoprene layer

#### 4.4 Finite-element Modeling

Numerical simulations were conducted both before and after physical testing took place. Pre-experimental modeling was utilized to identify idealized connections that were suitable for testing, while post-testing models were used to verify the assumptions used in the model, thus calibrating the model to realistic behavior, and draw conclusions. The results discussed below are for the calibrated simulations.

##### 4.4.1 Thermal Modeling

Heat transfer simulations were performed on a continuous beam thermal bridging configuration, with a varying parameter of beam size, as well as a thermal break configuration that consisted of a beam-to-beam end plate connection with a thermal break pad placed in the



connection. The thermal break configuration parameters were thermal break material, thermal break thickness, and bolt material. Results of the parametric study are detailed in the following sections.

#### *4.4.1.1 Continuous beam*

A variety of thermal bridges can exist in a steel structure. In this study, a structural steel beam penetrating normal to the vertical plane of the building envelope, as shown in Figure 4-9, is examined.

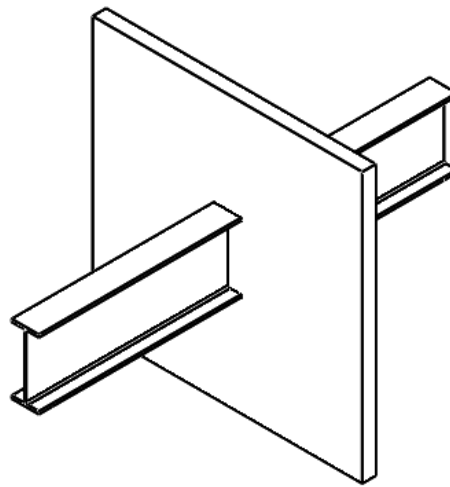


Figure 4-9: Idealized continuous beam thermal bridge model

Consider the simple example shown in Figure 4-9 where a beam penetrates a layer of insulation. There exists a field of three-dimensional heat flow near the thermal bridge, but the three-dimensional heat flow diminishes with distance from the bridge, until, at some distance from the insulation plane, the heat flow can be considered one-dimensional. Any plane sectioning the model at that location is considered adiabatic for modeling purposes. Figure 4-10 shows the diminishing rate of return for increased wall insulation thickness for the idealized continuous thermal bridging model shown in Figure 4-9.

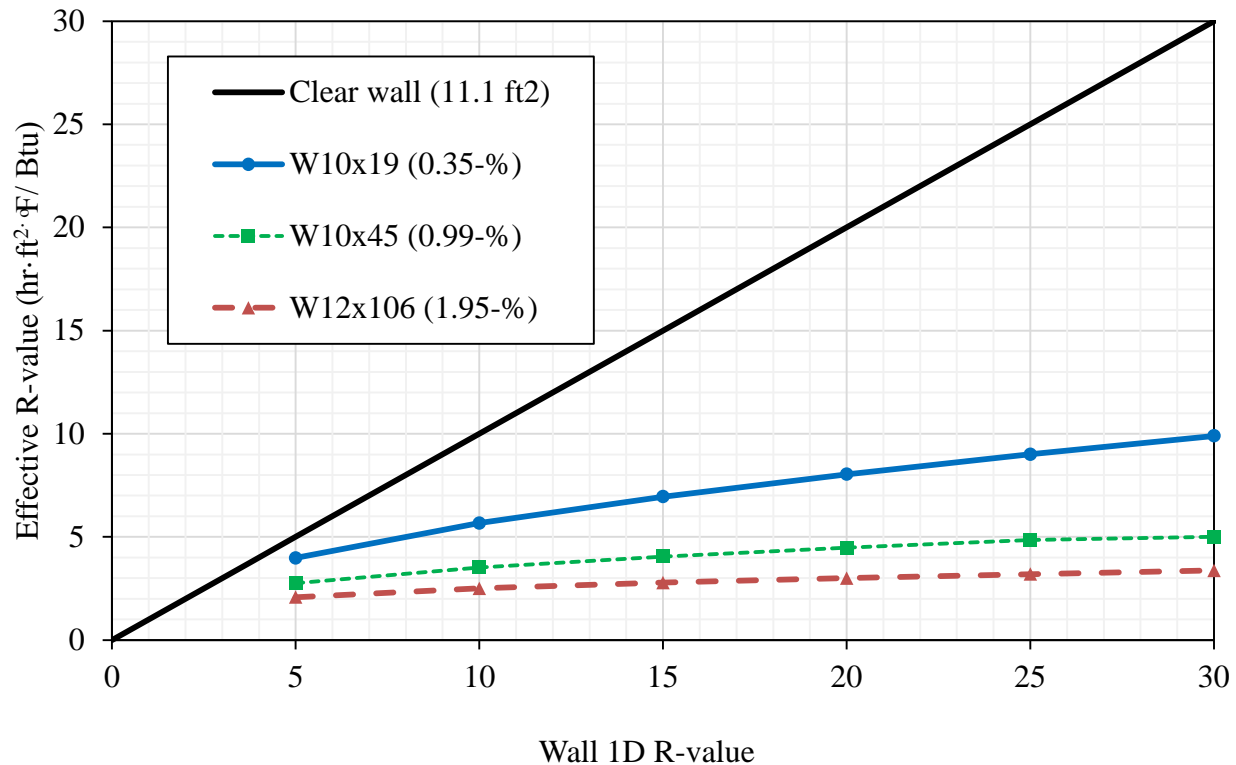


Figure 4-10: Effective versus nominal R-value for a structural steel thermal bridge

This figure illustrates how increasing the thickness of the insulation produces only a small relative benefit with the presence of a thermal bridge. Three curves are shown, each for a different ratio of steel cross-sectional area to total one-dimensional area. As the area of steel is increased in a section of insulation with constant width and height, the benefit of increasing the insulation thickness is greatly reduced.

A beam penetrating the building envelope, such as in Figure 4-9, acts as a cooling fin. In terms of heat transfer, fins are generally used to increase the heat transfer rate from surfaces which are convectively cooled by air, such as radiators or heat sinks. Single point steel thermal bridges are effectively and computationally identical to fins, although the goal of a fin is to increase the heat transfer rate, whereas for thermal bridging the converse is true. The derivation of heat transfer equations for fins and extended surfaces have been extensively studied and equations have been derived to solve general fin equations with a variety of boundary conditions. However, applying these equations to real-world thermal bridging scenarios can quickly become problematic due to the overly simplistic and general assumptions that must be made in order to

solve the differential equations. For example, it is assumed that the heat transfer coefficient,  $h$ , is constant and uniform over the entire surface of the extended fin, whereas its real-world value is a strong function of the air velocity at that point. Air velocity at a thermal bridge can be disrupted by a variety of building elements for which the structural member is responsible for supporting. Coatings and architectural fixtures also serve to manipulate the overall surface heat transfer coefficient.

Applying fin heat transfer equations to thermal bridging scenarios in real-world building envelope construction assemblies requires some broad simplifications in order to enable engineers to quickly and easily determine relatively reasonable values for heat flow and temperature factor in their details, and to their specific heating and cooling requirements. Therefore, in order to enable the use of general fin equations for continuous beam thermal bridges, they must be developed in a manner that can be applied efficiently and result in effective and approximately accurate and precise values for heat flow and temperature index.

There exist several solutions to the general fin equation depending on the fin tip conditions. This section presents the resulting equations for an infinite length tip conditions, where the fin is very long and at a certain length, any additional heat flow from the end of the fin is negligible. The following equation for the temperature distribution along a fin of uniform cross-sectional area and infinite length is derived from Fourier's law and the conservation of energy requirement:

$$T(x) = T_{\infty} + (T_b - T_{\infty})e^{-x\sqrt{\frac{hP}{kA_c}}} \quad (\text{Eq. 4-2})$$

where  $h$  is the convective heat transfer coefficient,  $P$  is the perimeter of the fin,  $k$  is the thermal conductivity of the fin material,  $A_c$  is the cross-sectional area,  $T_b$  is the temperature at the base of the fin, and  $T_{\infty}$  is the environmental air temperature. The temperature along the fin in this case decreases exponentially from the base temperature,  $T_b$ , to the environmental temperature,  $T_{\infty}$ , shown in Figure 4-11.

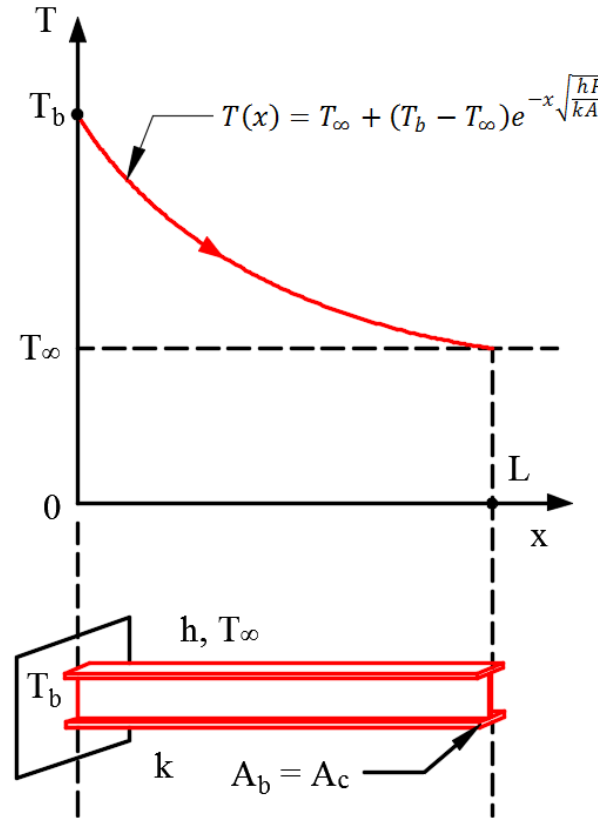


Figure 4-11: Temperature variation along a long W-section of uniform cross-sectional area

The resulting steady-state convective heat transfer rate from the entire fin is derived from Fourier's law resulting in:

$$Q = \sqrt{hPkA_c}(T_b - T_\infty) \quad (\text{Eq. 4-3})$$

Using constant values of  $k = 347 \text{ Btu}\cdot\text{in}/\text{hr}\cdot\text{ft}^2\cdot^\circ\text{F}$  and  $h = 1.5 \text{ Btu}/\text{hr}\cdot\text{ft}^2\cdot^\circ\text{F}$ , **Error! Reference source not found.** can be simplified, with only  $T_b$  left to be determined. These equations, and the assumption of infinite length, are compared to the results of finite element simulations. A three-dimensional finite-element model, similar to the one shown in Figure 4-9 was created using the simulation methodology outlined in Section 3.4 . A parametric analysis was performed on this model by varying the length of the beam and plotting the resulting heat flow rate from the inside environment ( $1^\circ\text{F}$ ) to the outside ( $0^\circ\text{F}$ ). Figure 4-12 shows the resulting heat flow compared to the length of beam extending beyond each face of the insulation plane.

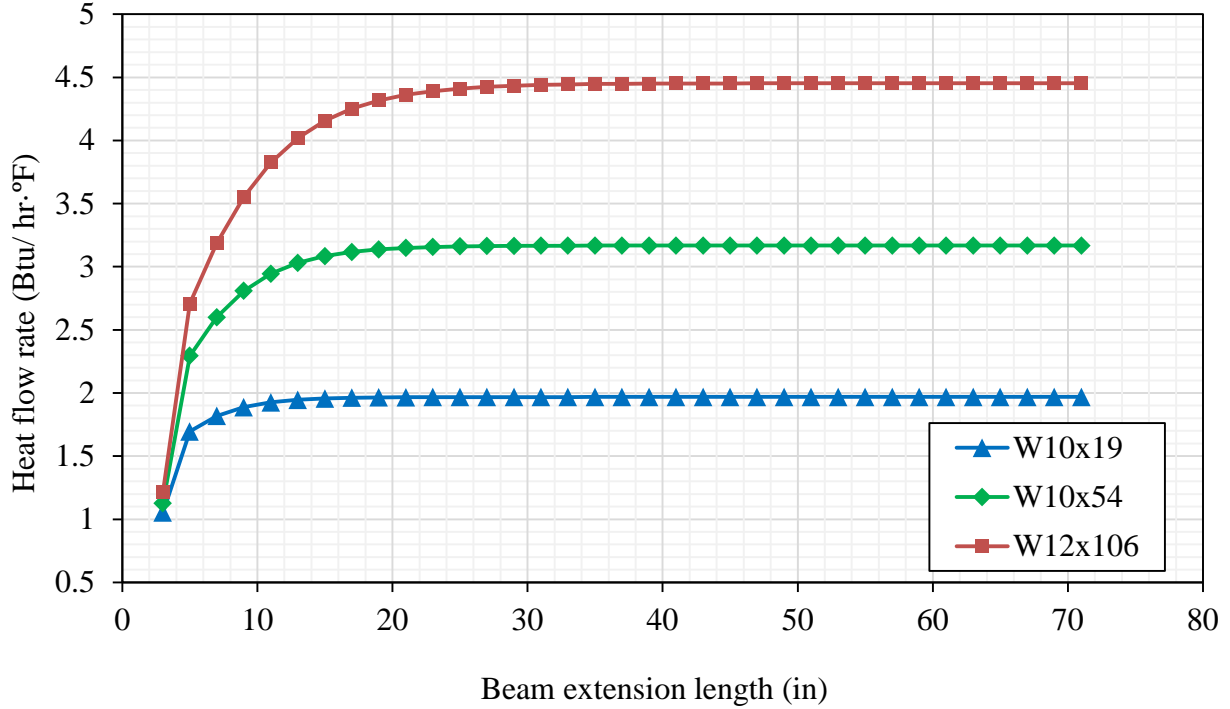


Figure 4-12: Total heat flow versus length of beam extending from insulation face

For the selected shapes shown in Figure 4-12, the heat flow quickly approaches its limit. For heat flow within 1% of the asymptotic limit, the infinite length assumption for a W10x19 is approximately 16in. From these distributions, it is evident that there is little additional heat transfer associated with extending the length of the beams beyond this length. This length is compared against the textbook assumption for infinite length of a fin (see [87] for derivation):

$$L_{infinite\ length} \geq 2.65 \sqrt{\frac{kAc}{hP}} \quad (\text{Eq. 4-4})$$

This equation reduces to 15.9in. for a W10x19 with a cross-sectional area of 5.62in<sup>2</sup>, a perimeter of 35.98in., and  $k = 347 \text{ Btu} \cdot \text{in} / \text{hr} \cdot \text{ft}^2 \cdot ^\circ\text{F}$  and  $h = 1.5 \text{ Btu} / \text{hr} \cdot \text{ft}^2 \cdot ^\circ\text{F}$ . For many structural application this length is almost always achieved, and for many scenarios, the actual length may be several times the length it takes to achieve the infinite length assumption for heat transfer. Thus, all FEA simulations in this study used a length of two times the calculated infinite length to ensure that the total heat flow accurately predicts the heat flow associated with a beam of

infinite length. Figure 4-13 shows the temperature distribution along the surface of a W10x19 steel beam for an inside temperature of 1°F to the outside temperature of 0°F.

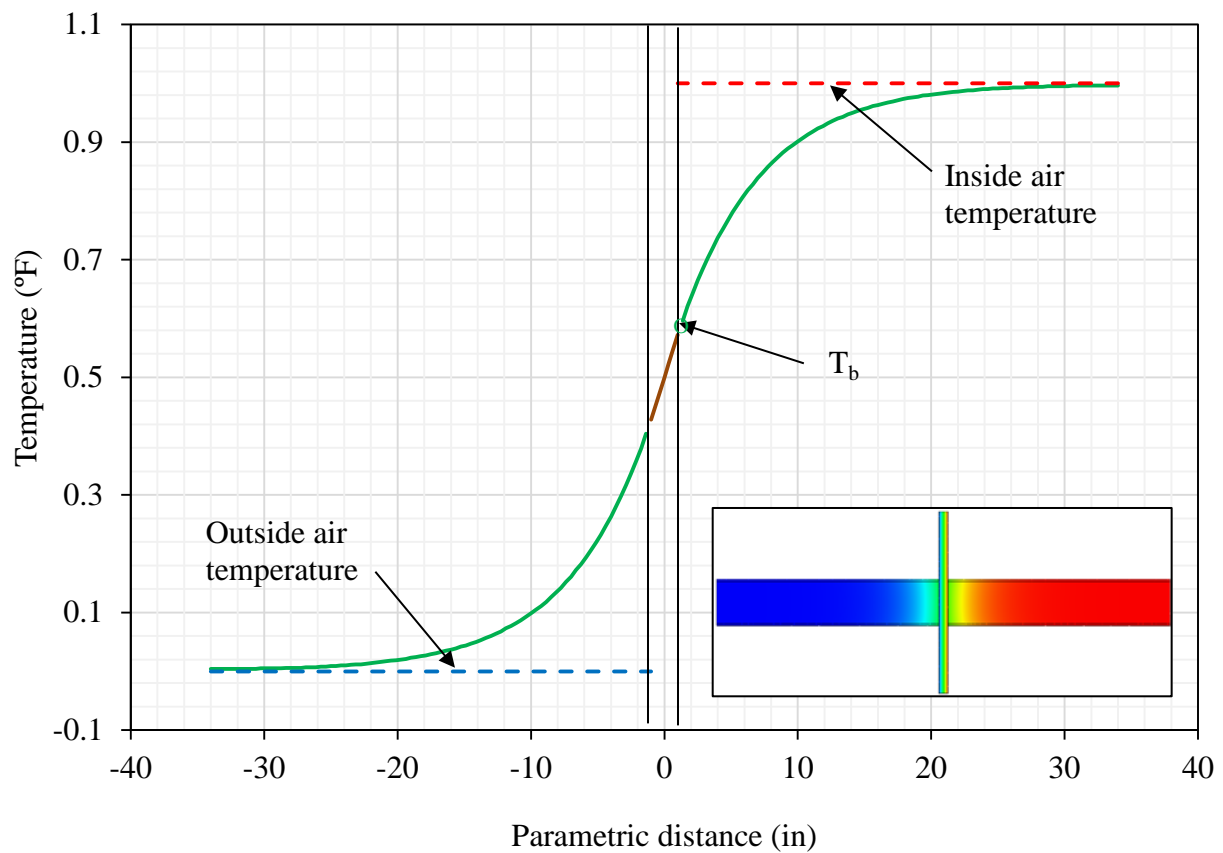


Figure 4-13: Temperature distribution along the surface of the beam flange

With identical surface heat transfer coefficients on both sides of the insulation, the temperature at the midpoint of the beam is the average of the environmental temperatures. The temperature along the beam inside the space occupied by the insulation is linear between an upper value nearing the indoor environmental temperature and a lower value that is nearer to the outside environmental temperature. Therefore, (Eq. 4-3) can be simplified to produce the modified general fin equation:

$$Q = \sqrt{hPkA_c} \left( \frac{T_i - T_o}{2} \right) \quad (\text{Eq. 4-5})$$

Continuous thermal bridge models, such as the one in Figure 4-9, were created for all steel wide-flange shapes ranging from W6x9 to W44x335 using 2in. thick insulation. The width and length of the insulation was fixed at 65in. by 65in. in all simulations to accommodate the largest sized beam. The results were used to determine base-line thermal transmittance values for each shape.

Figure 4-14 shows the relationship between the square-root of the perimeter times the cross-sectional area of several common steel beam shapes and the heat flow rate.

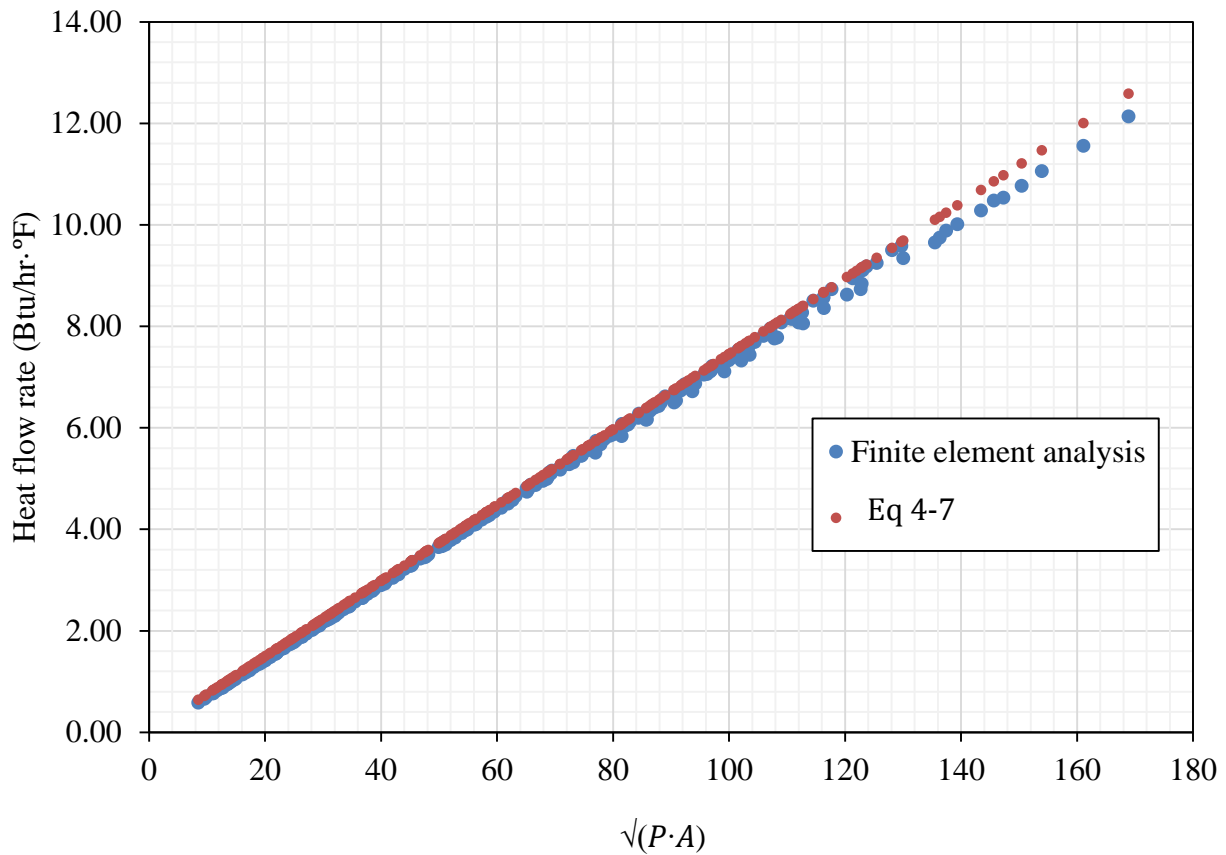


Figure 4-14: Relationship of heat flow rate to perimeter and area for all W-shapes

The results from the FEA simulations and the computed values are in good agreement. It is expected that the results would differ as the ratio of perimeter times the cross-sectional area is increased due to the assumption that  $T_b - T_\infty$  is approximately equal to the average of the indoor and outdoor temperatures. However, it was determined that selecting  $T_b$  as the average temperature of the indoor and outdoor temperatures will result in a slightly conservative estimate for the total heat flow of a symmetric fin. Increasing the insulation thickness and changing the

surface heat transfer coefficients, as well modifying any other assumptions, will all affect the resulting heat flow rate.

While Figure 4-14 provides a good indication on the linear relationship between the square root of the perimeter times the cross-sectional area and  $\chi$ -value, Figure 4-15, which indicates the relationship between the moment of inertia and  $\chi$ -value, may be more useful for structural engineers designing cantilever beam and column penetrations.

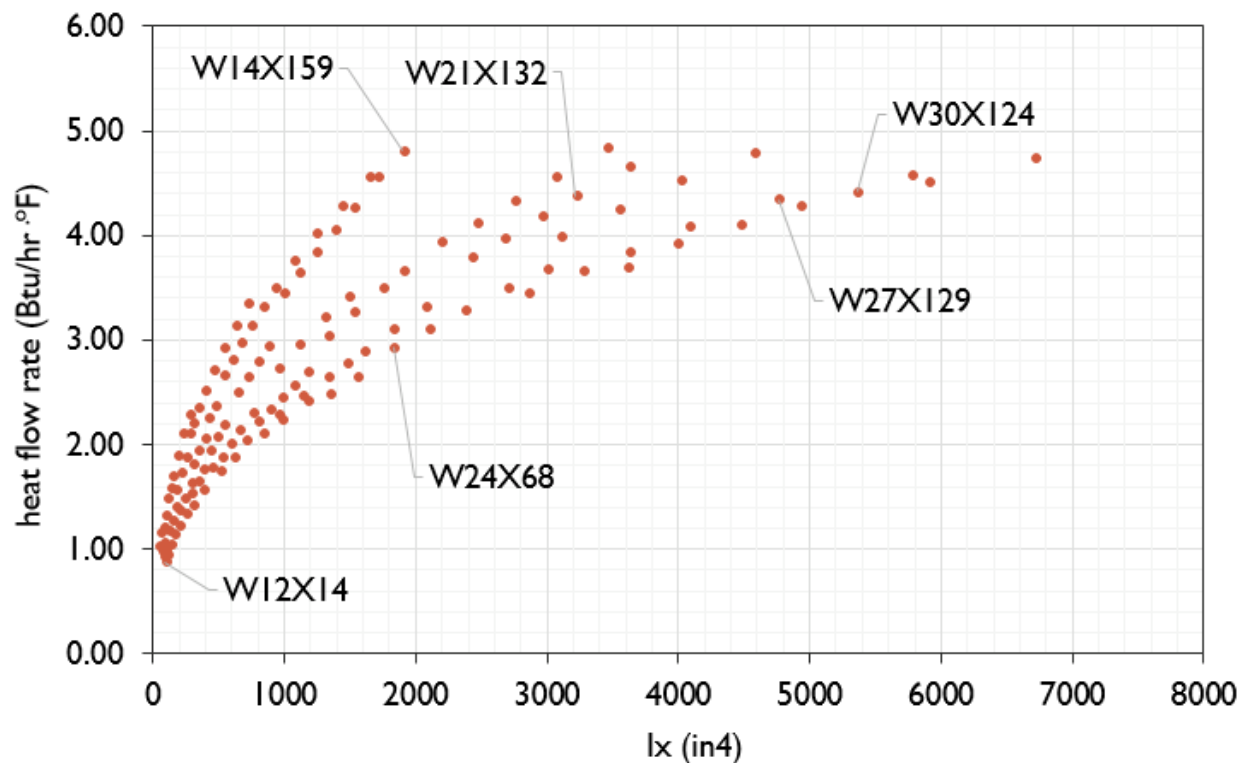


Figure 4-15: Comparison of heat flow rate and the area moment of inertia

Figure 4-15 can be used to determine the most thermally efficient shape for the necessary moment of inertia. Similar charts can be made available for other section properties, such as the elastic and plastic section moduli.

One of most common, and in some cases the only, method of dealing with structural steel beam thermal bridges is to surround the protruding beam with insulation, shown in Figure 4-16 (see Appendix A). This method serves to reduce the heat flow from the extended surface, and increase the exposed indoor surface temperature.



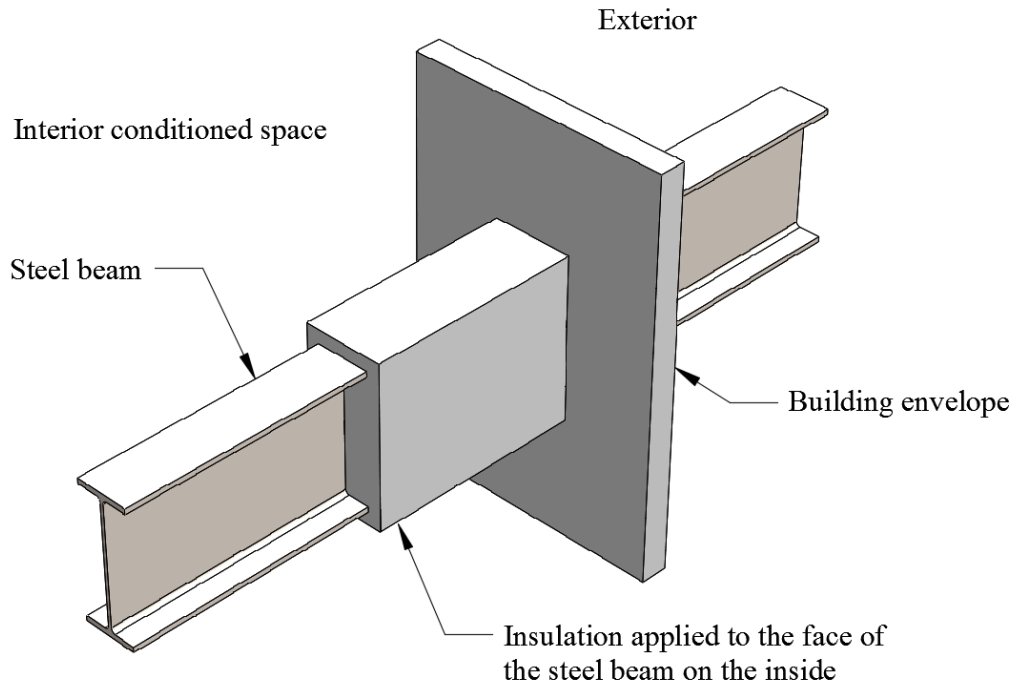


Figure 4-16: Covering insulation applied to an extended steel beam

Placement of insulation in a real-world building condition is highly dependent on architectural and requirements and space limitations. Steel beams, in addition to acting as structurally supporting elements, often serve as architectural highlights. Thus, insulation coverings may be in conflict with the architectural vision. Additionally, the nature of structural steel elements demands that they support some additional framework, such as floor slabs, mechanical dunnage, and exterior façade elements. Therefore, the application of additional covering insulation may not be a viable solution.

An ideal scenario, where a continuous beam penetrates a building envelope with a length that can be assumed infinite in both directions, is examined. In this model, a W10x19 steel beam penetrates a 2in. thick layer of insulation. An interior air temperature of 1°F and an exterior air temperature of 0°F were applied as the boundary conditions. Figure 4-17a shows the resulting temperature field and Figure 4-17b shows the heat flux. The heat flux field indicates the region of high heat flow, at which the beam would benefit most by the application of covering insulation. From the faces of the interior and exterior building envelope, additional insulation may be applied on the surface of the steel beam, of varying length and thickness.

Applying covering insulation at a thickness of 2in., and extending 12in. from each face of the wall insulation, to the region of greatest heat flux leads to the results shown in Figure 4-17c and Figure 4-17d.

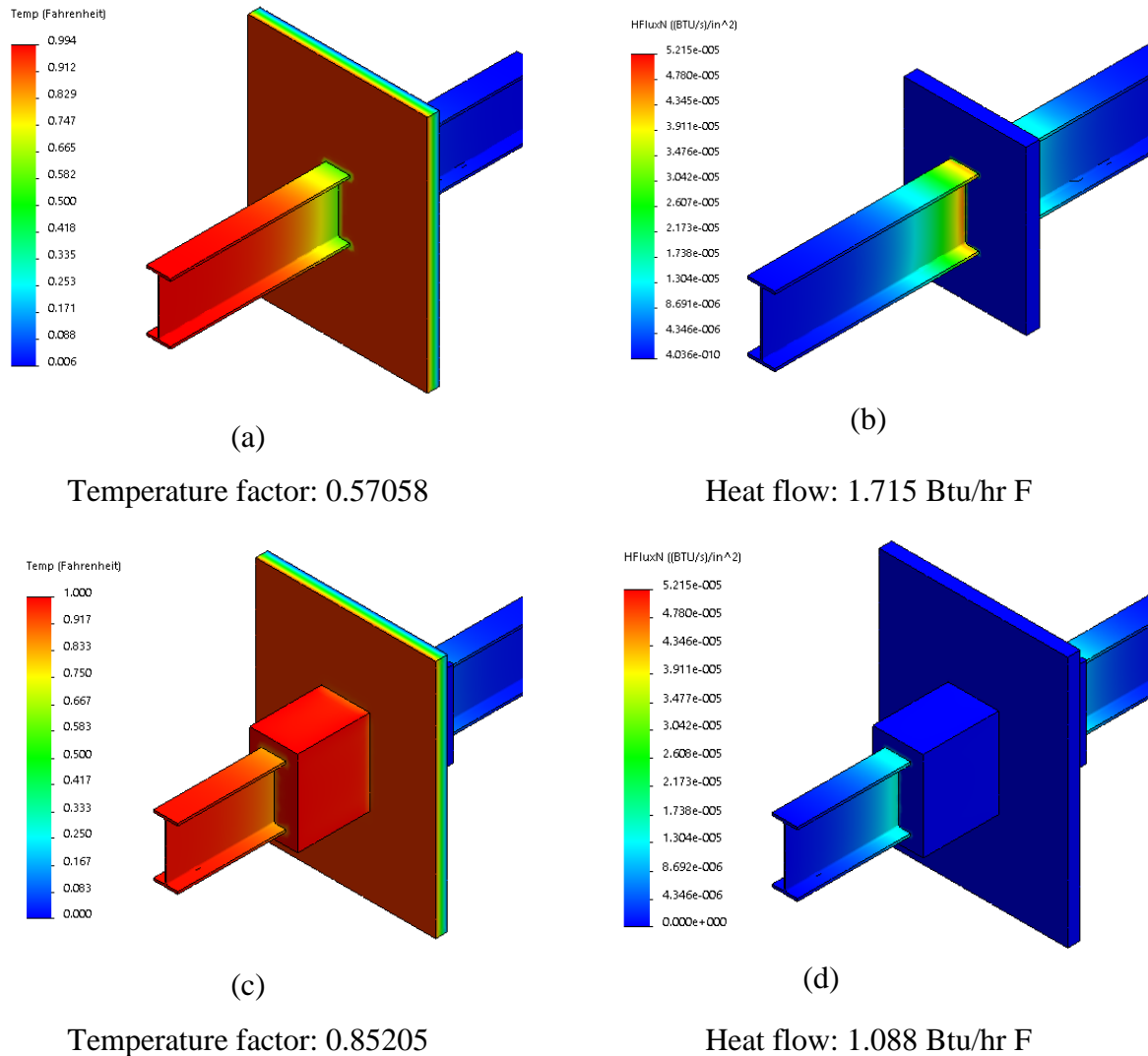


Figure 4-17: Temperature and heat flux for a continuous and covered beam thermal bridge

The temperature factor is increased significantly, from 0.57 to 0.85, and the heat flow is reduced 36.6 %, from 1.715 Btu/hr·°F to 1.088 Btu/hr·°F. Using the same method, insulation covering can be optimized for thickness and length by using the heat flux field from simulation data. Since the magnitude of the heat flux is parabolic along the length of the beam, similar to Figure 4-13, optimized insulation covering will follow the same magnitude in insulation thickness. Thus, an optimized covering for insulation would take the shape shown in Figure

4-18, which shows the temperature distribution of a continuous beam with insulation applied to the areas of greatest heat flux.

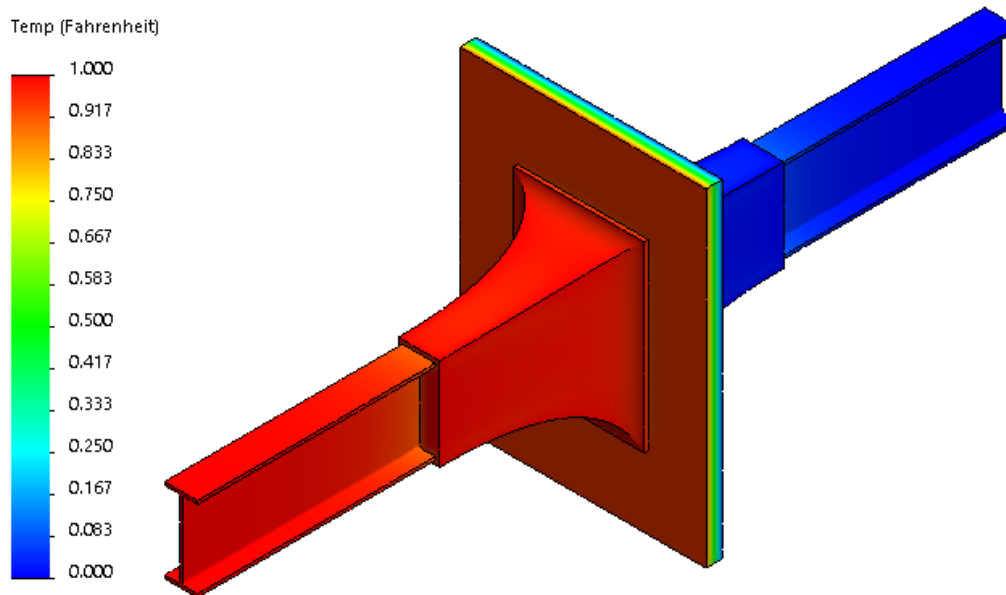


Figure 4-18: Optimum insulation covering. TI = 0.91. Heat flow = 0.927 Btu/hr °F

In this optimized scenario, the edges of the covering insulation were extended 20in. out from the face of the insulation, and 6in. out from the beam flange and web. The temperature index is increased to 0.91; sufficient enough to never warrant an issue with condensation, while the heat flow is reduced by 46 %, from 1.715 Btu/hr·°F to 0.927 Btu/hr·°F. Practical considerations, however, will obviously prevent the installation of covering insulation in the manner shown in Figure 4-18.

#### 4.4.1.2 Thermal break

This section presents the results of heat transfer simulations on an end-plate connection with various types and configurations of a thermal break. Thermal break strategies vary in more ways than thermal bridges can exist. Therefore, the thermal break configuration evaluated in this study involves a pad material placed between the faying surfaces of a structural steel connection. As stated previously, this is one of the most commonly used methods to implement a thermal break in a structural steel protrusion. These types of thermal breaks can be configured in a

variety of ways, depending on the thermal bridge and the demands of the thermal break. As such, the number of parameters becomes exceedingly large. Thus, only a few parameters were evaluated.

A representative beam end-plate connection, shown schematically in Figure 4-19, was designed following the procedure outlined in AISC Design Guide 16 [35].

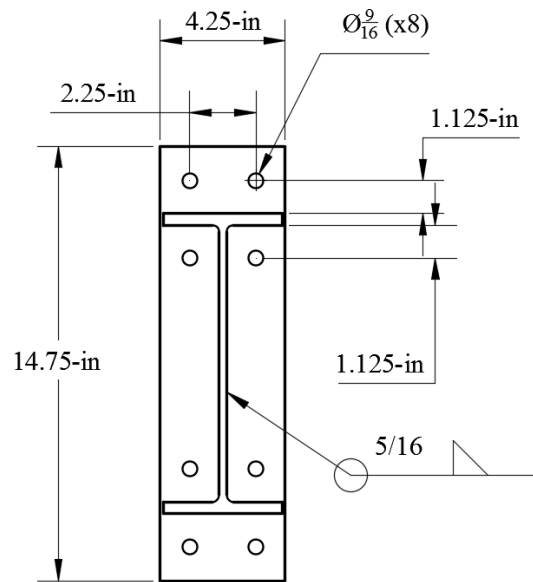


Figure 4-19: Beam-to-beam end-plate connection

The connection is a doubly-symmetric unstiffened 4-bolt end-plate moment connection that uses a W10x19 steel beam (A992 steel) with a 1/2-in thick steel end-plate (A572 Gr. 50 steel). The bolt holes are 9/16-in diameter. The dimensions of the end-plate measure 4.25-in by 14.75-in. The end-plate design uses a 5/16-in nominal weld using an E70XX filler metal to attach the end-plate to the end of the beam. Nuts used in the finite element model were simplified as cylinders with an outside radius of 0.88in. and an inside radius of 0.5in. Bolts were simplified in a similar manner, with a length determined using the minimum required bolt length for the grip thickness (AISC/ RCSC 2009, Table C-2.2, p. 16.2-13 [4]). The weld fillets were not modeled. These simplifications are assumed to have a negligible effect on the results of any analysis. The configuration of the three-dimensional finite element model is shown in Figure 4-20.

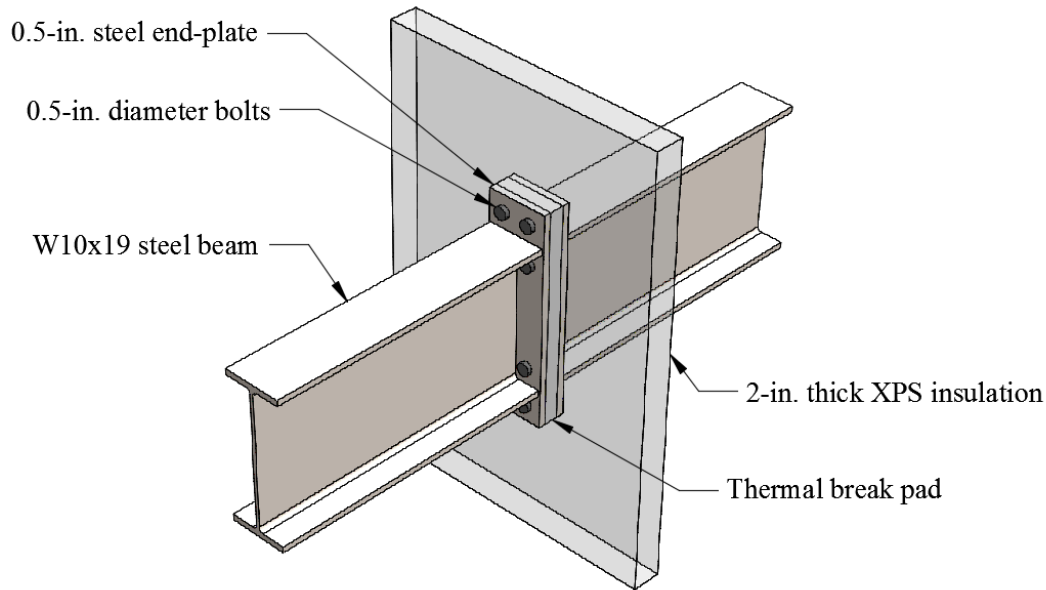


Figure 4-20: Finite element model of the thermal break connection

This type of thermal break was parametrically evaluated using a varying pad material and thickness, with all other dimensions and values fixed constant. Heat flow results are shown in Figure 4-21 for a thermal break pad of varying material and steel bolts.

When comparing heat flow rate between pad materials of the same thickness, it can be seen that an increase in the thermal conductivity of the thermal break material leads to an increase in heat flow. However, this increase is slight, with only a 6 % increase in heat flow between FRP and concrete, and 11 % increase between neoprene and FRP, for the 1in. thick pad. The difference in heat flow rate between pad materials is increased as the thermal break pad thickness is increased.

Contrary to the intent of the beam-to-beam end-plate thermal break pad connection, the heat flow for thin pads is higher than that of a continuous beam. This is due to the large surface area of the steel connection end-plates. In fact, for some configurations of a typical structural steel end-plate moment connection (such as this one), the cross-sectional area of steel in a continuous beam is less than the sum of the area of the bolts passing through the pad. This effect is not a novel finding, and has been investigated by other researchers [3], [15], [27]. However, this may not yet be common knowledge in the architectural community, as evidenced by common practices and marketing of structural thermal break pad materials and structural thermal break assemblies that employ a similar method.

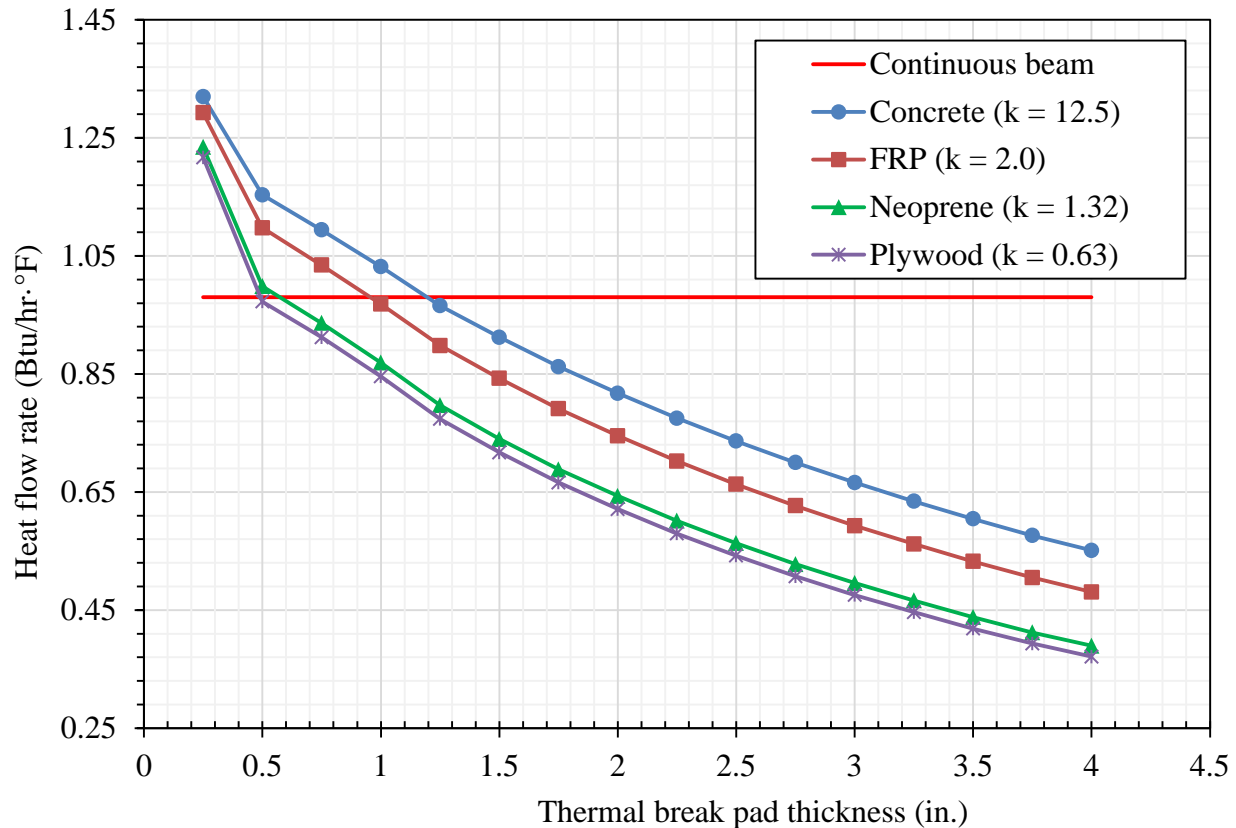


Figure 4-21: Comparison of heat flow rate and thermal break pad thickness

An increase in the pad thickness causes a downward trend to the heat flow rate through the thermal break. The negative effect of a beam-to-beam end-plate connection is overcome at a certain thickness of pad material, approximately 1.0in. for GRFP and 0.5in. for neoprene. However, increasing the thickness of the pad material can potentially conflict with structural limit states, notably deflection. For a moment connection, such as this modeled one, the rotation of the connection under load is an important design consideration, typically for user comfort and serviceability requirements. The additional rotation of the connection due to the presence of a thermal break within the connection can be significant, and will increase with increasing thickness of the pad. Also, an increase in the pad thickness can potentially lead to shear deflection within the thermal break that must be accounted for.

An analysis was performed with different bolt materials. Figure 4-22 shows a comparison between heat flow through a thermal break with different neoprene pad thicknesses and bolt materials, as well as the corresponding temperature index.

A significant improvement in heat flow for non-steel bolts is evidenced. Heat flow through a thermal break with a 0.5in. neoprene pad material is reduced by 20 % using stainless-steel bolts instead of steel bolts. Surface temperatures of a neoprene pad thermal break were compared against the continuous beam case. The right axis of Figure 4-22 compares the temperature index for a neoprene thermal break and the continuous beam case for different pad thicknesses. An improvement in the temperature index relative to the continuous beam is immediately noted, even at the 1/2in. pad thickness using steel bolts. For a 1in. neoprene pad, the temperature index is improved by 21 %. The minimum interior surface temperature for the thermal break is at the point where the bolt head is in contact with the steel plate, at the outer row of bolts. Thus, an improvement to the temperature index can be made by applying covering insulation to the bolts, nuts, and exposed end-plate steel.

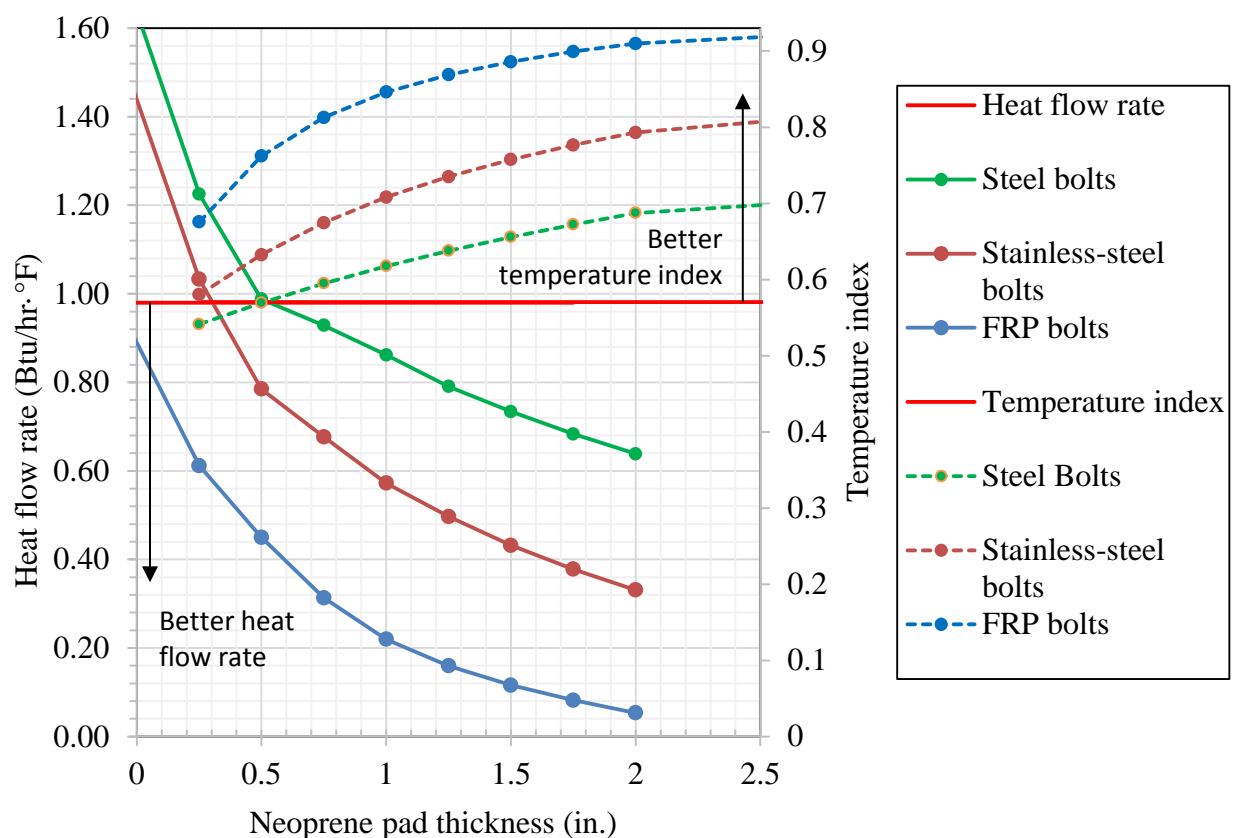


Figure 4-22: Comparison of heat flow against neoprene pad thickness for different bolt types

Figure 4-23 illustrates the heat flow in the bolts by comparing the total one-dimensional heat flow in the bolts to the heat flow through the thermal break.

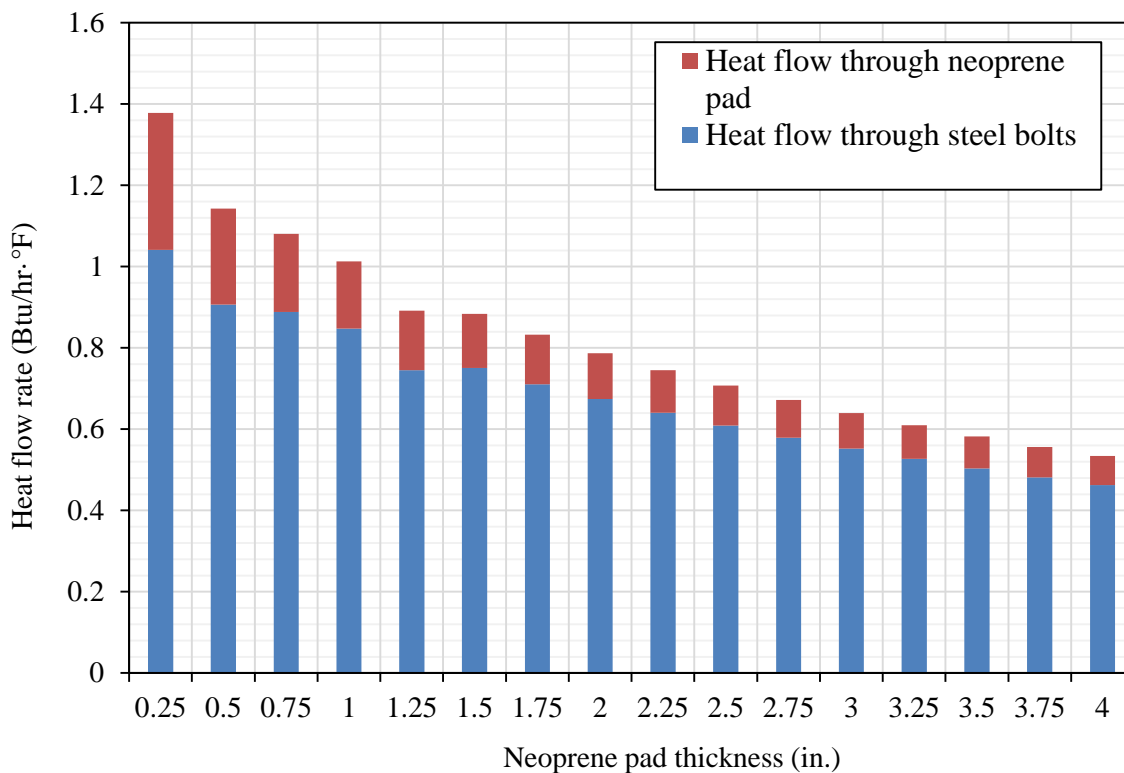


Figure 4-23: Comparison of heat flow through the pad material and steel bolts

This condition, where an increase in the thickness of the pad material provides a diminishing return in heat flow, is similar to the overall diminishing return of increasing the insulations thickness in a region of a thermal bridge, as shown in Figure 4-10. The results of this analysis conclude that the majority of heat flow exists in the bolts, rather than the pad material. To put it another way, bolts are the thermal bridge in the thermal break. Any decrease in the thermal conductivity of the bolts provides a significant return in decreased heat flow. Thus, in a structural engineering sense, it can potentially be more beneficial to use a pad material with a higher thermal conductivity and higher stiffness, while decreasing the strength of the bolts by using FRP or stainless steel bolts. These tradeoffs, however, are highly dependent on the structural requirements of the thermal bridging details, and must be made on a case-by-case basis.



#### 4.4.1.3 Comparison with Experimental Testing

The results of both measurements and finite-element analysis are presented in Table 4-3. The percent difference between results is also provided in Table 4-3.

Table 4-3: Comparison between experimental and finite-element analysis results

| Specimen description                   | Measured heat flow<br>(Btu/hr °F) | FEA heat flow<br>(Btu/hr °F) | Percent difference<br>(%) |
|--|-----------------------------------|------------------------------|---------------------------|
| XPS insulation (no thermal bridge)     | 1.02 ± 0.03                       | 0.985                        | -3.4                      |
| Continuous beam                        | 1.98 ± 0.03                       | 1.961                        | -1.0                      |
| End-plate connection (no pad)          | 2.27 ± 0.03                       | 2.399                        | +5.7                      |
| 0.5in. neoprene, steel bolts           | 2.01 ± 0.04                       | 2.082                        | +3.6                      |
| 0.5in. neoprene, stainless-steel bolts | 1.95 ± 0.06                       | 1.914                        | -1.8                      |
| 0.5in. FRP, steel bolts                | 1.99 ± 0.07                       | 2.100                        | +5.5                      |
| 0.5in. FRP, stainless-steel bolts      | 1.92 ± 0.03                       | 1.954                        | +1.7                      |
| 1.0in. neoprene, steel bolts           | 1.85 ± 0.05                       | 1.945                        | +5.1                      |
| 1.0in. neoprene, stainless-steel bolts | 1.72 ± 0.04                       | 1.707                        | -0.8                      |
| 1.0in. FRP, steel bolts                | 1.91 ± 0.03                       | 1.964                        | +2.8                      |
| 1.0in. FRP, stainless-steel bolts      | 1.80 ± 0.03                       | 1.749                        | -3.3                      |
| 1.5in. neoprene, steel bolts           | 1.75 ± 0.05                       | 1.913                        | +9.3                      |

Of interest is the percent difference between the measured and FEA values, which occurs because of the result of experimental construction flaws and FEA assumptions and simplifications. It is expected that the XPS insulation and the continuous beam specimens would provide the most accurate results, due to the simplicity of their construction and assembly. Therefore, the results for the XPS insulation and continuous beam tests will give the best possible comparison between measured and FEA results. This comparison, however, will not be consistent between specimens, as the thermal break connection provides additional complexity in construction assembly.

The constructed thermal break assembly is fitted in a rectangular space in the XPS insulation sheet and the gap between the steel end-plates and the insulation is filled with expanding foam. The thickness of the expanding foam in the gap was not precisely controlled,

and left to expand and fill the 2in. gap, allowing overflow. The expanding spray foam has a thermal conductivity slightly higher than the XPS insulation, which may reduce the overall measured heat flow. Additionally, it is expected that since the bolt diameter is 1/16in. smaller than the holes in the end plates and pad, some additional contact resistance is provided which, is not accounted for in the FEA model, where the hole perimeter and bolts are assumed to be bonded with no contact resistance. The total contact resistance through the thermal break assembly is increased with additional plies of end-plates, bolts, and thermal break pad materials in a way that cannot be precisely or accurately implemented in the FEA model.

It is not immediately clear from Table 4-3 whether the FEA values under- or overestimate the measured heat flow. It is expected, however, that due to the simplifications in geometry of the model, and the assumption that the surface heat transfer coefficient is constant on all exposed surfaces, the FEA should overestimate the heat flow, and for most specimens, that is the case. In all the cases with steel bolts, the heat flow was overestimated in the finite element model. This could be due to several factors, among them The cause of this is almost certainly the additional thermal resistance provided by contacting faces. For the simulations that underestimate the heat flow, three of the four tests use stainless steel bolts. A possible conclusion that can be drawn from this observation is that perhaps the value for thermal conductivity of the stainless-steel bolts in the FEA model may need to be adjusted.

Surface temperatures along the beam are shown in **Error! Reference source not found..** Surface temperatures are in good agreement, although it seems that the finite element model tends to underestimate and overestimate the surface temperatures on the hot and cold side (respectively). This is almost certainly a measurement error due to radiative heating of the temperature sensors from the surrounding enclosure. The temperature sensors were attached to the face of the steel without any protective coatings.

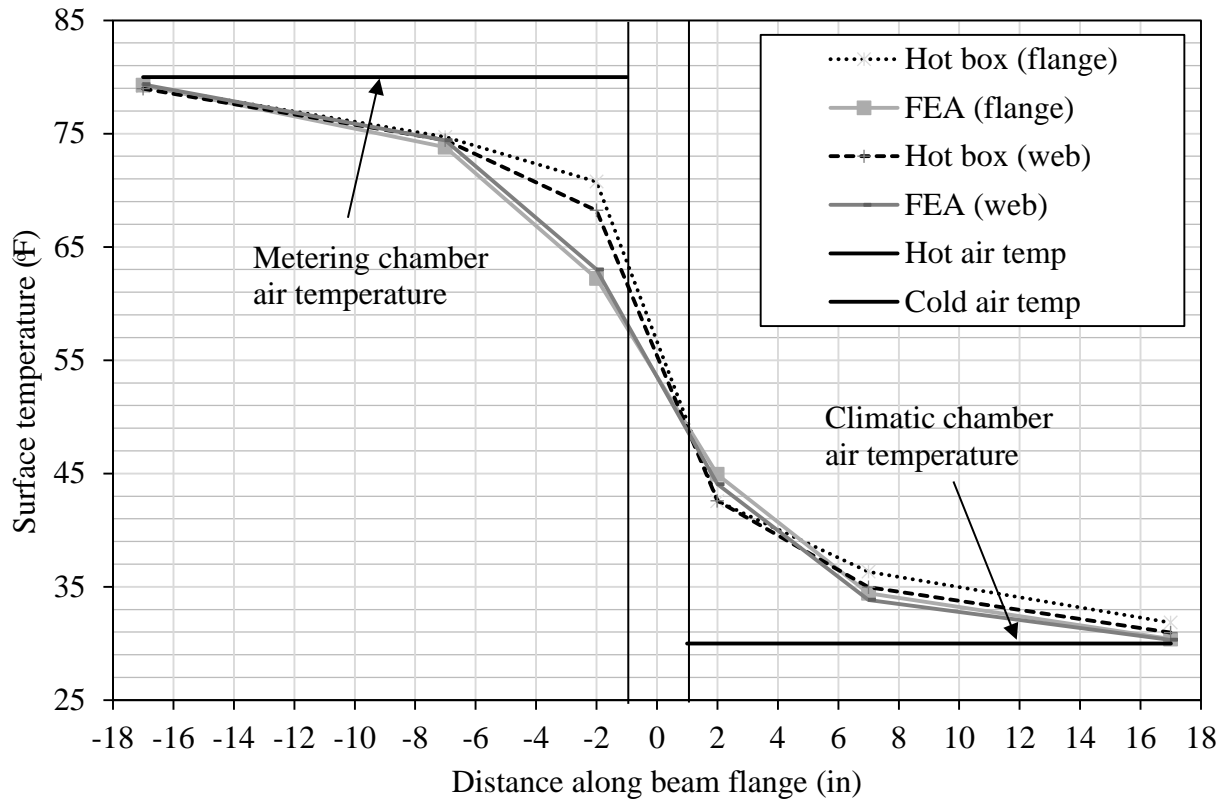
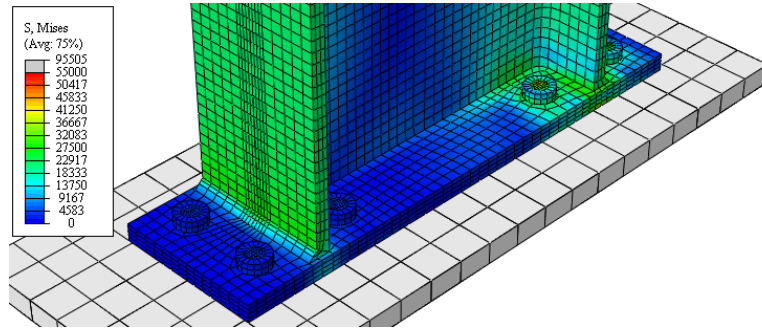


Figure 4-24: Comparison of surface temperatures along the beam for continuous beam test

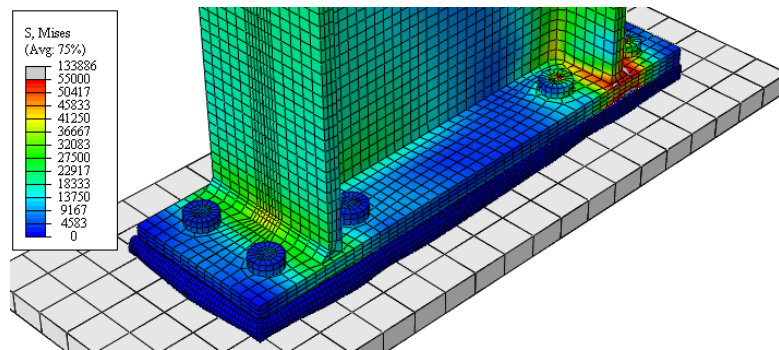
For the most part, the experimental results are in relatively good agreement with FEA results. Without a complete and thorough analysis of the air velocity in the hot box, the surface heat transfer coefficient on each surface of the thermal bridge, the radiative heat transfer component and its contribution to the overall heat transfer coefficient, as well as an experimental measurement of the thermal conductivity measurement of each material, and the contact resistance between mating surfaces, the assumptions made to develop the FEA simulations in this study are considered to be reasonably accurate.

#### 4.4.2 Mechanical Behavior

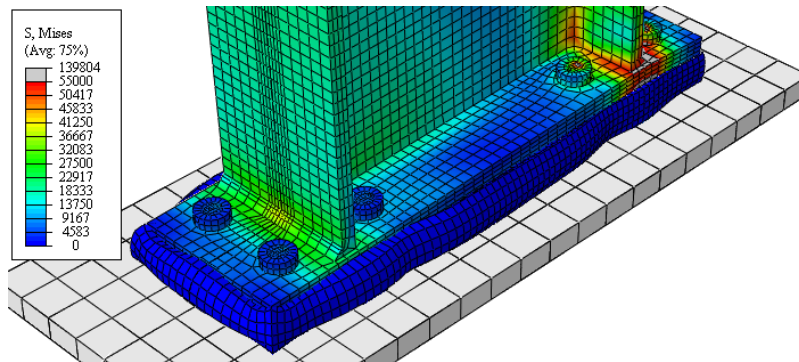
Figure 4-25 shows an overview of the compression region of each connection showing the von Mises stresses.



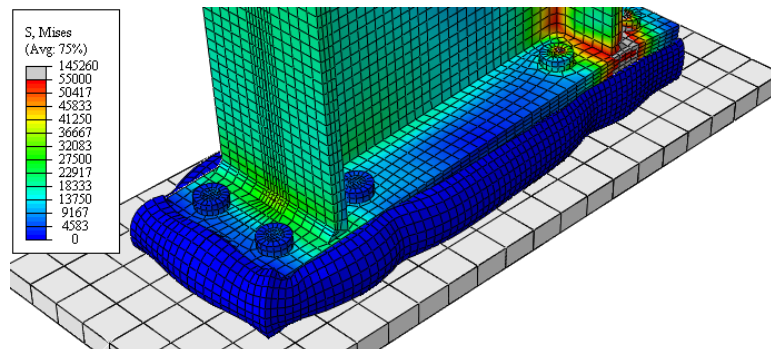
(a) No neoprene



(b) 0.5in neoprene



(c) 1.0in neoprene



(d) 1.5in neoprene

Figure 4-25: Deformed isometric view of each connection.

Validation of the finite element model was performed by comparing the results with the experimental test data discussed earlier in the text. Moment-rotation curves were determined from the finite element analyses using the force applied to the beam at 45.9-in from the column face and multiplying it by the moment arm. Rotation data was determined in the same manner as that of the experimental bending test; by using the displacement of the beam at 12-in. from the column face and applying it to  $\theta = \tan^{-1}(d/12)$  to determine the rotation of the connection. Since beam bending and shear deflections are accounted for in the finite element model, it was not necessary to offset these additional deflections. Hence, deflections and forces were directly compared against each other. The moment-rotation curve for the steel end-plate connection is shown in Figure 4-26.

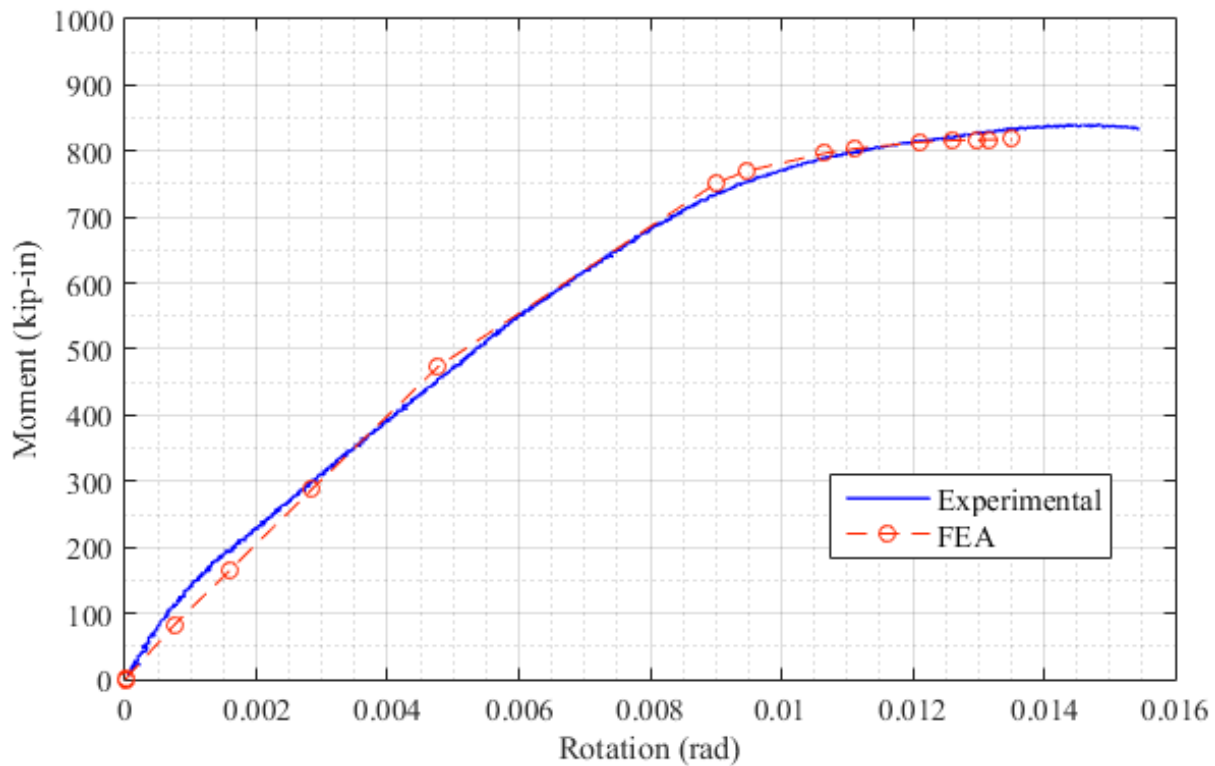


Figure 4-26: Experimental and FEA moment-rotation curves for steel connection

A good correlation between experimental and finite element moment-rotation curves was found. It can be seen that the initial stiffness of the finite element model slightly underestimates the experimentally determined curve, although the discrepancy diminishes at an increasing

moment. For the modeled connection, the post-yield rotational stiffness of the connection is highly dependent on the bolt geometry and material definition, as well as the end-plate bending stiffness. Yield and post-yield material definitions are integral to the results of the post-yield behavior of the connection, especially so for this modeled connection. The connection was constructed and designed to use a thick end-plate in order for bolt rupture to control the failure mechanism, which occurs prior to plate yield. Therefore, the stiffness of the connection is highly dependent on the stiffness of the tension region, which is predominantly controlled by the elastic bending deformation in the plate, and the inelastic (post-yield) behavior of the tension bolt group. Reasonably accurate assumptions made in this study indicate that the predicted values of yield stress and strain, as well as post-yield nonlinearity, closely approximate the experimental conditions.

A comparison between experimental and finite element moment-rotation curves was made for all the bending tests, shown in Figure 4-27.

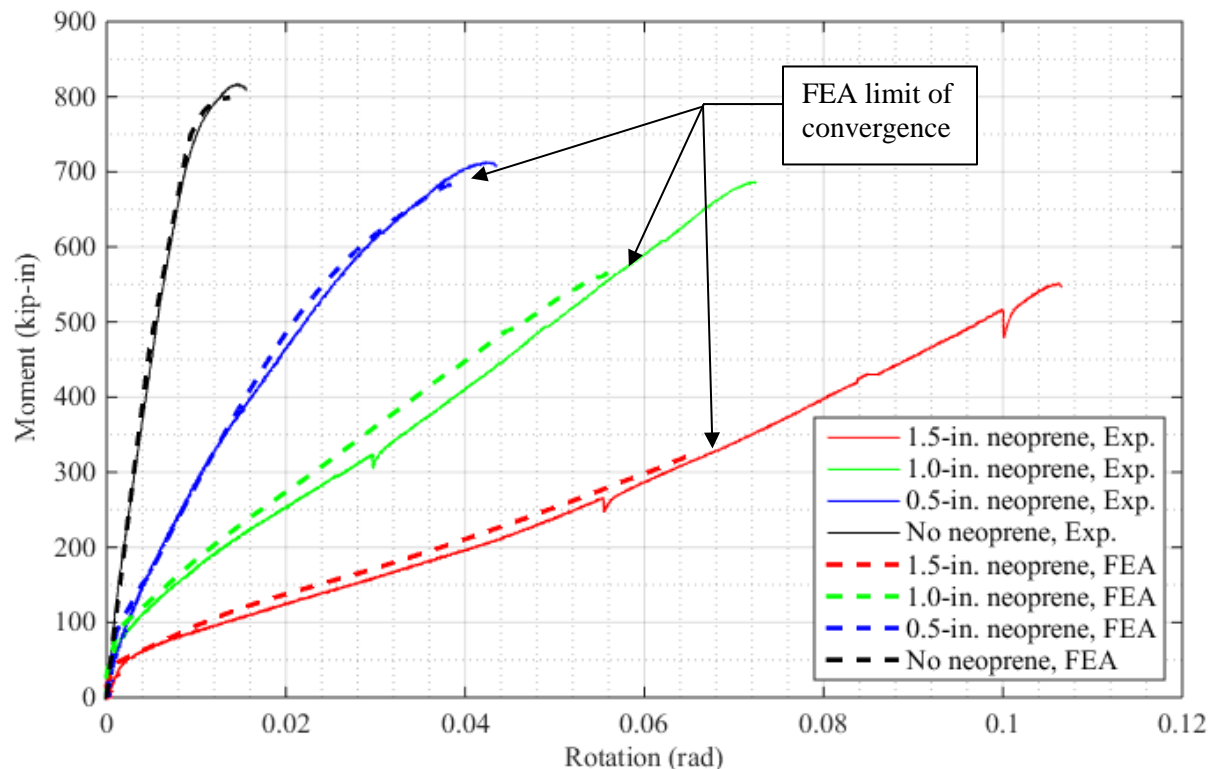


Figure 4-27: Experimental and FEA moment-rotation curves all bending tests

Reasonable agreement was found between the experimental finite element analysis moment-rotation curves. Finite element analysis convergence proved difficult, due to excessive deformation of elements in the neoprene pad resulting in termination of the analysis before reaching the end of the defined step. Hybrid formulation, fully-integrated elements, and adaptive meshing techniques were used to progress the solution further towards completion of the loading step, but complete experimental reproduction was not possible using these techniques. Regardless, finite element analyses show that the assumptions and approximations made in the model result in remarkably good agreement with experimental results.

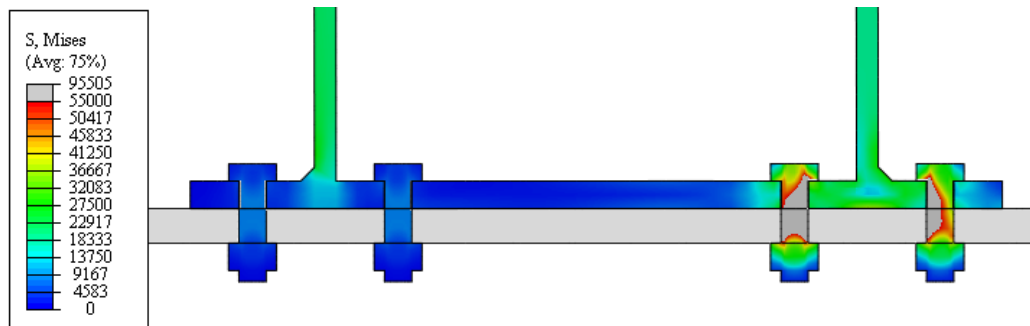
Failure of steel elements in the connection can be reasonably predicted using the von Mises stress criterion. The von Mises stress represents the stress in the material corresponding to von Mises failure (yield) theory. In this theory, yielding occurs for a complex stress state when the von Mises stress, defined by Equation 4-12, at any point in the material becomes equal to the yield stress from a simple tension test.

$$\sigma = \sqrt{\frac{(\sigma_1 - \sigma_2)^2 + (\sigma_2 - \sigma_3)^2 + (\sigma_3 - \sigma_1)^2}{2}} \quad (\text{Eq. 4-6})$$

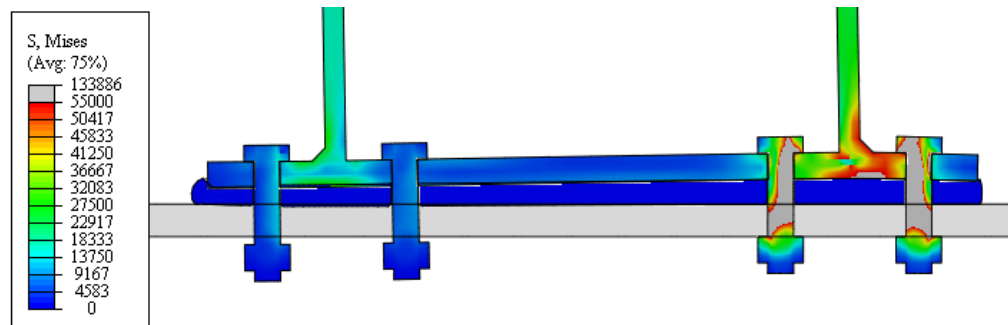
where  $\sigma_1$ ,  $\sigma_2$ ,  $\sigma_3$ , are the maximum, intermediate, and minimum principal stresses, respectively.

Figure 4-28 shows a cross-sectional cut through the connection and the resulting von Mises stresses under an applied moment of 200-kip·in for each thickness of neoprene. Of interest is the tension region in the end-plate. It can be seen that under the same applied moment, the stresses in the tension flange region are much greater for the cases with a neoprene pad.

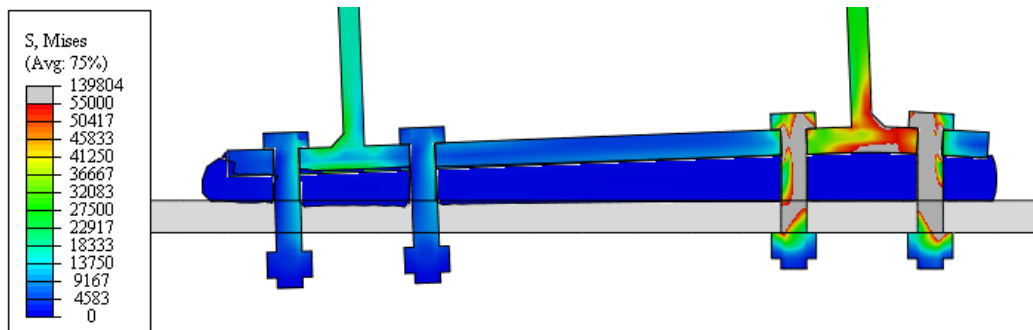
Stresses in the bolts were investigated in the finite element model results. Figure 4-29 shows the von Mises stresses in bolt 8 (outer row of tension bolt group) of the connection for each test with no deformation scale for an applied moment of 200 kip-in.



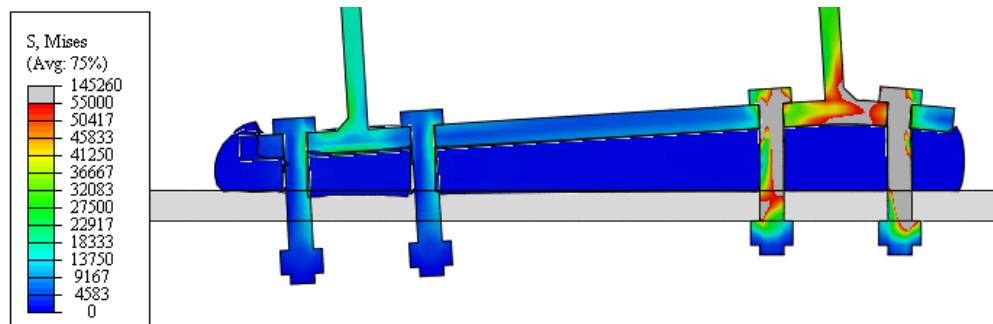
(a) No neoprene



(b) 0.5-in. neoprene



(c) 1.0-in. neoprene



(d) 1.5-in. neoprene

Figure 4-28: Deformation of connection for each thickness of neoprene.



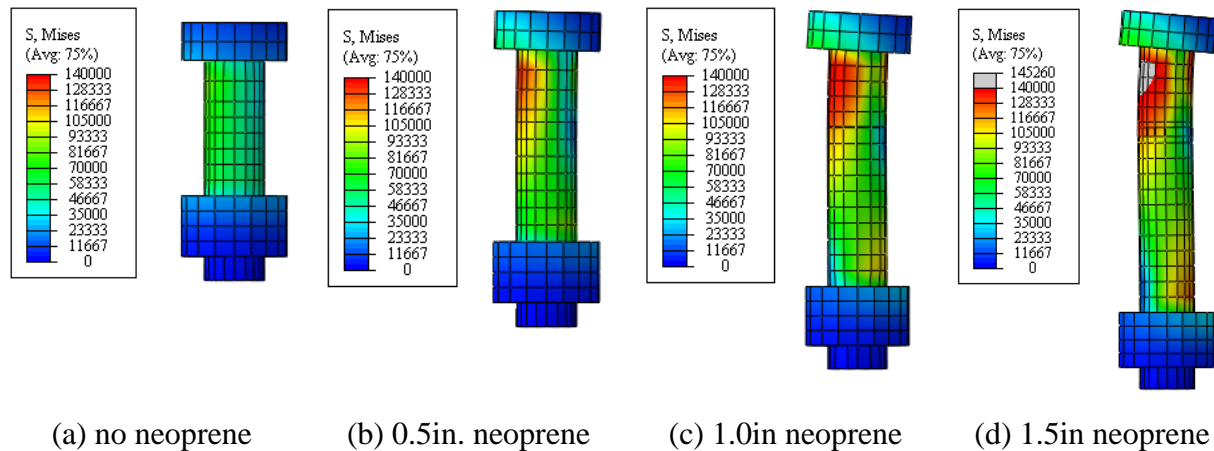


Figure 4-29: von Mises stress distribution in bolt 8 at 200 kip-in applied moment.

Under an identically applied moment, maximum stresses in the bolt are increased as the neoprene pad becomes thicker. It is clear that the additional rotational capacity of the connection due to the elastomeric pad produces prying forces on the tension group of bolts

Comparison between experimental and finite element deformation of the neoprene is compared in Figure 4-30.

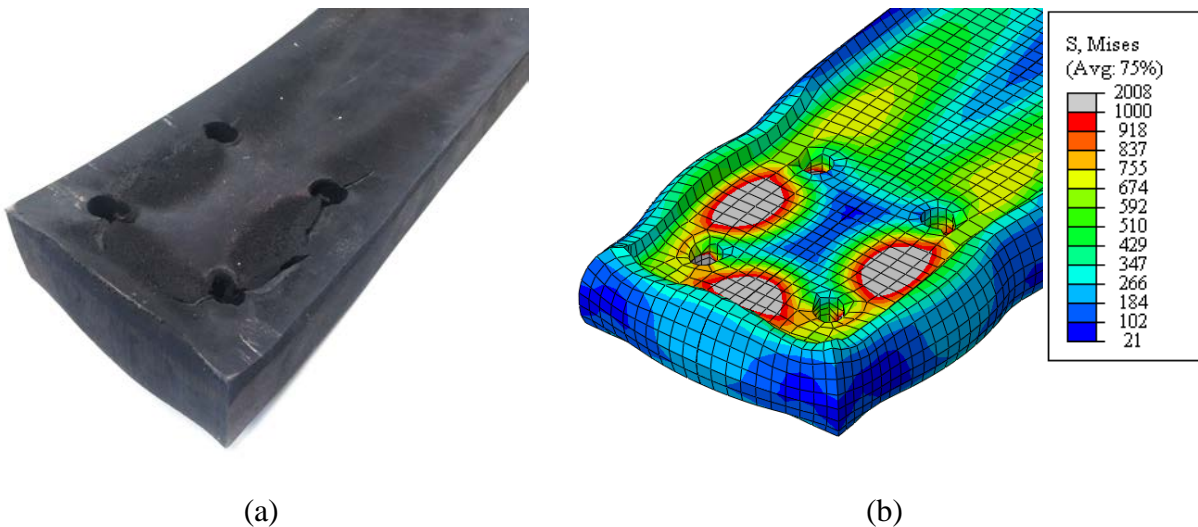


Figure 4-30: 1.5-in. neoprene pad for (a) experimental bending and (b) FEA stresses

It is seen that high stresses occur in the regions between adjacent holes. In bridge bearing pad design practice, holes in elastomeric bearing pads are strongly discouraged by American

Association of State Highway and Transportation Officials (AASHTO) for this very reason, because they increase the free area where the elastomeric pad can bulge leading to localized stress areas in regions near the bolt holes.

Failure criteria in elastomers are difficult to define. No unified criterion exists for predicting the rupture of elastomers under multiaxial loading conditions [88]. However, bridge bearing pad design authorities, namely AASHTO, have set forth limits on the maximum compressive stresses in plain and reinforced bearing pads. These limits, however, are derived from experimental research performed for the specific purpose of determining suitable limits for bridge bearing pad conditions. It is well known that the friction coefficient, the shape factor and other parameters significantly affect the resultant stresses in an incompressible material. In many ways, bridge bearing pad design principles are similar to those of steel connections with an intermediate bearing pad. However, the practice of simply placing an elastomeric pad between the faying surfaces of a connection differs from the application of design procedures for bridge bearing pads to be applied to structural steel moment connection due to the yet un-researched parameters such as large rotations, prying action due to large rotations, and holes in the elastomeric pad. Simply, the design practices of bridge bearing pads cannot be carried over to structural steel moment connection without further research.

#### **4.5 Limitations**

The experimental results of the calibrated hot box were in relatively good agreement with numerical heat flow analysis results. However, the constructed thermal bridge specimens were idealized, namely, using only a 2-in. thick layer of XPS insulation to represent the continuous insulation layer. In reality, typical building envelope constructions have several layers of insulation, through which the thermal bridge or thermal break protrudes. The additional layers of insulation can have an impact on the resulting heat flow. A plethora of thermal bridge and thermal break detailing scenarios exist, many of which must be idealized in order to represent archetypal conditions. Experimental testing on every possible permutation of thermal bridge or break is not possible, nor is it helpful to engineers and architects. Finite element heat transfer, however, can be applied to specific design details. Regardless, when considering numerical results and experimental test results, it should be noted that the assumptions made in the

experimental test conditions and validated by the finite element simulations may not represent the actual constructed conditions of the thermal break.

Heat transfer finite element analyses were performed on idealized thermal bridging and thermal break configurations. Numerous parameters can all affect heat flow through a thermal bridge, and these parameters can either contribute to the effectiveness of a thermal break solution, or reduce it. For example, the surface heat transfer coefficient can have a large effect on the resulting heat flow, and depending on the conditions of the thermal bridge or break, this one parameter can make the difference between an effective or ineffective thermal break. Constant surface heat transfer values were used in the heat transfer simulations, which were appropriated from ASHRAE design values. Although deemed reasonable for typical wall constructions, a thermal bridge or thermal break has exposed surfaces of varying orientations, sizes, and coverings and may have different values.

Similarly, the structural tests were also limited, with experimental and numerical tests performed on a single type of thermal break connection. Thermal breaks can employ a variety of gasket materials, thicknesses, geometries, and many other parameters, and the variety of steel connection types, bolts, and steel materials that make up a thermal break assemblage can all affect the resulting mechanical behavior. Therefore, extrapolation of results from the study performed in Chapter 4 is extremely limited, and cannot be promulgated towards other thermal break configurations. In lieu of costly experimental testing, parametric finite element analysis can be performed on various thermal break configurations. However, finite element modelling has its own limitations, requiring the input of simplified material behavior, geometry, loading conditions, etc., which makes it difficult to produce recommendations based on finite element analysis alone.

The cost efficiency of thermal break implementation was not investigated in this project. The general assumption of a thermal break is that it should reduce heat flow, effectively reducing the cost of conditioning the structure. Speculatively, however, the payback period of the additional cost in implementing a thermal break strategy into the structural design may not be reached in the lifetime of the structure, making the thermal break option an unnecessary expenditure of resources.

THIS PAGE INTENTIONALLY LEFT BLANK

## Chapter 5: Conclusions and Recommendations

### 5.1 Hot-Box

A constructed hot box was constructed, calibrated, and utilized to experimentally determine the point transmittance value of a continuous beam and thermally broken structural steel connections with reasonable accuracy. The thermal conductivity value of a 2in thick XPS panel was determined using this hot box, resulting in accurate results compared to the manufacturer specified value. The thermal bridge and thermal breaks tested using this hot box were compared to a simplified three-dimensional finite element model and resulted in relatively good agreement. The finite element model predicted the  $\chi$ -value of the thermally broken connection with steel bolts to be higher (1.96 versus 1.91 Btu/hr·°F), and lower for the stainless-steel bolts (1.75 to 1.80 Btu/hr·°F) resulting in percent differences of two, over and under, respectively. The simplification of the finite element model is likely the cause, as there are several additional thermal resistances (i.e. resistance between touching faces), whereas the model did not account for such interactions. The model also assumes a constant and identical value for the surface heat transfer coefficient on both sides, whereas the in the constructed hot box that was likely not the case. The assumed surface heat transfer coefficient value lumps the radiative heat transfer component with the convective component. This contributes to the error, as the radiation heat transfer component is a function of the measured surface temperatures; the measured surface temperatures of a thermal bridging specimen can be significantly different from the enclosure air temperature. Overall, the idealized finite element heat transfer model was shown to agree relatively well with experimentally determined values using the constructed hot box.

### 5.2 Structural Testing

The behavior of a steel end-plate moment connection with an intermediate neoprene pad placed between the faying surfaces of the plate and column was investigated. The end-plate connection was tested in bending using a cantilever configuration, and in shear with bolts in double-shear. Each experimental test was conducted using three different thicknesses of

neoprene, 0.5-in, 1.0-in, and 1.5-in, as well as an unaltered test case without neoprene. Finite element analysis was performed and results were validated against the experimental bending test.

Experimental testing revealed that the introduction of a neoprene pad within an end-plate connection significantly reduces the following quantities:

- Rotational stiffness
- Ultimate strength
- Shear stiffness

The rotational stiffness of end-plate connection with a neoprene pad decreases approximately linearly as the thickness of the neoprene pad increases. The initial rotational stiffness of an end-plate connection is a function of the bolt pretension and the apparent compression stiffness of the neoprene pad. Once the pre-load on the compression bolts is lost, the resulting rotational stiffness increases linearly up to bolt rupture.

An end-plate connection with a neoprene pad reduces the ultimate strength of the connection. Bolt rupture occurs at less than the ultimate applied moment of an unaltered connection, and decreases with increasing pad thickness. Because the rotational stiffness of an end-plate connection with a neoprene pad is linear past the initial stiffness, **bolt rupture occurs without prior warning.**

It was revealed that the neoprene pad undergoes significant deformation and damage near the compression flange region. Tearing occurs at the bolt holes, as well as the regions between adjacent bolt holes due to the incompressibility of the neoprene material.

The shear stiffness of a bolted end-plate connection decreases as the thickness of the neoprene pad is increased. Shear stiffness decreases exponentially with increased neoprene pad thickness. Significant bending of the bolts occurs with increased neoprene pad thickness. Bending in the bolts closely approximates a member fixed at each end with applied displacement at one end.

Comparison of experimental results with finite-element analysis determined that a well-defined and calibrated finite-element analysis model can reasonably predict the rotational stiffness of an end-plate connection with a neoprene pad.

Results of the experimental testing and finite element analyses lead to the conclusion that the behavior of structural steel connection in combination with low-stiffness bearing pad is

complex, and further research is required before guidance can be put forth towards recommendations for applying such connections in construction practices.

While there can exist a variety of configurations of thermally-broken connections, the extensive research performed on quantifying end-plate behavior and the research performed on neoprene and rubber bearing pads in the structural bridge industry suggests that further research be performed to develop understating of the behavior of bearing pad end-plate connections using developed elastomeric design practices from the bridge bearing industry. However, based on the results of this study, thermally-broken structural steel moment connections using elastomeric bearing pads cannot be recommended for use, because they pose the risk of sudden failure if the localized and excessive stresses due to holes in the elastomeric pad, excessive rotations leading to prying action and yielding of steel elements, and time-dependent creep and relaxation deflections, and many other yet unknown parameters are not considered in the design. Additional research must be performed before thermally broken moment connections using elastomeric pads are to be considered for use in structural applications.

### **5.3 Finite-element Modeling**

Structural steel thermal bridges often occur in steel frames in the form of linear or point penetrations through the building envelope. While linear thermal bridges typically provide a greater source of heat loss than point penetrations overall, extended steel beams and columns that protrude through the insulation and beyond act as fins, increasing heat flow and reducing the interior surface temperature in the area around the thermal bridging element. Thermal bridging at structural steel point penetrations is generally mitigated by covering the exposed steel with insulation or by installing a thermal break pad or proprietary thermal break assembly. This study presents steady-state analyses of a continuous beam thermal bridge and a thermal break with several pad materials, thicknesses, and bolt materials, and compared heat flow rate results with experimentally determined values.

It was found that experimentally determined heat flow values closely agreed with finite element heat flow rates. Finite element results showed that for extended single point thermal bridges, the heat flow rate,  $\chi$ -value, can be determined by using Eq. 3-8 with ASHRAE values for the convective heat transfer and thermal conductivity of the bridging element. It was found

that without thermal break action, reducing the perimeter and/ or cross-sectional area of the bridging element will provide a linear reduction in heat flow. That is not to say that reducing the cross-sectional area of the high conductivity material passing through the building envelope, then enlarging it again beyond the plane of insulation is effective, since the increase in perimeter and area beyond only serves to increase heat flow through the bridge due to the fin effect. For example, a reasonable application of the results of this study would be to use an HSS section instead of a W-shape. An HSS is efficient thermal bridging since the cross-sectional area can be increased (by increasing the wall thickness) to add strength or stiffness while the perimeter that is exposed to air flow remains roughly the same. That is assuming that the interior cavity of the HSS is either capped or filled with insulation. In situ thermal bridges, or unavoidable structural bridging members, can be alleviated by applying insulation around the thermal bridge. **It was found that heat flow through a continuous beam thermal bridge is reduced significantly with the application of covering insulation. Covering insulation also increases the temperature index significantly.**

Results for a thermally-broken connection using a low-conductivity pad show that the process of segmenting the beam, welding end-plates, and bolting a low-conductivity thermal break pad between them can actually increase the heat flow for thin pads, as well as reducing the economy of this thermal break strategy. Thicker thermal break pads provide a significant reduction in heat flow, but with diminishing returns. Using stainless-steel or FRP bolts provides a significant reduction in heat flow, since the greater majority of heat flow exists in the bolts rather than the thermal break pad.

Results show that thermal breaks provide benefit in terms of increasing the temperature index, even with thin thermal break pads. It is expected that applying insulation to outside of the connection will increase the temperature index and also reduce the total heat flow through the thermal break. The combination of a thermal break and covering insulation may potentially be the most effective and efficient solution, but needs to be explored in future research.



## 5.4 Recommendations

Based on the results of this project, the following are recommended:

- Whenever possible, structural steel thermal bridges should be encompassed with insulation and sealed with an impermeable vapor barrier.
- Using the heat flow rate calculated using the fin equation (Eq. 4-5), an analysis should be performed to determine the cost of a thermal bridge over the lifetime of the structure. This cost can then be compared to the cost of a thermal break solution.
- When a thermal break is used, the design should consider the use of stainless-steel bolts. In cases where appropriate, the thermal break design should also consider the application of covering insulation to be applied to the face of the thermal break.
- If a building or structure consists of many thermal bridges or thermal breaks, it is recommended that a steady-state three-dimensional heat transfer analysis be performed in order to determine the most efficient thermal break solution. Numerous finite-element heat transfer programs are readily available, and the use of these programs can be sourced to engineering firms that specialize in building science, since the work can be performed remotely.
- When situations require a thermally-broken structural steel connection, soft elastomeric pads should not be used for connections resisting bending forces. Thin pads (less than 1-in.) of this type do not provide adequate thermal protection, while thicker pads (greater than 1-in.) reduce the rotational stiffness of the connection and produce significant bending stresses in the bolts due to prying forces.
- Soft elastomeric pads can be used for thermally-broken connections that resist only axial forces, e.g. a compression base plates. These connections should be carefully considered to ensure that they are designed to provide adequate thermal protection and structural resistance, including the effects of long-term loading.
- A325 structural steel bolts should be used for connections with thermal-break pads. Although stainless-steel and FRP bolts significantly reduce heat flow, their use is not recommended due to their limited strength and ductility. The presence of a elastomeric pad produces additional forces on the bolts, which must be ductile and resistant to fatigue

loading. A490 bolts should not be used since they have little ductility and are required to be fully pre-tensioned [4], which may not be possible without damage or significant deformation to the underlying elastomer.

- FRP materials show promise as a thermal-break material, but are beyond the scope of this project.
- Although manufactured thermal break assemblies (MSTBAs) are touted by manufactures and marketed to engineers as effective thermal break solutions, structural engineers should be aware when specifying them of possible issues with stiffness, creep, and fire-ratings.

## **5.5 Future Research**

Thermally broken structural steel connections provide an effective and efficient solution to excessive heat flow and condensation due to thermal bridging. This has resulted in an emerging need for allowing the use of non-steel materials in a structural steel connection. For this reason, the structural engineering community is interested in obtaining simple and effective design guidance on structural steel connections such as these. Future research should focus on the development of non-proprietary thermally broken steel connections and design guidance.

## References

- [1] American Society of Heating Refrigerating and Air Conditioning Engineers, “ANSI/ASHRAE/ IES Standard 90.1-2013 -- Energy Standard for Buildings Except Low-Rise Residential Buildings.” ASHRAE, Atlanta, GA, 2013.
- [2] R. P. Tye, J. P. Silvers, D. L. Brownell, and S. E. Smith, “New Materials and Concepts to Reduce Energy Losses through Structural Thermal Bridges,” ASHRAE/DOC/BTECC Thermal Performance of the Exterior Envelopes of Buildings III, 1986.
- [3] SEI/ AISC, “Minimizing Structural Steel’s Impact on Building Envelope Energy Transfer,” Modern Steel Construction, 2012.
- [4] American Institute of Steel Construction, RCSC Specification for Structural Joints Using High-Strength Bolts, 2009th ed. Chicago: American Institute of Steel Construction, 2009.
- [5] J. Kosny and J. E. Christian, “Thermal evaluation of several configurations of insulation and structural materials for some metal stud walls,” Energy and Buildings, vol. 22, pp. 157–163, 1995.
- [6] Morrison Hershfield, “Thermal and Whole building Energy Performance of Thermal Break Technology for Concrete Balconies in High-Rise Multi-unit Residential Buildings,” 2013.
- [7] K. W. Childs, “Analysis of Seven Thermal Bridges Identified in a Commercial Building,” 1988.
- [8] L. Lidia-Maria and M. Ioan, “Linear Thermal Bridges at Vertical Elements of Building Structures,” Journal of Applied Engineering Sciences, vol. 2 (15), no. 1/2012, pp. 59–64, 2012.
- [9] B. P. Barnes, A. Pagán-Vázquez, A. P. Heffron, B. B. Mehnert, M. P. Case, A. Kumar, J. L. Lattimore, R. J. Liesen, L. D. Stephenson, J. C. Trovillion, and J. B. Allen, “Analysis Techniques, Materials, and Methods for Treatment of Thermal Bridges in Building Envelopes,” Vicksburg, 2013.
- [10] J. Rose, C. Eng, and S. Svendsen, “Validating Numerical Calculations against Guarded Hot Box Measurements,” Nordic Journal of Building Physics, vol. 4, 2004.
- [11] Fabreeka, “Structural Thermal Break Pad / Connection.” Altrincham, Cheshire, England, UK, 2014.
- [12] Armadillo Noise & Vibration Ltd., “Thermal Break Pads Armatherm Grade FR - Ultra High Strength , High Performance.” Armadillo Noise & Vibration Ltd., Shipley, West Yorkshire, England, 2016.
- [13] Schöck USA Inc, “Thermal Bridge Solutions . Schöck Isokorb ® Product Guide . Guide to Thermal Breaks . Innovative Design in Practice .” Schöck USA Inc., New York, NY, 2016.
- [14] Farrat, “Thermal Break Connections (Farrat).” Farrat.
- [15] Insula, “Thermal Break Connections (Insula).” .
- [16] K. Martin, A. Campos-Celador, C. Escudero, I. Gómez, and J. M. Sala, “Analysis of a thermal bridge in a guarded hot box testing facility,” Energy and Buildings, vol. 50, pp. 139–149, 2012.

- [17] J. Kosny and P. Childs, "Accuracy of Hot Box Testing of Steel Stud Wall," *Insulation Materials: Testing and Applications*, vol. 4th Volume, no. ASTM STP 1426, pp. 147–158, Jan. 2002.
- [18] ASTM International, C1199-00: Standard Test Method for Measuring the Steady-State Thermal Transmittance of Fenestration Systems Using Hot Box Methods. ASTM International, 2000.
- [19] ASTM International, "C1363-11: Standard Test Method for Thermal Performance of Building Materials and Envelope Assemblies by Means of a Hot Box Apparatus." ASTM, 2011.
- [20] GOST 26602.1-99, "Windows and doors. Methods of determination of resistance of thermal transmission," 1999.
- [21] F. Asdrubali and G. Baldinelli, "Thermal transmittance measurements with the hot box method: Calibration, experimental procedures, and uncertainty analyses of three different approaches," *Energy and Buildings*, vol. 43, pp. 1618–1626, 2011.
- [22] J. Kosny, A. O. Desjarlais, and J. E. Christian, "Steel-framed buildings: impacts of wall detail configurations on the whole wall thermal performance," in *ASHRAE Transactions*, 1998.
- [23] J. A. D'Aloisio, "Steel Framing & Building Envelopes," *Modern Steel Construction*, vol. January, 2010.
- [24] P. G. Schild and P. Blom, "Good practice guidance on thermal bridges & construction details, Part I: Principles (P188)," 2010.
- [25] Morrison Hershfield, "Thermal Performance of Building Envelope Details for Mid-and High-Rise Buildings," no. 5085243, p. 189, 2011.
- [26] J. Kosny, J. E. Christian, C. E. Barbour, and J. Goodrow, "Thermal performance of steel-framed walls," 1994.
- [27] Morrison Hershfield, "Building Envelope Thermal Bridging Guide," Vancouver, BC, 2014.
- [28] N. Norris, P. Ropell, and M. Lawton, "The concept of linear and point transmittance and its value in dealing with thermal bridges in building enclosures," *Building enclosure science & technology conference*, pp. 1–10, 2012.
- [29] International Organization for Standardization, "ISO 10211:2007 Thermal bridges in building construction - Heat flows and surface temperatures - Detailed calculations." International Organization for Standardization, Geneva, Switzerland, 2007.
- [30] Schock, *Design Guide Solutions to Prevent Thermal Bridging* (Schock). Schock Canada Inc, 2014.
- [31] Fabreeka, "Properties of Fabreeka's Thermal Insulation Material." Fabreeka, 2011.
- [32] C. C. Kendrick, "Thermal Performance of Steel Beam Junctions using Different Connection Methods (Schoeck)," 2013.
- [33] BS 5250, "Code of practice for control of condensation in buildings," vol. 3, no. 1, p. 100, 2011.

- [34] J. W. Baldwin, "Report of the Kemper Arena roof collapse of June 4, 1979, Kansas City, Missouri," Kansas City, Missouri, 1979.
- [35] T. M. Murray and W. L. Shoemaker, "Steel Design Guide 16: Flush and Extended Multiple-Row Moment End-Plate Connections," AISC Steel Design Guide Series. American Institute of Steel Construction, Chicago, Illinois, p. 72, 2003.
- [36] T. M. Murray and E. A. Sumner, "Steel Design Guide 4: Extended End-Plate Moment Connections. Seismic and Wind Applications," AISC Steel Design Guide Series. American Institute of Steel Construction, Chicago, Illinois, 2003.
- [37] T. M. Murray, "Recent developments for the design of moment end-plate connections," *Journal of Constructional Steel Research*, vol. 10, pp. 133–162, 1988.
- [38] E. A. Sumner, "Unified Design of Extended End-Plate Moment Connections Subject to Cyclic Loading," Virginia Polytechnic Institute, 2003.
- [39] J. T. Borgsmiller, "Simplified Method for Design of Moment End-Plate Connections," Virginia Polytechnic Institute, 1995.
- [40] A. N. Sherbourne and M. R. Bahaari, "Finite Element Prediction of End Plate Bolted Connection Behavior. I: Parametric Study," *Journal of Structural Engineering*, vol. 123, pp. 157–164, 1997.
- [41] M. Mohamadi-Shooreh, "Empirical Model of the Moment-Rotation Curve of Beam-to-Beam Bolted Flush Endplate Connections," *Journal of Structural ...*, vol. 139, no. January, pp. 66–72, 2012.
- [42] C. P. Chasten, R. B. Fleischman, L. Lu, and G. C. Driscoll, "Semi-Rigid Steel Connections and Their Effects on Structural Steel Frames," 1987.
- [43] K. M. Abdalla and W. F. Chen, "Expanded database of semi-rigid steel connections," *Computers and Structures*, vol. 56, no. 4, pp. 553–564, 1995.
- [44] C. Faella, V. Piluso, and G. Rizzano, *Structural Steel Semirigid Connections: Theory, Design, and Software*. CRC Press, 1999.
- [45] C. Daz, P. Mart, M. Victoria, and O. M. Querin, "Review on the modelling of joint behaviour in steel frames," *Journal of Constructional Steel Research*, vol. 67, no. 5, pp. 741–758, 2011.
- [46] A. N. Gent, *Engineering with Rubber - How to Design Rubber Components*, 2nd ed. Cincinnati: HanserGardner Publications Inc., 2001.
- [47] R. A. Cook and D. T. Allen, "Stiffness Evaluation of Neoprene Bearing Pads Under Long-Term Loads," Gainesville, 2009.
- [48] J. V Muscarella and J. A. Yura, "An Experimental Study of Elastomeric Bridge Bearings with Design Recommendations," Austin, 1995.
- [49] G. L. Bradley, P. C. Chang, and A. W. Taylor, "Determination of the Ultimate Capacity of Elastomeric Bearings Under Axial Loading," Gaithersburg, 1998.
- [50] TRANSPORTATION RESEARCH BOARD, NCHRP Report 596: Rotation Limits for Elastomeric Bearings. 2008.

- [51] TRANSPORTATION RESEARCH BOARD, NCHRP Report 449: Elastomeric Bridge Bearings : COOPERATIVE HIGHWAY PROGRAM. .
- [52] U.S. Department of Transportation, “Steel Bridge Design Handbook,” vol. 15, 2015.
- [53] K.-S. Lee, C.-P. Fan, R. Sause, and J. Ricles, “Simplified design procedure for frame buildings with viscoelastic or elastomeric structural dampers,” *Earthquake Engineering & Structural Dynamics*, vol. 34, no. 10, pp. 1271–1284, Aug. 2005.
- [54] U. Gerhaher, A. Strauss, and K. Bergmeister, “Numerical modeling of elastomeric bearings in structural engineering,” *Advances in Materials Sciences*, vol. 11, pp. 51–63, 2011.
- [55] M. J. Asl, M. M. Rahman, and A. Karbakhsh, “Numerical Analysis of Seismic Elastomeric Isolation Bearing in the Base-Isolated Buildings,” *Open Journal of Earthquake Research*, vol. 2014, no. February, pp. 1–4, 2014.
- [56] G. Milani and F. Milani, “Stretch–Stress Behavior of Elastomeric Seismic Isolators with Different Rubber Materials: Numerical Insight,” *Journal of Engineering Mechanics*, vol. 138, no. 5, pp. 416–429, 2012.
- [57] D. B. Cleary and W. T. Riddell, “Progress Report: Moment-Rotation Testing of Armatherm Barrier,” Glassboro, 2014.
- [58] D. B. Cleary and W. T. Riddell, “Shear Testing of Armatherm Barrier,” Glassboro, 2014.
- [59] D. B. Cleary and W. T. Riddell, “Compression Testing of Armatherm Barrier,” Glassboro, 2014.
- [60] L. Nasdala, B. Hohn, and R. Rühl, “Design of end-plate connections with elastomeric intermediate layer,” *Journal of Constructional Steel Research*, vol. 63, no. 4, pp. 494–504, Apr. 2007.
- [61] Z. Sulcova, Z. Sokol, and F. Wald, “STATIC DESIGN OF THERMAL INSULATING STEEL CONNECTIONS,” in *Central Europe towards Sustainable Building, Advanced Building Design*, 2010, pp. 1–5.
- [62] ASHRAE, 2009 ASHRAE Handbook of Fundamentals IP Edition, 2009th ed. Atlanta: ASHRAE.
- [63] S. Yuan, A. G. Russell, and W. P. Goss, “Uncertainty Analysis of a Calibrated Hot Box,” *Insulation Materials: Testing and Applications*, vol. 4th Volume, no. ASTM STP 1426, pp. 189–202, 2002.
- [64] S. Yuan, “Experimental and analytical heat transfer analyses for a calibrated hot box and fenestration systems,” University of Massachusetts Amherst.
- [65] American Institute of Steel Construction, *Specification for Structural Steel Buildings*. 2010.
- [66] G. S. Prinz, A. Nussbaumer, L. Borges, and S. Khadka, “Experimental testing and simulation of bolted beam-column connections having thick extended endplates and multiple bolts per row,” *Engineering Structures*, vol. 59, pp. 434–447, 2014.
- [67] E. A. Sumner, T. W. Mays, and T. M. Murray, “End-Plate Moment Connections: Test Results and Finite Element Method Validation,” in *4th International Workshop on Connections in Steel Structures*, 2000, pp. 82–93.

- [68] C. Lim, W. Choi, and E. A. Sumner, "Low cycle fatigue life prediction using a four-bolt extended unstiffened end plate moment connection," *Engineering Structures*, vol. 41, pp. 373–384, Aug. 2012.
- [69] K. Kaushik, A. K. Sharma, and R. Kumar, "A Review on Finite Element Analysis of Beam to Column Endplate Bolted Connection," *IOSR Journal of Mechanical and Civil Engineering (IOSR-JMCE)*, vol. 8, no. 1, pp. 97–103, 2013.
- [70] M. S. M. Abel, "Four-bolt Extended Unstiffened Moment End-plate Connections," Virginia Polytechnic Institute and State University, 1993.
- [71] T. W. Mays, "Application of the finite element method to the seismic design and analysis of large moment end-plate connections," Virginia Polytechnic Institute and State University, 2000.
- [72] A. K. Dessouki, A. H. Youssef, and M. M. Ibrahim, "Behavior of I-beam bolted extended end-plate moment connections," *Ain Shams Engineering Journal*, vol. 4, no. 4, pp. 685–699, Dec. 2013.
- [73] M. Ghassemieh, M. Jalalpour, and A. A. Gholampour, "Numerical Evaluation of the Extended Endplate Moment Connection Subjected to Cyclic Loading," *Current Advances in Civil Engineering*, vol. 2, no. 1, pp. 35–43, 2014.
- [74] MSC Software, "Nonlinear finite element analysis of elastomers," *Computers & Structures*, vol. 26, no. 4, p. 75, 2010.
- [75] H. Najm, H. Nassif, and N. O. Bezgin, "Circular Elastomeric Bearings," Piscataway, NJ, 2002.
- [76] ABAQUS Inc, "ABAQUS User's Theory and Scripting Manuals." Dassault Systemes Simulia Corp., Providence, USA, 2012.
- [77] B. Kim, S. B. Lee, J. Lee, S. Cho, H. Park, S. Yeom, and S. H. Park, "A comparison among Neo-Hookean model, Mooney-Rivlin model, and Ogden model for Chloroprene rubber," *International Journal of Precision Engineering and Manufacturing*, vol. 13, no. 5, pp. 759–764, 2012.
- [78] R. W. Ogden, G. Saccomandi, and I. Sgura, "Fitting hyperelastic models to experimental data," *Computational Mechanics*, vol. 34, no. 6, pp. 484–502, 2004.
- [79] F. Xiao, Y. Chen, and H. Hua, "Comparative Study of The Shock Resistance of Rubber Protective Coatings Subjected to Underwater Explosion," *Journal of Offshore Mechanics and Arctic Engineering*, vol. 136, no. 2, p. 21402, 2014.
- [80] H. Augusto, L. Simões da Silva, C. Rebelo, and J. M. Castro, "Characterization of web panel components in double-extended bolted end-plate steel joints," *Journal of Constructional Steel Research*, vol. 116, pp. 271–293, Jan. 2016.
- [81] O. S. Bursi and J. P. Jaspart, "Benchmarks for finite element modelling of bolted steel connections," *Journal of Constructional Steel Research*, vol. 43, pp. 17–42, 1997.
- [82] A. M. Girão Coelho, F. S. K. Bijlaard, and L. Simões da Silva, "Experimental assessment of the ductility of extended end plate connections," *Engineering Structures*, vol. 26, no. 9, pp. 1185–1206, Jul. 2004.

- [83] L. Simoes da Silva and A. G. Coelho, "Ductility model for steel connections," *Journal of Constructional Steel Research*, vol. 57, no. 1, pp. 45–70, 2001.
- [84] W. Y. Wang, G. Q. Li, and Y. L. Dong, "Experimental study and spring-component modelling of extended end-plate joints in fire," *Journal of Constructional Steel Research*, vol. 63, no. 8, pp. 1127–1137, 2007.
- [85] F. Block, I. Burgess, B. Davison, and R. Plank, "A Component Approach to Modelling Steelwork Connections in Fire: Behaviour of Column Webs in Compression," in *Structures*, 2004, pp. 1–8.
- [86] K. Urbonas and A. Daniūnas, "Component method extension to steel beam-to-beam and beam-to-column knee joints under bending and axial forces," *Journal of Civil Engineering and Management*, vol. XI, no. 3, pp. 217–224, 2005.
- [87] M. E. M. M. Yovanovich, "Fins or Extended Surfaces," pp. 1–5.
- [88] A. Hamdi, M. N. Abdelaziz, N. A. Hocine, P. Heuillet, U. M. R. Cnrs, P. Lille, V. Ascq, and V. S. Seine, "Fracture Criteria of Rubber-Like Materials Under Plane."









## **Appendices**

THIS PAGE INTENTIONALLY LEFT BLANK

## Appendix A Industry Survey of Thermal Break Practices





**Information about you and your company/ firm. Please check only the questions you'd like to provide answers to.**

Table A-1: Question 1. General information.

| # | Answer            |   | Responses | %   |
|---|-------------------|---|-----------|-----|
| 1 | Company/ Firm:    |  | 88        | 75% |
| 2 | # of Employees:   |  | 77        | 66% |
| 3 | Primary Services: |  | 103       | 88% |
| 4 | Surveyee Name:    |  | 75        | 64% |
| 5 | Surveyee Title:   |  | 84        | 72% |
| 6 | Surveyee E-mail:  |  | 68        | 58% |



**How often do you encounter a detailing situation where the design requires a steel member or steel element to protrude through a buildings thermal envelope?**

Table A-2: Question 2. Thermal bridging frequency.

| # | Answer                          |   | Responses | %    |
|---|---------------------------------|---|-----------|------|
| 1 | Every project                   |   | 39        | 24%  |
| 2 | Sometimes, depending on project |  | 99        | 60%  |
| 3 | Rarely, unique situations only  |  | 21        | 13%  |
| 4 | Never                           |  | 6         | 4%   |
|   | Total                           |   | 165       | 100% |

**You have answered that you have never encountered a detailing situation where the design required a steel member or steel element to protrude through a buildings thermal envelope. If so, the following survey may not be relevant to you. Would you like to proceed through the rest of the survey anyway?**

Table A-3: Question 3. Contingency exit.

| # | Answer                               |  | Responses | %    |
|---|--------------------------------------|--|-----------|------|
| 1 | Yes, continue with survey questions  |   | 1         | 17%  |
| 2 | No, this survey does not apply to me |  | 5         | 83%  |
|   | Total                                |  | 6         | 100% |

**Which thermal bridging detailing situations do you find to be more common? Check all that apply.**

Table A-4: Question 4. Thermal bridging detail type frequency





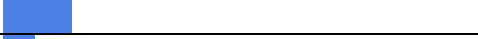
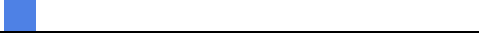
| # | Answer                   |  | Response | %   |
|---|--------------------------|--|----------|-----|
| 1 | Cantilever levels/ beams |  | 113      | 74% |
| 2 | Facade elements          |  | 113      | 74% |
| 3 | Roof protrusions         |  | 96       | 63% |
| 4 | Foundation penetrations  |  | 30       | 20% |
| 5 | External braces          |  | 22       | 14% |
| 6 | Other                    |  | 10       | 7%  |

Table A-5: Question 4. Other responses

|  |
|--|
| Other                                    |
| External columns at ground level         |
| Roof appurtenance supports               |
| Canopies                                 |
| Canopies                                 |
| Canopies and Awnings                     |
| Exposed columns                          |
| Entry canopies                           |
| not applicable                           |
| Wall Studs                               |
| long structures like pipe rack structure |

**How does your company currently address thermal bridging of steel members that protrude through a building's thermal envelope? Check all that apply.**

Table A-6: Question 5. Thermal break methods

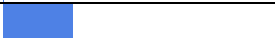



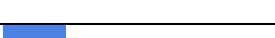


| # | Answer   |  | Response | %   |
|---|--|--|----------|-----|
| 1 | Avoid entirely (e.g., double columns, etc.)  |  | 39       | 27% |
| 2 | Use gasket material (e.g., plywood, neoprene, fiberglass, etc.)                      |  | 67       | 46% |
| 3 | Use a Manufactured Structural Thermal Break Assembly (MSTBA)                         |  | 34       | 23% |
| 4 | Replace member with less conductive material (such as stainless steel, timber, etc.) |  | 35       | 24% |
| 5 | Surround protruding steel member with insulating material                            |  | 104      | 71% |
| 6 | Do nothing   |  | 63       | 43% |
| 7 | Other  |  | 17       | 12% |

Table A-7: Question 5. Other responses

|  |
|--|
| Other  |
| Use high capacity foam insulation, autoclaved aeraed concrete, and frp in structural connection load path  |
| Gernerally depends on the architect and what the owner wants to pay for.   |
| Each situation is addressed based on the project needs.  |
| FRP structural plates and shapes   |
| create specific envelope to the intrusion  |
| Use Tnemec 971 Aerolon Fluid Applied Aerogel coating   |
| whine at architect to no avail   |
| Architect driven unless LEED cert. sought  |
| in-house designed thermal break assemblies   |
| we deal with insulation to isolate the high temperature steel equipment from other structural members  |
| We typically design the thermal envelope to be as continuous as possible, entirely exterior of the structure and with drying potential in at least one direction, in order to minimize condensation potential and to provide resiliency in the system for inevitable leaks, exfiltration, etc. |
| Try to minimize the thermal break with different details   |
| provide expansion joints to allow growth due to temperature. Isolate the structure to keep growth to allowable settings  |
| Special conditioning by mechanical   |
| Minimize bridge size   |
| Change detail to minimize bridging using same materials  |

**You have selected that you've used Manufactured Structural Thermal Break Assemblies (MSTBAs). Please provide the following:**

Table A-8: Question 6. Manufactured structural thermal break assembly responses

| # | Answer                        | Response | %    |
|---|-------------------------------|----------|------|
| 1 | Manufacturer:                 | 20       | 100% |
| 2 | Approximate number installed: | 12       | 60%  |
| 3 | Installed unit cost:          | 5        | 25%  |

Table A-9: Question 6. MSTBA manufacturers

| Manufacturer: | Approximate number installed: | Installed unit cost:            |
|---------------|-------------------------------|---------------------------------|
| Shock         |                               |                                 |
| Armadillo     |                               |                                 |
| Fabreeka      |                               |                                 |
| Fabreeka      | 6                             |                                 |
| Armadillo     |                               |                                 |
| Schock        | 20                            |                                 |
| Fabreeka      | 6                             | unknown, contractor said it was |

|                                      |           |           |
|--------------------------------------|-----------|-----------|
|                                      |           | expensive |
| aerolon                              | 3         |           |
| Schoek                               | 20        |           |
| various                              | thousands | unknown   |
| Schock Isokrob                       |           |           |
| Isokorb                              | 30        |           |
| Fabreeka                             | 25        |           |
| Schock Isokorb 5                     | Not sure  | ?         |
| Wausau Windows thermal break system. |           |           |
| Fabreeka                             |           |           |
| Fabreeka                             |           |           |
| Fabreeka, halfen                     | 35        |           |
| Halfan, Farat                        | 1000      | Expensive |

**Which of the following materials does your company employ to mitigate thermal bridging effects? Check all that apply.**

Table A-10: Question 7: Thermal break materials











| # | Answer                           |   | Response | %   |
|---|----------------------------------|---|----------|-----|
| 1 | Neoprene                         |   | 43       | 56% |
| 2 | Nitrile                          |  | 1        | 1%  |
| 3 | High Density Polyethylene (HDPE) |  | 31       | 40% |
| 4 | Wood/ engineered wood            |  | 35       | 45% |
| 5 | Fibre-reinforced polymer (FRP)   |  | 26       | 34% |
| 6 | Fibre-reinforced polymer bolts   |  | 5        | 6%  |
| 7 | Stainless steel                  |  | 31       | 40% |
| 8 | Stainless steel bolts            |  | 29       | 38% |
| 9 | Other (list as many as apply)    |  | 9        | 12% |

Table A-11: Question 7: Other responses

|  |
|--|
| Other (list as many as apply)                          |
| high capacity foam (column bearing blocks); aac        |
| Whatever Fabreeka makes                                |
| specific envelope                                      |
| Tnemec 971 Aerolon Fluid Applied Thermal Break coating |
| micarta  |
| 8in composite insulation                               |
| Insulated Thermal Block Systems (masonry)              |
| polymer shim similar to korolath                       |

**Would you be willing to provide thermal break construction details which may be modeled using thermal analysis software, and/or made publicly available?**



Table A-12: Question 8: Thermal break details

| # | Answer   |  | Response | %    |
|---|--|--|----------|------|
| 1 | Yes, provide ONLY for research purposes                  |  | 12       | 9%   |
| 2 | No   |  | 118      | 86%  |
| 3 | Yes, provide for research purposes AND public disclosure |  | 7        | 5%   |
|   | Total  |  | 137      | 100% |

**Questions 9-10 omitted for privacy.**

**Have you done any thermal modeling or thermal imaging to evaluate the efficacy of your thermal break strategies?**

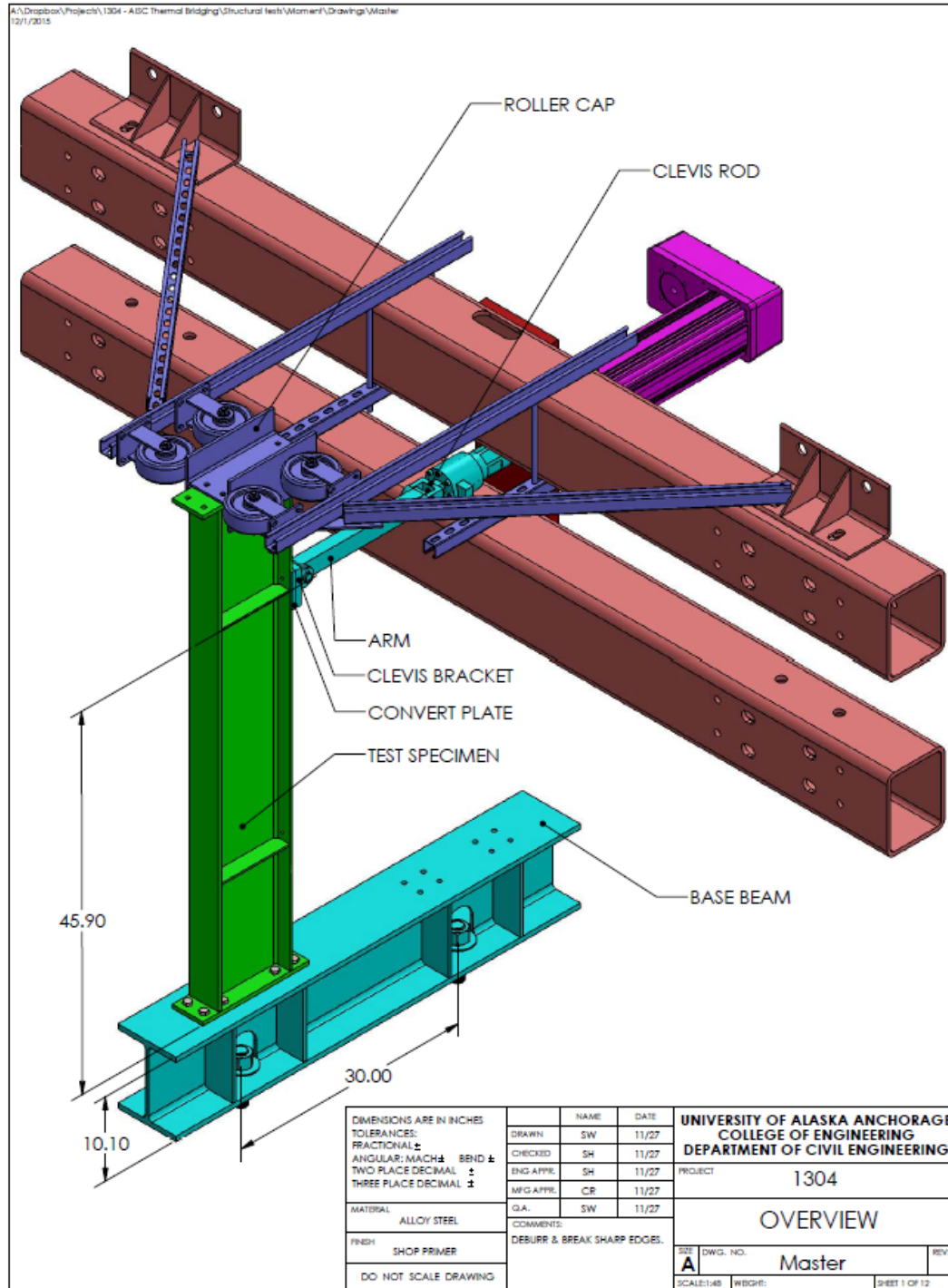
Table A-13: Question 11. Thermal modeling or thermal imaging on thermal breaks

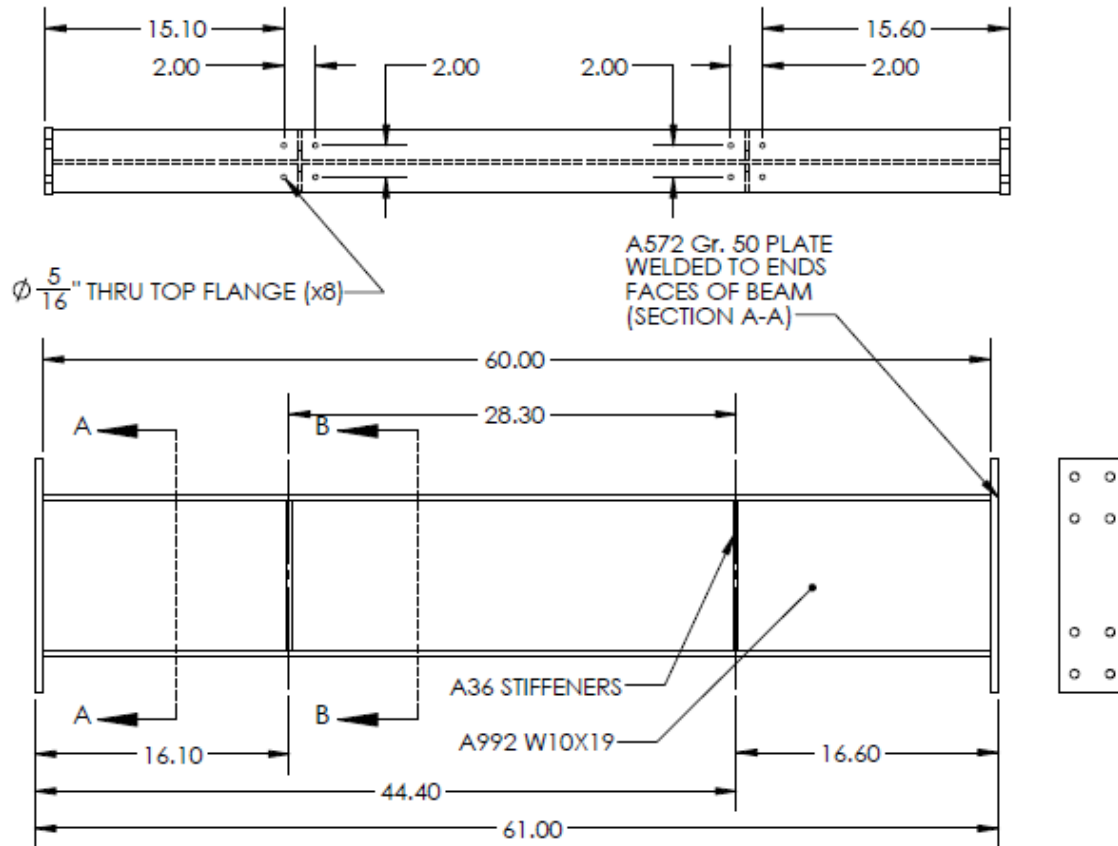
| # | Answer |   | Response | %    |
|---|--------|---|----------|------|
| 1 | Yes    |   | 21       | 14%  |
| 2 | No     |  | 125      | 86%  |
|   | Total  |   | 146      | 100% |

THIS PAGE INTENTIONALLY LEFT BLANK

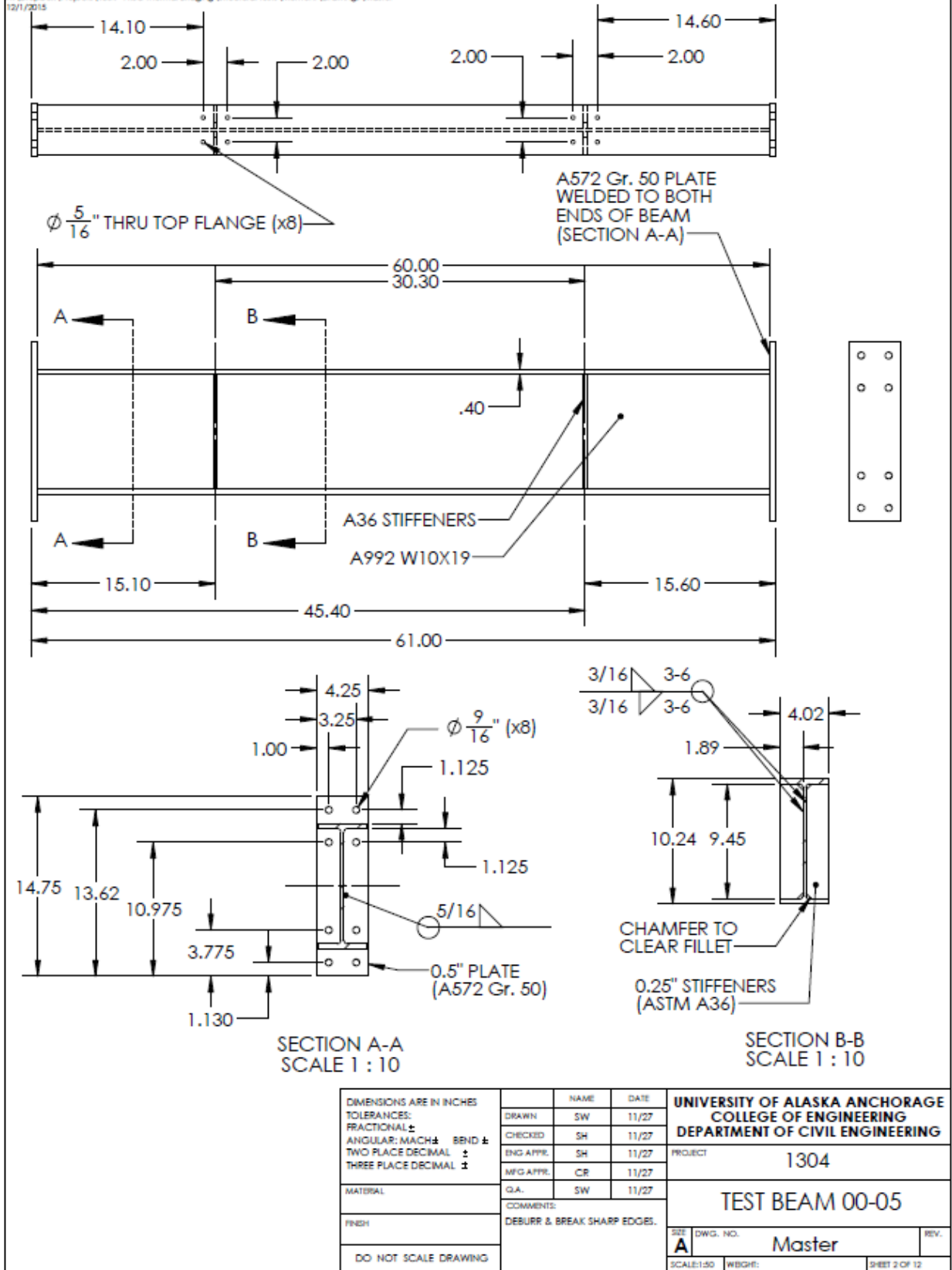


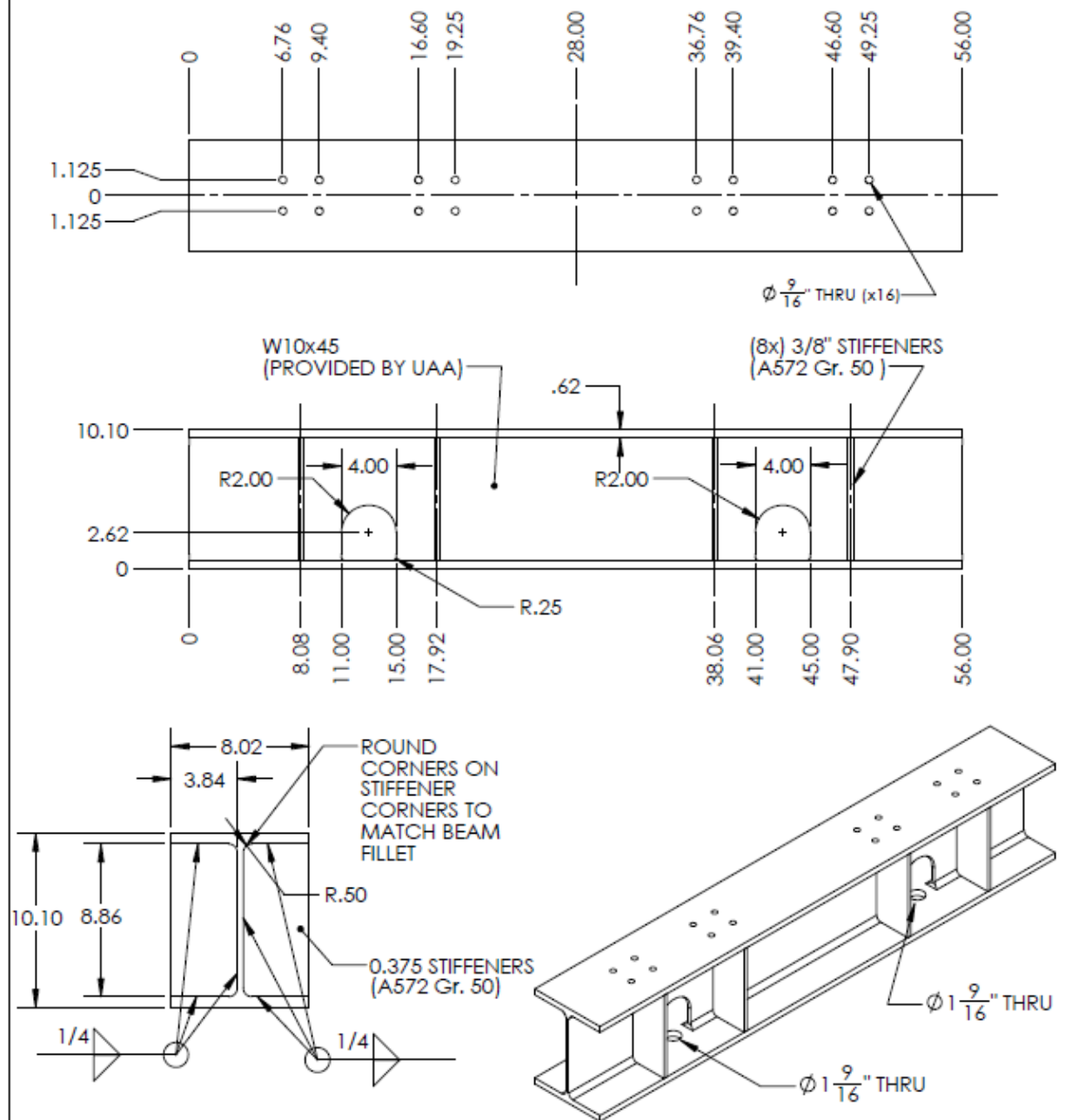
## Appendix B Experimental Test Drawings



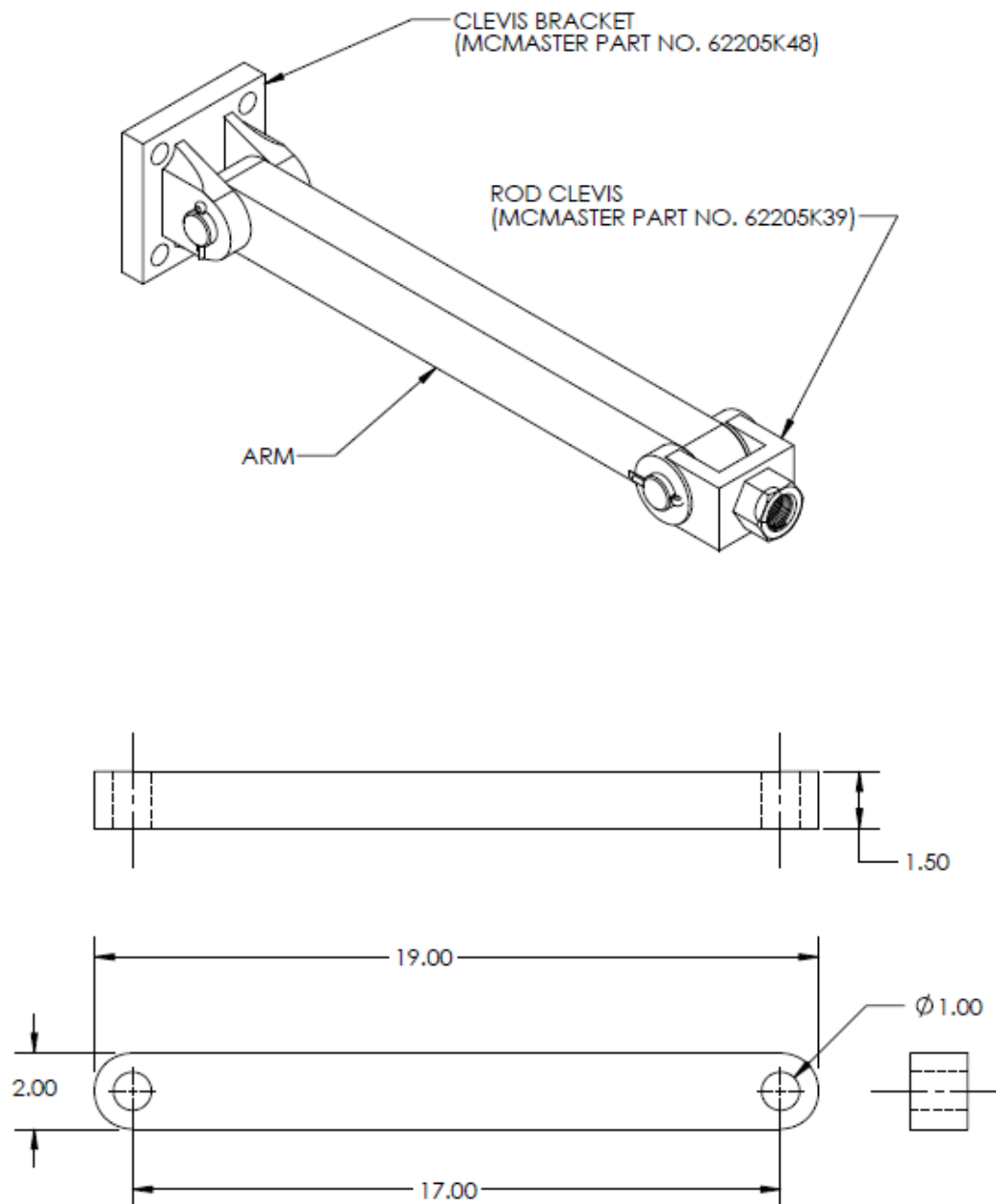


|  |  |                             |  |                 |  |   |  |
|--|--|-----------------------------|--|-----------------|--|---|--|
| DIMENSIONS ARE IN INCHES<br>TOLERANCES:<br>FRACTIONAL: ±<br>ANGULAR: MACH ± BEND ±<br>TWO PLACE DECIMAL ±<br>THREE PLACE DECIMAL ± |  | NAME                        |  | DATE            |  | UNIVERSITY OF ALASKA ANCHORAGE<br>COLLEGE OF ENGINEERING<br>DEPARTMENT OF CIVIL ENGINEERING |  |
|  |  | DRAWN                       |  | SW 11/27        |  |   |  |
|  |  | CHECKED                     |  | SH 11/27        |  |   |  |
|  |  | ENG APPR.                   |  | SH 11/27        |  |   |  |
|  |  | MFG APPR.                   |  | CR 11/27        |  |   |  |
| MATERIAL   |  | Q.A.                        |  | SW 11/27        |  | PROJECT 1304  |  |
| FINISH   |  | COMMENTS:                   |  | TEST BEAM 10-15 |  |   |  |
|  |  | DEBURR & BREAK SHARP EDGES. |  |                 |  |   |  |
| DO NOT SCALE DRAWING   |  | SIZE                        |  | DWG. NO.        |  | REV.  |  |
|  |  | A                           |  | Master          |  |   |  |
|  |  | SCALE:1:50                  |  | WEIGHT:         |  | SHEET 3 OF 12   |  |

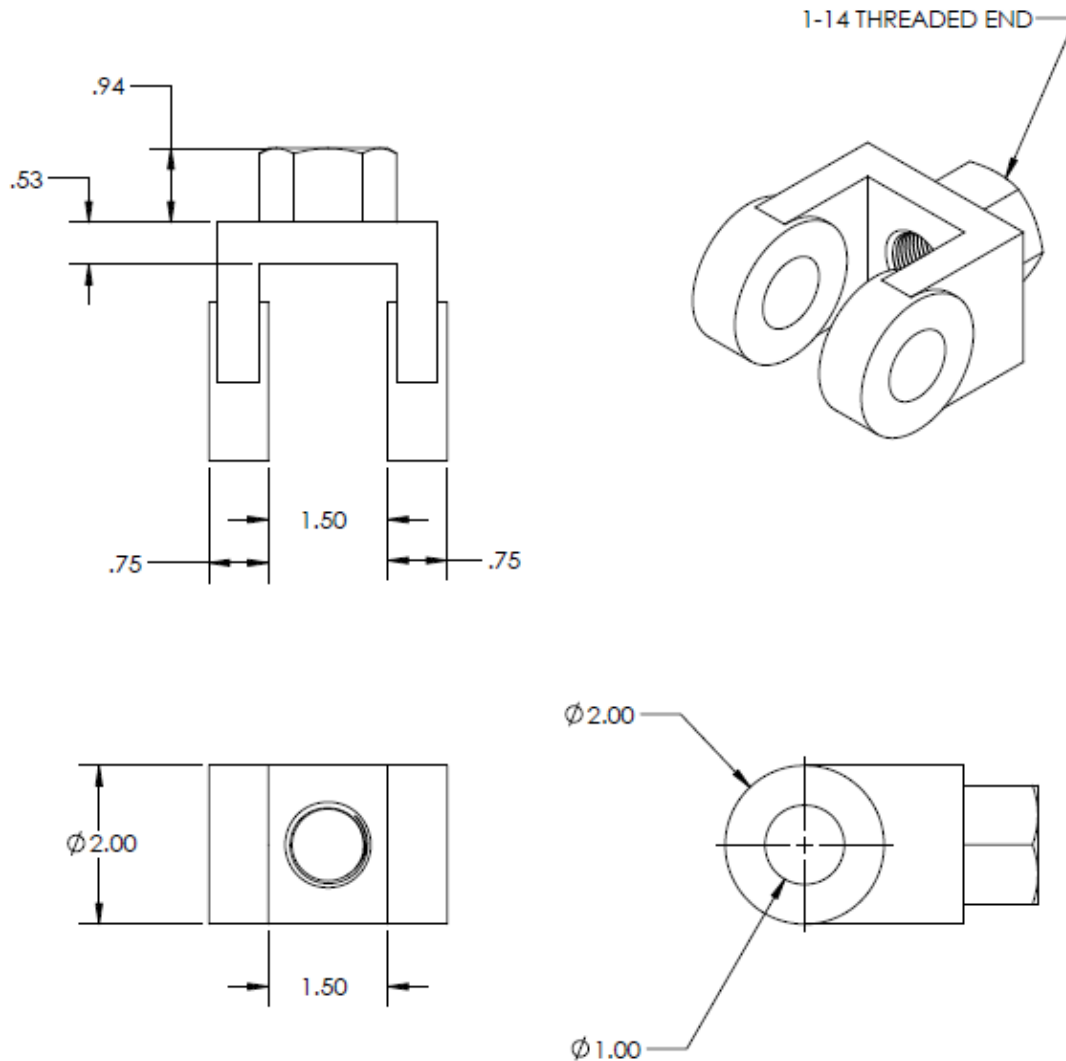




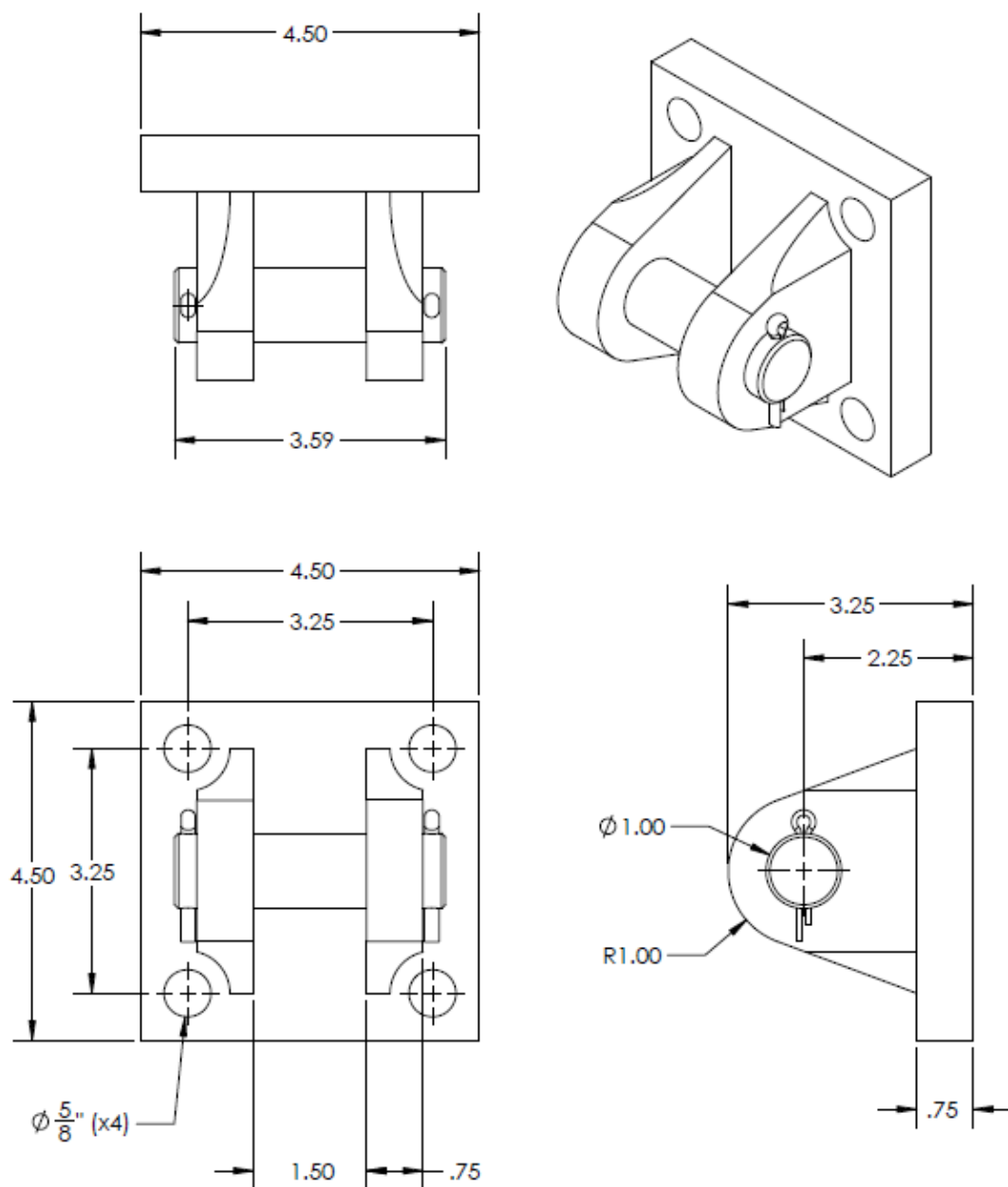
|  |                             |      |       |   |                        |               |
|--|-----------------------------|------|-------|---|------------------------|---------------|
| DIMENSIONS ARE IN INCHES<br>TOLERANCES:<br>FRACTIONAL ±<br>ANGULAR: MACH ±<br>BEND ±<br>TWO PLACE DECIMAL ±<br>THREE PLACE DECIMAL ± |                             | NAME | DATE  | UNIVERSITY OF ALASKA ANCHORAGE<br>COLLEGE OF ENGINEERING<br>DEPARTMENT OF CIVIL ENGINEERING |                        |               |
|  | DRAWN                       | SW   | 11/27 |   |                        |               |
|  | CHECKED                     | SH   | 11/27 | PROJECT<br><br>1304   |                        |               |
|  | ENG APPR.                   | SH   | 11/27 |   |                        |               |
|  | MFG APPR.                   | CR   | 11/27 |   | BASE BEAM              |               |
|  | Q.A.                        | SW   | 11/27 |   |                        |               |
| MATERIAL   | COMMENTS:                   |      |       | SIZE<br><b>A</b>  | DWG. NO.<br><br>Master | REV.          |
| FINISH   | DEBURR & BREAK SHARP EDGES. |      |       |   |                        |               |
| DO NOT SCALE DRAWING   |                             |      |       | SCALE:1:50  | WEIGHT:                | SHEET 4 OF 12 |



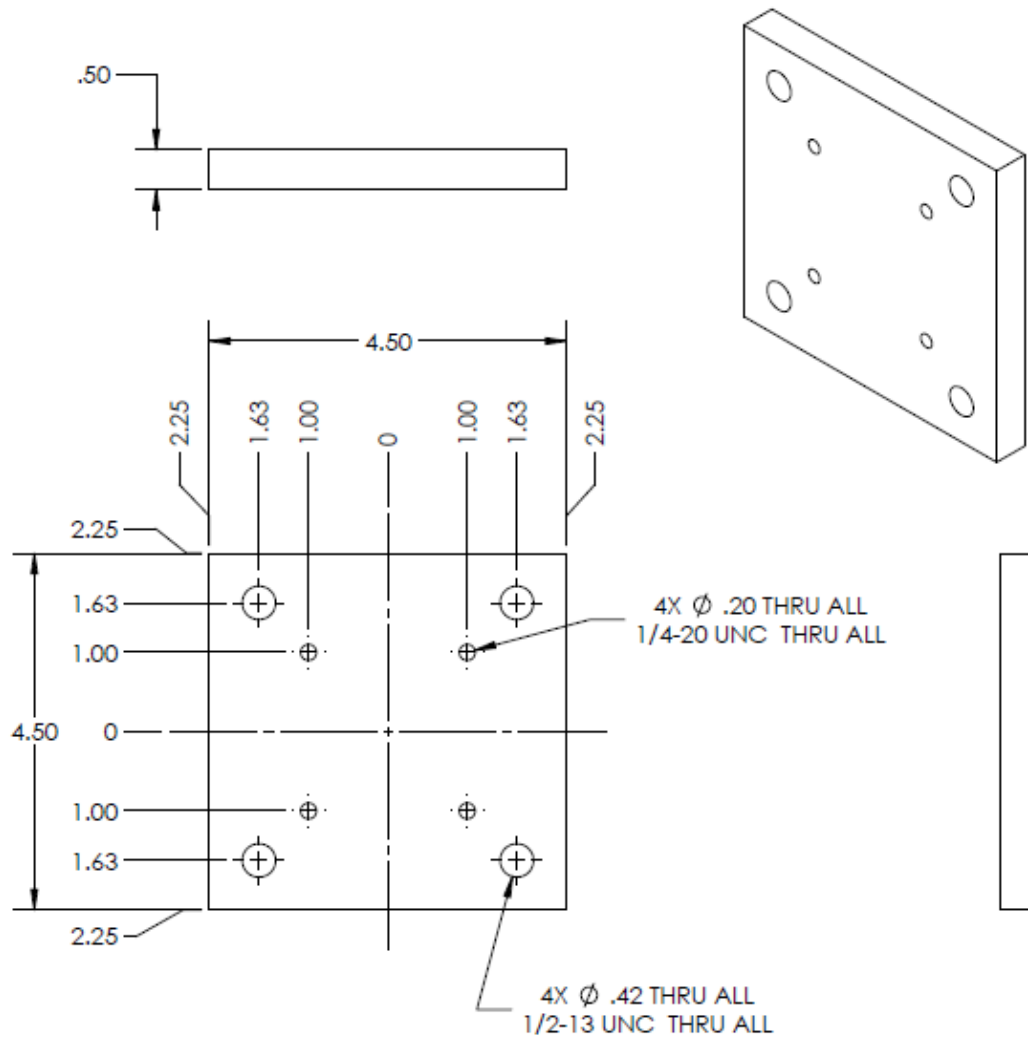
|                          |  |                             |      |                                |                                 |
|--------------------------|--|-----------------------------|------|--------------------------------|---------------------------------|
| DIMENSIONS ARE IN INCHES |  | NAME                        | DATE | UNIVERSITY OF ALASKA ANCHORAGE |                                 |
| TOLERANCES:              |  | DRAWN                       | SW   | 11/27                          | COLLEGE OF ENGINEERING          |
| FRACTIONAL: ±            |  | CHECKED                     | SH   | 11/27                          | DEPARTMENT OF CIVIL ENGINEERING |
| ANGULAR: MACH ±          |  | ENG APPR.                   | SH   | 11/27                          | PROJECT<br>1304                 |
| TWO PLACE DECIMAL ±      |  | MFG APPR.                   | CR   | 11/27                          |                                 |
| THREE PLACE DECIMAL ±    |  | Q.A.                        | SW   | 11/27                          | ARM                             |
| MATERIAL                 |  | COMMENTS:                   |      |                                |                                 |
| FINISH                   |  | DEBURR & BREAK SHARP EDGES. |      |                                | SIZE<br>A                       |
| DO NOT SCALE DRAWING     |  |                             |      |                                |                                 |
|                          |  |                             |      |                                | DWG. NO.<br>Master              |
|                          |  |                             |      |                                | SCALE: 1:8                      |
|                          |  |                             |      |                                | WEIGHT:                         |
|                          |  |                             |      |                                | SHEET 5 OF 12                   |



|                          |  |                             |  |      |  |                                |  |                                 |  |
|--------------------------|--|-----------------------------|--|------|--|--------------------------------|--|---------------------------------|--|
| DIMENSIONS ARE IN INCHES |  | NAME                        |  | DATE |  | UNIVERSITY OF ALASKA ANCHORAGE |  |                                 |  |
| TOLERANCES:              |  | DRAWN                       |  | SW   |  | 11/27                          |  | COLLEGE OF ENGINEERING          |  |
| FRACTIONAL ±             |  | CHECKED                     |  | SH   |  | 11/27                          |  | DEPARTMENT OF CIVIL ENGINEERING |  |
| ANGULAR: MACH ± BEND ±   |  | ENG APPR.                   |  | SH   |  | 11/27                          |  | PROJECT                         |  |
| TWO PLACE DECIMAL ±      |  | MFG APPR.                   |  | CR   |  | 11/27                          |  | 1304                            |  |
| THREE PLACE DECIMAL ±    |  | Q.A.                        |  | SW   |  | 11/27                          |  | CLEVIS ROD END                  |  |
| MATERIAL                 |  | COMMENTS:                   |  |      |  | SIZE                           |  | DWG. NO.                        |  |
| FINISH                   |  | DEBURR & BREAK SHARP EDGES. |  |      |  | A                              |  | Master                          |  |
| DO NOT SCALE DRAWING     |  |                             |  |      |  | SCALE: 1/2                     |  | SHEET 4 OF 12                   |  |
|                          |  |                             |  |      |  | WEIGHT:                        |  | REV.                            |  |

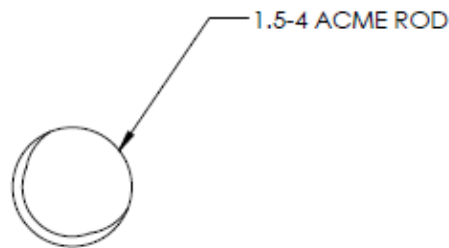
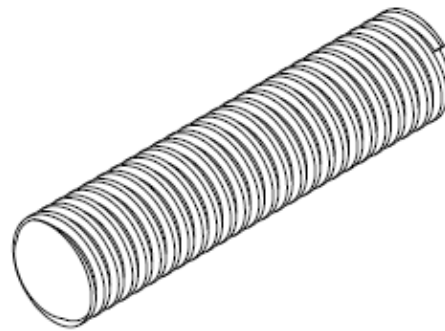
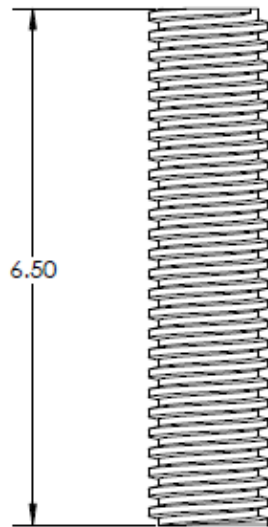


|                          |  |                                  |      |   |   |
|--------------------------|--|----------------------------------|------|---|---|
| DIMENSIONS ARE IN INCHES |  | NAME                             | DATE | UNIVERSITY OF ALASKA ANCHORAGE<br>COLLEGE OF ENGINEERING<br>DEPARTMENT OF CIVIL ENGINEERING |   |
| TOLERANCES:              |  | DRAWN                            | SW   | 11/27   | PROJECT<br><br>1304<br><br>CLEVIS BRACKET |
| FRACTIONAL: ±            |  | CHECKED                          | SH   | 11/27   |   |
| ANGULAR: MACH ± BEND ±   |  | ENG APPR.                        | SH   | 11/27   |   |
| TWO PLACE DECIMAL ±      |  | MFG APPR.                        | CR   | 11/27   |   |
| THREE PLACE DECIMAL ±    |  | Q.A.                             | SW   | 11/27   |   |
| MATERIAL                 |  | COMMENTS:                        |      |   | SIZE<br><b>A</b> DWG. NO. Master REV.     |
| FINISH                   |  | DEBURR & BREAK SHARP EDGES.      |      |   |   |
| DO NOT SCALE DRAWING     |  | SCALE: 1:2 WEIGHT: SHEET 7 OF 12 |      |   |   |

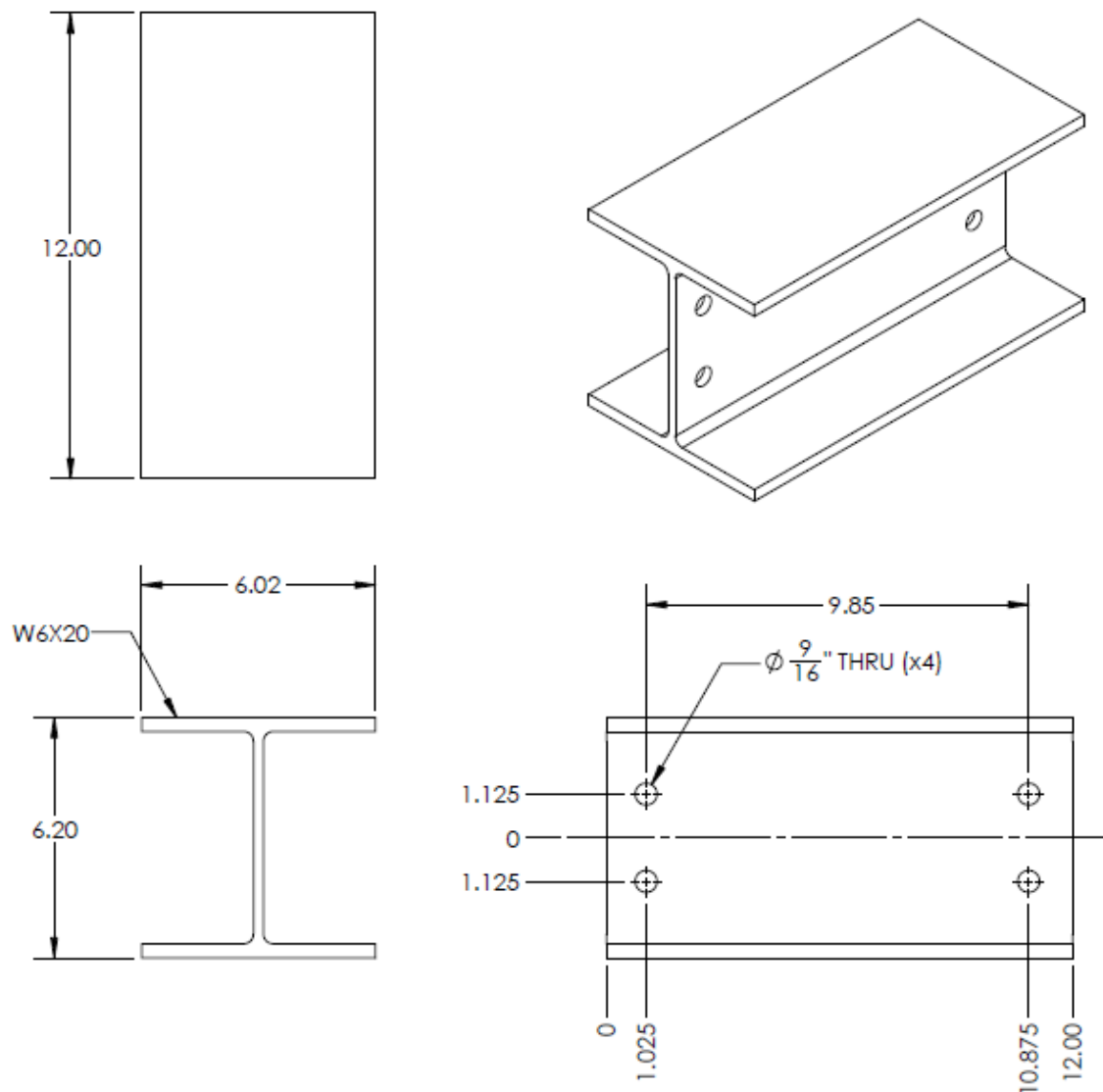


|                          |  |                             |      |   |                                |
|--------------------------|--|-----------------------------|------|---|--------------------------------|
| DIMENSIONS ARE IN INCHES |  | NAME                        | DATE | UNIVERSITY OF ALASKA ANCHORAGE<br>COLLEGE OF ENGINEERING<br>DEPARTMENT OF CIVIL ENGINEERING |                                |
| TOLERANCES:              |  | DRAWN                       | SW   | 11/27   | PROJECT 1304                   |
| FRACTIONAL: ±            |  | CHECKED                     | SH   | 11/27   |                                |
| ANGULAR: MACH ± BEND ±   |  | ENG APPR.                   | SH   | 11/27   | CONVERT PLATE                  |
| TWO PLACE DECIMAL ±      |  | MFG APPR.                   | CR   | 11/27   |                                |
| THREE PLACE DECIMAL ±    |  | Q.A.                        | SW   | 11/27   | SIZE DWG. NO. Master REV.<br>A |
| MATERIAL                 |  | COMMENTS:                   |      | SCALE: 1:2 WEIGHT: SHEET 8 OF 12  |                                |
| FINISH                   |  | DEBURR & BREAK SHARP EDGES. |      |   |                                |
| DO NOT SCALE DRAWING     |  |                             |      |   |                                |

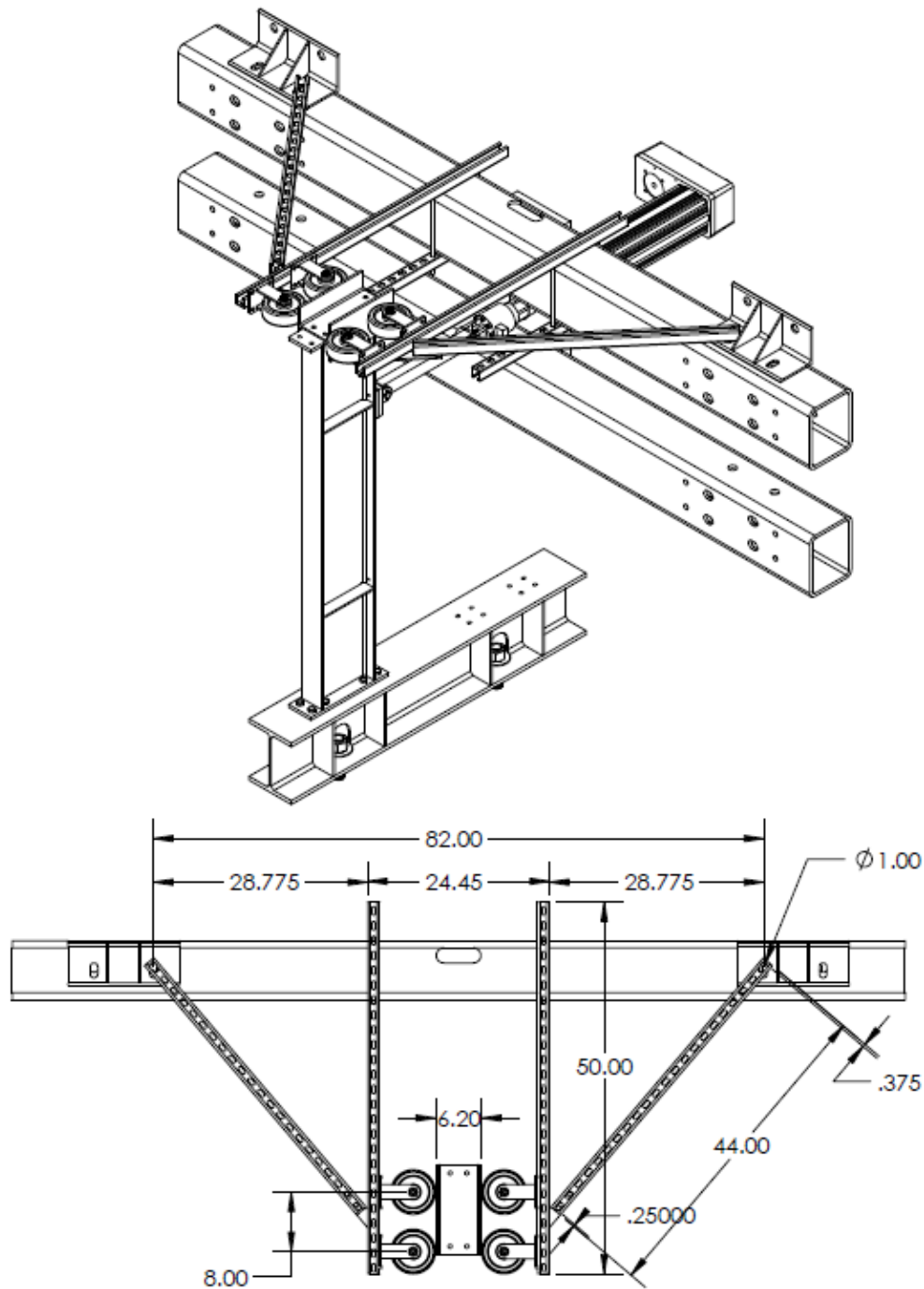




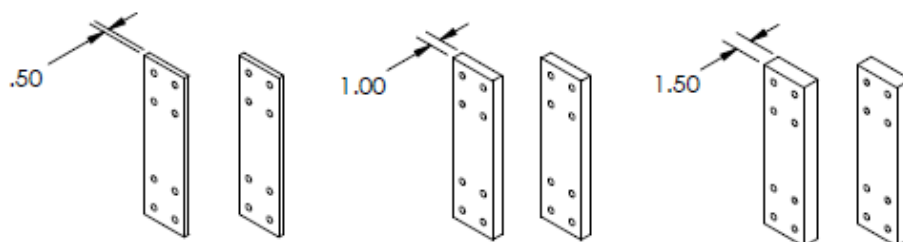
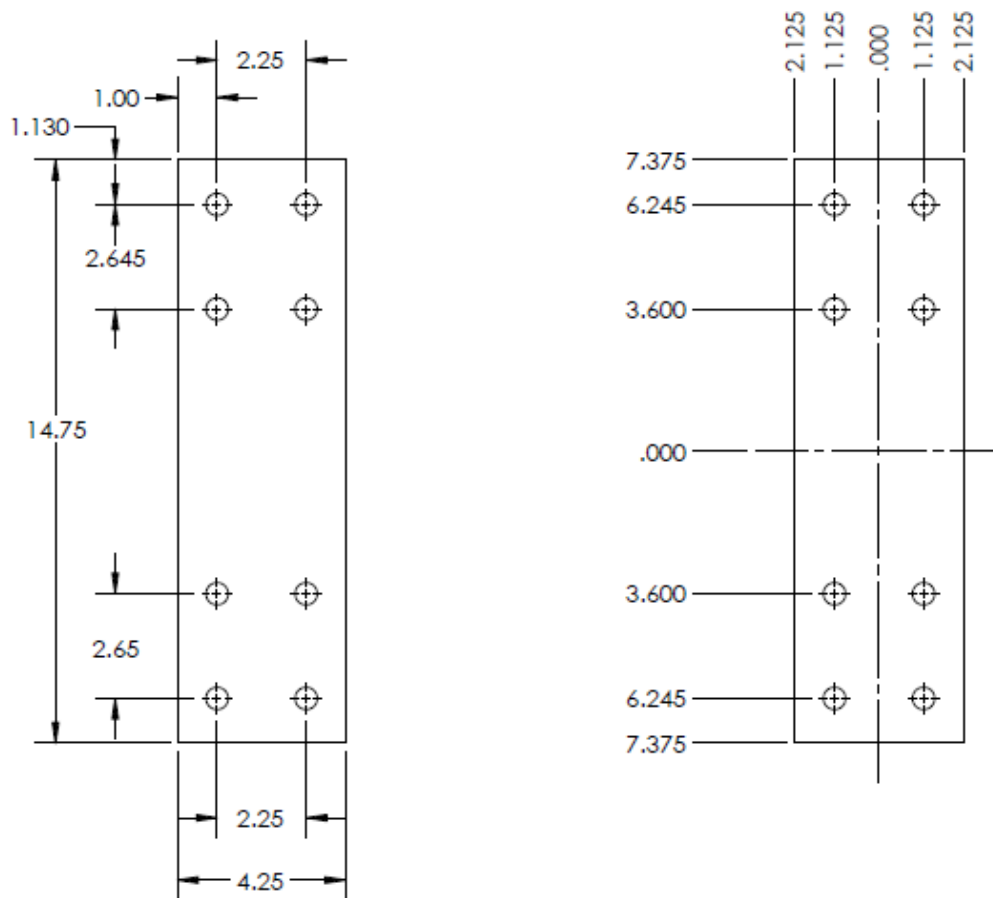
|  |  |  |  |      |  |   |  |                     |  |                    |  |               |  |
|--|--|--|--|------|--|---|--|---------------------|--|--------------------|--|---------------|--|
| DIMENSIONS ARE IN INCHES<br>TOLERANCES:<br>FRACTIONAL: ±<br>ANGULAR: MACH ± BEND ±<br>TWO PLACE DECIMAL ±<br>THREE PLACE DECIMAL ± |  | NAME                                     |  | DATE |  | UNIVERSITY OF ALASKA ANCHORAGE<br>COLLEGE OF ENGINEERING<br>DEPARTMENT OF CIVIL ENGINEERING |  |                     |  |                    |  |               |  |
|  |  | DRAWN                                    |  | SW   |  |   |  |                     |  | 11/27              |  |               |  |
|  |  | CHECKED                                  |  | SH   |  | 11/27   |  | PROJECT<br>1304     |  |                    |  |               |  |
|  |  | ENG APPR.                                |  | SH   |  | 11/27   |  |                     |  |                    |  |               |  |
|  |  | MFG APPR.                                |  | CR   |  | 11/27   |  |                     |  |                    |  |               |  |
| MATERIAL   |  | Q.A.                                     |  | SW   |  | 11/27   |  | 1.5-4 ACME ROD (x2) |  |                    |  |               |  |
| FINISH   |  | COMMENTS:<br>DEBURR & BREAK SHARP EDGES. |  |      |  |   |  |                     |  |                    |  |               |  |
| DO NOT SCALE DRAWING   |  |  |  |      |  |   |  | SIZE<br><b>A</b>    |  | DWG. NO.<br>Master |  | REV.          |  |
|  |  |  |  |      |  |   |  | SCALE: 1/4"         |  | WEIGHT:            |  | SHEET 9 OF 12 |  |



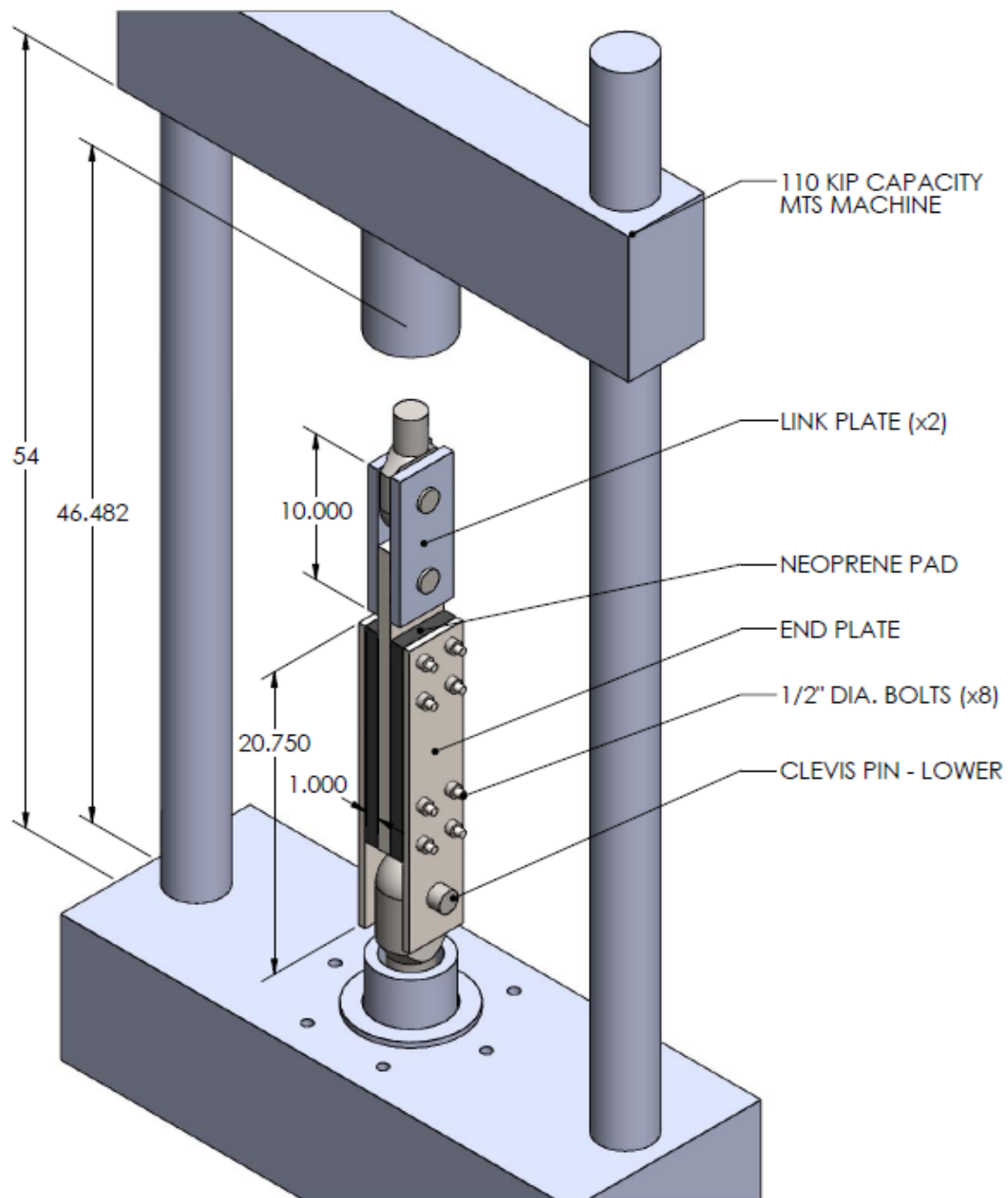
|                          |  |                             |  |      |  |                                |             |                                 |          |      |                |  |      |  |
|--------------------------|--|-----------------------------|--|------|--|--------------------------------|-------------|---------------------------------|----------|------|----------------|--|------|--|
| DIMENSIONS ARE IN INCHES |  | NAME                        |  | DATE |  | UNIVERSITY OF ALASKA ANCHORAGE |             |                                 |          |      |                |  |      |  |
| TOLERANCES:              |  | DRAWN                       |  | SW   |  | 11/27                          |             | COLLEGE OF ENGINEERING          |          |      |                |  |      |  |
| FRACTIONAL: ±            |  | CHECKED                     |  | SH   |  | 11/27                          |             | DEPARTMENT OF CIVIL ENGINEERING |          |      |                |  |      |  |
| ANGULAR: MACH ± BEND ±   |  | ENG APPR.                   |  | SH   |  | 11/27                          |             | PROJECT                         |          | 1304 |                |  |      |  |
| TWO PLACE DECIMAL ±      |  | MFG APPR.                   |  | CB   |  | 11/27                          |             | ROLLER CAP                      |          |      |                |  |      |  |
| THREE PLACE DECIMAL ±    |  | G.A.                        |  | SW   |  | 11/27                          |             |                                 |          |      |                |  |      |  |
| MATERIAL                 |  | COMMENTS:                   |  |      |  |                                |             |                                 |          |      |                |  |      |  |
| FINISH                   |  | DEBURR & BREAK SHARP EDGES. |  |      |  |                                | SIZE        |                                 | DWG. NO. |      | Master         |  | REV. |  |
| DO NOT SCALE DRAWING     |  |                             |  |      |  |                                | SCALE: 1/8" |                                 | WEIGHT:  |      | SHEET 10 OF 12 |  |      |  |



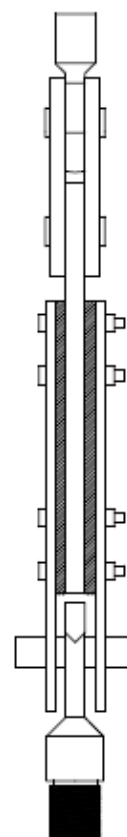
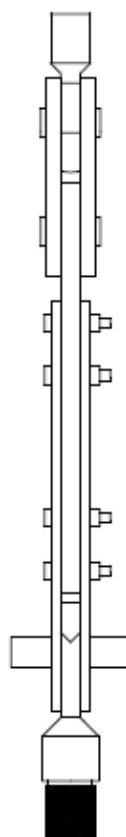
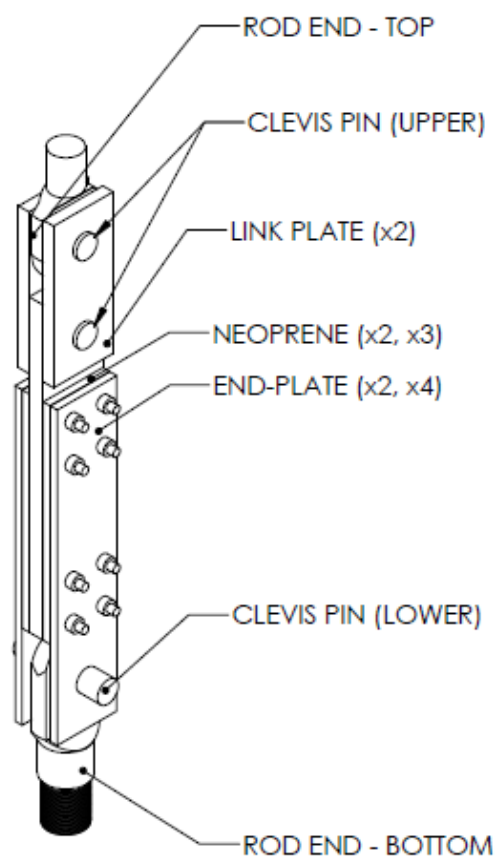
|                             |             |                             |      |                                   |  |
|-----------------------------|-------------|-----------------------------|------|-----------------------------------|--|
| DIMENSIONS ARE IN INCHES    |             | NAME                        | DATE | UNIVERSITY OF ALASKA ANCHORAGE    |  |
| TOLERANCES:                 |             | DRAWN                       | SW   | 11/27                             | COLLEGE OF ENGINEERING                   |
| FRACTIONAL: ±               |             | CHECKED                     | SH   | 11/27                             | DEPARTMENT OF CIVIL ENGINEERING          |
| ANGULAR: MACH: ±    BEND: ± |             | ENG APPR.                   | SH   | 11/27                             | PROJECT 1304                             |
| TWO PLACE DECIMAL: ±        |             | MFG APPR.                   | CR   | 11/27                             |  |
| THREE PLACE DECIMAL: ±      |             | G.A.                        | SW   | 11/27                             | OVERVIEW                                 |
| MATERIAL                    | ALLOY STEEL | COMMENTS:                   |      | SIZE A    DWG. NO. Master    REV. |  |
| FINISH                      | SHOP PRIMER | DEBURR & BREAK SHARP EDGES. |      |                                   | SCALE: 1/4"    WEIGHT:    SHEET 11 OF 12 |
| DO NOT SCALE DRAWING        |             |                             |      |                                   |  |



|                          |  |                             |      |                                |                                 |                |
|--------------------------|--|-----------------------------|------|--------------------------------|---------------------------------|----------------|
| DIMENSIONS ARE IN INCHES |  | NAME                        | DATE | UNIVERSITY OF ALASKA ANCHORAGE |                                 |                |
| TOLERANCES:              |  | DRAWN                       | SW   | 11/27                          | COLLEGE OF ENGINEERING          |                |
| FRACTIONAL: ±            |  | CHECKED                     | SH   | 11/27                          | DEPARTMENT OF CIVIL ENGINEERING |                |
| ANGULAR: MACH ± BEND ±   |  | ENG APPR.                   | SH   | 11/27                          | PROJECT<br>1304                 |                |
| TWO PLACE DECIMAL ±      |  | MFG APPR.                   | CR   | 11/27                          |                                 |                |
| THREE PLACE DECIMAL ±    |  | Q.A.                        | SW   | 11/27                          | NEOPRENE                        |                |
| MATERIAL                 |  | COMMENTS:                   |      |                                |                                 |                |
| FINISH                   |  | DEBURR & BREAK SHARP EDGES. |      |                                | SIZE<br>A                       |                |
| DO NOT SCALE DRAWING     |  |                             |      |                                |                                 |                |
|                          |  | DWG. NO.                    |      |                                | Master                          | REV.           |
|                          |  | SCALE:1/8                   |      |                                | WEIGHT:                         | SHEET 12 OF 12 |

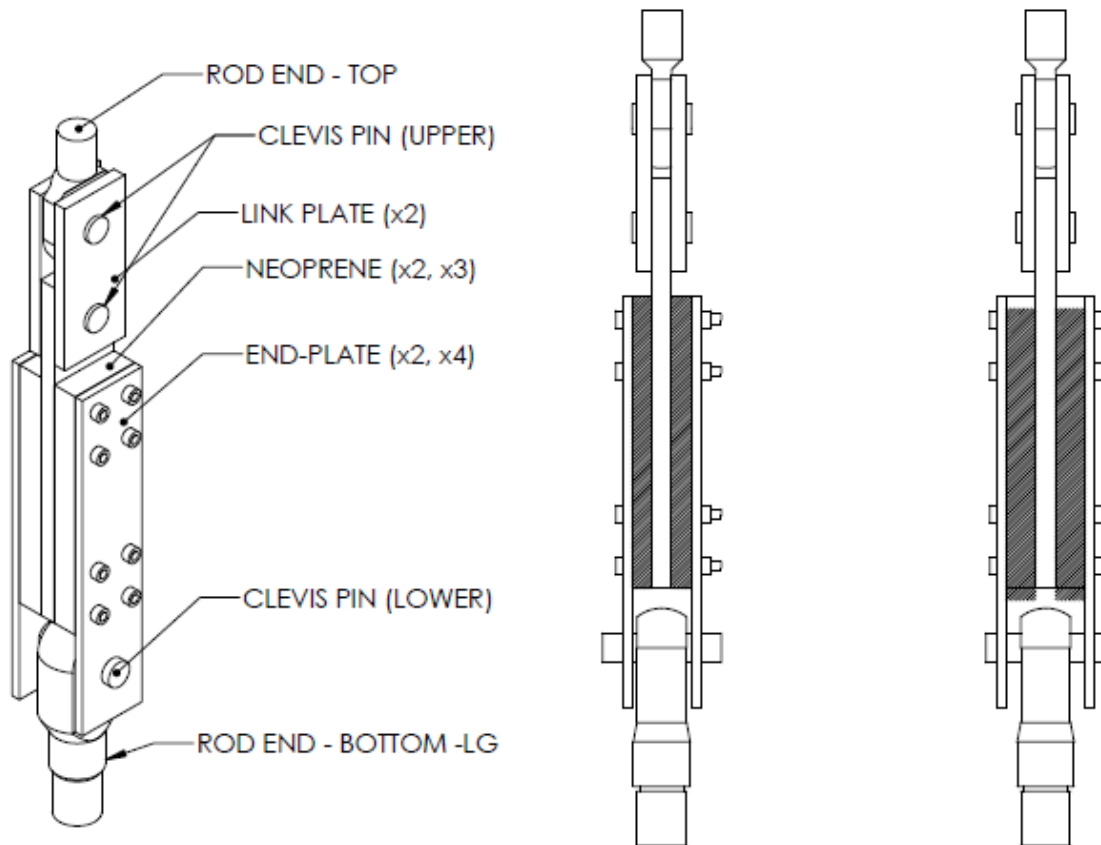


|  |                             |      |      |   |       |               |
|--|-----------------------------|------|------|---|-------|---------------|
| DIMENSIONS ARE IN INCHES<br>TOLERANCES:<br>FRACTIONAL: ±<br>ANGULAR: MACH ± BEND ±<br>TWO PLACE DECIMAL ±<br>THREE PLACE DECIMAL ± |                             | NAME | DATE | UNIVERSITY OF ALASKA ANCHORAGE<br>COLLEGE OF ENGINEERING<br>DEPARTMENT OF CIVIL ENGINEERING |       |               |
|  | DRAWN                       | SW   | 12/7 |   |       |               |
|  | CHECKED                     | SH   | 12/7 | PROJECT<br>1304   |       |               |
|  | ENG APPR.                   | SH   |      |   |       |               |
|  | MFG APPR.                   | CR   | 12/8 | GENERAL   |       |               |
|  | Q.A.                        | SW   | 12/8 |   |       |               |
| MATERIAL   | COMMENTS:                   |      |      | SITE DWG. NO. MasterShear   |       |               |
| FINISH   | DEBURR & BREAK SHARP EDGES. |      |      |   |       |               |
| DO NOT SCALE DRAWING   |                             |      |      | SCALE: 1:20   | WGHT: | SHEET 1 OF 12 |



**CONFIGURATION FOR TEST OF NONE & 0.5" PAD**

|  |  |    |      |  |
|--|--|----|------|--|
| DIMENSIONS ARE IN INCHES<br>TOLERANCES:<br>FRACTIONAL: $\pm$<br>ANGULAR: MACH $\pm$ BEND $\pm$<br>TWO PLACE DECIMAL $\pm$<br>THREE PLACE DECIMAL $\pm$<br>MATERIAL<br>FINISH<br>DO NOT SCALE DRAWING | DRAWN                                    | SW | 12/7 | <b>UNIVERSITY OF ALASKA ANCHORAGE</b><br><b>COLLEGE OF ENGINEERING</b><br><b>DEPARTMENT OF CIVIL ENGINEERING</b><br>PROJECT <b>1304</b><br>SITE <b>A</b> DWG. NO. <b>MasterShear</b> 10<br>SCALE: 1:20 WEIGHT: SHEET 2 OF 12 |
|  | CHECKED                                  | SH | 12/7 |  |
|  | ENG APPR.                                | SH |      |  |
|  | MFG APPR.                                | CR | 12/8 |  |
|  | Q.A.                                     | SW | 12/8 |  |
|  | COMMENTS:<br>DEBURR & BREAK SHARP EDGES. |    |      |  |



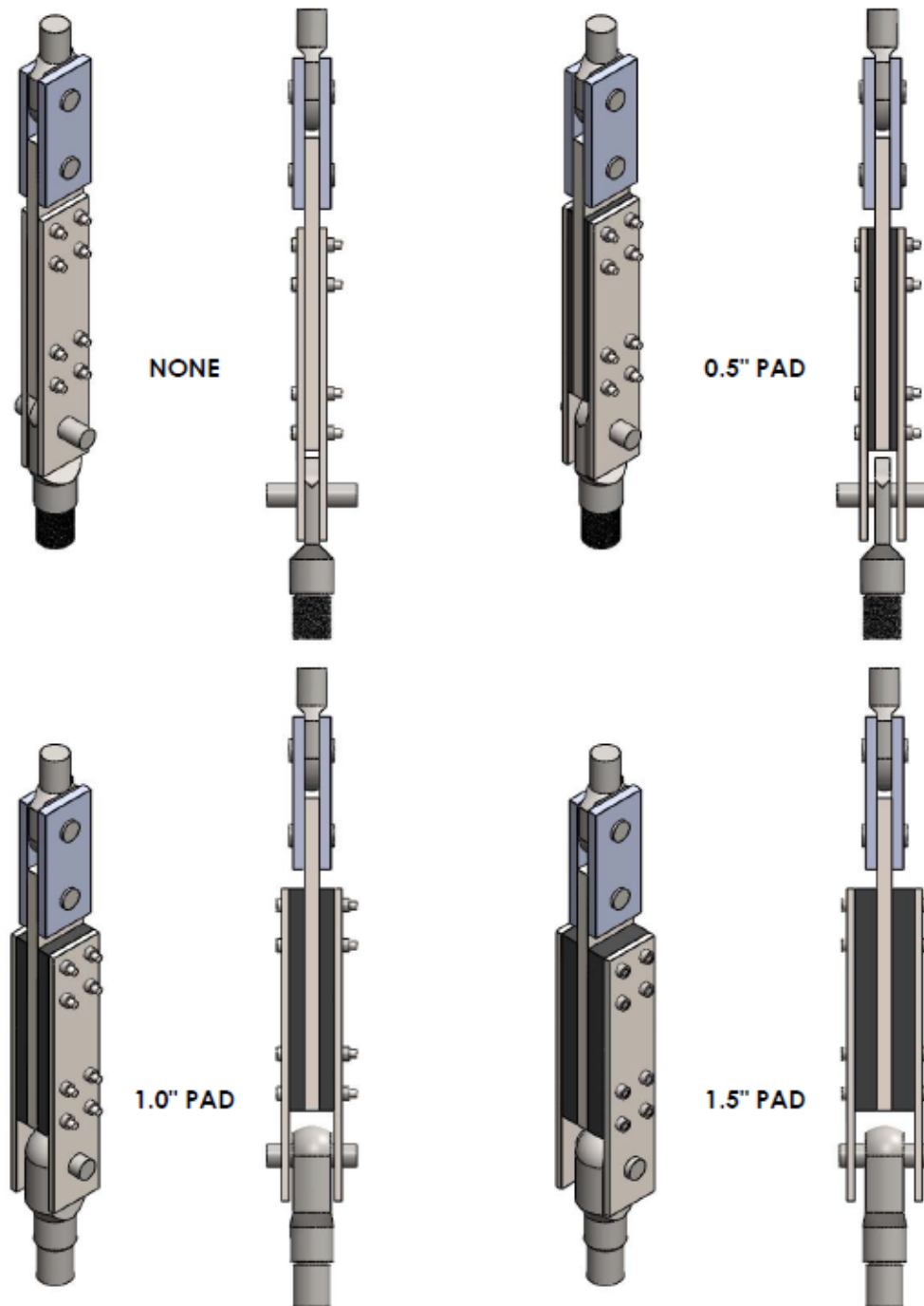
**CONFIGURATION FOR TEST OF 1.0" PAD & 1.5" PAD**

|  |  |    |      |  |
|--|--|----|------|--|
| DIMENSIONS ARE IN INCHES<br>TOLERANCES:<br>FRACTIONAL: $\pm$<br>ANGULAR: MACH $\pm$ BEND $\pm$<br>TWO PLACE DECIMAL $\pm$<br>THREE PLACE DECIMAL $\pm$<br>MATERIAL<br>FINISH<br>DO NOT SCALE DRAWING | DRAWN                                    | SW | 12/7 | <b>UNIVERSITY OF ALASKA ANCHORAGE</b><br><b>COLLEGE OF ENGINEERING</b><br><b>DEPARTMENT OF CIVIL ENGINEERING</b><br>PROJECT <b>1304</b><br><b>GENERAL</b><br>SEE DWG. NO. <b>MasterShear</b> 10<br>SCALE: 1/2" = 1'-0" WEIGHT: SHEET 3 OF 12 |
|  | CHECKED                                  | SH | 12/7 |  |
|  | ENG APPR.                                | SH |      |  |
|  | MFG APPR.                                | CR | 12/8 |  |
|  | Q.A.                                     | SW | 12/8 |  |
|  | COMMENTS:<br>DEBURR & BREAK SHARP EDGES. |    |      |  |

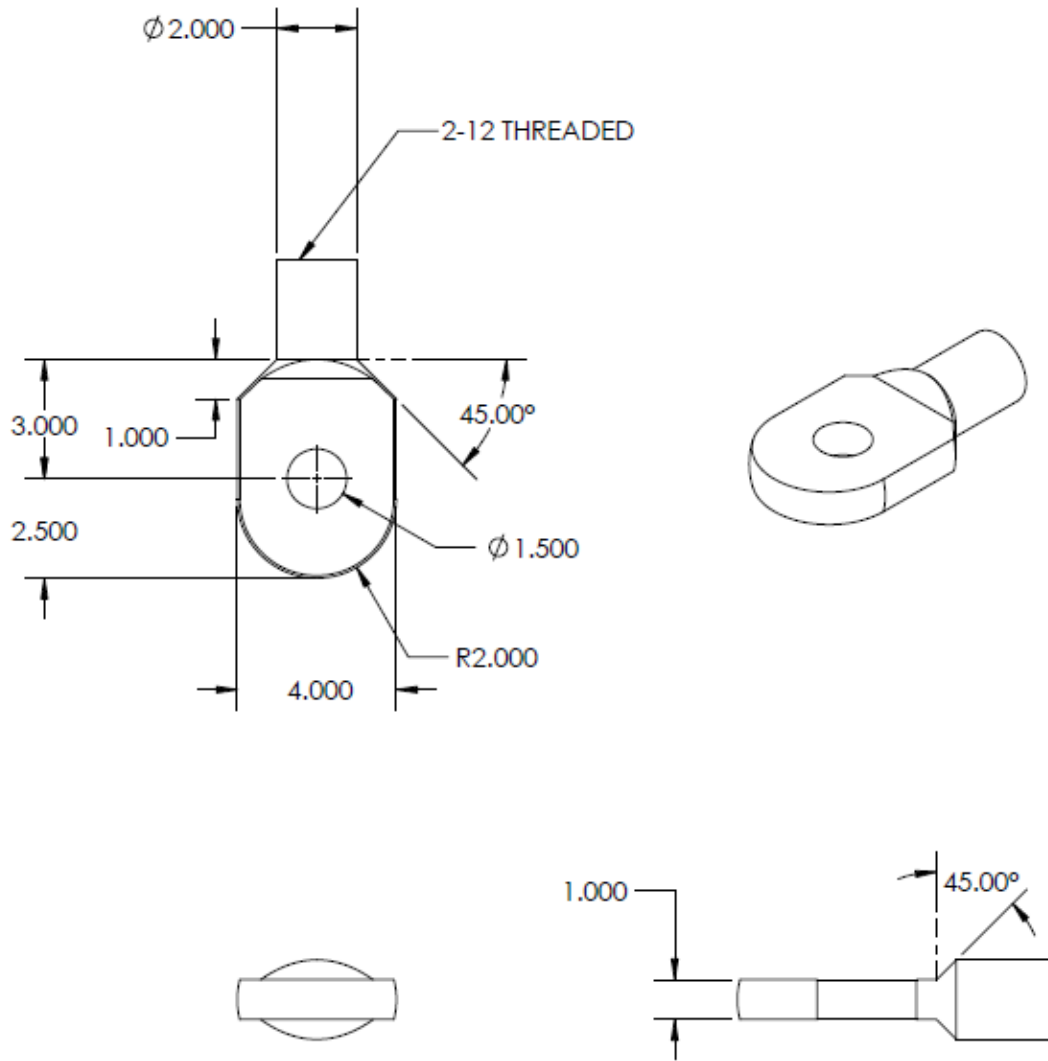
| ITEM NO.      | PART                | QTY | MATERIAL                | MATERIAL SRC              | MATERIAL DIM SPEC       | PRICE   | SHIP   |
|---------------|---------------------|-----|-------------------------|---------------------------|-------------------------|---------|--------|
| 1             | BULL EYE            | 2   | 1144 STEEL (90KSI)      | MCMMASTER                 | 4"D 12"L                | 360.74  | 353.00 |
| 2             | LINK PLATE          | 2   | A514 (100 KSI)          | STEELFAB                  | 0.75"x5"x10"            | 41.48   | 0.00   |
| 3             | PULL PLATE          | 1   | A514 (100KSI)           | STEELFAB                  | 1.0"x20.75"x4.25        | 48.55   | 0.00   |
| 4             | END PLATE           | 8   | A572 Gr 50 (50 KSI)     | STEELFAAB                 | 0.5"x20.75"x4.25"       | 155.76  | 0.00   |
| 5             | NEOPRENE            | 2   | CR DURO 60              | ALASKA RUBBER & SUPPLY CO | 2x<br>0.5"x14.75"x4.25" | 21.03   | 0.00   |
| 6             | NEOPRENE            | 2   | CR DURO 60              | ALASKA RUBBER & SUPPLY CO | 2x<br>1.0"x14.75"x4.25" | 41.80   | 0.00   |
| 7             | NEOPRENE            | 2   | CR DURO 60              | ALASKA RUBBER & SUPPLY CO | 2x<br>1.5"x14.75"x4.25" | 65.00   | 60.70  |
| 8             | BOLTS               | 8   | A325                    | FASTENERS & FIRE          | 0.5"D x 2.5"L           | 3.19    | 0.00   |
| 9             | BOLTS               | 8   | A325                    | FASTENERS & FIRE          | 0.5"D x 3.5"L           | 4.20    | 0.00   |
| 10            | BOLTS               | 8   | A325                    | WHOLESALE BOLTS.COM       | 0.5"D x 4.5"L           | 7.56    | 0.00   |
| 11            | BOLTS               | 8   | A325                    | WHOLESALE BOLTS.COM       | 0.5"D x 5.5"L           | 11.37   | 42.92  |
| 12            | CLEVIS PIN - LOWER  | 1   | 300M STEEL (210 ksi)    | MCMMASTER                 | 1.5"D x 1'L             | 83.88   | 0.00   |
| 13            | ROD END EYE         | 1   | 1144 STEEL (90KSI)      | MCMMASTER                 | 4"D 12"L                | 180.37  | 0.00   |
| 14            | CLEVIS PINS - UPPER | 2   | A193, Grade B7 (125ksi) | FASTENERS & FIRE          | 1.5-6 6"L               | 4.30    | 0.00   |
| <b>TOTAL:</b> |                     |     |                         |                           |                         | 1029.23 | 456.62 |

|   |  |  |                                      |  |
|---|--|--|--------------------------------------|--|
| DIMENSIONS ARE IN INCHES<br>TOLERANCES:<br>FRACTIONAL ±<br>ANGULAR: MACH ± BEND ±<br>TWO PLACE DECIMAL ±<br>THREE PLACE DECIMAL ± |  | NAME<br>DRAWN: SW<br>CHECKED: SH<br>ENG APPR: SH<br>MFG APPR: CR<br>Q.A.: SW | DATE<br>12/7<br>12/7<br>12/8<br>12/8 | <b>UNIVERSITY OF ALASKA ANCHORAGE</b><br><b>COLLEGE OF ENGINEERING</b><br><b>DEPARTMENT OF CIVIL ENGINEERING</b><br>PROJECT 1304 |
| MATERIAL<br>FINISH<br>DO NOT SCALE DRAWING  | COMMENTS:<br>DEBURR & BREAK SHARP EDGES. |  | SCALE: 1/20<br>WBDH:                 | DWG. NO. MasterShear<br>10<br>SHEET 4 OF 12  |

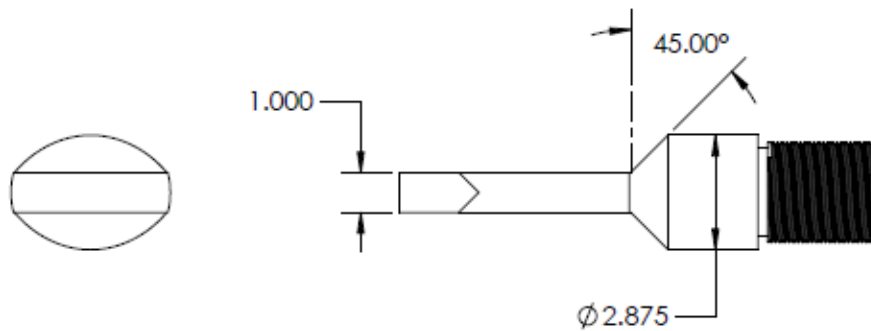
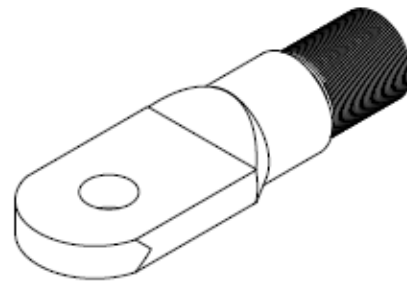
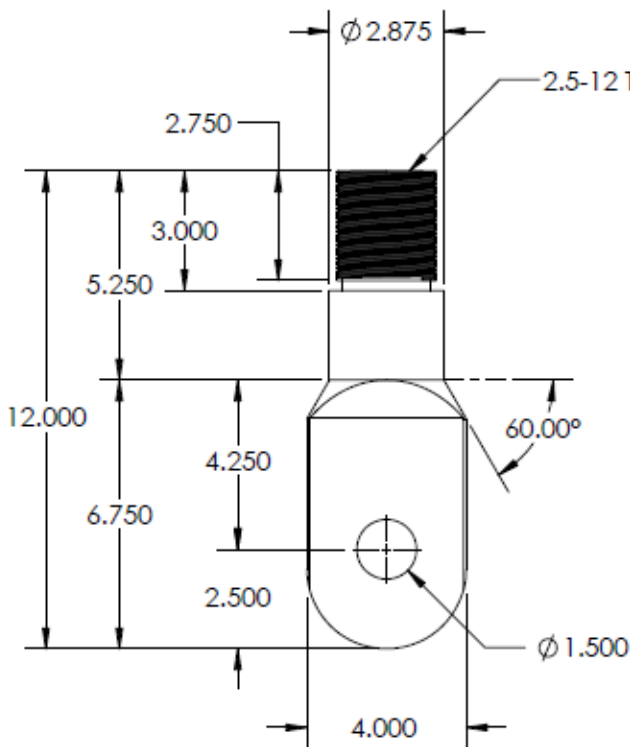




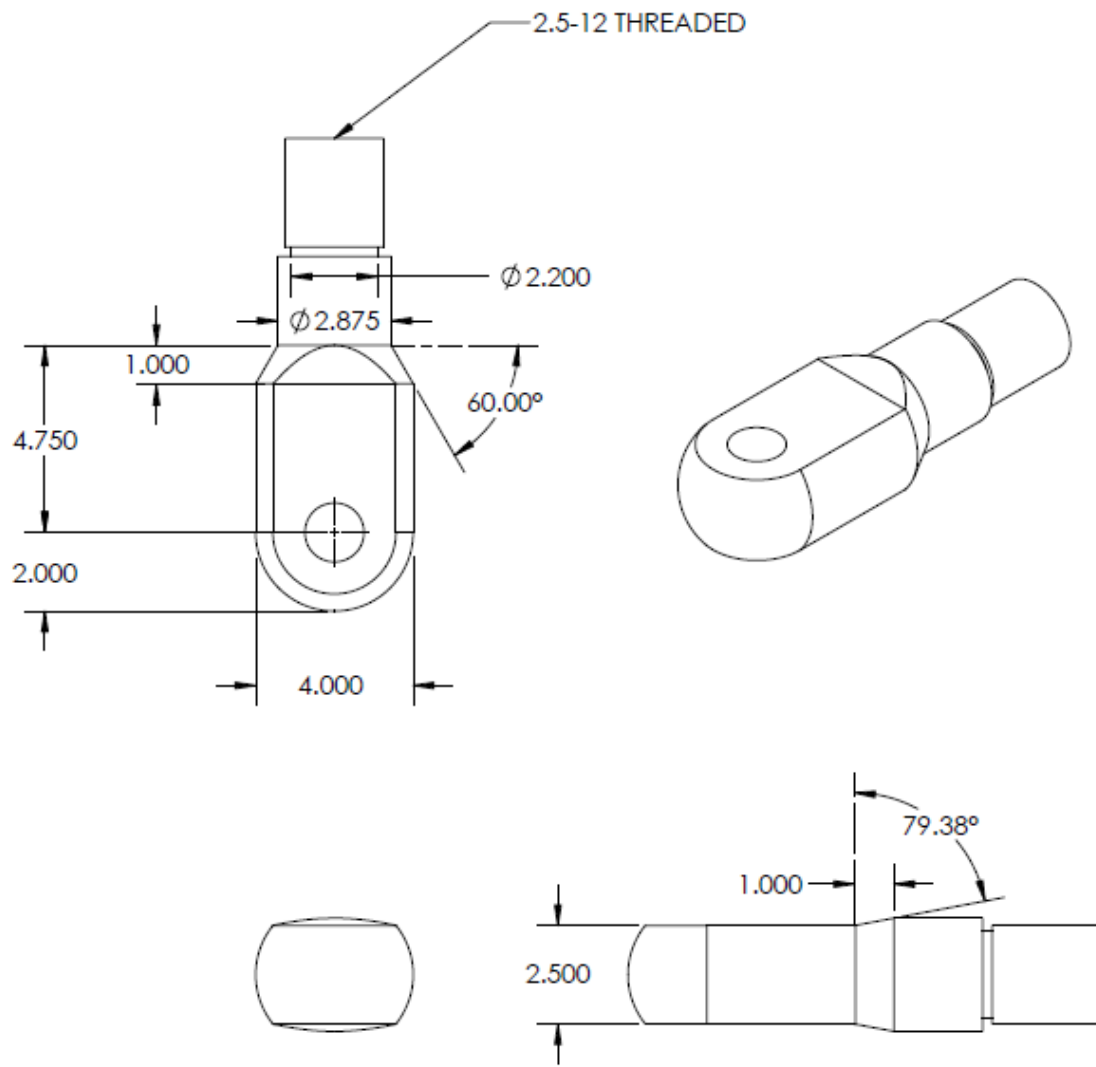
|                          |  |  |  |                      |  |   |  |
|--------------------------|--|--|--|----------------------|--|---|--|
| DIMENSIONS ARE IN INCHES |  | NAME                                     |  | DATE                 |  | UNIVERSITY OF ALASKA ANCHORAGE<br>COLLEGE OF ENGINEERING<br>DEPARTMENT OF CIVIL ENGINEERING |  |
| TOLERANCES:              |  | DRAWN                                    |  | 12/7                 |  |   |  |
| FRACTIONAL ±             |  | CHECKED                                  |  | 12/7                 |  |   |  |
| ANGULAR: MACH ±          |  | ENG APPR.                                |  | SH                   |  |   |  |
| TWO PLACE DECIMAL ±      |  | MFG APPR.                                |  | 12/8                 |  |   |  |
| THREE PLACE DECIMAL ±    |  | Q.A.                                     |  | 12/8                 |  | PROJECT 1304  |  |
| MATERIAL                 |  | COMMENTS:<br>DEBURR & BREAK SHARP EDGES. |  |                      |  | CONFIGURATIONS  |  |
| FINISH                   |  |  |  |                      |  |   |  |
| DO NOT SCALE DRAWING     |  | SIZE A                                   |  | DWG. NO. MasterShear |  | REV. 10   |  |
|                          |  | SCALE: 1/20                              |  | WEIGHT:              |  | SHEET 5 OF 12   |  |



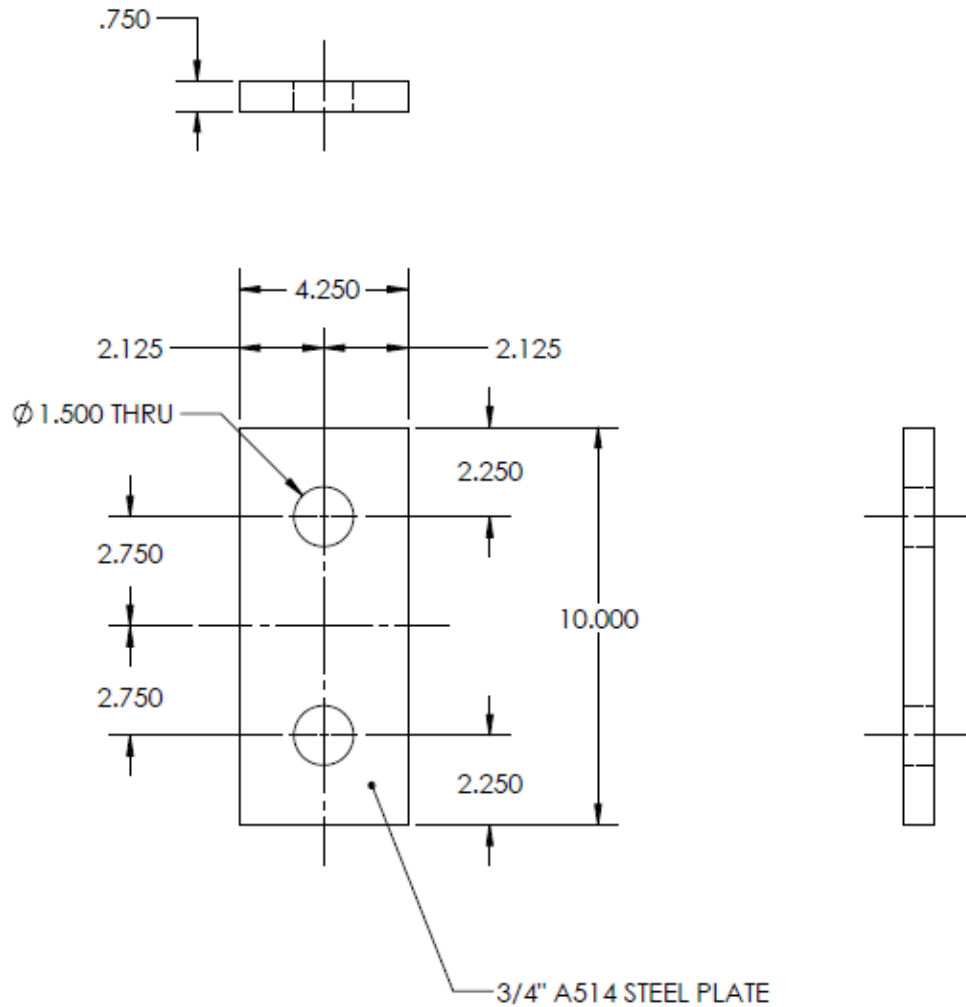
|                          |  |                             |  |      |  |                                |  |                                 |  |
|--------------------------|--|-----------------------------|--|------|--|--------------------------------|--|---------------------------------|--|
| DIMENSIONS ARE IN INCHES |  | NAME                        |  | DATE |  | UNIVERSITY OF ALASKA ANCHORAGE |  |                                 |  |
| TOLERANCES:              |  | DRAWN                       |  | SW   |  | 12/7                           |  | COLLEGE OF ENGINEERING          |  |
| FRACTIONAL: ±            |  | CHECKED                     |  | SH   |  | 12/7                           |  | DEPARTMENT OF CIVIL ENGINEERING |  |
| ANGULAR: MACH ± BEND ±   |  | ENG APPR.                   |  | SH   |  |                                |  | PROJECT                         |  |
| TWO PLACE DECIMAL ±      |  | MFG APPR.                   |  | CR   |  | 12/8                           |  | 1304                            |  |
| THREE PLACE DECIMAL ±    |  | G.A.                        |  | SW   |  | 12/8                           |  | ROD END - TOP (x1)              |  |
| MATERIAL                 |  | COMMENTS:                   |  |      |  | SIZE                           |  | DWG. NO.                        |  |
| FINISH                   |  | DEBURR & BREAK SHARP EDGES. |  |      |  | A                              |  | MasterShear                     |  |
| DO NOT SCALE DRAWING     |  |                             |  |      |  | SCALE: 1:20                    |  | WEIGHT:                         |  |
|                          |  |                             |  |      |  |                                |  | REV. 10                         |  |
|                          |  |                             |  |      |  |                                |  | SHEET 4 OF 12                   |  |



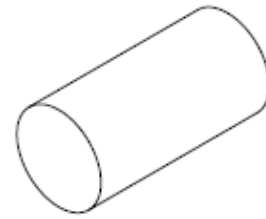
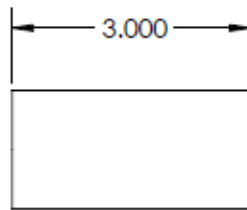
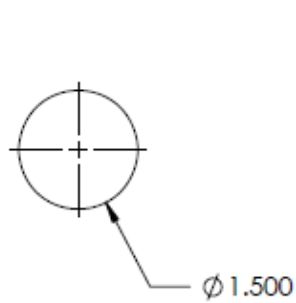
|  |  |      |      |   |                         |               |
|--|--|------|------|---|-------------------------|---------------|
| DIMENSIONS ARE IN INCHES<br>TOLERANCES:<br>FRACTIONAL: ±<br>ANGULAR: MACH ± BEND ±<br>TWO PLACE DECIMAL ±<br>THREE PLACE DECIMAL ± |  | NAME | DATE | UNIVERSITY OF ALASKA ANCHORAGE<br>COLLEGE OF ENGINEERING<br>DEPARTMENT OF CIVIL ENGINEERING |                         |               |
|  | DRAWN                                    | SW   | 12/7 |   |                         |               |
|  | CHECKED                                  | SH   | 12/7 | PROJECT<br>1304   |                         |               |
|  | ENG APPR.                                | SH   |      |   |                         |               |
|  | MFG APPR.                                | CR   | 12/8 |   |                         |               |
| MATERIAL   | Q.A.                                     | SW   | 12/8 | ROD END - BOTTOM (x1)   |                         |               |
| FINISH   | COMMENTS:<br>DEBURR & BREAK SHARP EDGES. |      |      |   |                         |               |
| DO NOT SCALE DRAWING   |  |      |      | SIZE<br>A   | DWG. NO.<br>MasterShear | REV.<br>T0    |
|  |  |      |      | SCALE: 1:20   | WEIGHT:                 | SHEET 7 OF 12 |



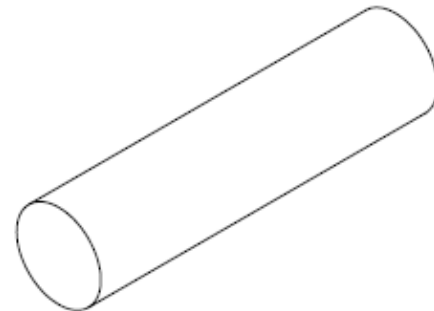
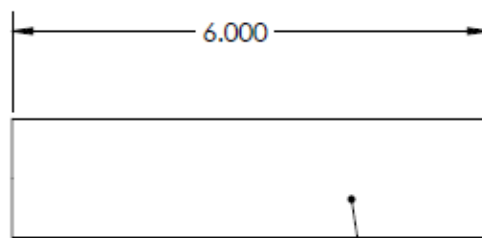
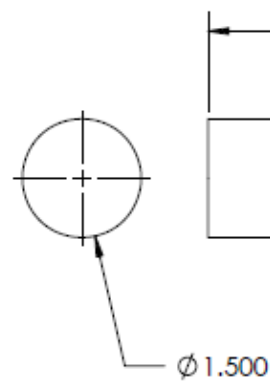
|  |                             |      |      |   |                       |
|--|-----------------------------|------|------|---|-----------------------|
| DIMENSIONS ARE IN INCHES<br>TOLERANCES:<br>FRACTIONAL: ±<br>ANGULAR: MACH ± BEND ±<br>TWO PLACE DECIMAL ±<br>THREE PLACE DECIMAL ± |                             | NAME | DATE | UNIVERSITY OF ALASKA ANCHORAGE<br>COLLEGE OF ENGINEERING<br>DEPARTMENT OF CIVIL ENGINEERING |                       |
|  | DRAWN                       | SW   | 12/7 |   |                       |
|  | CHECKED                     | SH   | 12/7 | PROJECT<br>1304   |                       |
|  | ENG APPR.                   | SH   |      |   |                       |
|  | MFG APPR.                   | CR   | 12/8 |   |                       |
| MATERIAL   | Q.A.                        | SW   | 12/8 | ROD END - BOTTOM - LG (x1)  |                       |
|  | COMMENTS:                   |      |      |   |                       |
| FINISH   | DEBURR & BREAK SHARP EDGES. |      |      | SIZE  | DWG. NO.              |
| DO NOT SCALE DRAWING   |                             |      |      | A   | MasterShear           |
|  |                             |      |      | SCALE: 1:20   | WEIGHT: SHEET 8 OF 12 |



|                          |  |                             |  |             |  |   |  |      |  |
|--------------------------|--|-----------------------------|--|-------------|--|---|--|------|--|
| DIMENSIONS ARE IN INCHES |  | NAME                        |  | DATE        |  | UNIVERSITY OF ALASKA ANCHORAGE<br>COLLEGE OF ENGINEERING<br>DEPARTMENT OF CIVIL ENGINEERING |  |      |  |
| TOLERANCES:              |  | DRAWN                       |  | SW          |  |   |  | 12/7 |  |
| FRACTIONAL: ±            |  | CHECKED                     |  | SH          |  |   |  | 12/7 |  |
| ANGULAR: MACH ± BEND ±   |  | ENG APPR.                   |  | SH          |  |   |  |      |  |
| TWO PLACE DECIMAL ±      |  | MFG APPR.                   |  | CR          |  |   |  | 12/8 |  |
| THREE PLACE DECIMAL ±    |  | G.A.                        |  | SW          |  | 12/8  |  |      |  |
| MATERIAL                 |  | COMMENTS:                   |  |             |  | PROJECT<br><br>1304   |  |      |  |
| FINISH                   |  | DEBURR & BREAK SHARP EDGES. |  |             |  |   |  |      |  |
| DO NOT SCALE DRAWING     |  |                             |  |             |  | LINK PLATE (x2)   |  |      |  |
|                          |  | SIZE                        |  | DWG. NO.    |  | REV.  |  |      |  |
|                          |  | A                           |  | MasterShear |  | 10  |  |      |  |
|                          |  | SCALE: 1/2"                 |  | WEIGHT:     |  | SHEET 9 OF 12   |  |      |  |



**CLEVIS PIN - UPPER**

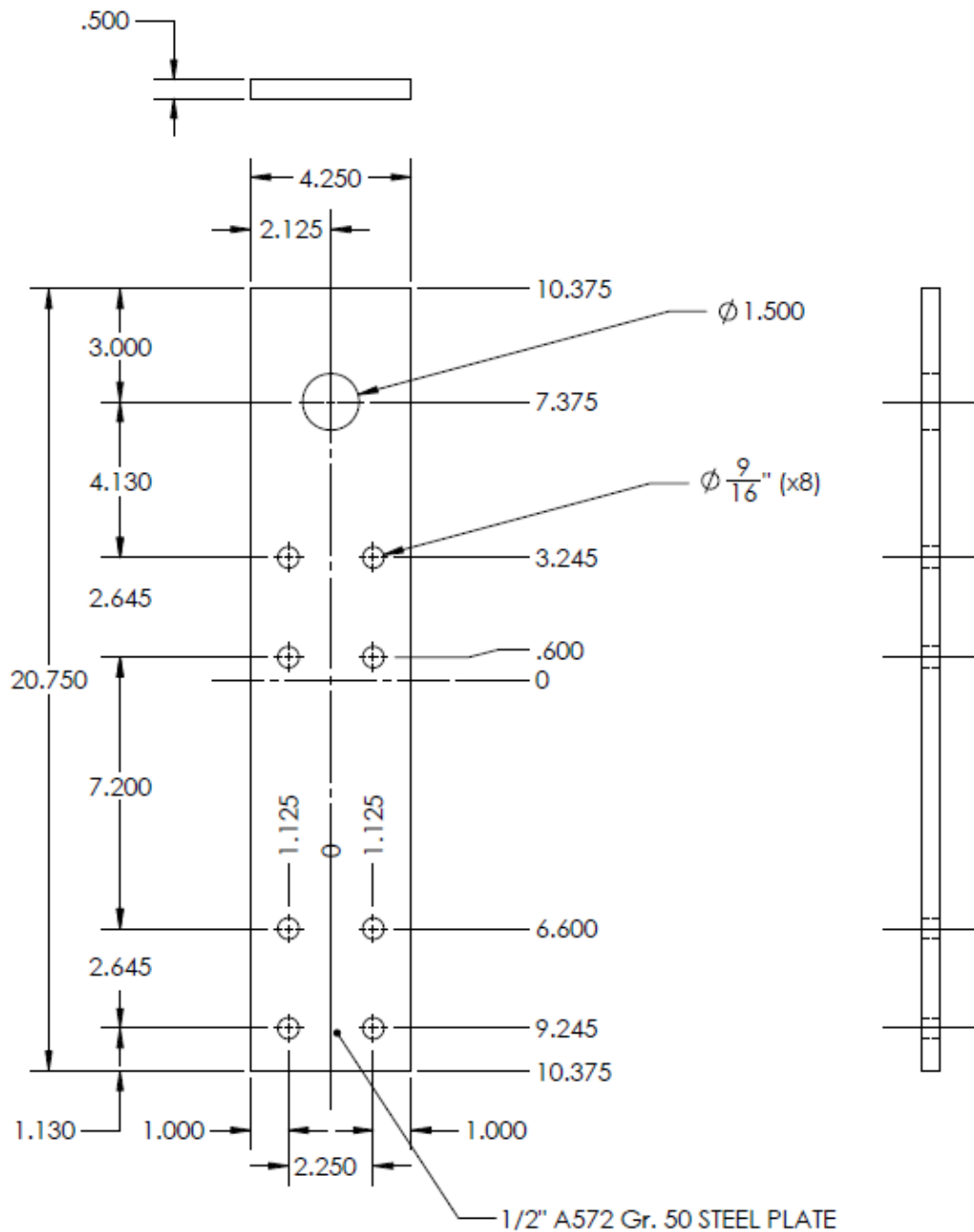


1.5" DIA 300M STEEL ROD

**CLEVIS PIN - LOWER**

|                          |  |                                    |      |   |                |
|--------------------------|--|------------------------------------|------|---|----------------|
| DIMENSIONS ARE IN INCHES |  | NAME                               | DATE | UNIVERSITY OF ALASKA ANCHORAGE<br>COLLEGE OF ENGINEERING<br>DEPARTMENT OF CIVIL ENGINEERING |                |
| TOLERANCES:              |  | DRAWN                              | SW   |   | 12/7           |
| FRACTIONAL: ±            |  | CHECKED                            | SH   |   | 12/7           |
| ANGULAR: MACH ± BEND ±   |  | ENG APPR.                          | SH   |   |                |
| TWO PLACE DECIMAL ±      |  | MFG APPR.                          | CR   | 12/8  | PROJECT 1304   |
| THREE PLACE DECIMAL ±    |  | Q.A.                               | SW   | 12/8  |                |
| MATERIAL                 |  | COMMENTS:                          |      |   |                |
| FINISH                   |  | DEBURR & BREAK SHARP EDGES.        |      |   |                |
| DO NOT SCALE DRAWING     |  | SIZE DWG. NO. <b>A</b> MasterShear |      |   | REV. 10        |
|                          |  | SCALE: 1:20 WEIGHT:                |      |   | SHEET 10 OF 12 |





|                                |  |                             |             |   |
|--------------------------------|--|-----------------------------|-------------|---|
| DIMENSIONS ARE IN INCHES       |  | NAME                        | DATE        | UNIVERSITY OF ALASKA ANCHORAGE<br>COLLEGE OF ENGINEERING<br>DEPARTMENT OF CIVIL ENGINEERING |
| TOLERANCES:                    |  | DRAWN                       | SW          |   |
| FRACTIONAL: $\pm$              |  | CHECKED                     | SH          |   |
| ANGULAR: MACH $\pm$ BEND $\pm$ |  | ENG APPR.                   | SH          |   |
| TWO PLACE DECIMAL $\pm$        |  | MFG APPR.                   | CR          |   |
| THREE PLACE DECIMAL $\pm$      |  | G.A.                        | SW          | 12/8  |
| MATERIAL                       |  | COMMENTS:                   |             | PROJECT 1304  |
| FINISH                         |  | DEBURR & BREAK SHARP EDGES. |             | END PLATE (x8)  |
| DO NOT SCALE DRAWING           |  | SIZE                        | DWG. NO.    | REV   |
|                                |  | A                           | MasterShear | 10  |
|                                |  | SCALE: 1/20                 | WEIGHT:     | SHEET 12 OF 12  |





THIS PAGE INTENTIONALLY LEFT BLANK

## Appendix C End-plate design

### End plate design strength:

#### Given:

$$P := 11.2 \text{ kip}$$

$$d := 45.9 \text{ in}$$

$$V_u := P = 11.2 \text{ kip}$$

$$M_u := P \cdot d = 514.08 \text{ kip} \cdot \text{in}$$

#### Beam:

W10x19

#### Geometric properties:

ASTM A992

$$d := 10.2 \text{ in}$$

$$t_w := 0.25 \text{ in}$$

$$F_y := 50 \text{ ksi}$$

$$b_f := 4.02 \text{ in}$$

$$t_f := 0.395 \text{ in}$$

$$F_u := 65 \text{ ksi}$$

$$Z_x := 21.6 \text{ in}^3$$

#### Plate:

ASTM A572 Gr. 50

$$F_{yp} := 50 \text{ ksi}$$

$$F_{up} := 65 \text{ ksi}$$

#### Solution:

Extended end-plate geometric properties:

$$b_p := 4.5 \text{ in}$$

$$g := 2.25 \text{ in}$$

$$p_{ft} := 1.125 \text{ in}$$

$$p_{fo} := 1.125 \text{ in}$$

$$h_o := d + p_{fo} - \frac{t_f}{2} = 11.128 \text{ in}$$

$$h_I := d - p_{ff} - t_f - \frac{t_f}{2} = 8.483 \text{ in}$$

#### Required bolt diameter assuming no prying action

From Design guide 4 Equation 3.5, determine the required bolt diameter:

$$F_m := 90 \text{ ksi}$$

$$\phi := 0.75$$

$$d_{b\_req'd} := \sqrt{\frac{2 \cdot M_u}{\pi \cdot \phi \cdot F_m \cdot (h_o + h_I)}} = 0.497 \text{ in}$$

$$d_{b\_req'd} = 0.497 \text{ in}$$

$$d_b := 0.5 \text{ in}$$

$$\frac{d_{b\_req'd}}{d_b} = 0.994$$

$$R_u := \pi \cdot \left(\frac{d_b}{2}\right)^2 \cdot F_m = 17.671 \text{ kip}$$

#### Required end-plate thickness:

The end-plate yield line mechanism parameter is:

$$s := \sqrt{\frac{b_p \cdot g}{2}} = 2.25 \text{ in}$$

$$p_{ff} := \min(p_{ff}, s) = 1.125 \text{ in}$$

From Design Guide 4 Table 3.1:

$$Y_p := \frac{b_p}{2} \cdot \left( h_I \cdot \left( \frac{1}{p_{ff}} + \frac{1}{s} \right) + h_o \cdot \left( \frac{1}{p_{fo}} - \frac{1}{2} \right) + \frac{2}{g} \cdot (h_I \cdot (p_{ff} + s)) \right) = 72.025 \text{ in}$$

$$P_t := F_{nt} \cdot \left( \frac{\pi \cdot d_b^2}{4} \right) = 17.671 \text{ kip}$$

$$M_{np} := 2 \cdot P_t \cdot (h_o + h_1) = 693.075 \text{ kip} \cdot \text{in}$$

The no prying bolt available flexural strength is:  $h_1$

$$\phi := 0.75$$

$$\phi_b := 0.90$$

$$t_{p\_req'd} := \sqrt{\frac{1.11 \cdot \phi \cdot M_{np}}{\phi_b \cdot F_{yp} \cdot Y_p}} = 0.422 \text{ in}$$

$$t_p := 0.5 \text{ in}$$

$$\frac{t_{p\_req'd}}{t_p} = 0.844$$

With a plate thickness of  $t_p$ , the design strength is:

$$\phi_b := 0.90$$

$$M_{pl} := \frac{F_{yp} \cdot t_p^2 \cdot Y_p}{1.11} = 67.591 \text{ kip} \cdot \text{ft}$$

$$\frac{M_u}{\phi_b \cdot M_{pl}} = 0.704$$

And bolt rupture is:

$$\frac{M_u}{\phi \cdot M_{np}} = 0.989$$

Check thick plate behavior:

$$M_{pl} = 67.591 \text{ kip} \cdot \text{ft}$$

$$M_{np} = 57.756 \text{ kip} \cdot \text{ft}$$

$$\frac{1.1 M_{np}}{M_{pl}} = 0.94$$

### **Beam flange force**

The required force applied to the end plate through the beam flange is:

$$F_{fu} := \frac{M_u}{d - t_f} = 52.43 \text{ kip}$$

### **Shear yielding of the extended end plate**

Available strength due to shear yielding on the extended portion of the end plate

$$\phi := 0.90$$

$$R_n := 0.6 \cdot F_{yp} \cdot b_p \cdot t_p = 67.5 \text{ kip}$$

$$R_u := \frac{F_{fu}}{2} = 26.215 \text{ kip}$$

$$\frac{R_u}{\phi \cdot R_n} = 0.432$$

### **Shear rupture of the extended end plate**

Available strength due to shear rupture on the extended portion of the end plate

$$A_n := \left( b_p - 2 \cdot \left( d_b + \frac{1}{16} \text{ in} + \frac{1}{16} \text{ in} \right) \right) \cdot t_p = 1.625 \text{ in}^2$$

$$\phi := 0.75$$

$$R_n := 0.6 \cdot F_{up} \cdot A_n = 63.375 \text{ kip}$$

$$R_u := \frac{F_{fu}}{2} = 26.215 \text{ kip}$$

$$\frac{R_u}{\phi \cdot R_n} = 0.552$$

### **Bolt shear and bearing**

Try the minimum of four bolts at the compression flange.

$$F_m := 54 \text{ ksi} \quad (\text{A325, threads not excluded})$$

$$F_m := 68 \text{ ksi} \quad (\text{A325, threads excluded})$$

$$d_b = 0.5 \text{ in}$$

$$n := 8$$

$$\phi := 0.75$$

$$A_b := \left( \frac{\pi}{4} \cdot d_b^2 \right)$$

$$R_n := n \cdot F_m \cdot A_b = 84.823 \text{ kip}$$

$$R_u := V_u = 11.2 \text{ kip}$$

$$\frac{R_u}{\phi \cdot R_n} = 0.176$$

### **Bolt bearing on the end plate:**

$$\phi := 0.75$$

$$l_c := d_b + 0.375 \text{ in} \quad \text{Edge distance}$$

$$n := 2$$

$$R_n := \min(1.5 \cdot l_c \cdot t_p \cdot F_{up}, 3.0 \cdot d_b \cdot t_p \cdot F_{up}) = 42.656 \text{ kip}$$

$$R_u := \frac{V_u}{n} = 5.6 \text{ kip}$$

$$\frac{R_u}{\phi \cdot R_n} = 0.175$$

**Beam web to end-plate fillet weld:**

Determine the required size of the beam web to end-plate fillet weld in the tension-bolt region to develop the yield strength of the beam web. The minimum weld size required to match the shear rupture strength of the weld to the tension yield strength of the beam web, per unit length, is:

For:

$$F_{EXX} := 70 \text{ ksi}$$

$$D := 5$$

$$l := 1 \text{ in} = 1 \text{ in}$$

$$\phi := 0.75$$

$$R_n := 2 \cdot 1.5 \cdot 0.60 \cdot F_{EXX} \cdot \left( \frac{\sqrt{2}}{2} \right) \cdot \left( \frac{D}{16} \right) \cdot l = 27.842 \frac{\text{kip}}{\text{in}}$$

$$R_u := 0.90 F_y \cdot t_w = 11.25 \frac{\text{kip}}{\text{in}}$$

$$\frac{R_u}{\phi \cdot R_n} = 0.539$$

OR:

$$\phi := 0.90$$

$$D_{min} := \frac{\phi \cdot F_y \cdot t_w}{2 \cdot 1.5 \cdot 1.392 \frac{\text{kip}}{\text{in}}} = 2.694$$



**Weld size required for the end-reaction:**

*The end reaction,  $R_u$  or  $R_a$ , is resisted by the lesser of the beam web-to-end-plate weld 1) between the mid-depth of the beam and the inside face of the compression flange, or 2) between the inner row of tension bolts plus two bolt diameters and the inside face of the beam compression flange.*

$$D_{min\_2} := D_{min}$$

$$l := \frac{d}{2} - t_f = 4.705 \text{ in}$$

$$R_u := V_u = 11.2 \text{ kip}$$

$$D_{min\_1} := \frac{R_u}{2 \cdot 1.392 \frac{\text{kip}}{\text{in}} \cdot l} = 0.855$$

$$D_{min} := \min(D_{min\_1}, D_{min\_2}) = 0.855$$

Use:

$$D := 5 \quad \text{"sixteenths"}$$

$$\frac{D_{min}}{D} = 0.171$$

**Connecting elements rupture strength at welds:**

$$t_{min} := \frac{0.60 F_{EXX} \cdot \left( \frac{\sqrt{2}}{2} \right) \cdot \frac{D_{min}}{16}}{0.6 \cdot F_u} \cdot \text{in} = 0.041 \text{ in} \quad (\text{Manual Eq. 9-2})$$

$$\frac{t_{min}}{t_w} = 0.163$$

THIS PAGE INTENTIONALLY LEFT BLANK

## Appendix D Neoprene material model

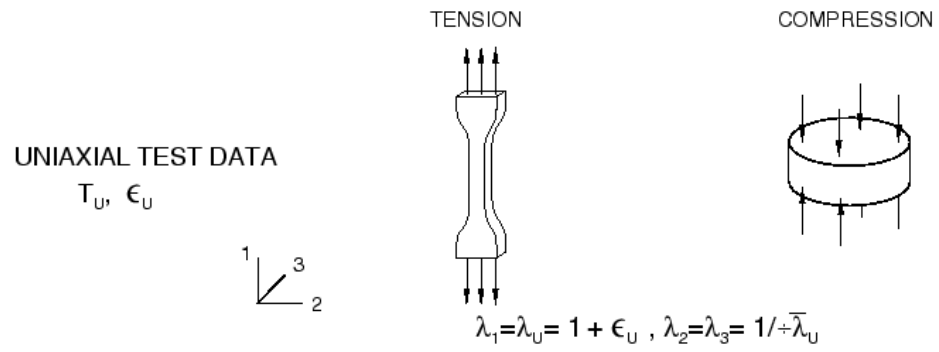


Figure D-1: Uniaxial test description

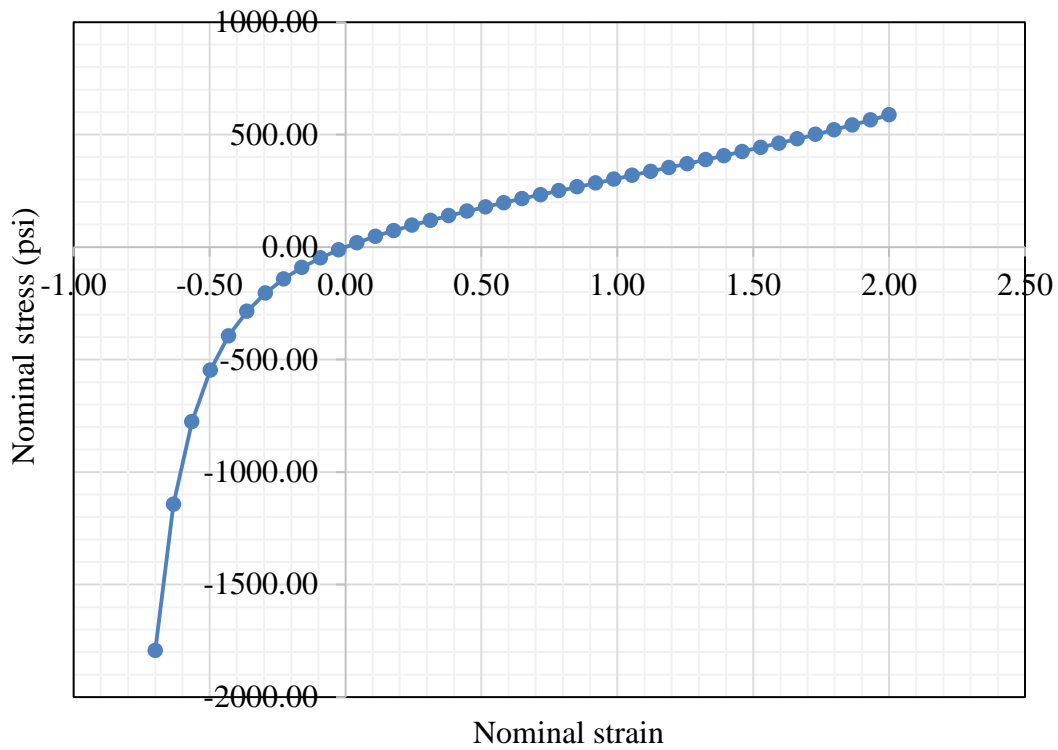


Figure D-2: Uniaxial nominal stress-strain curve

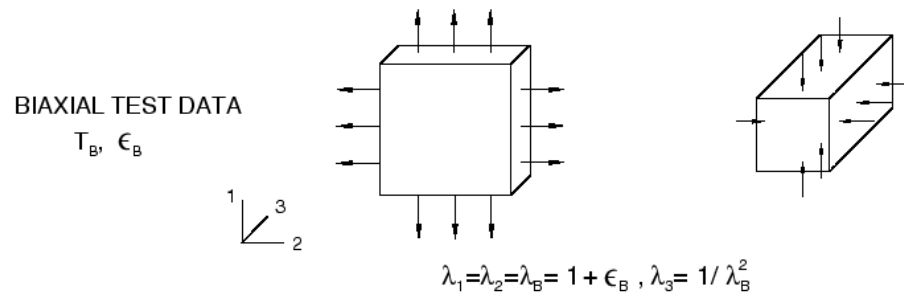


Figure D-3: Biaxial test description

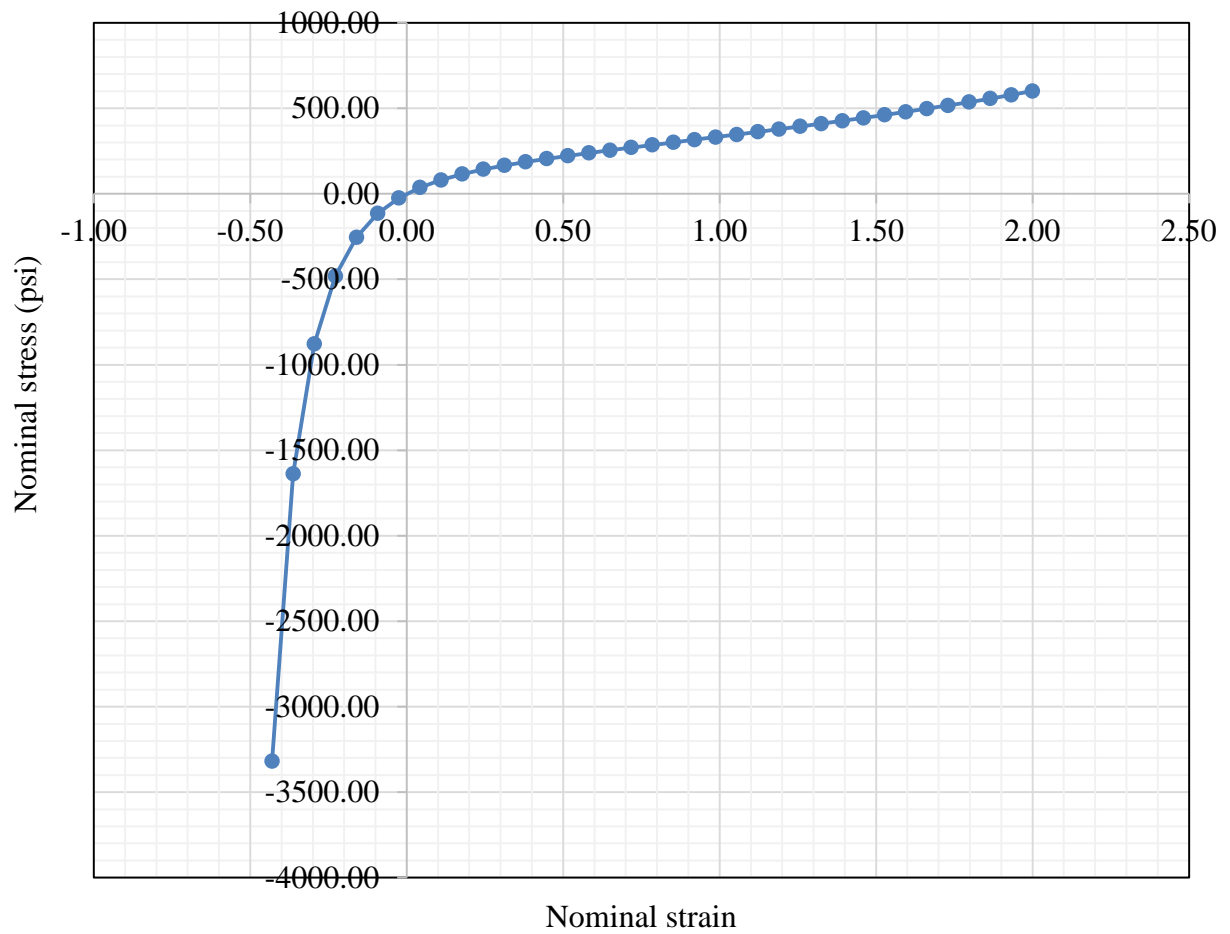


Figure D-4: Biaxial stress-strain curve

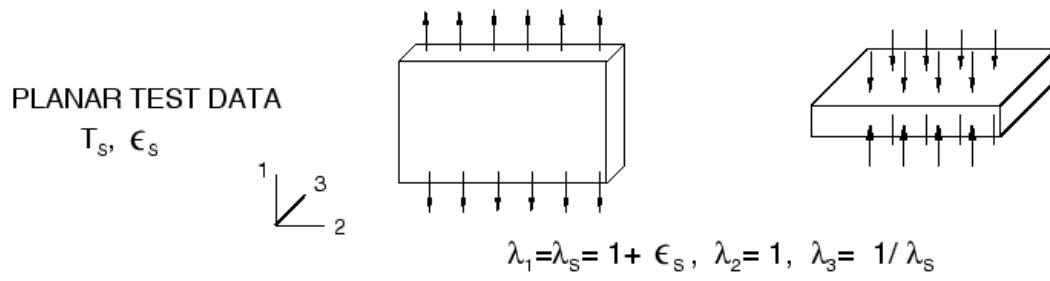


Figure D-5: Planar test description

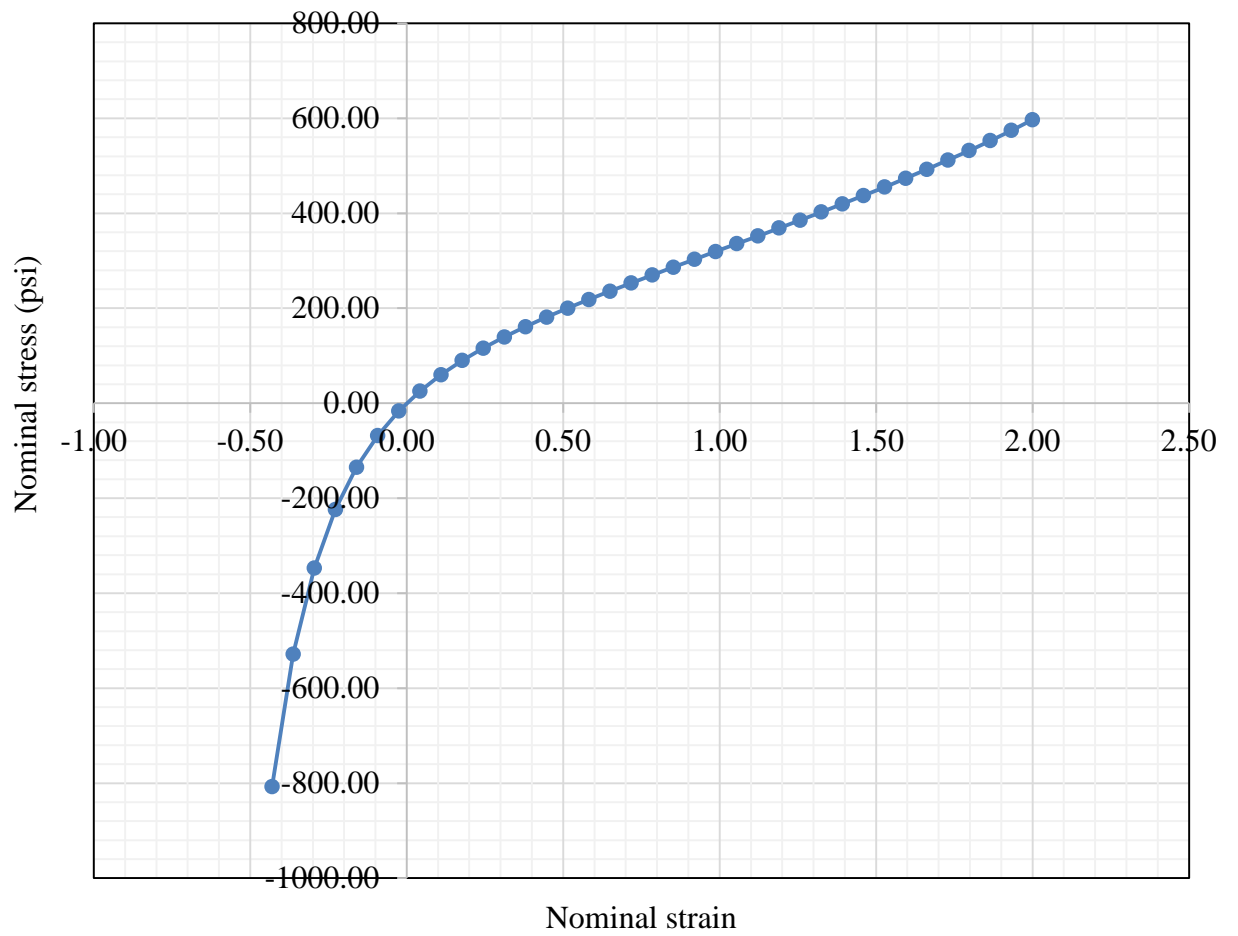


Figure D-6: Planar stress-strain curve

THIS PAGE INTENTIONALLY LEFT BLANK

## **Appendix E Material Reports**

THIS PAGE INTENTIONALLY LEFT BLANK



Customer Name: University of Alaska

Customer PO: Cash/CC

Ht #N07311



EVRAZ INC. NA

Evraz Oregon Steel 14400 N. Rivergate Blvd., Portland, Oregon 97203

## REPORT OF CHEMICAL/PHYSICAL TESTS

ISO 9001

REGISTERED

U.S. PLATE PRODUCER

S  
O  
L  
D  
T  
O

STEELFAB

2132 Railroad Ave  
Anchorage, AK 99501

STEELFAB

2132 Railroad Ave  
Anchorage, AK 99501

|                    |              |      |
|--------------------|--------------|------|
| CERTIFICATE NO.    | DATE         | PAGE |
| 1443433            | May 21, 2015 | 6    |
| MILL ORDER NO.     | DATE         |      |
| 136736             |              |      |
| CUSTOMER ORDER NO. |              |      |
| PLATE SALES-1      |              |      |
| JOB/REQ. NO.       |              |      |
| SHIPPING NO.       | DATE         |      |
| 1443433            | 05/21/2015   |      |
| CARRIER            |              |      |
| UNKNOWN            |              |      |
| CAR/TRUCK NO.      |              |      |
| P12671-SFA         |              |      |

THIS MATERIAL HAS BEEN MANUFACTURED, TESTED AND FOUND TO MEET THE SPECIFICATIONS AND PURCHASE ORDER REQUIREMENTS  
EOS CARBON REGULAR QUALITY PLATE EXCESS PRIME STEEL PLATE.

## PHYSICAL PROPERTIES

| ITEM NO | DESCRIPTION   | HEAT NO. | SLAB | YIELD<br>PSI X 100 | TENSILE<br>PSI X 100 | % ELONG<br>8" 2" | % RA | HARDNESS<br>BHN | BEND<br>TEST | IMPACTS |
|---------|---|----------|------|--------------------|----------------------|------------------|------|-----------------|--------------|---------|
| 2       | HSLA STRUCTURAL QUALITY PLATE<br>ASTM A572-13A GRADE 50<br>ASME SA572 GRADE 50 2013<br><br>0.5118 X 62.000 X 526.000<br><br>1 PC 4734 LBS | N07311   |      | 640                | 815                  | 23               |      |                 |              |         |

## CHEMICAL ANALYSIS

| HEAT NO.   | C   | Mn   | P    | S    | Si  | Cu  | Ni  | V    | Co   | Al   | Cr  | Mo  | Ti   | B | N     | Ca | CE | McQuaid Ehn<br>Grain Size |
|--|-----|------|------|------|-----|-----|-----|------|------|------|-----|-----|------|---|-------|----|----|---------------------------|
| N07311   | .13 | 1.38 | .011 | .002 | .27 | .01 | .05 | .017 | .046 | .031 | .02 | .00 | .014 |   | .0053 |    |    |                           |
| HEATS INDICATED WITH (+) WERE MELTED & MANUFACTURED IN THE USA. HEATS INDICATED WITH (^) WERE ROLLED IN THE USA. |     |      |      |      |     |     |     |      |      |      |     |     |      |   |       |    |    |                           |

I certify the above to be correct as contained in the records of EVRAZ INC. NA

By

QUALITY COORDINATOR

Customer Name: University of Alaska Customer PO: Cash/CC Ht #N06955

**EVRAZ** EVRAZ INC. NA  
Evraz Oregon Steel 14400 N. Rivergate Blvd., Portland, Oregon 97203

**REPORT OF CHEMICAL/PHYSICAL TESTS**

|                       |              |      |
|-----------------------|--------------|------|
| CERTIFICATE NO.       | DATE         | PAGE |
| 1424451               | Jan 28, 2015 | 1    |
| MILL ORDER NO.        | DATE         |      |
| 283421                |              |      |
| CUSTOMER ORDER NO.    |              |      |
| 0052664               |              |      |
| JOB/REQ. NO.          |              |      |
|                       |              |      |
| SHIPPING NO.          | DATE         |      |
| 1424451               | 01/28/2015   |      |
| CARRIER               |              |      |
| HELSEBROS TRANSFER CO |              |      |
| CAR/TRUCK NO.         |              |      |
| ST46                  |              |      |

|  |                |   |   |
|--|----------------|---|---|
| <b>ISO 9001</b><br>REGISTERED<br>U.S. PLATE PRODUCER | <b>SOLD TO</b> | RJH INC DBA STEELFAB<br>2132 RAILROAD AVE<br>ANCHORAGE, AK 99501<br>USA | RJH INC DBA STEELFAB<br>2132 RAILROAD AVE<br>ANCHORAGE, AK 99501<br>USA |
|  |                |   |   |

THIS MATERIAL HAS BEEN MANUFACTURED, TESTED AND FOUND TO MEET THE SPECIFICATIONS AND PURCHASE ORDER REQUIREMENTS  
BOS ALLOY STRUCTURAL QUALITY PLATE ASTM A514-09 GR B.

**PHYSICAL PROPERTIES**

| ITEM NO | DESCRIPTION   | HEAT NO. | SLAB | YIELD<br>PSI X 100 | TENSILE<br>PSI X 100 | % ELONG<br>8" 2" | % RA | HARDNESS<br>BHN | BEND<br>TEST | IMPACTS |
|---------|---|----------|------|--------------------|----------------------|------------------|------|-----------------|--------------|---------|
| >>> 1   | 0.7500 X 96.000ME X 288.000   |          |      |                    |                      |                  |      |                 |              |         |
|         | THE FOLLOWING PLATES WERE AUSTENITIZED AT 1660 DEGS F FOR 34 MINUTES AND WATER QUENCHED<br>THEN TEMPERED AT 1270 DEGS F FOR 38 MINUTES AND AIR COOLED |          |      |                    |                      |                  |      |                 |              |         |
|         | 1 PC 5881 LBS 15A5829 ^ N06955 A21 1030 1120 37 53.1  |          |      |                    |                      |                  |      |                 |              |         |
|         | THE FOLLOWING PLATES WERE AUSTENITIZED AT 1660 DEGS F FOR 34 MINUTES AND WATER QUENCHED<br>THEN TEMPERED AT 1270 DEGS F FOR 38 MINUTES AND AIR COOLED |          |      |                    |                      |                  |      |                 |              |         |
| 2       | 0.6250 X 96.000ME X 288.000   |          |      |                    |                      |                  |      |                 |              |         |
|         | THE FOLLOWING PLATES WERE AUSTENITIZED AT 1660 DEGS F FOR 30 MINUTES AND WATER QUENCHED<br>THEN TEMPERED AT 1280 DEGS F FOR 34 MINUTES AND AIR COOLED |          |      |                    |                      |                  |      |                 |              |         |
|         | 1 PC 5881 LBS 15A5830 ^ N06955 A21 1070 1150 38 60.0  |          |      |                    |                      |                  |      |                 |              |         |
|         | THE FOLLOWING PLATES WERE AUSTENITIZED AT 1660 DEGS F FOR 29 MINUTES AND WATER QUENCHED<br>THEN TEMPERED AT 1280 DEGS F FOR 34 MINUTES AND AIR COOLED |          |      |                    |                      |                  |      |                 |              |         |

**CHEMICAL ANALYSIS**

| HEAT NO.   | C   | Mn  | P    | S    | Si  | Cu  | Ni  | V    | Co   | Al   | Cr  | Mo  | Ti   | B     | N     | Ca | CE | McQuaid Grain Size |
|--|-----|-----|------|------|-----|-----|-----|------|------|------|-----|-----|------|-------|-------|----|----|--------------------|
| N06955   | .18 | .96 | .012 | .003 | .32 | .01 | .06 | .038 | .000 | .042 | .60 | .18 | .039 | .0023 | .0039 |    |    |                    |
| N06957   | .19 | .92 | .012 | .003 | .32 | .01 | .06 | .038 | .000 | .043 | .59 | .18 | .039 | .0022 | .0044 |    |    |                    |
| HEATS INDICATED WITH (+) WERE MELTED & MANUFACTURED IN THE USA. HEATS INDICATED WITH (^) WERE ROLLED IN THE USA. |     |     |      |      |     |     |     |      |      |      |     |     |      |       |       |    |    |                    |

I certify the above to be correct as contained in the records of EVRAZ INC. NA By

Richard Deschand Quality Coordinator

Customer Name: University of Alaska Customer PO: Cash/CC Ht #3502586

**NUCOR** P.O.Box 279  
Winton, NC 27986  
**PLATE MILL** (252) 356-3700

## Mill Test Report

Page 1



Issuing Date : 05/20/2013 B/L No. : 358103 Load No. : 380760 Our Order No. : 108986/1 Cust. Order No. : 29085  
Vehicle No: WTI 4109L Sold To: ASTRALLOY STEEL PRODUCTS Ship To: ASTRALLOY  
Specification : 1.0000" x 96.000" x 288.000" P.O Box 170974 251 WHEELER PLACE  
ASTM A514-05 Grade B NUHEAT BIRMINGHAM, AL 35217 SHARON, PA 16146

Marking : 14072

| Heat No            | C    | Mn    | P            | S       | Si      | Cu     | Ni         | Cr     | Mo   | Al(tot) | V              | Nb                      | Ti    | N      | Ca     | B      | Sn                      | CEQ  | PCM  |     |     |
|--------------------|------|-------|--------------|---------|---------|--------|------------|--------|------|---------|----------------|-------------------------|-------|--------|--------|--------|-------------------------|------|------|-----|-----|
| 3502586            | 0.17 | 0.86  | 0.013        | 0.000   | 0.24    | 0.11   | 0.06       | 0.43   | 0.15 | 0.027   | 0.047          | 0.002                   | 0.031 | 0.0083 | 0.0006 | 0.0023 | 0.009                   | 0.45 | 0.28 |     |     |
| Plate Serial<br>No |      |       | Tensile Test |         |         |        | Heat Treat |        |      |         | Charpy Impacts |                         |       |        |        |        |                         |      |      |     | BHN |
|                    |      |       | Dir.         | Yield   | Tensile | Elong. | R.A.       | Quench | Time | Temper  | Time           | Absorbed Enrgy (Ft-lbs) |       |        |        |        | Lateral Expansion (In.) |      |      |     |     |
| Pieces             | Tons | (psi) |              | (psi)   | % In 2" | %      | "F         | (min)  | "F   | (min)   | 1              | 2                       | 3     | Ave    | Min    | 1      | 2                       | 3    | Ave  | Min | "F  |
| 3502586-07-1       | 1    | 3.92  | T            | 108,800 | 118,800 | 36.2   | 56.4       | 1665   | 41   | 1250    | 51             |                         |       |        |        |        |                         |      |      |     |     |

Manufactured to fully killed fine grain practice by Electric Arc Furnace. Welding or weld repair was not performed on this material. Mercury has not been used in the direct manufacturing of this material. Produced as continuous cast discrete plate on rectangular specimens, unless otherwise noted in Specification.

Yield by 0.5EUL method unless otherwise specified.  $Ceq = C + (Mn/5) + ((Cr + Mo + V)/5) + ((Cu + Ni)/15)$

$PCM = C + (Si/30) + (Mn/20) + (Cu/20) + (Ni/60) + (Cr/20) + (Mo/15) + (V/10) + 5B$

Melted and manufactured in the USA, ISO 9001:2008 certified (#008063) by SRI Quality System Registrar (#0985-09). PED 97/23/EC 7/2 Annex 1, Para. 4.3 Compliant. DIN 50049 3.1.B/EN 10204 3.1B(2004), DIN EN 10204 3.1(2005) compliant. For ABS grades only. Quality Assurance certificate 09-MMPQA-548

We hereby certify that the contents of this report are accurate and correct. All test results and operations performed by the material manufacturer are in compliance with the applicable specifications, including customer specifications.

*T. A. Depretis*

T. A. Depretis, Metallurgist

05/20/2013 4:50:53 PM

151248

## Economy Grade Neoprene Sheet Grade 60

| Test             | Typical Value | Units               | ASTM Method |
|------------------|---------------|---------------------|-------------|
| Hardness         | 60 +/- 5      | Shore "A" Durometer | D2240       |
| Tensile Strength | 500           | PSI                 | D412        |
| Elongation       | 200           | %                   | D412        |
| Tear Value       | 50            | PL                  |             |

### Heat Aging

|   |        |                  |      |
|---|--------|------------------|------|
| Heat Resistance @ 100° C after 70 hours |        |                  | D573 |
| Change in hardness                      | 10     | %                |      |
| Change in Tensile                       | -16%   | %                |      |
| Change in Elongation                    | -60%   | %                |      |
| Compression set                         | 50%    | 22 hours @ 70° C |      |
| Lowest Working Temp                     | -40° F |                  |      |
| Highest Working Temp.                   | 134° F |                  |      |

|                   |      |                   |
|-------------------|------|-------------------|
| Oil Swell: #3 Oil | 120% | 22 hours @ 100° C |
|-------------------|------|-------------------|

### Product Range

Color: Black

Thickness: 0.8 mm - 50.8 mm (1/32" - 2")

Length: 17' - 150'

Width: 4" - 72"

Width Tolerance:

48" Widths +/- .177"

All other Widths +/- .063"

Gage Tolerances:

1/8", 1/4", 3/8" +/- .032"

1/2" +/- .047"

3/4" +/- .094"

1" +/- .100"

1 1/8" +/- .110"

1 1/2" +/- .114"

Pattern: Smooth both sides.

Fabric Finish available one side or two sides upon request and at an additional charge.

## Appendix F Drawings and Photos of Calibrated Hot Box

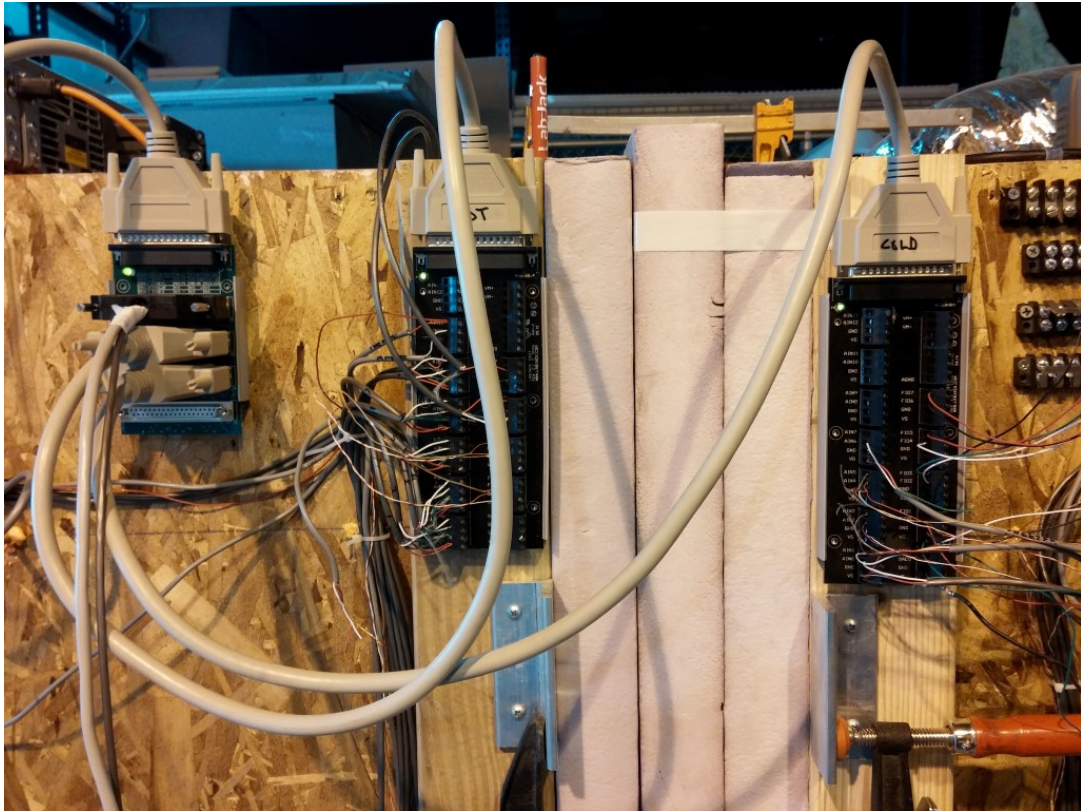




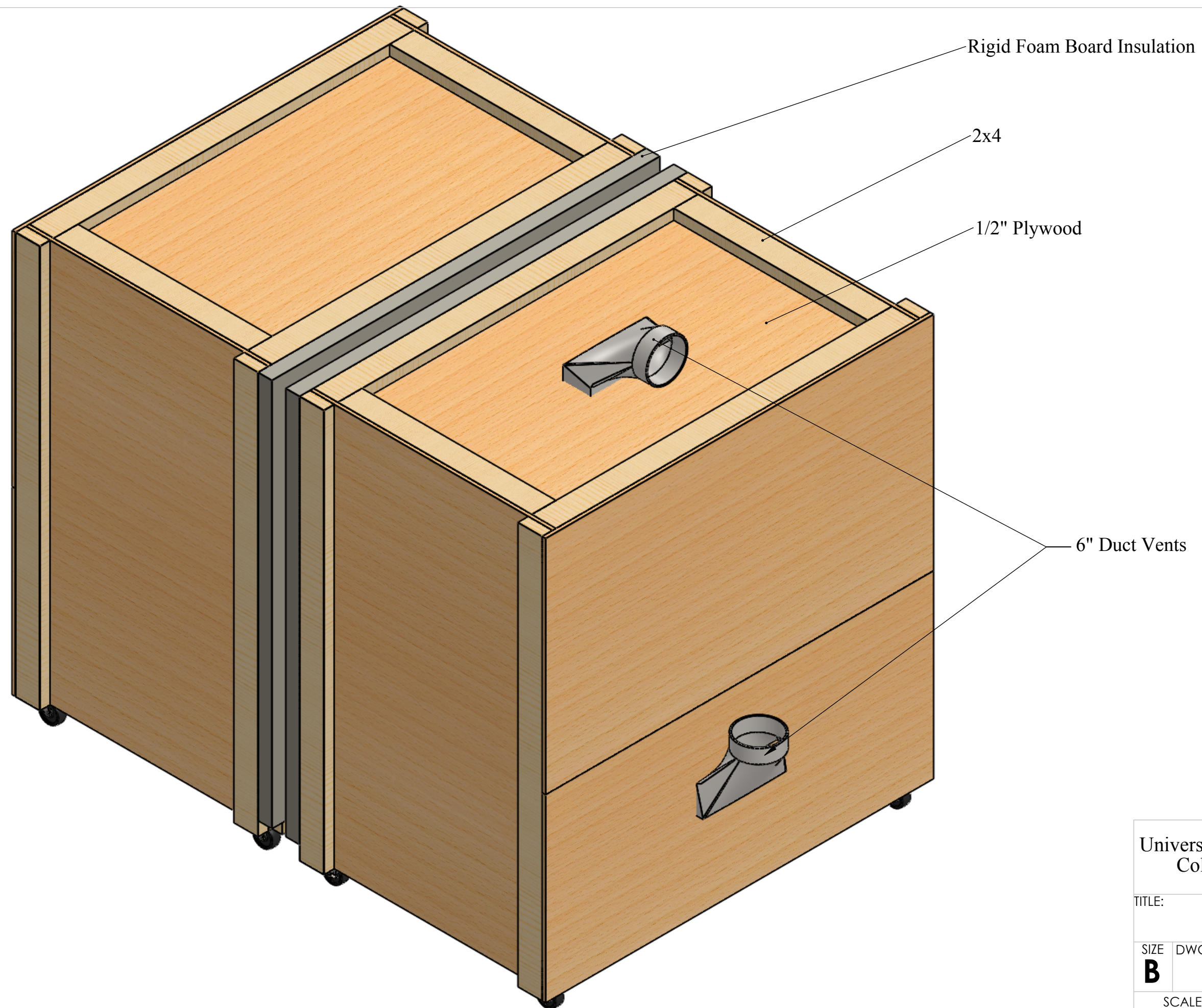






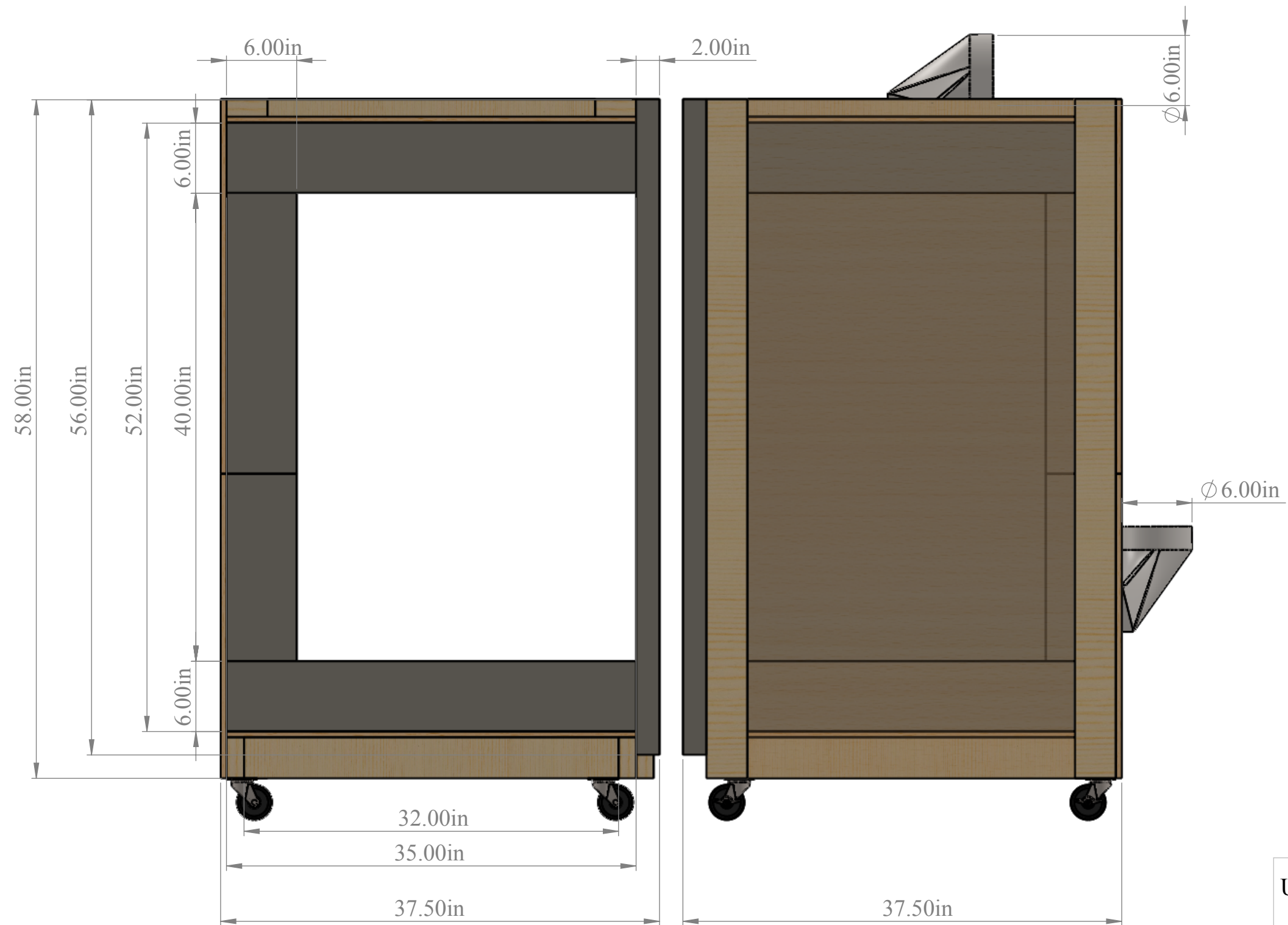






|  |                      |              |
|--|----------------------|--------------|
| University of Alaska Anchorage<br>College of Engineering |                      |              |
| TITLE: Hot Box   |                      |              |
| SIZE<br><b>B</b>   | DWG. NO.<br>Assembly | REV<br>0     |
| SCALE: 1:10  |                      | SHEET 1 OF 5 |





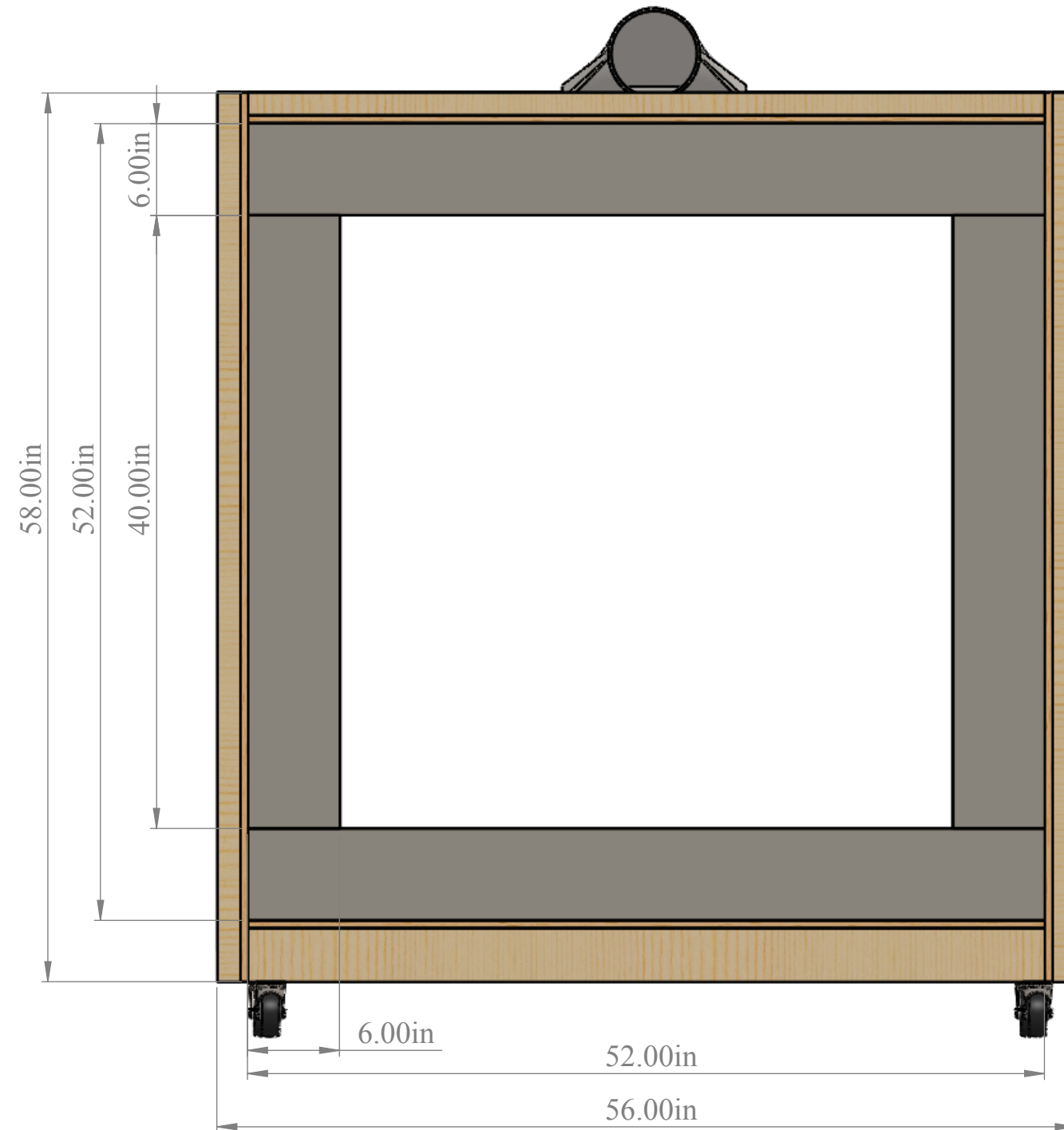
University of Alaska Anchorage  
College of Engineering

TITLE: **Hot Box**

| SIZE     | DWG. NO. | REV      |
|----------|----------|----------|
| <b>B</b> | Front    | <b>0</b> |

SCALE: 1:10

SHEET 2 OF 5



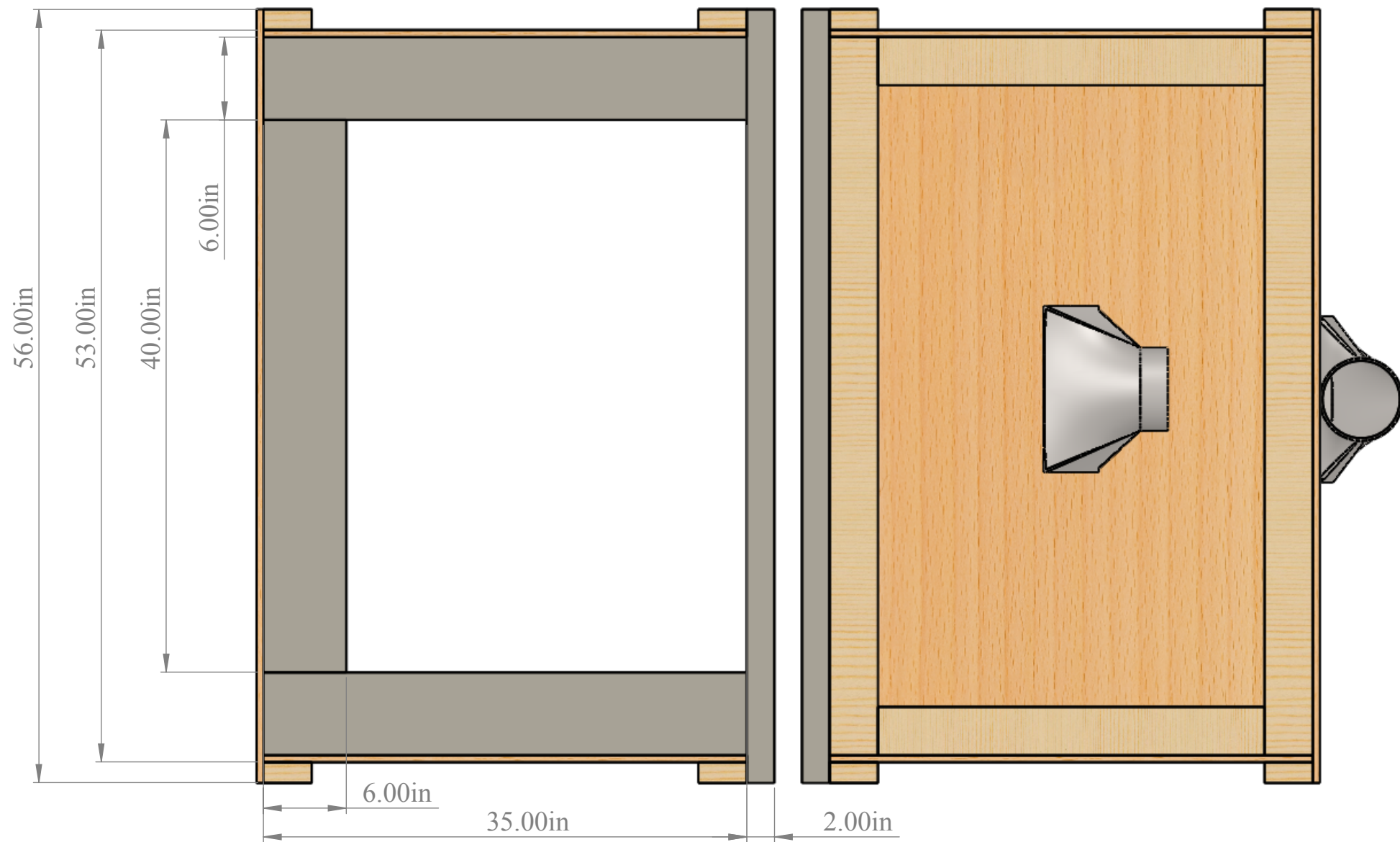
University of Alaska Anchorage  
College of Engineering

TITLE: **Hot Box**

| SIZE     | DWG. NO. | REV      |
|----------|----------|----------|
| <b>B</b> | Right    | <b>0</b> |

SCALE: 1:10

SHEET 3 OF 5



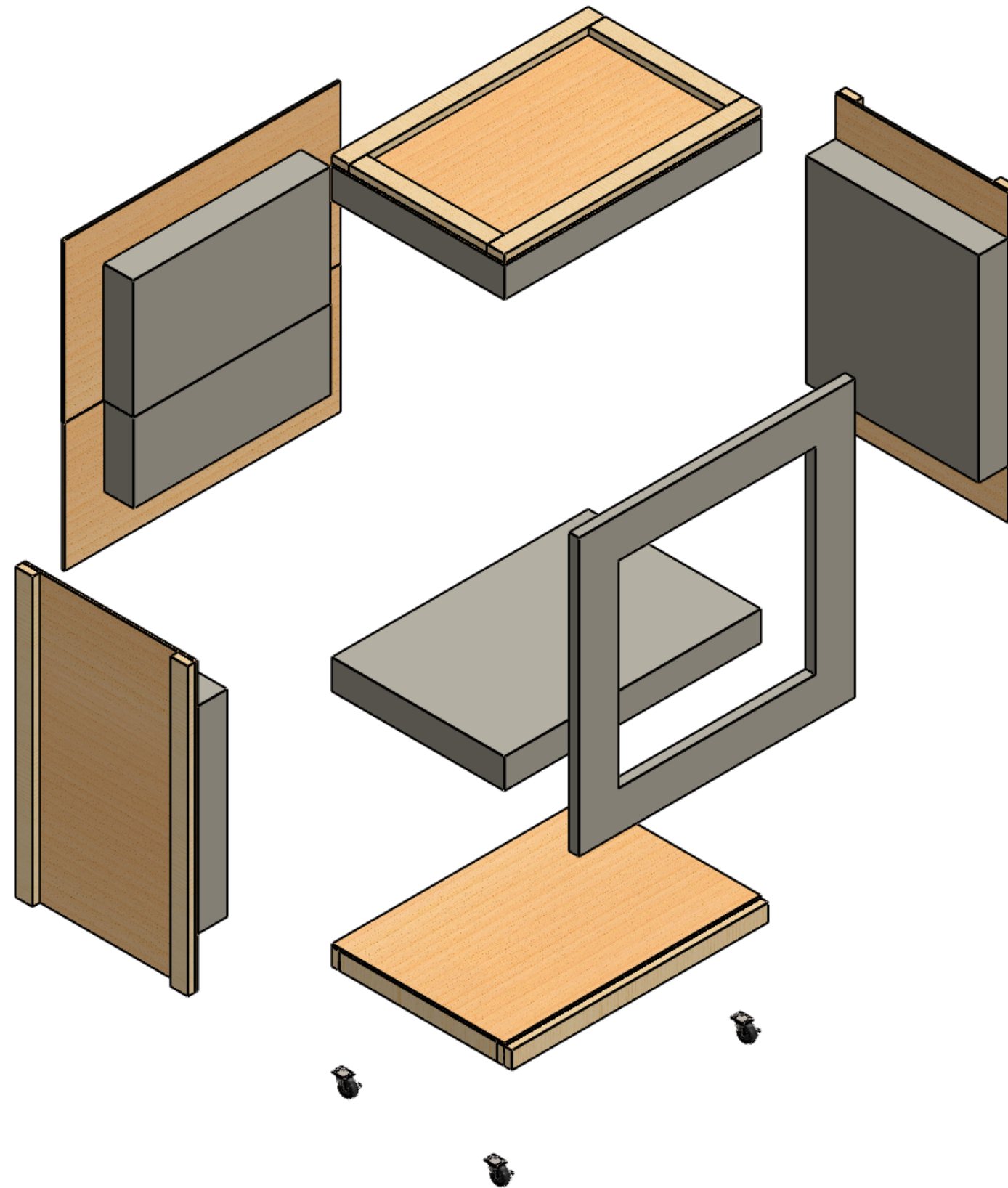
University of Alaska Anchorage  
College of Engineering

TITLE: **Hot Box**

| SIZE     | DWG. NO.   | REV      |
|----------|------------|----------|
| <b>B</b> | <b>Top</b> | <b>0</b> |

SCALE: 1:10

SHEET 4 OF 5



University of Alaska Anchorage  
College of Engineering

TITLE: **Hot Box**

|          |                      |          |
|----------|----------------------|----------|
| SIZE     | DWG. NO.             | REV      |
| <b>B</b> | <b>Exploded View</b> | <b>0</b> |

SCALE: 1:20

SHEET 5 OF 5